2010

CHARACTERIZATION OF Ni-RICH NiTiHf BASED HIGH TEMPERATURE SHAPE MEMORY ALLOYS

Gurdish S. Ded

University of Kentucky, gurdish.ded@gmail.com

Click here to let us know how access to this document benefits you.

ABSTRACT OF THESIS

CHARACTERIZATION OF Ni-RICH NiTiHf
BASED
HIGH TEMPERATURE SHAPE MEMORY ALLOYS

Among the potential high temperature shape memory alloys, due to its low cost, medium ductility and high work output NiTiHf seems to be the most promising HTSMA for a wide range of applications in the 100-250ºC. A detailed investigation into the shape memory properties and transformation behavior for the Ni-rich HTSMA with the compositions of $Ni_{45.3}Cu_5Ti_{29.7}Hf_{20}$, $Ni_{50.3}Ti_{29.7}Hf_{20}$ and $Ni_{45.3}Pd_5Ti_{29.7}Hf_{20}$ was carried out. It is possible to form Ni-rich precipitates in Ni-rich NiTiHf alloys and tailor the TTs by heat treatments that results in increased strength and stable response at high temperatures. The coherent Ni-rich precipitates deplete the Ni content from the matrix increasing the transformation temperatures and strengthen the material by hindering the dislocation motion. The effect of aging on the microstructure, shape memory and mechanical properties are revealed. Optimum aging conditions have been found determined to get the most favorable combination of high transformation temperatures with stable and good shape memory properties. The $Ni_{50.3}Ti_{29.7}Hf_{20}$ and $Ni_{45.3}Pd_5Ti_{29.7}Hf_{20}$ aged at 500ºC-600 ºC were found to be formidable candidates for high temperature applications.

KEYWORDS: HTSMA, NiTiHf, precipitate hardening, Ni-rich SMA, mechanical testing.

Gurdish S. Ded

13th August, 2010

CHARACTERIZATION OF Ni-RICH NiTiHf
BASED
HIGH TEMPERATURE SHAPE MEMORY ALLOYS

By

Gurdish S. Ded

<div style="text-align:right">

Dr. Haluk E.Karaca

Director of Thesis

Dr. James M. McDonough

Director of Graduate Studies

13th August, 2010

</div>

RULES FOR THE USE OF THESES

Unpublished theses submitted for the Master's degree and deposited in the University of Kentucky Library are as a rule open for inspection, but are to be used only with due regard to the rights of the authors. Bibliographical references may be noted, but quotations or summaries of parts may be published only with the permission of the author, and with the usual scholarly acknowledgments.

Extensive copying or publication of the thesis in whole or in part also requires the consent of the Dean of the Graduate School of the University of Kentucky.

A library that borrows this thesis for use by its patrons is expected to secure the signature of each user.

  Name   Date

_____

_____

_____

_____

_____

_____

_____

_____

_____

THESIS

Gurdish S. Ded

The Graduate School

University of Kentucky

2010

CHARACTERIZATION OF Ni-RICH NiTiHf
BASED
HIGH TEMPERATURE SHAPE MEMORY ALLOYS

_____

THESIS

_____

A thesis submitted in partial fulfillment of the
requirements for the degree of Master of Science in
Mechanical Engineering in the College of Engineering
at the University of Kentucky

By

Gurdish S. Ded

Lexington, Kentucky

Director: Dr. Haluk E. Karaca, Assistant Professor of Mechanical Engineering

Lexington, Kentucky

2010

This work is dedicated to my family and friends, who have always been there, especially when I needed them the most.

ACKNOWLEDGEMENTS

I am thankful to a lot of people both in my professional and personal walks of life on the completion of my thesis, without whom it would have not been possible for me to make it till here.

I would like to express my gratitude towards my advisor Dr. Haluk E. Karaca for his guidance, time, support in carrying out this research project and teaching me how to do scientific research. This thesis could not have been made possible without his tremendous help and valuable comments. I would also like to take this opportunity for thanking Dr. Ronald Noebe for his timely guidance, comments and providing the alloys for carrying out the research, without which the experimental work would have not been possible. I would also like to thank Dr. Maier for all his help on the TEM work and the valuable comments about the findings.

I would also like to thank Dr. I.S. Jawahir and Dr. Balk for for serving as members of my defense committee. I would also like to thank Dr. Stephens for giving me gudiance and the TA when I first joined the department and Dr. Menguc for his guidance also.

I am grateful to my parents for showing constant trust in me and showing me that nothing is impossible to achieve. I am blessed to have wonderful two sisters and their families. I am grateful for their timely piece of advise and pushing me forward to realize my dreams. I am also lucky to have my uncle and aunt here in Kentucky, and am thankful to them for making Kentucky my home away from home. I want to take this oppurtunity

to thank my office partners Mohammad, Sayed, Sadi for putting up with and gettting used to the constant punjabi music in the backround and laughing even at my not so funny jokes. I am thankful to Sayed for all his help for running the experiments and Dr. Burak Basaran for making sure we had accurate and running systems for running the experiments and Micah for proof reading my chapters . I would also like to thank all my friends I made in Lexington during my masters who made sure that I never felt away from home. I would like to thank Amir for giving me suggestions throughout my stay and Vivek for showing me that no matter how hard I work, he has already done more. Vishnu, Henry, Lius and Cisco for showing me way around the campus and planning all the funtrips to make sure I got my mind free for the short intervals before I came back to the lab. I am grateful to my friends Ankur and Subu for their comments and guidance. I am also grateful to all the help I got from the staff in the mechanical engineering department, especially from Josh and Herb. This thesis would have not been possible without my friends Aman, Ankush, Bikram, Gurinder, Harpreet and Kabir.

Finally I would like to thanks NASA Epscor foundation for funding the project, without which this work would have not been possible.

TABLE OF CONTENTS

LIST OF TABLES

LIST OF FIGURES

xi

LIST OF FILES

File Name	File Size
1. Gurdish_Ded_thesis.pdf	9.4 MB

Chapter One

Introduction

1.1 History and overview

During their research on the bending behavior of Gold-Cadmium bars, Chang and Read [1] observed an unusual phenomenon. During the application of load, the Au-Cd bar deformed as expected, but upon the removal of load followed by subsequent heating, the bar recovered to its original undistorted shape. This was the first time that shape memory effect (SME) was observed and the term for behavior of the material to remember its original shape upon heating was termed as SME, however the underlying unique thermoelastic behavior was not completely understood. Later similar behavior was observed later in Cu-Zn and In-Tl alloys, but the scientific community did not give much attention into the utilization of this unique behavior until 1963 [2]. The discovery of SME in nearly equiatomic nickel titanium alloy by Buehler [3] and his coworkers, while researching the heat shielding properties of the alloy at the Naval Ordinance Laboratory (NOL) drew attention towards the potential use of this extraordinary property in actual applications. During their research at NOL, Buelher and his team-members noticed that along with the good mechanical properties, the material had the capability to recover its original shape. This discovery led to the coining of the term "NiTiNOL", derived from its composition and place of discovery. Since the Ni-Ti alloy has many complicated structures associated with it, the development of understanding for the underlying phenomenon for SME was not possible till early 1980s. It was with the discovery of SME in Cu-Al-Ni [4] alloy that made it possible to relate the SME with the thermoelastic martensitic transformation.

NiTi alloy has been at the helm of most shape memory alloys (SMA) research because of its high tensile strength, low density, corrosion resistance, superelasticity and shape memory behavior. These properties have motivated both scientists and innovators in the past few decades to utilize this unique property of SMAs for use as functional materials in various applications and actuation roles. One of the first commercial SMA applications was called as Cryofit [5-6], in which the SMA was used for making pipe couplings used in F-14 fighter jets. The transformation temperatures for Cryofit were so low that the couplings were transported in liquid nitrogen to avoid accidental actuation. Later research led to the development of NiTiNb [7] system with a comparably higher transformation temperature in 1989, which found its application in battle damage and nuclear reactors repair. In the last few decades many advances have been made in the improvement of SMAs. In 1999 Miyazaki [8] showed the improved fatigue life of NiTiCu, hence opening way for wide range of applications in engineering.

Ever since the discovery of NiTi in 1963, numerous industrial applications were being developed but it was in early 1970's when the idea of using NiTi in the field of biomedical applications was first conceived, and later in that decade first wide-scale biomedical application in the field of orthodontics was already available, and later in the early 1990's the first SMA based NiTi stents were made commercially available. Apart from this breakthrough in the field of medicine, applications in air conditioning vents, temperature sensitive valves, electronic cable connectors, etc. had already been developed [7]. In the past decade, a strong demand of SMAs for actuation in high temperature environment has been seen in the field of aerospace, the automobile sector and the oil industry. In comparison with conventional actuators such as hydraulic

actuators, pneumatic devices, bimetallic strips and electric motors, studies have shown that SMAs are more desirable because of their force capabilities, low weight, compact size, high energy density, noiseless and frictionless operation [9-11]. Their ability to simultaneously act as sensors makes them a unique self contained smart system.

Shape memory alloys have this unique ability to evoke the state of previously memorized shape by utilization of an external stimulus such as temperature or stress because of a reversible crystallographic, thermoelastic-martensitic transformation. The martensitic transformations can be defined as a lattice tranfomation involving a shear deformation and resulting from cooperative atomic movement [12]. The transformation is diffusionless and the concentration of solute atoms dissolved in martensite phase remains the same as in the parent phase. The transformation is accompanied by a definite value in shape change. The SMA properties rely on this transformation from a high temperature parent phase to a low temperature martensite phase. This high temperature parent phase is called as the austenite phase. There are four temperature points associated with these two phases. The martensite start (M_s) temperature is one at which the martensite phase starts to form when cooling down from austenite phase and martensite finish (M_f) temperature is that at which the transformation from austenite to martensite finishes upon cooling. Similarly, upon heating when the austenite start temperature (A_s) is the one at which austenite starts to form from martensite and austenite finish (A_f) temperature is the one at which the transformation from martensite to austenite finishes upon heating.

1.2 Shape memory properties:

SMAs exhibit chiefly two different properties, namely shape memory effect and superelastic effect (SE) depending on the alloy's transformation temperatures and the operating temperature. Shape memory effect is described as the ability of the alloy to recover any deformation imparted by heating it above A_f. While superelasticity is a phenomenon which takes place at a temperature higher than A_f, as a result of stress induced martensitic transformation during loading and subsequent reverse transformation upon unload.

1.2.1 One-Way shape memory effect

SME or one way shape memory effect is described as the phenomenon in which the material is deformed in martensite recovers its original shape upon heating up to austenite phase. Figure 1.1(a) shows an illustration in which the SMA spring is deformed in martensite upon application of load. While the load is still applied, upon heating the SMA spring to a temperature higher than A_f, the spring returns to its original undeformed state. When twinned martensite is subjected to stress, the process of reorientation starts and as a result more favorable variants of martensite start forming at the expense of less favorable variants. The material when unloaded retains this detwinned state and the reverse transformation starts only after heating beyond A_f. Further in the illustration it is seen that when the spring cools down and transforms to martensite, since the load is still present the spring starts to deform again. Illustration represented in Figure 1.1(b) shows a case in which the load is taken off after initially deforming the SMA spring in martensite phase. Upon heating the spring recovers to its original shape as in the previous

illustration but it does not change its shape upon cooling since there is no external stress available for deformation. Thus the phenomenon is named "one-way shape memory effect".

(a)   (b)
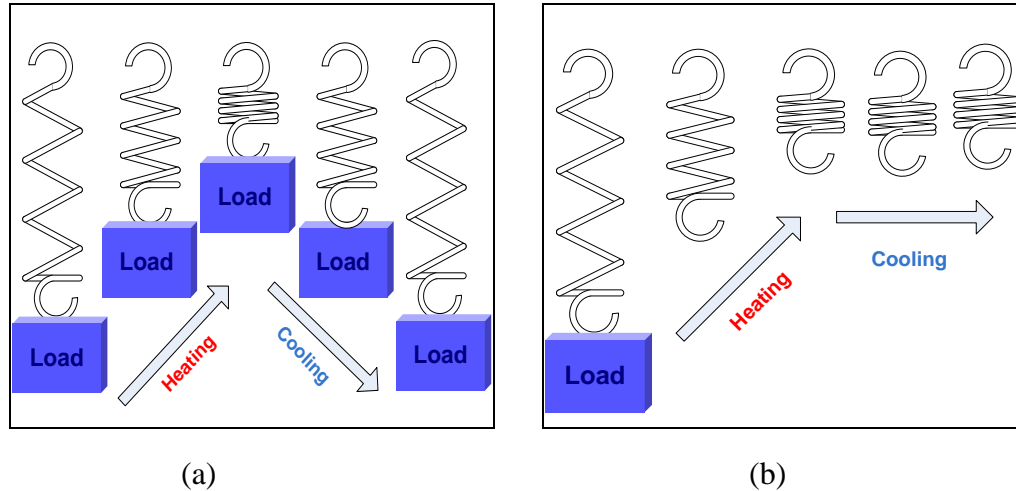
Figure1.1: Schematic representing a SMA spring SME under load (a) and no load (b) condition

The reason behind the phenomenon of one-way shape memory effect is the formation of self accommodating martensite upon cooling, and hence resulting in no shape change. During no load condition or when there are no internal stresses present, they form self accommodating structures in order to minimize energy. When a force is applied on the structure, some favorable variants grow at the expense of others. The austenite phase has a high order of symmetry with no variants and after transformation, the different variants formed during the deformation in martensite are transformed into the same structure. The configuration of the material in the martensite does not have any effect on the parent shape and it remains the same.

1.2.2 Two-way shape memory effect

In contrast to one way shape memory effect where only the shape of the parent phase is remembered, in two way shape memory effect it is possible to memorize the shape of martensite phase also in some cases as depicted by the schematic presented in Figure 1.2. With thermal cycling under no load, the specimen changes its shape in both ways. This phenomenon is called as two way shape memory effect (TWSME) because of the ability of the SMA to memorize shape in both martensite and austenite phase. The underlying reason behind this phenomenon is the introduction of internal stresses due to dislocations, defects and precipitates that disrupts self-accommodating structure and favors formation of selective martensite variants. The dislocations and defects don't dissolve with the transformation, and upon cooling the stress fields present around the dislocations favors formation of particular variants. Hence, a shape change is observed during cooling also.
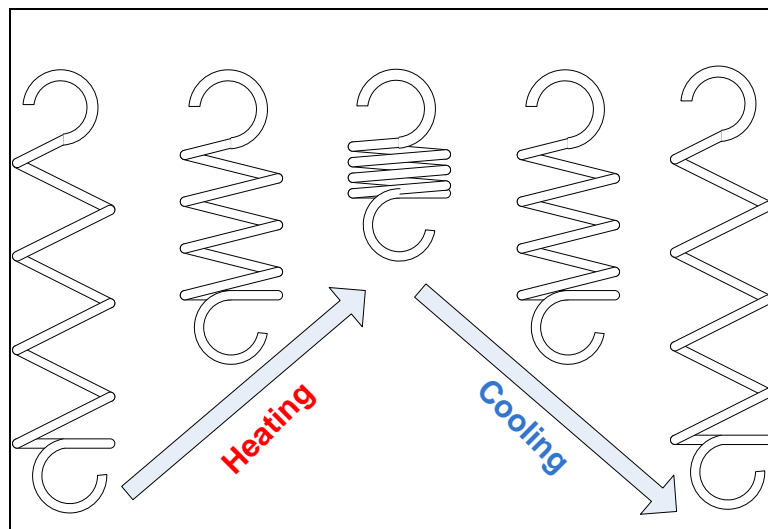
Figure1.2: Sping made of SMA showing the behavior of TWSME

1.2.3 Superelastic effect

Superelastic effect also known as pseudoelastic effect, is the phenomenon associated with reversible large strains when the SMA is deformed above A_f temperature. During loading at temperatures above A_f, stress induced transformation leads to formation of martensite at sufficiently high stress levels and upon removal of the load, reverse transformation from martensite to austenite is observed. At temperature where austenite is stable, during loading the stress level intersects the level for initiation for stress induced martenistic transformation as shown in phase diagram in Figure 1.3. Since the SMA is being loaded at temperature above A_f, under stress free condition austenite is stable and hence upon unloading back transformation occurs accompanied by large recoverable strains.
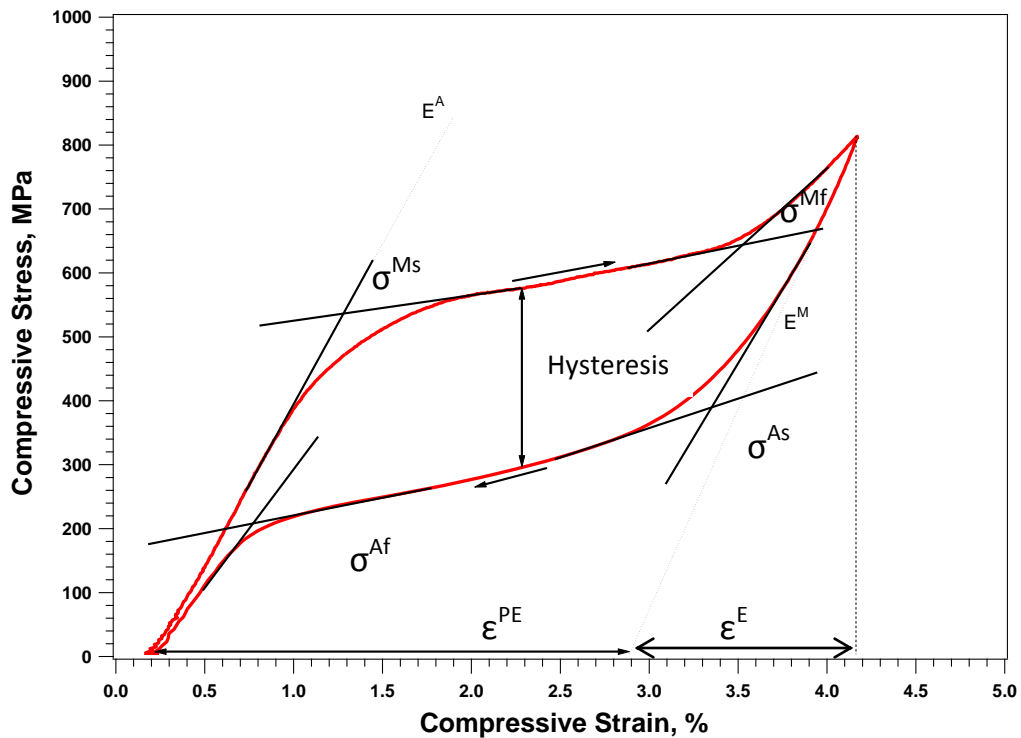
Figure1.3: Typical plot showing the stress-strain curve for Super elastic behavior

Figure 1.3 highlights the critical points important to the understanding of the SE cycle. The load level reffered to σ^{Ms} is the defined as the critical stress required to initiate the process of stress induced martensite (SIM) which ends at σ^{Mf}, followed by elastic loading of the martensite. In the unloading part of the curve the σ^{As} represents the critical stress at which the SIM begins to transform back to austenite which ends at stress level of σ^{Af}. ε^{PE} represents the total amount of SE strain that is recovered upon unloading and ε^{E} represents the elastic part of the strain upon unloading. The hysteresis mentioned in the plot depicts the difference in the critical stresses for forward and back transformation. E^{A} and E^{M} represent the Youngs Modulus of Elasticity for austenite phase and martensite phase, respectively.
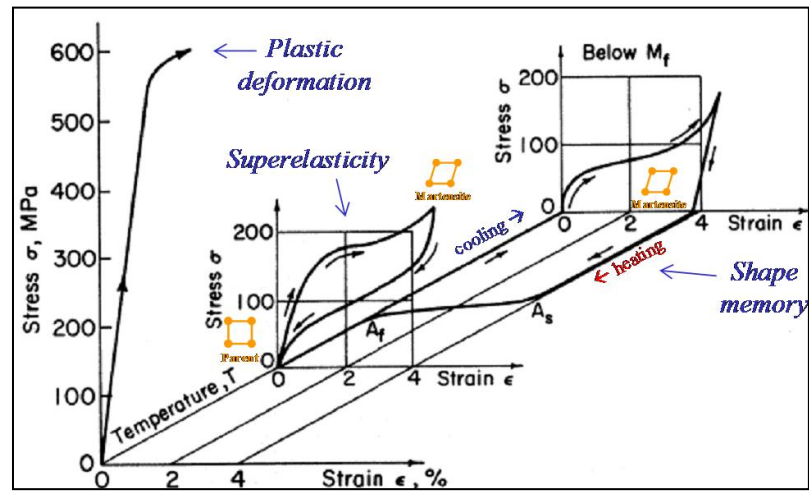
Figure 1.4: Schematic of stress-strain, SME and SE in 3-D [9]

Figure 1.4 depicts the relationship between stress, strain and temperature for SMA. As seen from the Figure 1.4 it can be seen that the SME is a consequence of changing the temperature and SE occurs due to applied mechanical stress. The Clausius-Clapeyron linear relationship best describes the temperature-stress dependence of

martenistic transformations in SMAs. The relationship for uniaxial stress can be written as follows,

$$\frac{d\sigma}{dT} = -\frac{\Delta S}{\varepsilon} = -\frac{\Delta H^*}{\varepsilon T_0}$$

where σ is the uniaxial stress, ε is the transformation strain in the direction of the uniaxial stress, ΔS is the entropy of transformation per unit volume, and ΔH^* is the enthalpy of transformation per unit volume. ΔH^* is dictated by the chemistry and crystallography of the transformation, T_0 is the equilibrium temperature of transformation and is determined from the enthalpy and entropy changes of the transformation. Since all the parameters mentioned above are constants for a given system, hence the relation between stress and temperature is linear. The slope of the curve for near equiatomic NiTi varies between 5-8MPa/°C [13].

Figure 1.5 depicts the schematic representing the region of SE as a function of stress and temperature. The SME and SE can be observed in the same specimen depending on the temperature of testing, provided the stress applied is below critical strees for inducing slip. It is noted from Figure 1.4 that the SME occurs below A_s upon heating beyond A_f where the martensite is unstable is absence of stress. The red line in the Figure 1.5 represents the critical stress required to induce martensite which follows the Clausius-Clapeyron relationship. It is known that the critical stress for slip should be higher than critical stress for SIM for PE to occur. The shaded portion in the Figure 1.5 represents the window or the combination of stress-temperature for the particular alloy for PE to occur. The steeper slope for Clausius-Clapeyron relation as depicted by the dotted curves for A and M can diminish or completely deplete the chance of SE to occur.

9

Another key point to be noted is that if the critical stress for slip is increased, the area depicting the possibility of PE increases. Hence one of the foremost methods to achieve improvement of both PE and SME obtained by means of hardening the alloy which in turn increases the critical stress for slip [10].
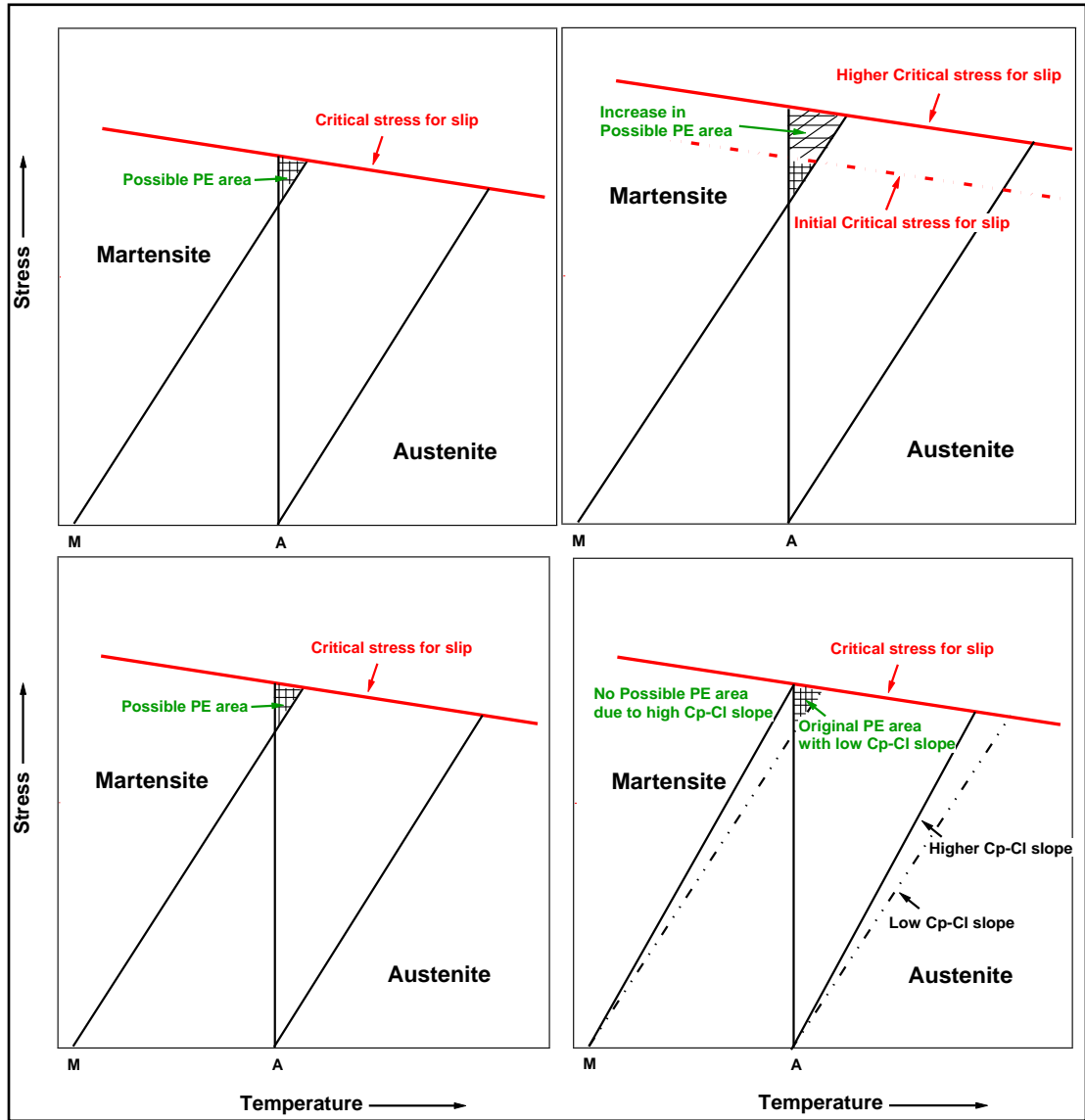
Figure 1.5: Schematic representing the relation between the critical temperatures and stresses for SMA

1.3 Introduction to High Temperature Shape Memory Alloys

The unique properties of SMAs are widely being used in the vicinity of room temperature for applications in form of electrical switches, eyeglass frames, couplings for pipes and other tubular products, temperature sensing valves and apart from these there are countless applications in medical and dental devices [14]. Since its most famously known and commercially available binary NiTi alloy cannot be utilized at temperature higher than 100°C

In recent years many material scientists have paid close attention to the development of SMAs which can operate at temperatures above 100°C because of the demand from automotive, robotic and aerospace industries [15]. One of the simplest examples of SME is unconstrained recovery in which the SMA wire recovers to its original shape after being deformed or twisted in any shape. This same concept has been utilized to put forward SMA based antenna arrays. The antennae for a satellite or a space rover can be rolled into a compact state for storage while the unit is being transported, but when the unit is in action the antenna can be deployed by passing a small amount of current through the SMA based antenna to prepare the antenna to function. Most orbital satellite utilizing this application would also require a high temperature shape memory alloy with transformation temperatures more than 100°C to avoid unintended actuation in case of exposure to direct sunlight. Another application area of SMAs is during constrained recovery in which the SMA component is prevented from going back to its original shape upon heating, which usually generates very high stresses [14]. This property can be used for fastening multiple components, connecting pipes or tubes etc. Due to material property degradation of currently available SMAs, they cannot be used

for above mentioned application because of their risk of failure due to material strength [14]. The high demand for HTSMAs is from the interest of utilizing them in solid state actuators. SMA based actuators have been found to have higher energy densities than pneumatic actuators and DC motors and at par with hydraulics while having the advantage of weighing significantly less. Along with the advantage of being lighter in weight, being frictionless and noiseless make SMA based solid state actuators a formidable candidate for application in weight critical systems such as jet turbine engines, spaceships and any other aerospace application. Hence, the development of HTSMA will play a pivotal role in the realization of the use of SMA in real life applications in aerospace such as clearance control in the compressor and turbine section of jet engine, variable area and geometry inlets for subsonic jets, self-damping components in fuel line clamps, down-well flow control valves, electrical appliances and actuators close to engine parts in automobiles. Currently available NiTi based SMAs can only operate at temperatures lower than 100°C due to their low TTs or poor mechanical behavior at high temperatures[14]. In this mentioned higher temperature range the martenstic transformation occurs at a temperature range where the diffusion controlled processes like decomposition, recrystallization, recovery, etc. could take place and might deteriorate the shape memory behavior

Some of the most common approaches suggested to meet the industry requirements of HTSMAs include the following [16-17]

- Development of new metallic alloys with high transformation temperatures.
- Addition of ternary or quaternary element(s) or solid solutioning the known alloys.
- Optimization of various thermo-mechanical treatments and process of SMAs.

In an attempt to distinguish HTSMAs from their lower TT counterparts, many a definitions have been put forward. One of the most widely accepted definition is given by Firstov et al. [15] where he describes HTSMAs as alloys of which the reverse transformation A_s starts above 390K in stress free conditions following any thermo-mechanical treatment. Some of most the extensively researched HTSMAs are based on Co-, Fe-Mn-S-, Cu-Al-Ni-, Ni-Mn-, Ni-Al-, Ti-Pt(Pd, Au, Rh)-, and Ni-Ti-compositions[15-16, 18]. Some of the recent discovered alloys consist of Ta-Ru, Nb-Ru [19] and Ni-Mn-Ga [20], Co-Ni-Al [21] ternary alloys. The Co-based and Fe-Mn-Si-based HTSMAs undergo a non-thermoelastic FCC↔HCP transformation [15]. This unique martenistic transformation (MT) includes the nucleation of martensite phase as a stacking fault in the parent FCC and its further growth in HCP martensite. This requires the movement of partial dislocations for progress of martensite and the reversibility of the process depends on this movement [10].

In the group of Cu-based SMAs, only the sub group of Cu-Al-Ni can be classified as HTSMA. Van Humbeeck et al. [22] showed that despite using various thermo-mechanical treatments to attain stable TTs for reverse martensite transformation, due to the possibility of the precipitation of equilibrium α and γ phases the degradation of TTs still continues to occur. Another problem that plagues this alloy system is the high brittle behavior due to large grain size, the large anisotropic energy and the tendency of impurities to collect in the grain boundaries [23]. This problem has been attempted to be solved by using single crystals and addition of quaternary elements like B, Ti and Zr in addition to thermo-mechanical treatments to improve ductility via finer grain size [24].

Ni-Mn and Ni-Al based HTSMAs have also received much attention in the past decades because of the occurrence of martensitic transformation between a temperature 920K and 1020K. However the problem of brittleness prohibits the use of Ni-Mn in commercial applications. Yang et al. [15, 25] and Potapov et al. gave good reviews to Ni-Mn-X [26-30] alloys furthering the interest in the alloy system. The addition of ternary element was found to improve the ductility and SME of the Ni-Mn system by a small amount but still without obtaining full recovery. Ni-Al based β-phase alloys have a wide range of TTs, varying from 0K to 1170K. Kainuma et al. [31-32] showed the effect of the addition of ternary element on the TTs and found that Cu, Co and Ag were the only elements that seemed to increase the M_s temperature. Limited ductility in polycrystalline form of alloy inhibits the commercial realization, however attempts have been made utilizing techniques such as micro-alloying, melt spinning and powder alloying to improve the ductility. The major drawback however in the system is the formation of Ni_5Al_3 phase at a temperature of about 550K which is responsible for suppressing the TTs.

There are some other alloys (e.g. CoNiAl, NiMnGa, RuTa,) with high TTs but they either have unsatisfactory mechanical or shape memory properties (e.g., low material strength and ductility, unstable cyclic behavior (creep and fatigue), low recoverable strain) at high temperatures or they are very expensive. Volatility of Mn remains a problem in Ni-Mn-Ga [33-34] system and the oxidation of Fe in Ni-Fe-Ga along with brittleness in both the mentioned systems limit their capacity as commercial alloy.

The determination of the continuous solid solution at high temperature between PdTi and NiTi was done by Boriskina and Kenina [35] with a high temperature B2 phase. The martensite start temperature decreases with a uniform trend, beginning from binary PdTi to the minimum values for ternary compositions containing 5-10 at.% Pd when substituted for Ni [9]. This has led to addition of Pd to NiTi alloys to increase the TTs by substitution for Ni. Initially when Pd is added to NiTi to replace Ni, the temperature for M_s is found to decrease for upto 10 at.% addition of Pd with the minimum observed value for M_s of -26°C however with the increase of Pd to about 20at.%, a substantial increase to about 100°C for M_s is seen. In yet another examination by Shimuzu et al. [36], the effect of stoichiometry on the TTs for $Ti_{50-x}Pd_{30}Ni_{20+x}$ with x ranging from -0.6 to 1.5% has been presented. The result show a very steep fall in TTs for Ti deficient alloys and only a moderate variation in TTs in Ti rich side. This is in line with the trend followed by binary NiTi alloys. Poor shape memory properties were observed for alloys containing over 40 at.% Pd mainly due to low critical stress for slip in the alloy. One of the different approaches adopted to improve the shape memory properties of the alloy is the addition of small amounts of boron. However in different studies conducted by Yang et al. [37] and Shimizu et al., [36] no significant effect on TTs and shape memory properties was observed upon the addition of boron, but it increased the ultimate tensile strength to about two times and was also attributed for the improvement in the ductility. In yet another attempt to improve shape memory properties Shimizu et al. used the concept of precipitation hardening for desired output. They deviated away from stoichiometric ratio in order to induce precipitation of homogenous Ti_2Ni particles in $Ti_{50.6}Pd_{30}Ni_{19.4}$ alloy. An increase of about 10% in recovery rate for comparable $Ti_{50}Pd_{30}Ni_{20}$ was observed due

to the homogeneous precipitate distribution. The requirement of a higher percentage of Pd to have a significant increase in the TTs outweighs the benefit for use a commercial alloy when the cost of the expensive component is considered.

NiTi alloys can be alloyed with various elements like Pd, Cu, Pt, Zr, Hf, etc. to form various ternary and quaternary alloys. The transformation temperatures(TTs) are very strongly dependent on the composition in NiTi alloys [14, 38]. In Ni-rich intermetallic compounds, even a slight increase of the Ni content away from the stoichiometry leads to a sharp decrease in the TTs while the Ti rich side of the intermetallic compound is much less sensitive to the mentioned compositional variation primarily due to precipitation of Ti_2Ni particles which counteract the compositional variation of the matrix. Addition of ternary element within the range of less than 10% usually decreases the M_s or usually has very little effect. Substitution of Fe, or Co in place of Ni; or Mn, Cr, V when substituted for Ti decreases the TTs very significantly. Addition of more than 10% of Au, Hf, Pd, Pt, and Zr to NiTi increases the transformation temperature [14]. Addition of Cu and Fe to NiTi followed by low temperature heat treatment reduces the hysteresis to only a few degrees while addition of Nb has opposite effect and increases the hysteresis to about a 100°C [39].

NiTiAu system has higher TTs for the same concentration of Au for Pd in NiTiPd system but very less work has been done on the NiTiAu alloy. In two contrasting studies done by Eckelmeyer [40] and Donkersloot and Van Vucht [41] the effect of 2 at.% Au and 40-50 at.% Au respectively were shown. With an inability to show TWSME, a significant one way shape memory was shown qualitatively by bending and recovery of the bar made of the higher content of Au composition. However the currently available

studies are limited to the TTs and the structures of the phases and no research has been performed on the mechanical behavior.

NiTiPt has also not been researched thoroughly till date. With respect to the relative increase in TTs for addition of ternary elements, the Pt containing alloys have higher TTs as compared to any other other NiTi based systems. With substitution of Ni with Pt, in the range of towards 10 at.% the TTs decrease slightly but after this threshold an almost linear increase in M_s to a staggering 1040°C for 50at.% Pt. In the studies conducted by Lindquist and Wayman [9] , narrow hysteresis for all Pt alloys were recorded with an anomaly for 30 at.% Pt which had a hysteresis of about 80°C as compared to a general recording of less than 20°C. The extremely low ductility of the alloy prevented the measurement of recoverable stains in the above mentioned study. In another study as reported by Hosoda et at. [42] the ductility was found to generally decrease with an increase in Pt content. Even with extremely high TTs, just like other mentioned HTSMAs this alloy also suffers serious drawbacks due to the cost of expensive components and a very low ductility.

1.4 NiTiHf Alloys

HTSMAs suffer from either very high costs due to expensive elemental components or high degree of brittleness which prohibits them from use in commercial applications. To improve upon the brittleness, many techniques including drawing single crystals have been employed but such techniques add large amounts of capital to material processing leading to high costs and outweighing the benefits. NiTiHf based alloys are a competitive alternative [43] to the previously mentioned systems containing precious

elements or high capital involved processing techniques. NiTiHf alloys have been found to have higher TTs when compared to NiTi(Pd) or Au ternary alloy systems for an equivalent amount of the ternary element. The maximum amount of Hf that can be added as a ternary element to the alloy is limited to around 30% because there is no solid solution between NiTi and NiHf. Even though this sub-class of HTSMAs is still brittle, it possesses enough ductility to undergo most thermo-mechanical treatments [44-45].

Similar to the previously mentioned systems containing precious metals, in NiTiHf alloy the TTs don't increase significantly till about 10 at% Hf when replaced for Ni. With the Hf content of greater than 10%, the TTs increase linearly to approximately 525°C alloys when the Hf content is 30 at.% [45-46]. In key studies done by Angst et al. [45] and Besseghini et al. [46] it was found that when Hf content was fixed at 10 at.% and Ni was varied from 40 to 50at.% (with balance Ti), the TTs remained almost the same, but when the at.% of Ni was increased even slightly over 50 at.%, a steep fall in TTs was observed. As an example, martensite peak (M_p) temperature is below 0°C for $Ni_{50.2}Ti_{xx}Hf_{yy}$ (at.%). Alloys containing a more than 15 at.% Hf have been reported to have a monoclinic B19' structure for martensite phase similar to the one found in binary NiTi, while the alloys with a higher content of Hf transform to B19 orthorombhic martenistic phase and both structures transform to austentic B2 phase. The NiTiHf alloys with deviation from stoichiometry have been reported to encompass a possibility of the formation of a number of phases upon varying conditions of thermo-mechanical processing [47]. Those phases can have a range of effects on the transformation characteristics and stability of the alloy. However there are not many studies available about the qualitative analysis of the microstructure, evolution of microstructure and the

net result on the properties of NiTiHf alloy. In a study conducted by Zhu et al, [48] precipitation of second phase was observed due to thermal cycling at A_f+10°C and aging at 500°C in two NiTiHf alloys studied, and was attributed for the decrement in TTs. In another study related to aging, Meng and his colleagues [49] found that $(Ti,Hf)_2Ni$ second phase was precipitated when $Ni_{49}Ti_{36}Hf_{15}$ alloy was aged at 700°C. It was also noted that the size and volume fraction of the second phase are increased with an increase in aging time. The effects of the second phase presented in the study show a decrease of Ms temperature by about 70°C. Olier et al. [50] showed that presence of a cubic $(Ti,Hf)_4Ni_2O_x$ phase in $Ni_{50}Ti_{38}Hf_{12}$ alloy, but the effect of this second phase was not studied in detail. Contrasting results were put forward in a study by Han et al., [51] in which precipitates were identified as face centered orthorhombic structure after aging for 150 hours at 600°C in $Ni_{48.5}Ti_{36.5}Hf_{15}$ alloy but these precipitates were not observed in the homogenized samples. In another related study on the same alloy, the structure and substructure of martensite has been reported in detail. The structure for the martensite phase was identified as monoclinic B19' type with $P2_1$/m space group with the lattice parameters as a=0.293nm, b=0.411nm, c=0.473nm and β=100.4°. The precipitate had the approximate composition of $(Ti_{0.6}Hf_{0.4})Ni$ and was identified as face centered orthorhombic with lattice parameters of a=1.287nm, b=0.874nm and c=2.622nm and space group F2/d 2/d 2/d [51].

Olier et al. [50] reported about 80% recovery for $Ni_{50}Ti_{38}Hf_{12}$ samples deformed at room temperature to a strain 2.5%. A large amount of stress, 535MPa, is required to begin the reorientation of martensite which can be considered approximately the same as the critical stress for inducing dislocations, was attributed to the poor SMA. But in the

same alloy, when the samples were deformed 4% in the higher temperature austenite phase, a full recovery was observed. In another investigation conducted by Firstov et al., [52] recoverable stains of about 3% were reported for $Ni_{49.42}Ti_{39.95}Hf_{14.63}$ based ternary alloy, and suggested that another 0.8% recoverable strain could be achieved if the alloy could be strengthened to overcome plastic strains induced by slip. In another study for a similar composition of $Ni_{49}Ti_{36}Hf_{15}$ tested by Meng et al. [49, 53], 3% fully recoverable strains in bending was observed when the sample was deformed at room temperature and 92% recovery of a strain of 4.5% when deformed at below 184C between M_s and A_s. Meng et al. studied the tensile behavior of $Ni_{49}Ti_{36}Hf_{15}$ at room temperature and contrary to NiTi [54] no stress plateau was observed. As mentioned earlier, the martensite reorientation was not observed at lower stress levels and at higher stress levels reorientation along with continuous yielding and work hardening was noted. In another study by Meng et al. [55] tensile behavior at temperatures higher than A_f were examined. No super-elastic behavior was observed in this study along with no stress plateau during the loading in the austenite phase. The stress induced martensite did not transform back to austenite even after the removal of stress when the temperature was above A_f. The reason behind this behavior can be attributed to the occurrence of dislocation slip simultaneously with stress induced martensite. As a result, work hardening and lower mobility of martensite variants is observed, deteriorating the back transformation due to the occurrence of plastic deformation.

One of the concerns regarding ternary HTSMAs containing Hf is the possibility of relatively large hysteresis of order of about 60-80°C which makes it less attractive for application in active control. Some studies conducted reported the hysteresis to be 40-

50°C for similar compositions. Despite the ordinary SME and problems like lower ductility and large hysteresis associated with the NiTiHf alloy system, when compared with other HTSMAs, NiTiHf stands out as one of the most competitive candidate for the use as commercial HTSMAs due its lower cost and reasonable ductility. Although very limited work has been done in order to improve the shape memory properties of NiTiHf system in order to optimize the desired characteristics and get optimal shape memory characteristics. The three of the most effective methods to improve the shape memory characteristics are (1) thermo-mechanical treatment such as cold rolling and/or annealing, (2) addition of quaternary element, and (3) aging to induce precipitate formation based on the findings presented by Otsuka and Ren for strengthening NiTi based HTSMAs. Meng et al. [56] has explored the option of addition of quaternary element in an investigation regarding addition of 3-5% of Cu to $Ni_{49-x}Cu_xTi_{36}Hf_{15}$ aiming to reduce the hysteresis. Contrary to the finding of Liang et al. he found that instead of a reduction in hysteresis a slight increase was observed. He has also aimed to increase the thermal stability, but no effect was observed. No mechanical testing was done to characterize the mechanical properties. In another study Meng et al. [49, 57] studied the evolution of precipitates in $Ni_{50.6}Ti_{29.4}Hf_{20}$ and $Ni_{50.8}Ti_{29.2}Hf_{20}$ alloys. It was reported that $(Ti+Hf)_3Ni_4$ precipitates were formed after aging. These precipitates were attributed for a rise in TTs and the precipitates themselves were found to grow from spherical shape to lenticular shape and eventually coarsen when the alloy was aged at 550°C for long times. Apart from these finding no effect on the mechanical part of SME was studied.

Chapter Two

Mechanical properties

2.1 Material deformation

2.1.1 Theory of Dislocations

In order to understand the basic concepts behind the effects of various thermo-mechanical treatments in SMAs, a basic understanding of the various phenomenon by which material deforms is necessary. The two kinds of deformation that a material may experience can be classified as elastic and plastic deformations. Plastic deformation is a permanent type of strain and strength and hardness are the characteristic properties of the material by virtue of which the material resists deformation. When looked upon at microscopic scale, the plastic deformation corresponds to the movement of atoms due to application of stress. During this process the interatomic bonds are broken and then reformed. Two processes by which the material deforms are namely, the dislocation motion or slip and twinning. The process by which dislocations move to produce plastic deformation is called slip and the plane along which the dislocation line moves is called the slip plane. The dislocations move with a different degree of freedom in different crystallographic planes. In most cases there exists a plane, along whose direction the dislocations occur. This preferred plane is termed as the slip plane. Even when a pure tensile or compressive stress is applied on a material, some shear components occur except in the directions parallel and perpendicular to the direction of applied stress. These components of stress are called the resolved shear stresses [58]. The magnitude of these shear stresses depend on the applied stress and also on the orientation of the slip plane and direction within this plane. The resolved shear stress (τ_R) can be written as

$$\tau_R = \sigma \cos \phi \cos \lambda$$

where is the applied stress, ϕ is the angle between the normal and slip plane and λ is the angle between slip and stress direction. Usually one of the slip systems is most favorably oriented and has the largest resolved shear stress.

$$\tau_R(\text{max}) = \sigma (\cos \phi \cos \lambda)_{\text{max}}$$

When the $\tau_R(\text{max})$ reaches a critical value called as critical resolved shear stress (τ_{crss}) slip begins to occur, this critical stress represents the minimum shear stress required to initiate slip. This is a characteristic property of individual material and it determines the yield strength of the material.

2.1.2 Theory of twinning

Another phenomenon by which the plastic deformation can occur in some metals is called as twinning. In this phenomenon shear force produces atomic displacement in a way such that atoms located on one side of a plane called as twin boundary are located in a mirror image position of the atoms on the other side. Twinning mostly occurs in metals with crystal structure of BCC and HCP. Other physical conditions that promote twinning are low temperatures and high loading rates, though the net plastic deformation produced by twinning is usually less than deformation caused by slip. More than plastic deformations, twinning plays an important role in crystallographic reorientations.

2.2 Metal strengthening Techniques

Since in a majority of cases the plastic deformations depend on the ease of the mobility of dislocations, any restriction or hindrance in the dislocation motion tends to

increase the strength of the material alongwith hardness. If the mobility of the dislocations is reduced, larger mechanical forces are required to initiate plastic deformation and as a result the mechanical strength is increased. Most of the metal strengthening techniques are based on this principle and often used by materials engineers to design alloys to meet the required specifications.

Some of the most common methods used to increase the metal strength are the following:

1. Grain size reduction
2. Precipitate hardening
3. Solid solution hardening
4. Work hardening

2.2.1 Grain Size Reduction

The mechanical properties depend on the average grain diameter, and it can be controlled to enhance the strength. Usually the adjacent grains have different crystallographic orientations along the common grain boundary and during plastic deformation the slip has to pass across the grain boundary. An excessive degree of mis-match or disorder among the two adjacent grains makes it more difficult for the slip to pass through the boundary since the slip has to change direction while passing through. This inhibits the motion of slip and hence adds to the material hardness and strength. Another effect that the atomic disorder at the grain boundary region can cause is the discontinuity of slip planes from one grain to another and hence inhibit slip. The materials having smaller grain size have higher grain boundary area and hence are stronger due to higher obstruction to dislocation motion. The above effect can be

summarized using the Hall-Petch equation which states the variation of yield strength (σ_y) with the average grain size.

$$\sigma_y = \sigma_0 + k_y d^{-\frac{1}{2}}$$

where d is the average grain diameter and σ_0 and k_y are material constants.

2.2.2 Solid Solution Strengthening

Solid solution strengthening is a technique in which an impurity atom is added to the pure metal to increase over all mechanical strength of the material. Generally, it is seen that the pure metals are softer than the alloys made of the same parent metal. The reason behind this phenomenon is that when an impurity is added to metal, the impurity imposes a lattice strain on the surrounding host atoms. These lattice strains interact with the dislocations and as a result the dislocation movement is inhibited. The solid solution strength can be represented as

$$\Delta\sigma_i = k_i c_i^{1/2}$$

where k_i is the strengthening constant for the solute i and the c_i is the concentration in at.% of the solute i.

2.2.3 Precipitate hardening

The most important technique for increasing material strength in relation to the present study is precipitate hardening. Forming finely dispersed precipitates in metallic alloys are a very useful technique to increase the overall strength of the metallic compound. The strengthening ability of the precipitates depends on the size, composition

and the spacing between the adjacent precipitates. The coherent precipitates increase the strength of the material by dislocation shearing and as these precipitates grow in size to become incoherent, the initial increment in the strength of the material fades away because of the Orowan dislocation looping. In case of dislocation shearing the yield strength increases because of the three mechanisms, coherency strengthening, order strengthening and modulus mismatch.

As mentioned earlier the precipitates act as an obstacle in the path of dislocation which results in the increase in the hardness or the strength of the material. The dislocation must cut through the precipitate in its path or must go around it. Both phenomena inhibit the propagation of the dislocation motion and as a result the material strength increases.

When the precipitates begin to form in the alloy, they are small in size and are dispersed finely within the alloy. In this stage the precipitates are said to be coherent with the matrix and the dislocation has to shear across the precipitate to propagate. This shearing mechanism requires additional stresses and hence inhibits the slip motion. When the dislocation encounters an obstacle in the form of a precipitate it begins to bow due to the applied stresses and continues to do so until the precipitate can no longer withstand the increasing stress. The dislocation finally bows out free until it encounters another precipitate. A key point in the phenomenon is when the dislocation bows more in order to break free, the length of the dislocation increases which further results in an increase in the probability of encountering another obstacle. The Orowan looping mechanism adds another possibility to this path for bigger precipitates which are at a larger distance from each other due to consolidation of smaller precipitates into larger precipitates and hence

decreasing the number of precipitates and increasing the distance amongst themselves. The Orowan looping mechanism comes into consideration when the distance has increased to a critical value by the above mentioned process that the dislocation segments can bend and pass through the adjacent particles. As the dislocation passes through, it leaves behind a dislocation ring around the particle while stress fields further inhibit the motion to the next passing dislocation. The change in mechanical strength with the increment in volume fraction of precipitates is mathematically represented by the following equation

$$\Delta\tau = \alpha_\varepsilon G \varepsilon^{3/2} \left(\frac{fr}{b}\right)^{\frac{1}{2}}$$

where b is the magnitude of burger vectors, f if the fraction of precipitates and ε is the constrained lattice mismatch and α_ε is material constant. The change in strength due to Orowan looping is represented by

$$\Delta\tau = K \frac{1}{(L-2r)} \frac{Gb}{2\pi\sqrt{1-v}} \ln\left(\frac{2r}{r_0}\right)$$

where v is the matrix Poisson's ratio, L is the inter-precipitate distance, r is the mean particle radius, G is the matrix shear modulus, r_0 is the dislocation core radius and b is the Burgers vector of the matrix.

In order to utilize the principle of precipitate hardening as described earlier in the section, Ni-rich alloys were chosen for the study based on the findings in the literature which point to formation of Ni_4Ti_3 precipitates in the mentioned class of alloys. Zheng et al.[59] in one of his studies has shown the mechanism if the growth of Ni_4Ti_3

precipitate's size with increasing aging time and temperature in Ti-50.9at.% Ni alloy. As true for all Ni-rich NiTi alloys, the Ni_4Ti_3 type precipitate is formed when aged.

As shown in Figure 2.1, small Ni_4Ti_3 type precipitate begin to form along the grain boundaries at lower aging temperature and time. With further increment the segregated precipitates are observed to grow in size and spread homogeneously throughout the matrix. Further increment in aging time or temperature leads further growth of precipitates in size and it leads to mix of coherent and larger incoherent precipitates.
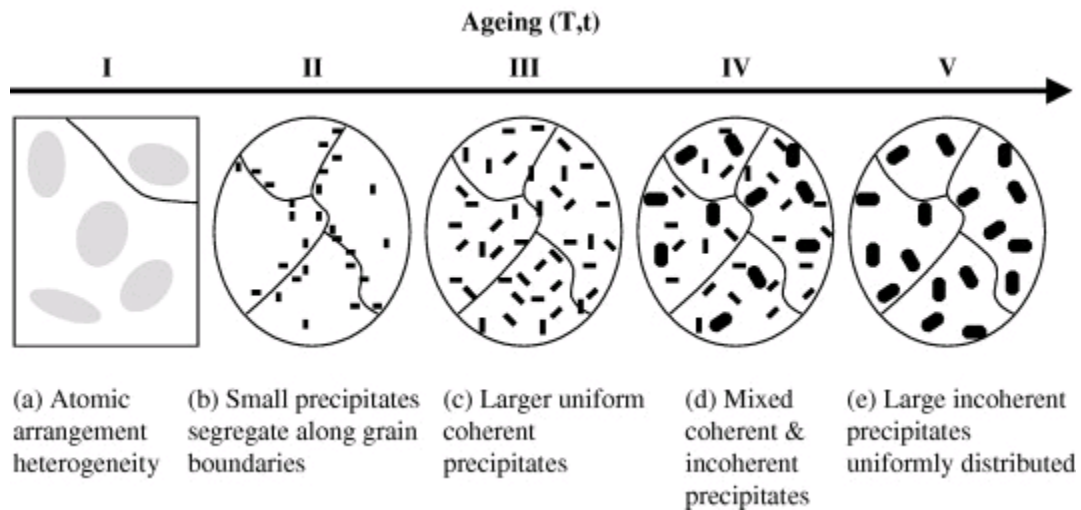
Figure2.1: Schematic depicting the evolution of precipitates as a function of the aging time and temperature [59]

With increase in aging time and temperature from even the finely dispersed coherent precipitates grow finally to form large incoherent precipitates. Since the precipitates formed are rich in Ni, the precipitation of these particles depletes the Ni in the matrix and hence makes the matrix more Ti-rich as compared to the original matrix with no precipitates as depicted in Figure 2.2. This not only strengthens the material but also increase the TTs of the alloys as mentioned earlier due to decrease in the Ni-content of the matrix.
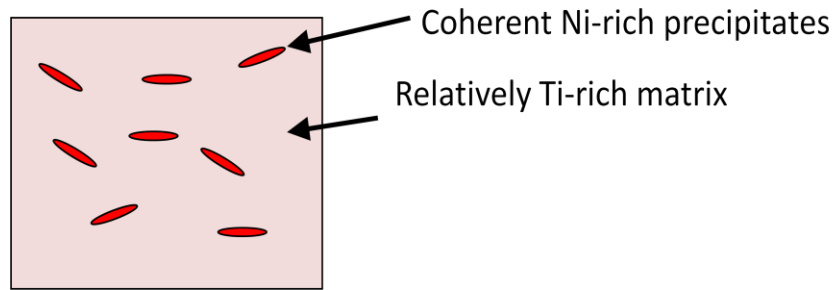
Figure2.2: Schematic depicting the depletion of Ni-content from the matrix with the formation of precipitates

Chapter Three

Experimental Setup

3.1 Sample Preparation

Alloys studied in the present work were synthesized by induction melting into 1" diameter rods which were then homogenized at 1050°C for 72 hours. The homogenized rods were extruded at 900°C with a reduction of 7:1 in diameter (hereafter referred to as as-extruded condition). These rods were then cut into small slices varying from 2~4mm in width using a variable speed MTI-4 cut-off saw. Resin bonded high concentration diamond blades, composed of an inner metal core and an outer rim were used to cut-off the wafers from the as-extruded rods for further processing. The rim consists of resin mixed with abrasive, cured under high temperature and pressure to bond the matrix together. The resin bonding creates less heat, provides better surface finish and is well suited for cutting hard, delicate or brittle materials.

(a)   (b)   (c)

Figure 3.1. Figure depicting the cast material(a) prior to extrusion on extreme left followed by extruded rod(b) in middle and the MTI saw(c) used to cut samples on extreme right.

3.2 Heat Treatments

Lindberg/Blue M BF514841 Box furnace was used to carry out all heat treatments on the alloys. Equipped with a UT150 controller, the furnace could be programmed to a single set-point while using desired ramp rate. With a chamber size of 38.1x38.1x38.1cm, the maximum temperature for the furnace was 1200°C. The BF514841 furnace came with factory installed air/atmosphere port with a capability of running most gases such as nitrogen, argon and helium however the furnace was not designed to be gas-tight atmosphere. The furnace was also equipped with a vent at the top to help remove contaminants from the furnace chamber. The furnace was set to the desired temperature and allowed to reach the set temperature before the sample was put in the furnace. After putting the sample in the furnace, the time was noted once the temperature reached the set temperature again. The heat treatments were followed by quenching the sample into water at room temperature.

Figure 3.2: Lindberg/BlueM box furnace (BF514841)

3.3 Differential Scanning Calorimetry (DSC)

The Perkin-Elmer DSC Pyris 1, differential scanning calorimeter was used to accurately measure the TTs. Typical temperature range is from -100°C to 400°C and the heating and cooling rate used to run the experiments was fixed at 10°C/minute. The temperature scale was calibrated using a two-point calibration, measuring the onset temperatures for melting points of high purity indium and zinc standards provided by Perkin Elmer. In addition to this the furnace was calibrated using the furnace calibration feature in Pyris software. The minimum and maximum setpoint is entered in the sub

menu for furnace calibration and the software calculates seven other points between the desired range, as specified by the user. The thermocouple temperature is matched to the programmed furnace temperature when this calibration is complete. The enthalpy scale was calibrated using the observed delta-H from an accurately known amount of indium.

Samples were encapsulated in disposable aluminum pans, typically using 20 – 40 milligrams of sample. There are two styles of pan available, one used for solids, and a hermetically sealed version for liquids. Aluminum pans Perkin Elmer part number 0219-0041 with a temperature range of -170°C to 600°C and volume capacity of 40μl were used. The sample pans ensured safety against material that can leak out into the DSC can contaminate and cause permanent damage to the DSC's furnace, particularly if there are metals present in the sample that could alloy with the platinum furnace holders.

There is a sample side and a reference side in the furnace. A blank pan was inserted into the reference side. For all samples it was noted that the sample had good contact with the bottom of the pan. This was done to ensure good contact with the sensor, especially when using large samples since the thermal gradient effects can increase. Large samples produce larger transition, hence are preferred for study even the small changes, but thermal gradient should be taken into account while using them.

Figure 3.4 depicts the graphical interpretation of the transformation temperatures determined from DSC plot.
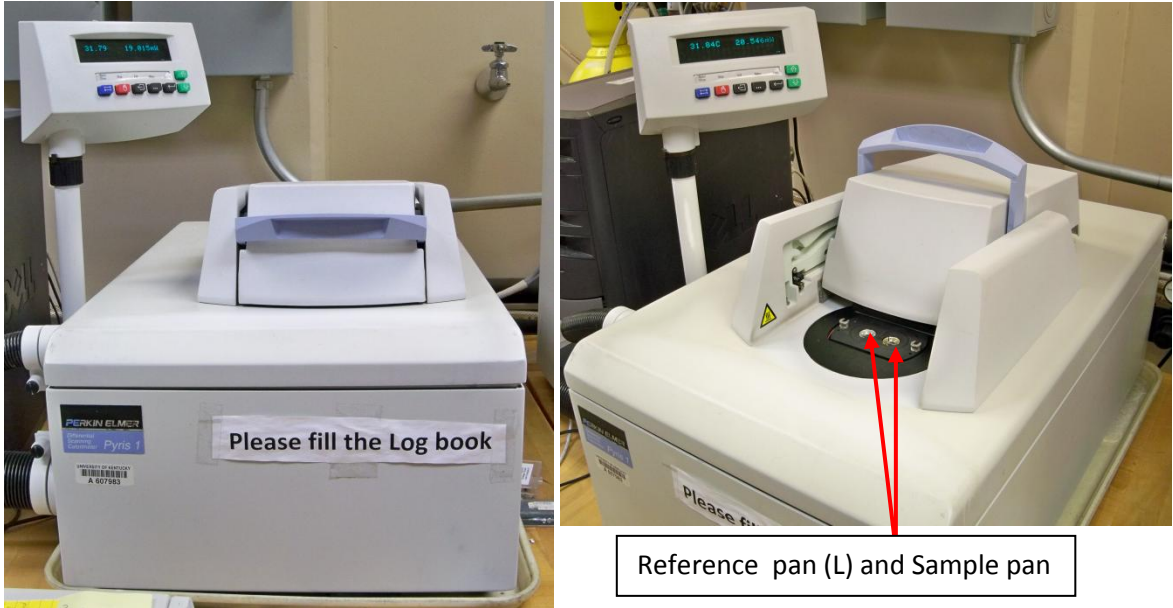
Figure 3.3: Pyris1 DSC used for finding the TTS
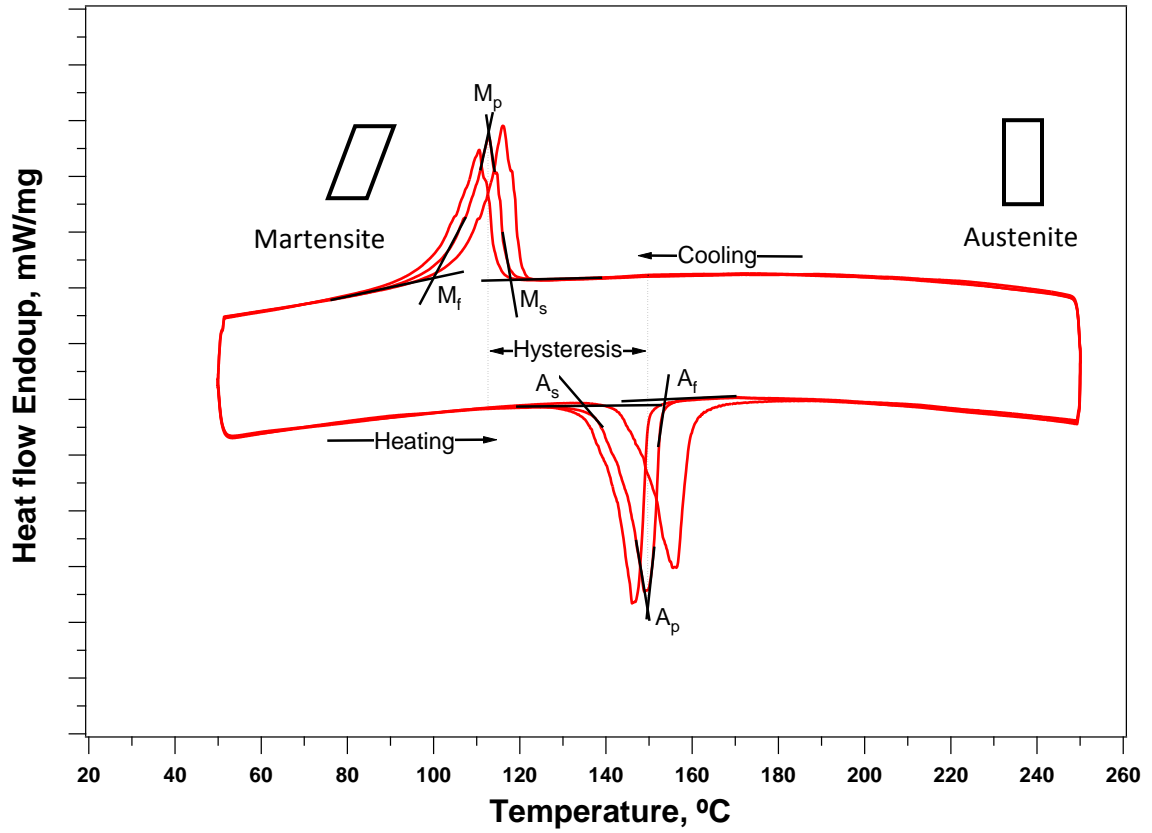
Figure 3.4: Typical plot from DSC

3.4 Mechanical Testing

Thermo-mechanical characterization was achieved by compression experiments on 4mm x 4mm x 8mm samples (cut by EDM) performed by a Landmark MTS hydraulic testing platform with 100 kN load cell and a custom built heating/cooling assembly. MTS High temperature extensometer is used to determine the strain between the compression plates thermal expansion and elastic deformation of compression plates were taken into account. The heating/cooling of the samples was achieved by conduction through the compression plates with a rate of 10°C/min. The plates were heated using heating bands and cooled by liquid nitrogen flowing through the tubing wrapped around the grips. An Omega CN8200 series temperature controller ensured stable heating-cooling rates with K type thermocouples attached to both the specimen and grips. A cryogenic grade, on/off solenoid valve commanded by the temperature controller was used to control the flow of liquid nitrogen.
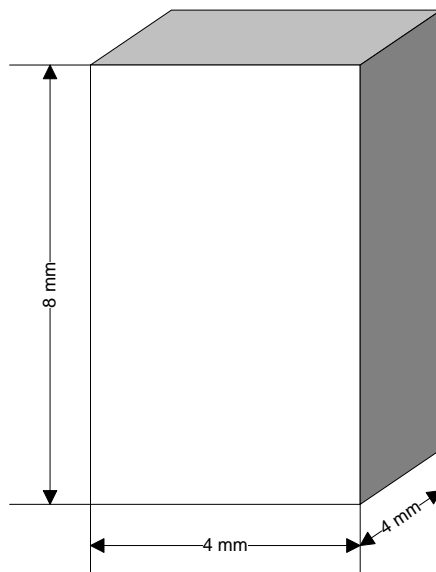
Figure 3.5: Schematic of compression mechanical specimen

The compression sample was polished mechanically with a 600 grit paper to remove the residue left after being cut by the EDM. Once the sample was ready, a K-type thermocouple was attached to the sample by fastening it with fine gauge copper wire, followed by placing the sample between the test setup in proper position. Typical loading rates used for isobaric cycling were 100N/sec for both loading and unloading, while 8×10^{-4} mm/sec was used for loading and 100N/sec was used for unloading in the isothermal mechanical cycling tests. The high temperature extensometer model number 632.54F-14 was used for all strain calculations. The gage length for the extensometer was 12mm, so required mathematical calculations were done to modify the data for the typical sample length of 8mm was used in the whole study for carrying out mechanical tests.

Figure 3.6 depicts the critical points for transformation determined by using graphical method. A with sub subscript "s" denoted the austenite start and with "f" denoted the finish temperatures for the transformation. M with the same subscripts depicts the transformations for martensite.

Figure3.5(a): MTS Landmark system(370.10)

Liquid Nitrogen Dewar

Force Sensor

Temperature Controller box

Heating Bands

Force Actuator
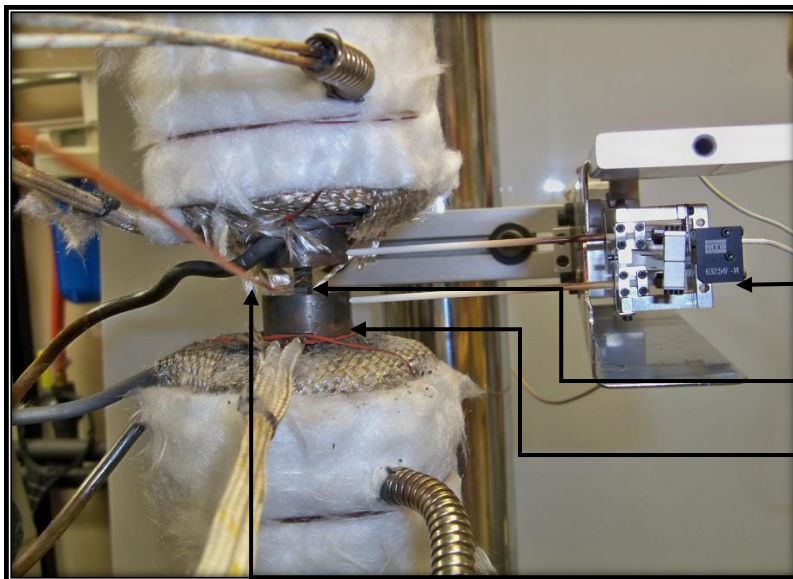
Figure 3.5(c): Picture depicting the sample ready to undergo mechanical test

Extensometer

Sample

Grips (H13)

Thermo-couple for sample temperature

Figure3.5(b): Picture depicting the sample ready to undergo mechanical test before the insulation is put on.
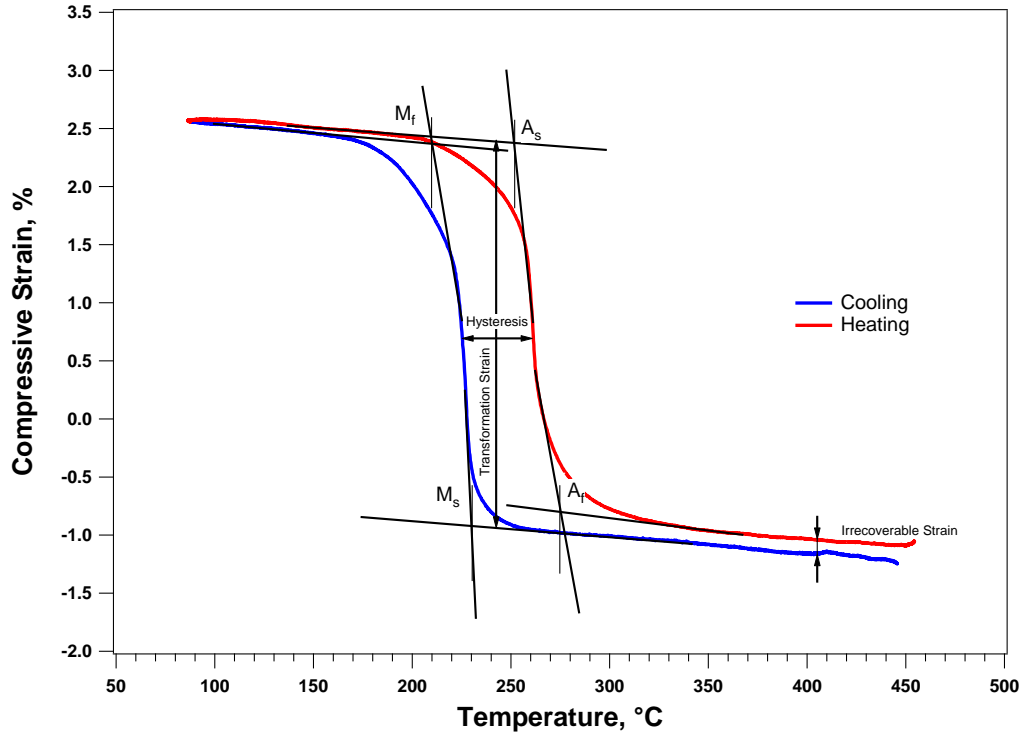
Figure 3.6: Typical plot from isobaric mechanical cycling under compression
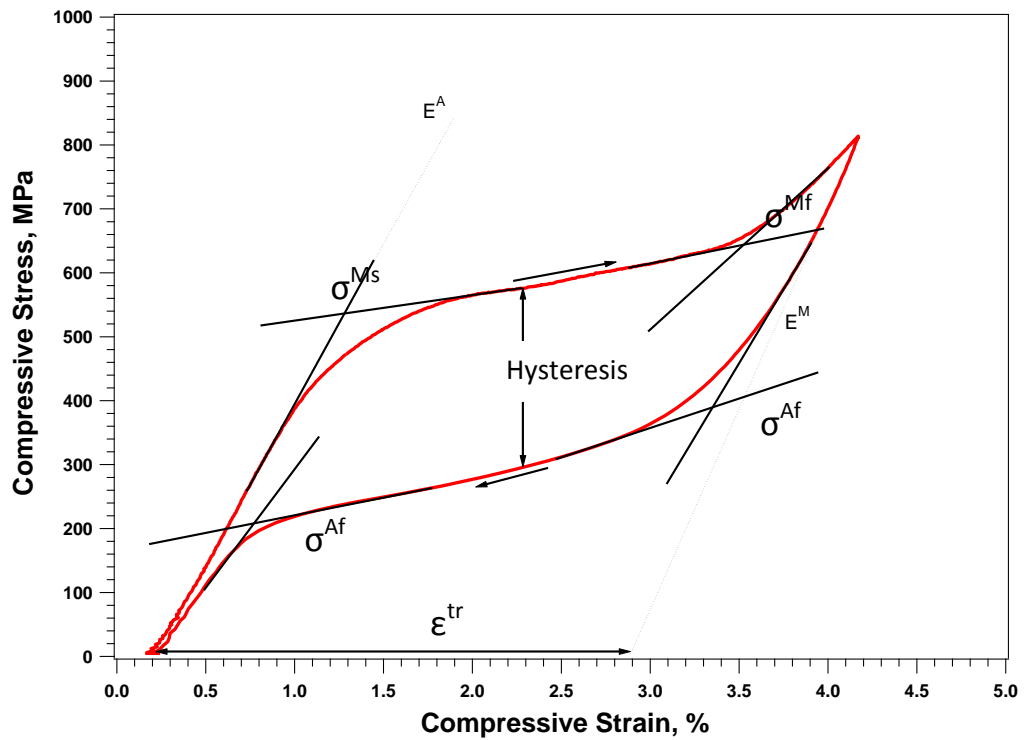
Figure 3.7: Typical plot from isothermal mechanical cycling under compression

3.5 XRD analysis

X-ray diffraction measurements to reveal the lattice parameters at different temperatures were carried out by a Bruker-AXS D8 Discover diffractometer. Powdercell and RefCell are used to determine the lattice parameters. The mechanically polished samples were scanned at both room temperature and elevated temperatures to capture the phase transformation. The stage for measurements at elevated temperatures was designed and manufactured in-house. Allen Bradley 900-TC8 temperature controller was used for maintaining desired temperatures.
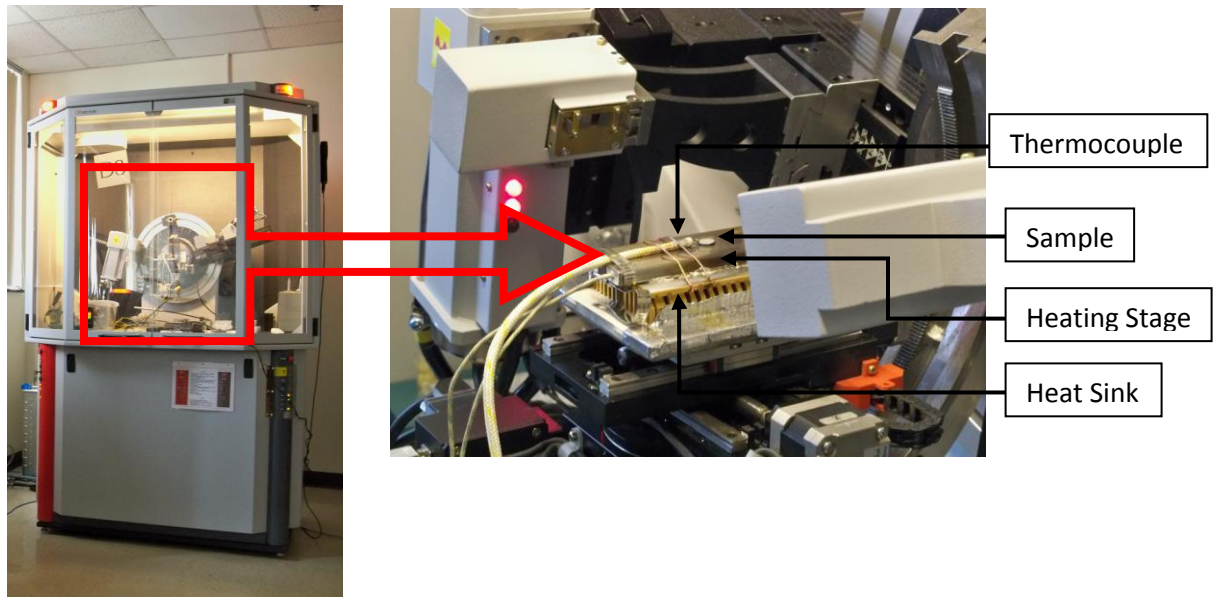
Figure 3.8: The picture showing the Bruker-AXS D8 diffractrometer and a close-up of

the sample on top of the custom built heating stage.

3.6 Optical and TEM Imaging

TEM samples were prepared by grounding the bulk material into 100 micron thick foils which in turn were cut into 3 mm diameter disks. Electron transparency was obtained by twin-jet electropolishing of the disks with an electrolyte consisting of 600 ml Methanol, 340 ml Butanol and 60 ml Perchloric acid at 30 V and -25°C.

3.7 Hardness Testing
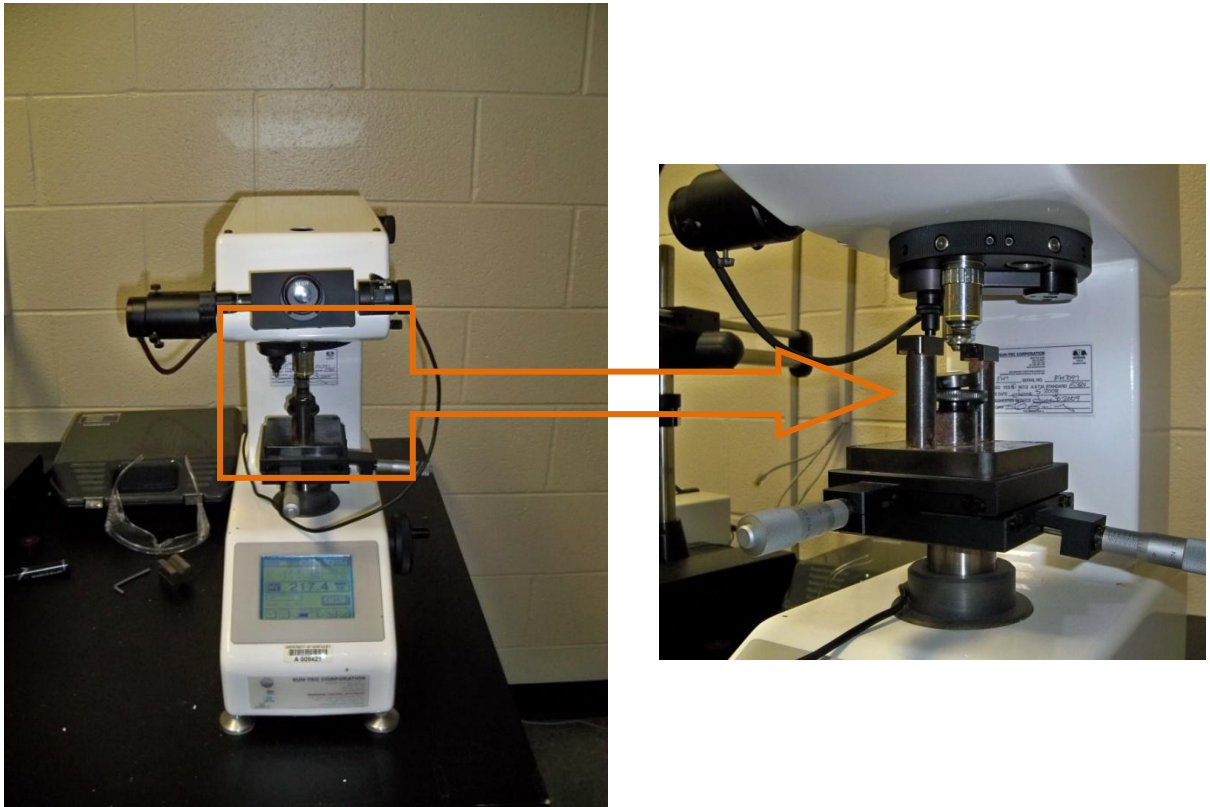
Figure 3.9.Microhardness testing setup used for measurements at room temperature

Harness results were obtained using Sun-tec model FM-7 microhardness testing setup. Samples mounted in epoxy were polished to mirror finish prior to measurements. Pyramidal indenter of 136° tip was used with a 100gf force and 15 seconds dwell time.

Ten reading were taken for each sample, the highest and the lowest reading were omitted

and the average of the remaining 8 readings were reported.

Chapter Four

Experimental Results: $Ni_{50.3}Ti_{29.7}Hf_{20}$

In this chapter the results on $Ni_{50.3}Ti_{29.7}Hf_{20}$ alloy will be presented and discussed. The chapter begins with the calorimetric analysis followed by the results from hardness testing for the samples of $Ni_{50.3}Ti_{29.7}Hf_{20}$ aged under various conditions. These results are followed by the XRD characterization and TEM micrographs. Mechanical characterization is discussed in the end along with comparison plots

4.1 Calorimetric Analysis

The variation in the TTs with aging temperature and time for $Ni_{50.3}Ti_{29.7}Hf_{20}$ alloy is discussed first. The $Ni_{50.3}Ti_{29.7}Hf_{20}$ was aged for 5 minutes to 48 hours and temperature ranging from 300°C to 900°C. DSC samples were then extracted from the aged specimen and run in the DSC to determine the change in TTs temperatures.

Figure 4.1 depicts the heat-flow vs temperature (DSC) curves for the $Ni_{50.3}Ti_{29.7}Hf_{20}$ alloy aged for 1 hour at temperatures ranging from 300°C to 900°C. All DSC samples were run for 3 cycles to determine cyclic stability, please note that the alloy was extruded at 900°C the first cycle in the DSC usually results in so called "First cycle effect" due to presence of dislocations. Hence the first cycle cannot be used without a sense of doubt for characterization, three cycles were run in the experiments to check for stability of the transformation. The DSC plot for as-extruded sample has been added to top of the plots for a comparison in change in behavior. The aging temperatures are indicated in the graph.
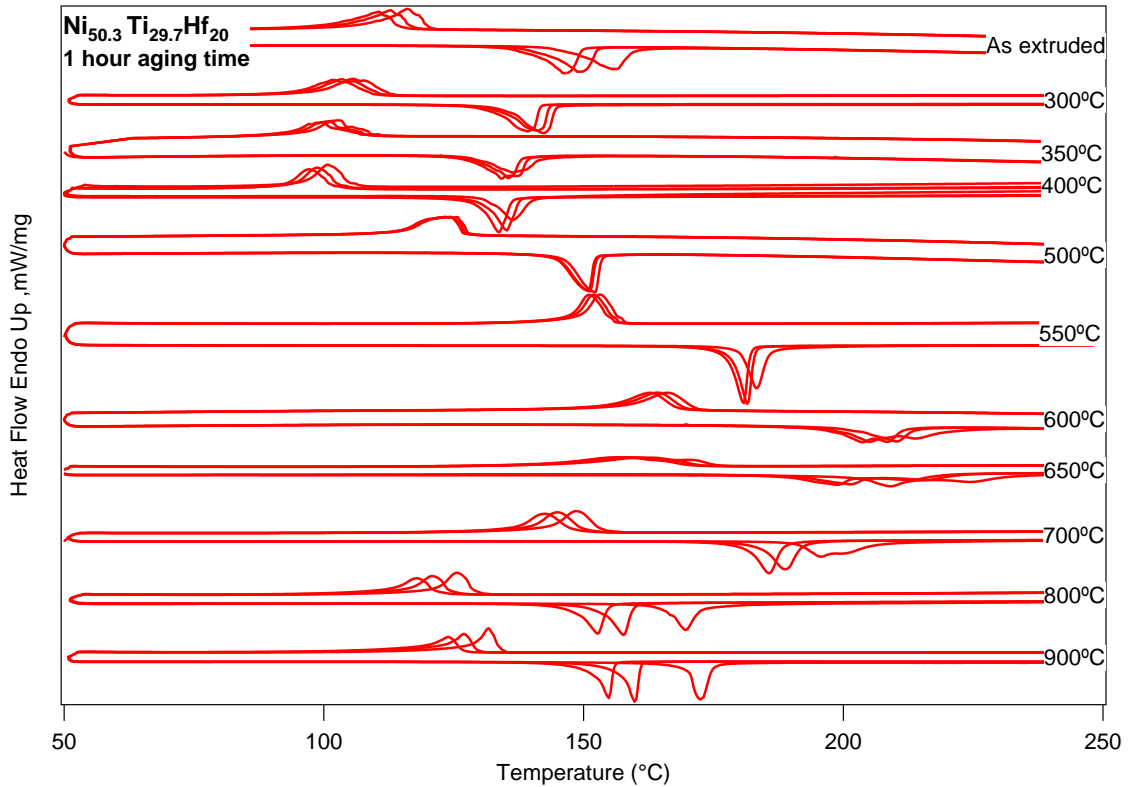
Figure 4.1: DSC curve for $Ni_{50.3}Ti_{29.7}Hf_{20,}$ aged for 1 hour for various temperatures

Figure 4.1 shows an initial decrease in the TTs when the alloy is aged for 1 hour from 300 to 400°C. After the initial drop the TTs become higher than the as-extruded condition for aging at 500°C. Even though the TTs are only slightly higher as compared to as-extruded condition for aging at 500°C, the peaks are sharper and stable. A substantial increase in the TTs is observed for the sample aged at 550°C with very stable sharp peaks. The TTs are observed to increase further with increasing the aging temperature to 600°C and 650°C. The heat flow peaks are determined to become wider and a decrease of about 5°C is recorded for both second and third cycle. The TTs were observed to start decreasing with increasing the aging temperature above 650°C to 700°C. The TTs then fell back to similar to as-extruded conditions for both aging temperatures of 800°C and 900°C.
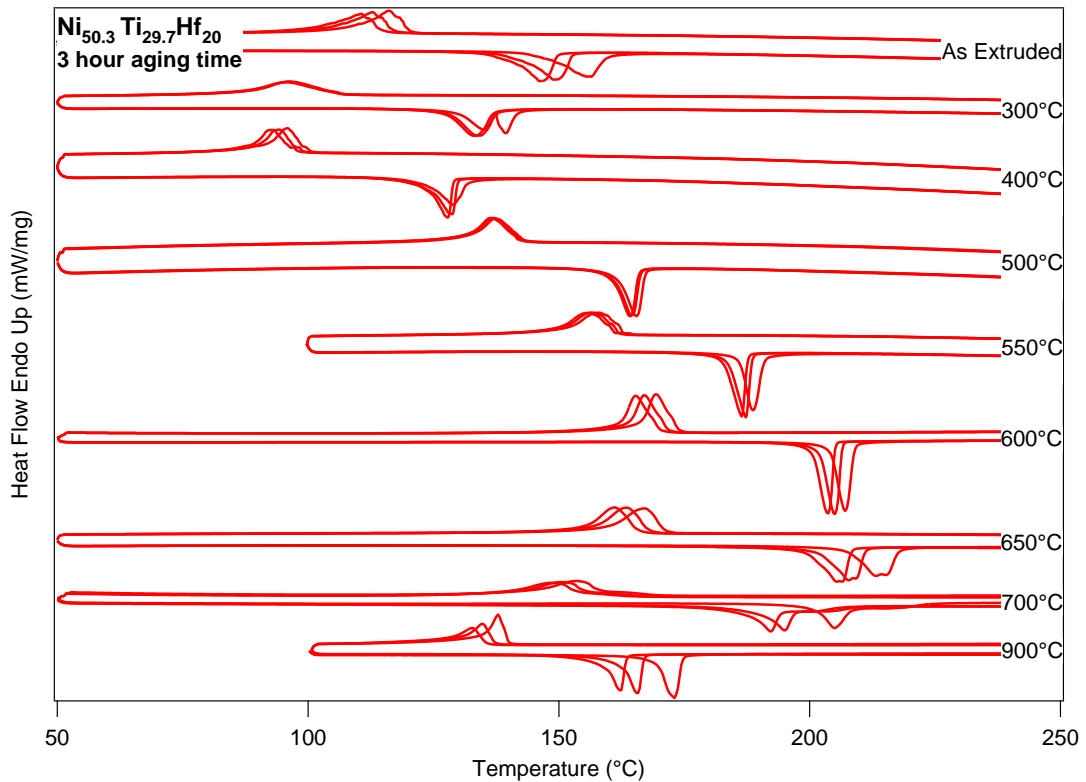
Figure 4.2: DSC curve for $Ni_{50.3}Ti_{29.7}Hf_{20,}$ aged for 3 hours for various temperatures

Figure 4.2 represents the DSC curves for the $Ni_{50.3}Ti_{29.7}Hf_{20}$ alloy aged at temperatures ranging from a minimum of 300°C to a maximum value of 900°C for 3 hours. Aging for 3 hours at 350°C and 800°C is not shown in the figure since no observable difference from their adjacent curves in the DSC plot. As similar to the variation in TTs with aging in 1 hour, the TTs fall below the TTs for as-extruded condition a for aging temperatures of both 300°C and 400°C. A notable difference in comparison behavior for same aging temperature but the aging time of 1hour, it is seen here that the second and third cycle are almost identical evidencing an increased stability for aging for 3 hours. For aging at 500°C an increase in the TTs along with an increased cyclic stability is observed. The TTs increase fractionally but the stability is very impressive, so much that the second and third cycle cannot be visibly distinguished. A significant increment in the TTs is observed when the aging temperature is increased

44

from 500°C to 550°C. The peaks for both the forward and reverse transformation are sharp indicating a strong and homogeneous matrix. The second and third cycles are also seen to be almost identical and hence stability is also maintained while increasing the TTs when the aging temperature is increased from 500°C to 550°C. The TTs are observed to increase about 25°C for an increase in aging temperature from 550°C to 600°C. Unlike the response at 500°C to 550°C, aging at 600°C produces a inferior cyclic stability where the TTs decrease by only a couple of degree for each cycle from first till last. The transformation peaks are still very sharp. The TTs did not change significantly for increasing the aging temperature to 650°C from 600°C, except for the first cycle which is slightly higher than the first cycle at aging at 600°C. The peaks are however observed to be broader with a characteristic double tipped forward transformation peak. The cyclic stability is further deteriorated without a substantial increase in TTs. When aged for 3 hours at 700°C the TTs begin to drop sharply especially after the first cycle. The TTs for the second cycle are sizably lower than the TTs for first cycle and they further decrease with the third cycle of 14°C. Aging at 900°C for 1 hour is resulted in a similar behavior as for aging for 3 hours. The TTs fall to slightly higher than the TTs for as-extruded condition but the cyclic stability deteriorated even further.
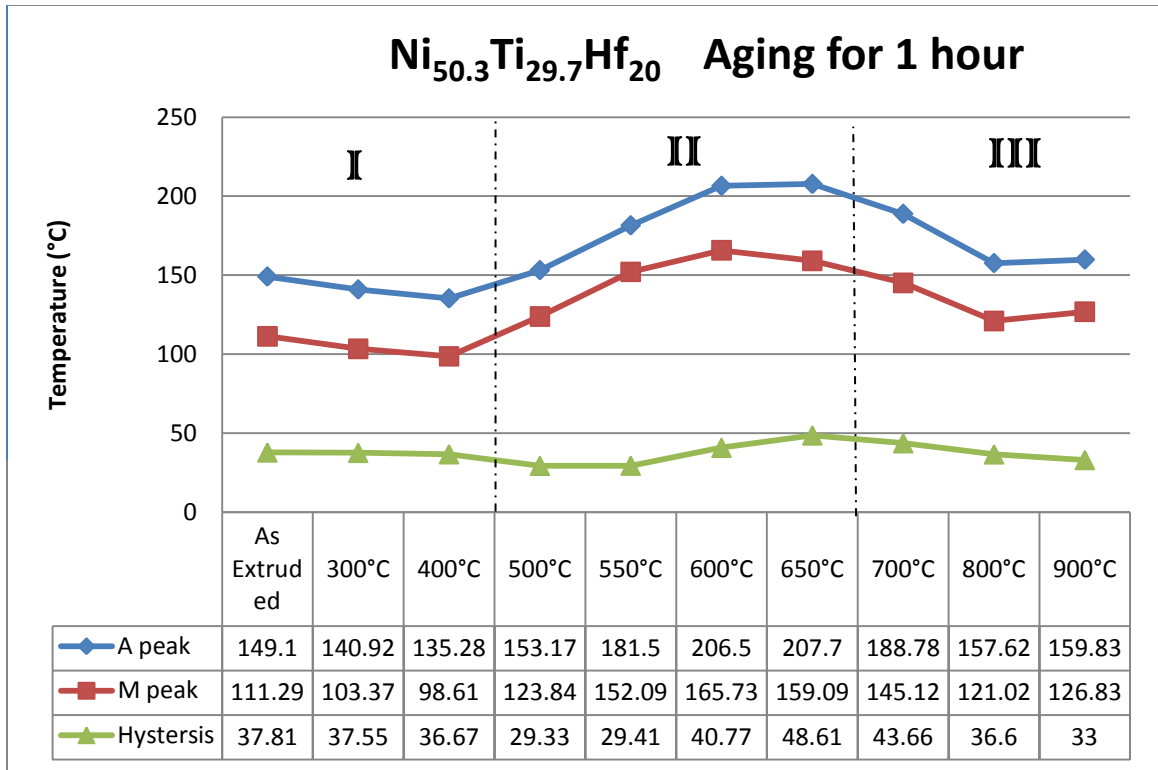
Figure 4.3: Comparison plot for peak values for the second cycle of specimen aged for 1 hour

The Figure 4.3 represents the A_p and M_p values along with peak hysteresis (A_p-M_p) for the second cycle of the samples run in the DSC aged for 1 hour at the respective temperatures as shown in the table below the curve. For the 1 hour aging time there was an initial decrease in the TTs for both forward and back martenistic transformations when the aging temperature is below 500°C. This initial dip in the TTs can be attributed to stress relief due to annealing at low temperatures along with the possibility of the formation of small volume fraction of particles in the material. The samples were extruded at 900°C with a reduction ratio of 7:1 before being aged at different conditions. The extrusion temperature was selected to be high to annihilate the dislocation formation during extrusion. But as it will be shown later by TEM results that dislocations are present in the material. The TTs start increasing as the aging temperature is increased

beyond 400°C into zone II. At the aging temperature of 500°C, the SMA has M_s much higher than 100°C which qualifies it well into the category of HTSMA and it is the lowest aging temperature found in the study to increase the TTs along with better cyclic stability as compared to as-extruded specimen. This increment in the TTs can be attributed to the theory presented in the literature for the evolution of Ni-rich precipitates[10, 51, 60] , which tend to form precipitate of the type Ni_4Ti_3 when aged beyond certain temperatures.

It is a well known fact that the TTs of NiTi based SMAs are highly compostition dependent, similarly the NiTiHf alloys have been reported to be highly sensitive to composition alternations [45-46]. Since the TTs are increasing, it can be ascertained that the matrix of the alloys is getting depleted in terms of Ni content. Further increasing the aging temperature to 550°C increased the TTs substantially. As known from the literature the precipitates grow in size with an increase in time and temperature [59]. Thus, increase in the TTs can be attributed to the growth of the size and volume fraction of precipitates with an increase in the aging temperature, which further depletes Ni from the matrix. The peaks were observed to be very sharp and stable, which can be attributed to the increased strength of the matrix due to the precipitation hardening. As a result of stronger matrix, there is no extensive plastic deformation introduced due to thermal cycling. The distribution of the precipitate can be regarded as homogenous since the transformation occurs with sharper peaks instead of broad ones. Along the lines on theory of precipitate evolution, the precipitates should become coherent with the matrix and provide optimal strength to the matrix before they begin to coarsen into larger incoherent precipitates with further increase in aging time and temperature. The growth of the precipitate size is

47

evident from the further elevation of TTs when the aging temperature is further increased to 600°C and 650°C. Larger precipitates further depleted Ni from the matrix and hence an increment in the TTs is observed. The reason behind the peaks becoming wide can be attributed to the formation of inhomogeneous precipitates. When the wide peaks observed closely as in Figure 4.4, the transformation occurs in two steps instead of single step as seen earlier. This further supports the reasoning of incoherent precipitates since the transformation occurs in partially in steps pointing towards the heterogeneous matrix.
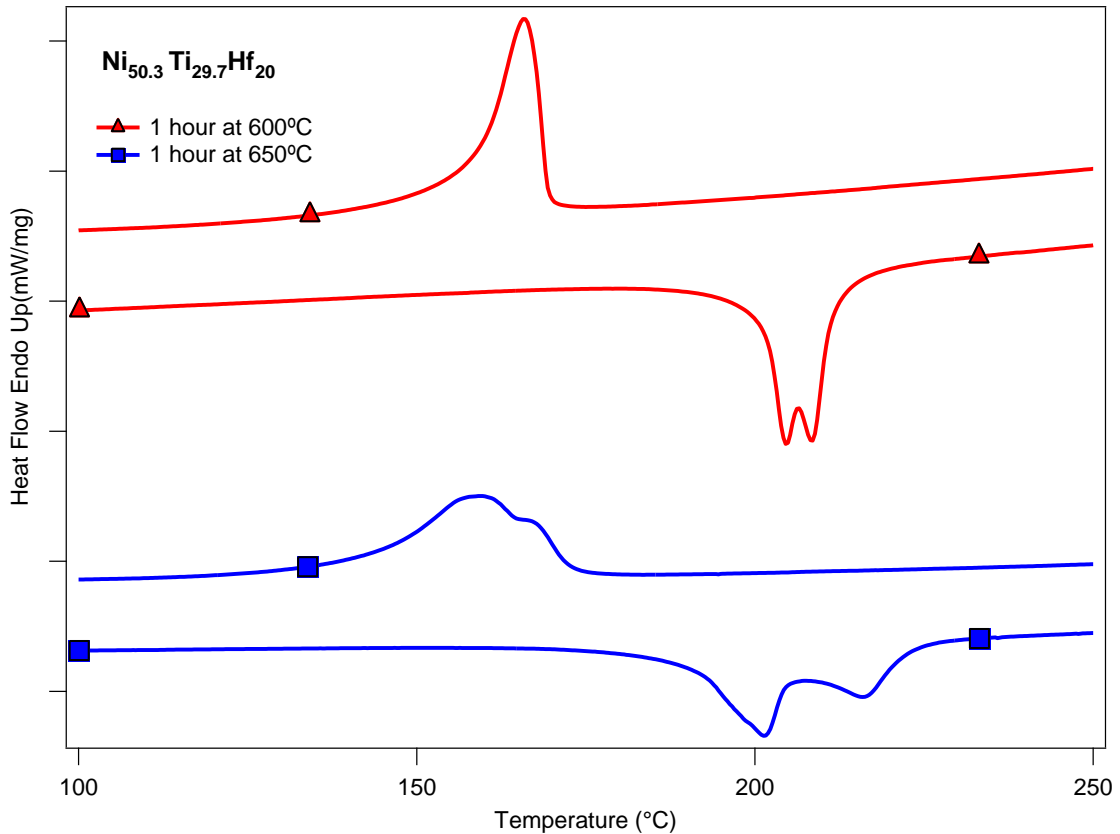
Figure 4.4: DSC plots for the second cycle for samples aged for 1 hour at 600°C and 650°C.

With increment of the aging temperature beyond 650°C to 700°C the fall in the TTs is the second change in the trend of TTs. The decline in the TTs lead to the hypothesis of the dissolution of the precipitates formed previously due to high

temperatures and/or formation of new type of precipitates and/or else recrystallization. Among three possibilities, the formation of new type of precipitates is least possible due to the high aging temperature. The later of the two above mentioned reasons are most likely due to the fact that in the literature it has been mentioned that the dissolution of Ni_4Ti_3 precipitates and the recrystalization temperature of NiTi start at this range of temperatures also, it is noted that the TTs decrease further for aging at 800°C and remain constant 900°C. This leads to the conclusion that the dissolution of the precipitates starts at temperature of 700°C and is almost complete by 800°C, the TTs don't fall further when the aging temperature is increased to 900°C.

Aging at 3 hours showed trends of change in TTs similar to 1 hour aging time with comparative TTs but with better cyclic stability. The TTs for aging at 300°C and 400°C are observed to be lower than the TTs for as-extruded condition and 1 hour aged samples. This leads to the idea of the precipitation of small precipitates along with stress relief which overshadows the effect on TTs due to the change in composition, and instead the small precipitates inhibit the nucleation of martensite and hence lower the TTs. The presence of second type of precipitates is unlikely since the change is not very sizable when the aging time is increased from 1 hour to 3 hours, during which the precipitates should have grown and led to further decline in TTs in contrast to what is seen.
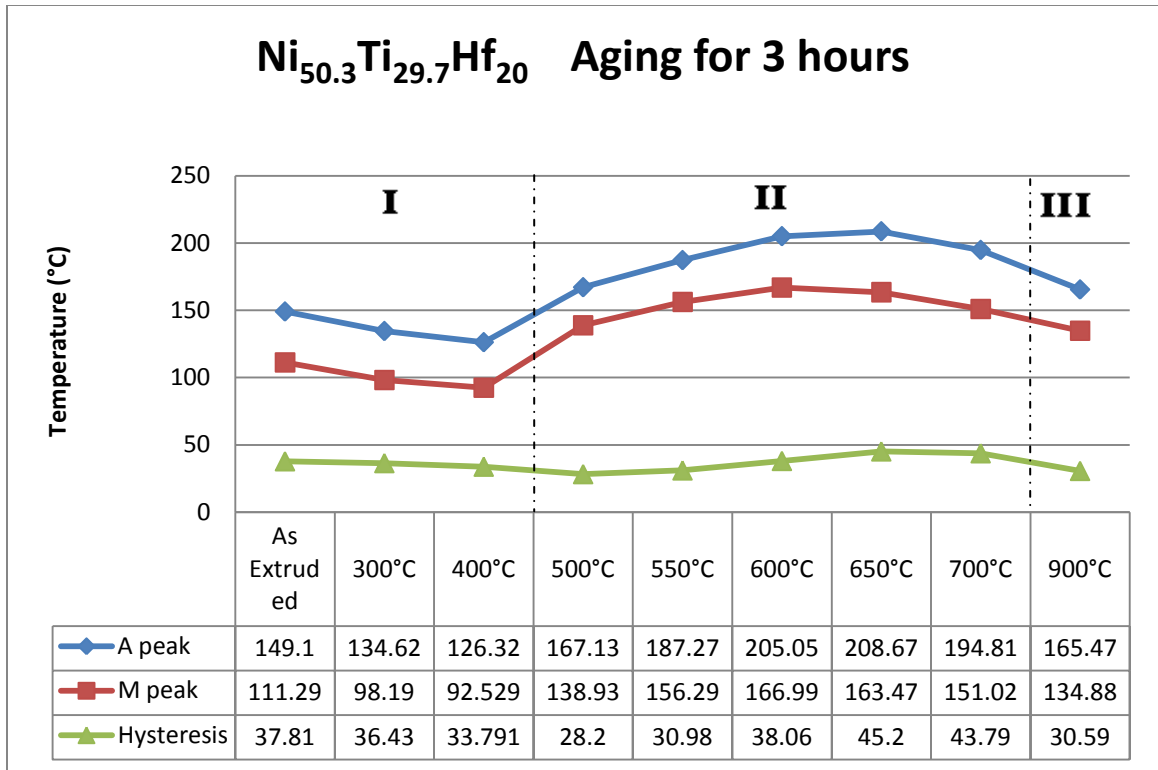
Figure 4.5: Comparison plot for peak temperatures for aging at 3hours for selected temperatures

Figure 4.5 depicts the peak temperatures for the $Ni_{50.3}Ti_{29.7}Hf_{20}$ alloy aged for 3 hours and varying temperatures. The elevated TTs after aging at 500°C as shown in Figure 4.5 can be attributed to the of growth of Ni-rich precipitates in the alloy with increasing aging time from 1 hour to 3 hours. Another notable feature of the TTs for the mentioned aging condition is the low hysteresis which could be a result of more compatible interface between the two phases. Strengthening of the matrix can be interpreted from the superb cyclic stability as observed in Figure 4.3, can also be attributed to the evolution of coherent precipitates. Further increase in the TTs is observed when the aging temperature is increased to 550°C. The increment in the TTs is sizable along with low hysteresis and high cyclic stability. This cements the theory of presence of coherent precipitates which in turn increased the TTs by changing the

composition and strengthened the matrix due to its size and placement. The TTs further increase for the aging temperature of 600°C and 650°C. This is a result of further growth of the precipitates in bigger size which alters the composition of the matrix to further depletion of Ni in the matrix and hence increases TTs. The change is TTs is accompanied by an increase in the hysteresis also which is an undesirable effect since it would inhibit the use of the HTSMA in active actuation. The TTs however are the highest for any aging temperature at 3 hours. The TTs fall for aging temperature of 700°C and reach almost the initial level of as-extruded condition for 900°C aging temperature evidencing the dissolution of the precipitates formed at lower temperatures.
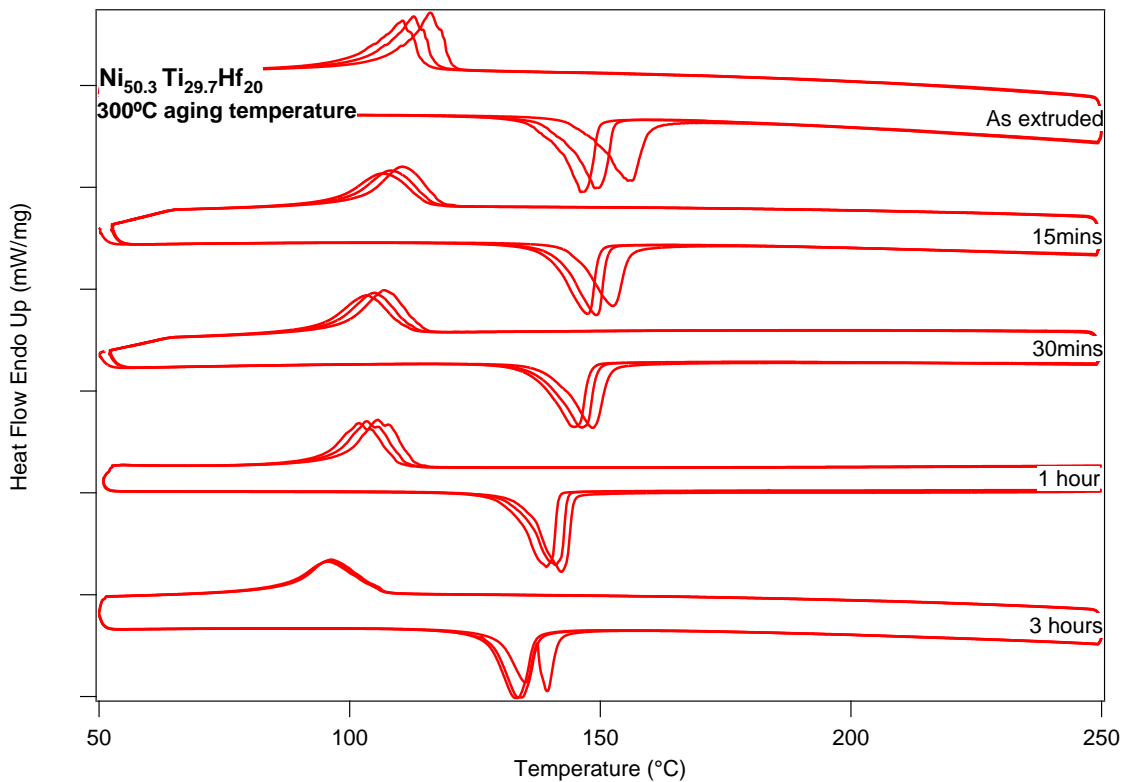
Figure 4.6: DSC curve for $Ni_{50.3}Ti_{29.7}Hf_{20,}$ aged at 300°C for various time durations.
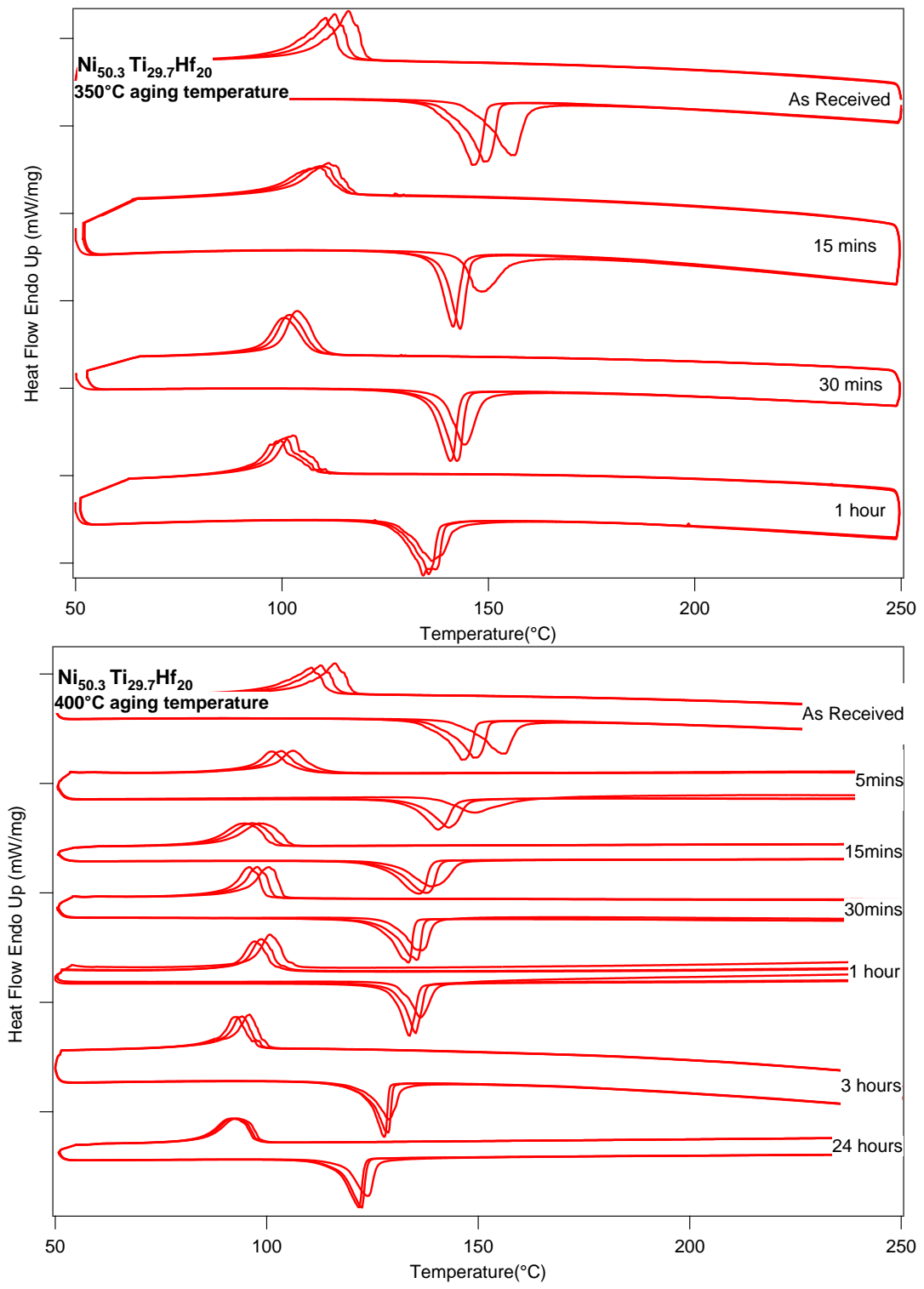
Figure 4.7(a,b): DSC curve for $Ni_{50.3}Ti_{29.7}Hf_{20,}$ aged at(a) 350°C(top) and (b)400°C(bottom) for various time durations.

Ni$_{50.3}$Ti$_{29.7}$Hf$_{20}$

	5min	15min	30min	1hour	3hour	24hour
(300°C) A p		149.19	146.25	140.92	133.63	
(300°C) M p		108.18	105.25	103.7	95.55	
(350°C) A p		143.01	142.37	135.44		
(350°C) M p		109.9	102.07	101.25		
(400°C) A p	143.14	137.8	135.51	135.28	128.65	122.55
(400°C) M p	103.3	96.561	97.799	98.611	94.04	92.628
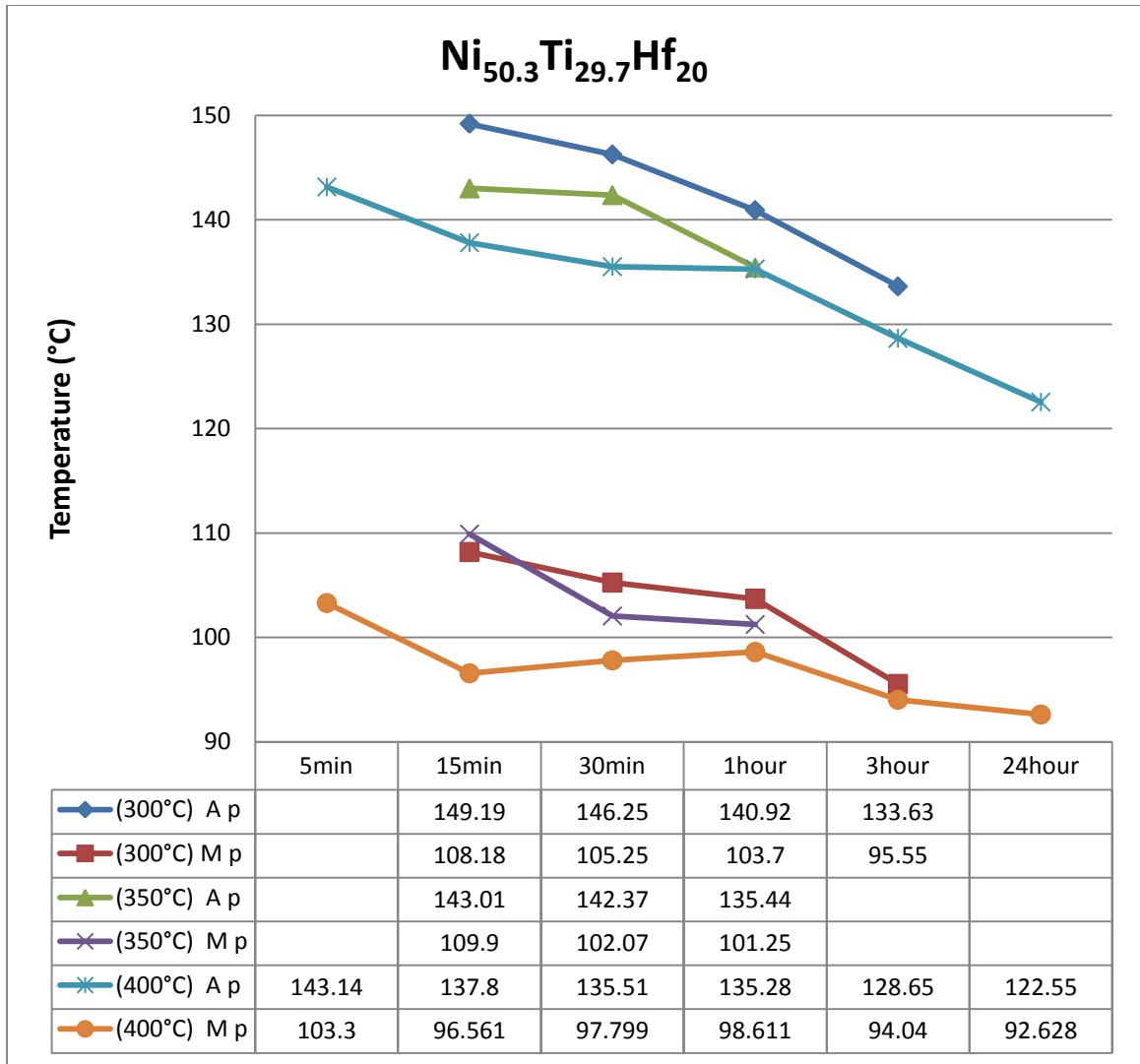
Figure 4.8: Comparison plot for transformation peaks Ni$_{50.3}$Ti$_{29.7}$Hf$_{20,}$ aged at 300°C, 350°C and 400°C for various time durations.

A detailed study was then conducted to reveal the effect of aging on variation in TTs in zone 1 as mentioned in the Figures 4.1 and 4.2. Figure 4.6 and Figure 4.7 show that the transformation temperatures kept decreasing with increase in aging temperature for aging at 300°C to 400°C. The TTs don't show any significant change in comparison with as extruded condition till an aging time of 30 minutes as evident from the DSC plots. The maximum drop for any aging time in the Zone 1 of aging temperature was for

24 hours at 400°C along with expectations since it was the maximum time for the mentioned temperature zone.
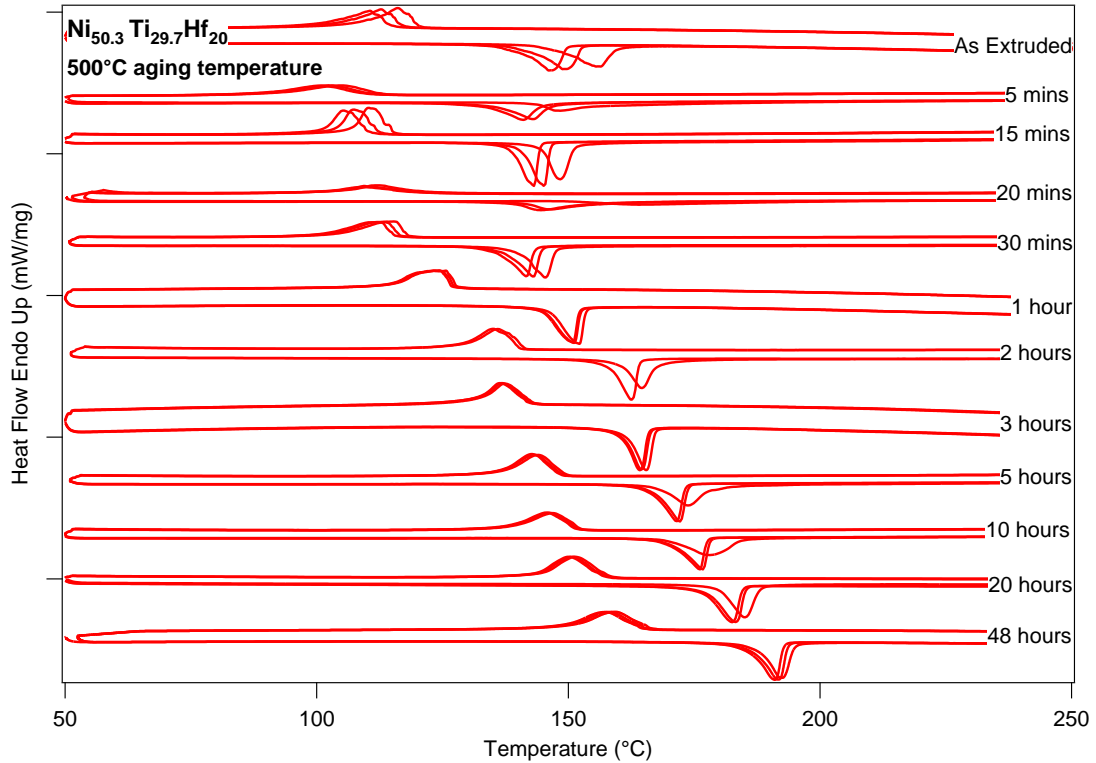
Figure 4.9: DSC curves for $Ni_{50.3}Ti_{29.7}Hf_{20,}$ aged at 500°C for various time durations.

The effect of aging time on the TTs in zone 2 was investigated by aging the sample at 500°C and 600°C from 5 minutes to 48 hours. The sample aged at 500°C for various time periods showed two different trends in the variation of TTs. For aging times less than 1 hour the TTs were observed to decrease to the level lower than the initial values. For aging time more than 30 minutes, the TTs were observed to increase with aging time. When the aging time was varied from 5 minutes to 48 hours with the intervals presented in the Figure 4.9 for the aging temperature of 500°C, the minimum TTs with values for M_p of 112.62°C and A_p of 142.89°C were observed for the aging time of 30 minutes. When the aging time was increased over 30 minutes, almost linear increase in

the TTs was observed for each interval as shown in Figures 4.9 and 4.10. Another key feature of aging at 500°C is the stable transformation that is observed for an aging time over 1 hour. The behavior of the increment is slightly different from the work reported by Meng et. al [61] in which a sharp increment in the TTs was observed with increasing the aging time to 5 hours at temperature of 550°C followed by stabilization of TTs in contrast to the linear increment observed here.

	As Extruded	5 mins	15 mins	20 mins	30 mins	1 hr	2 hrs	3 hrs	5 hrs	10 hrs	20 hrs	48 hrs
A peak	149.1	142.7	144.8	146.6	142.9	153.2	162.3	167.3	172.2	176.8	183.3	191.6
M peak	111.3	102.3	107.8	109.4	112.6	124.2	135.3	139.1	143.5	146.3	150.5	158.2
Hysteresis	37.81	40.32	36.98	37.24	30.27	29	27.06	28.26	28.72	30.47	32.78	33.36
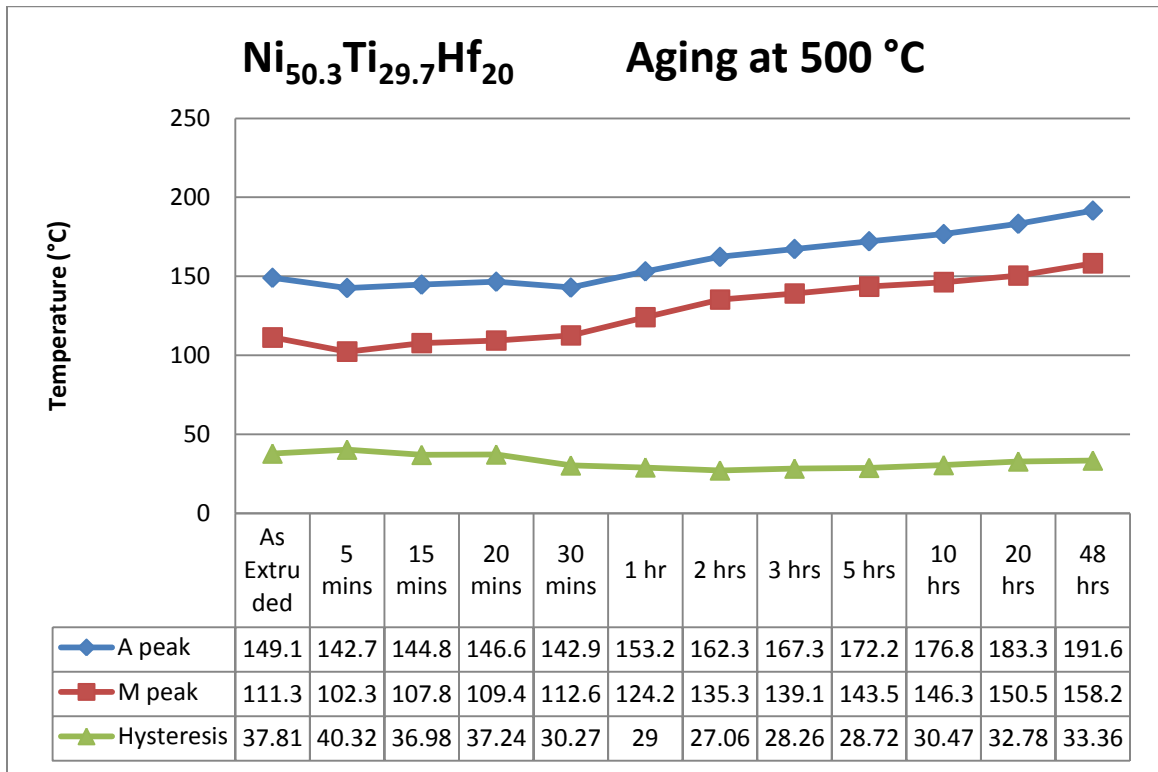
Figure 4.10: Comparison plot for transformation peaks $Ni_{50.3}Ti_{29.7}Hf_{20,}$ aged at 500°C for various time durations.

Figure 4.11 and 4.12 depicts the variation in TTs when the alloy is aged at 600°C for time range between 5 minutes and 48 hours. When aged at 600°C, as contrary to all lower aging temperatures, the variation showed a consistent trend of increase in the TTs without any drop even at 5 minutes. The uniqueness of 600°C aging temperature is the

evolution of a double peak transformation for 1 hour aging time. The transformation was not as stable as the 500°C aging time but the highest A_p of 217°C and M_p of 173 °C were observed for aging at 10 hours. These TTs are the highest observed TTs in the alloy system. The TTs increased sharply after aging for 30 minutes and followed by linear increase to reach their maximum values at aging for 10 hours.
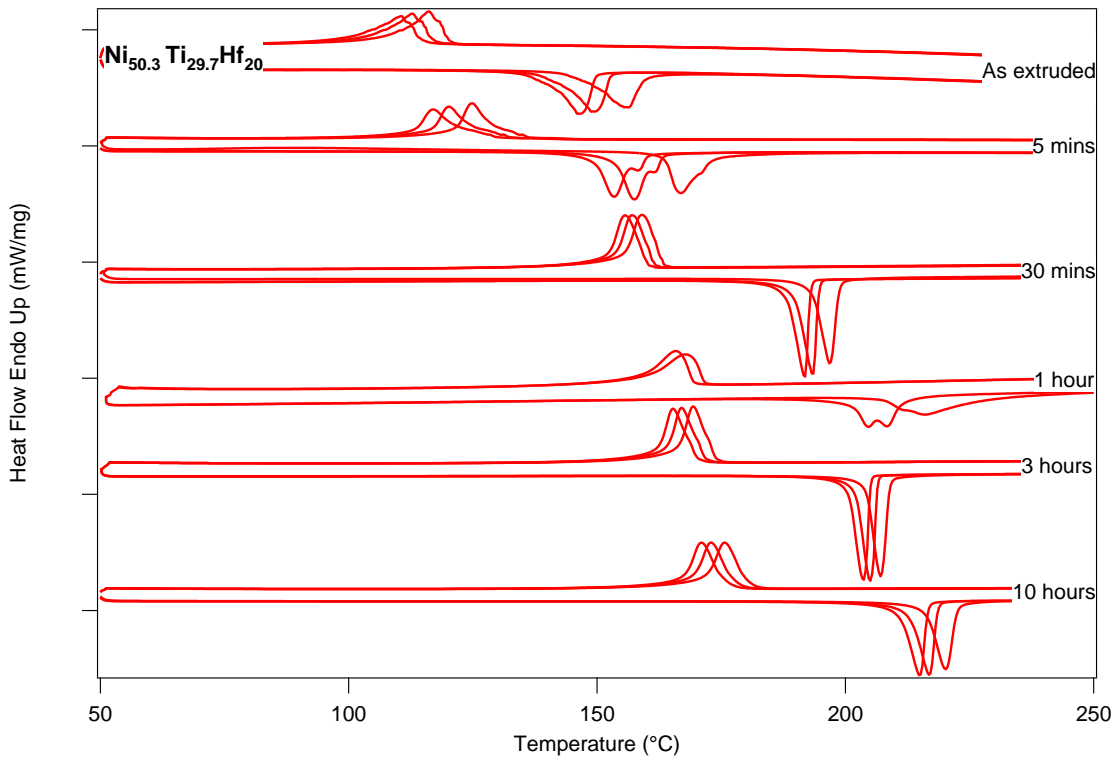
Figure 4.11: DSC curves for $Ni_{50.3}Ti_{29.7}Hf_{20,}$ aged at 600°C for various time durations.
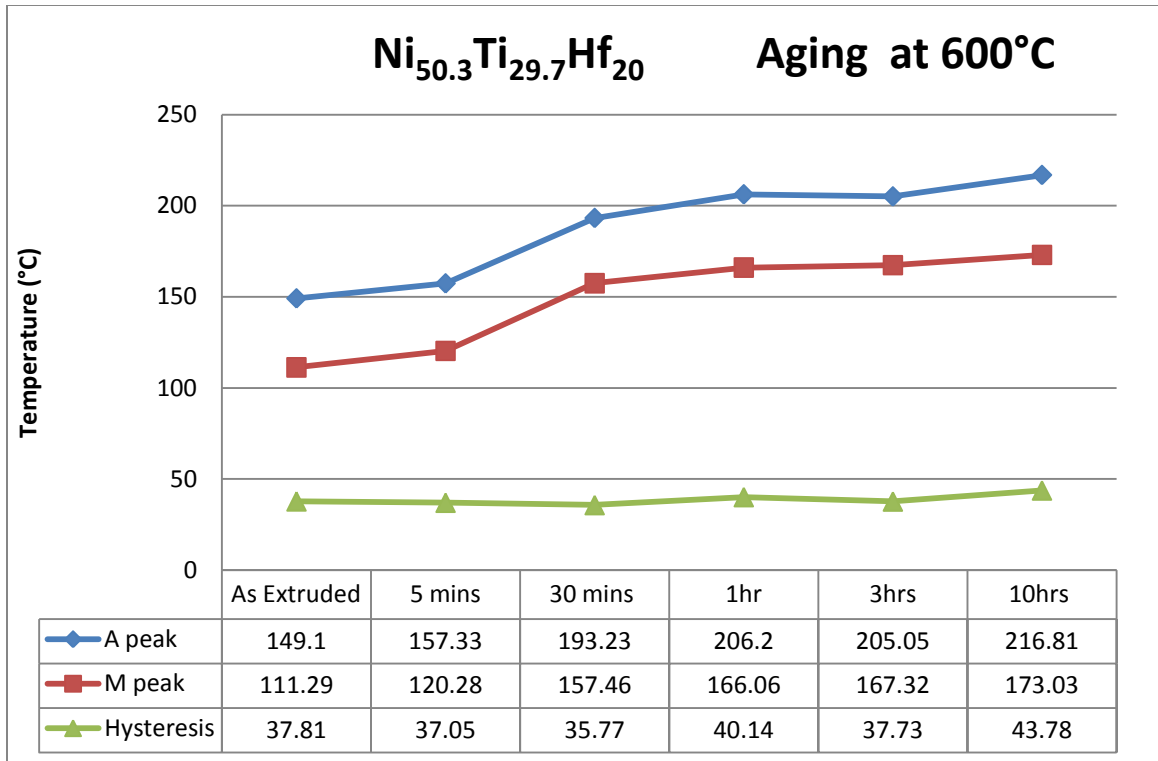
Figure 4.12: Comparison plot for transformation peaks $Ni_{50.3}Ti_{29.7}Hf_{20}$, aged at 600°C for various time durations.

The high degree of cyclic stability achieved while aging at 500°C was not achieved for the aging temperature of 600°C. Despite the elevation in TTs, the hysteresis for all aging times at 600°C was much higher in comparison with the lowest achieved hysteresis of 28°C for aging 3 hours at 500°C. The lowest achieved hysteresis for aging at 600°C was 36°C at aging for 30 minutes and the highest value for hysteresis at 10 hours of 43.78°C, which also coincides with the highest achieved TTs.
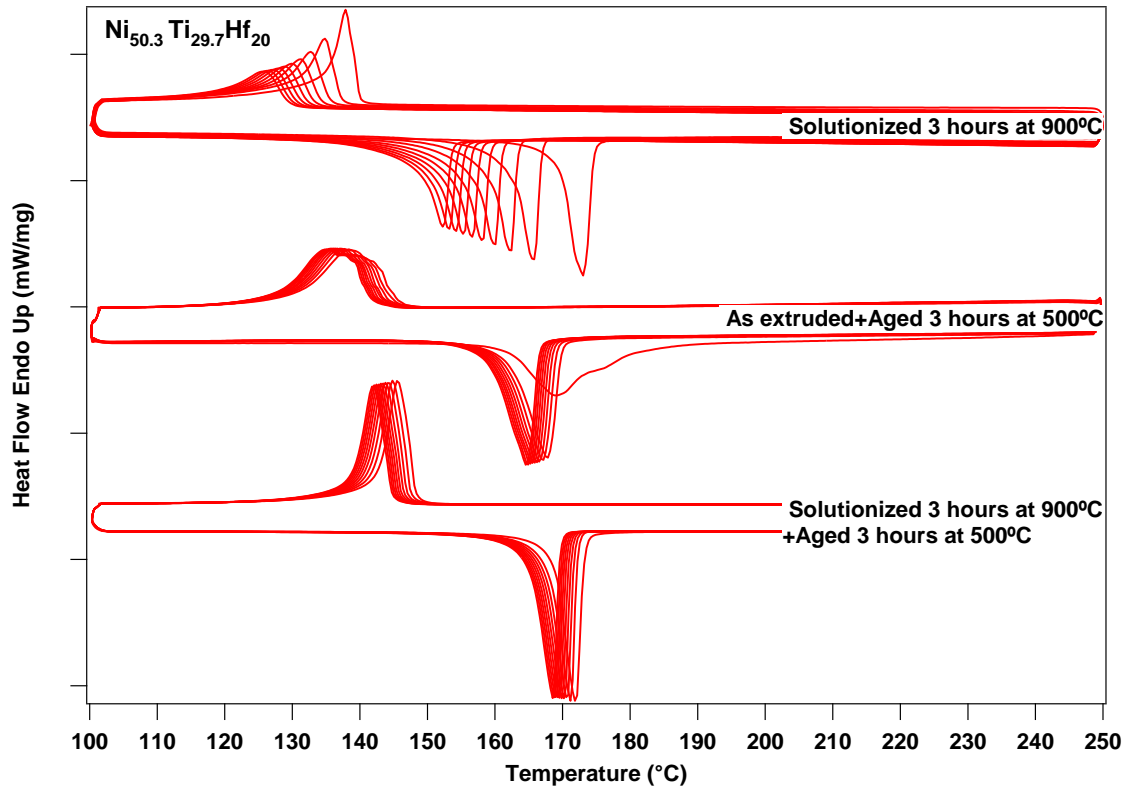
Figure 4. 13: DSC curves for $Ni_{50.3}Ti_{29.7}Hf_{20,}$ aged at various run for cyclic stablilty

A key characteristic required from the active materials for use in industrial applications is the precise range of actuation stimulus. Hence for the desirable output, the devices made of SMAs should actuate for a set range of temperatures in duty and should maintain the same characteristics even after several cycles of use. A systematic investigation carried out to investigate the stability is represented in Figure 4.13. It depicts the cyclic response for 10 cycles in DSC for the 3 samples solutionized at 900°C, aged for 3 hours at 500°C and solutionized 3 hours at 900°C followed by aging at 500°C respectively. Samples aged at mentioned conditions were run in the DSC for 10 cycles between 100°C and 250°C.

Amongst the various conditions for aging temperatures investigated earlier, 500°C was found to be most suitable for thermal stability and hence was chosen for the

58

detailed study of effects of aging on thermal stability. Results from the three samples mentioned above clearly show the effect of the aging on the thermal stability. The comparisons for the peak temperatures of each cycle are presented in Figure 4.14. The sample solutionized at 900°C for 3 hours was observed to have a very poor thermal stability and with each cycle the TTs degraded by about 3 to 5°C till the sixth cycle, after which the TTs decrease by about 1°C. In contrast, for the samples aged at 500°C, the degradation of TTs for each cycle is less than 1°C even for the first 3 cycles and the TTs became almost constant afterwards. The cyclic stability is very essential for applications and as shown it can be achieved by using suitable aging instead of combination of complicated and expensive cold working or severe plastic deformation along with aging techniques utilized in NiTi alloys.

The introduction of dislocations due to thermal cycling is attributed for the decrement of the phase TTs [61]. The smaller decrement in later cycles of the solutionized sample is due to the introduction of large number of dislocations in intial cycles which then begin to saturate and in turn inhibit introduction of more dislocations. While in contrast, the precipitates present in the aged specimen strengthen the matrix and prevent sternly the introduction of dislocations during the thermal cycling. As a result the increment in TTs in aged specimen is accompanied by enhanced stability making it more suitable to use these alloys in industrial applications.
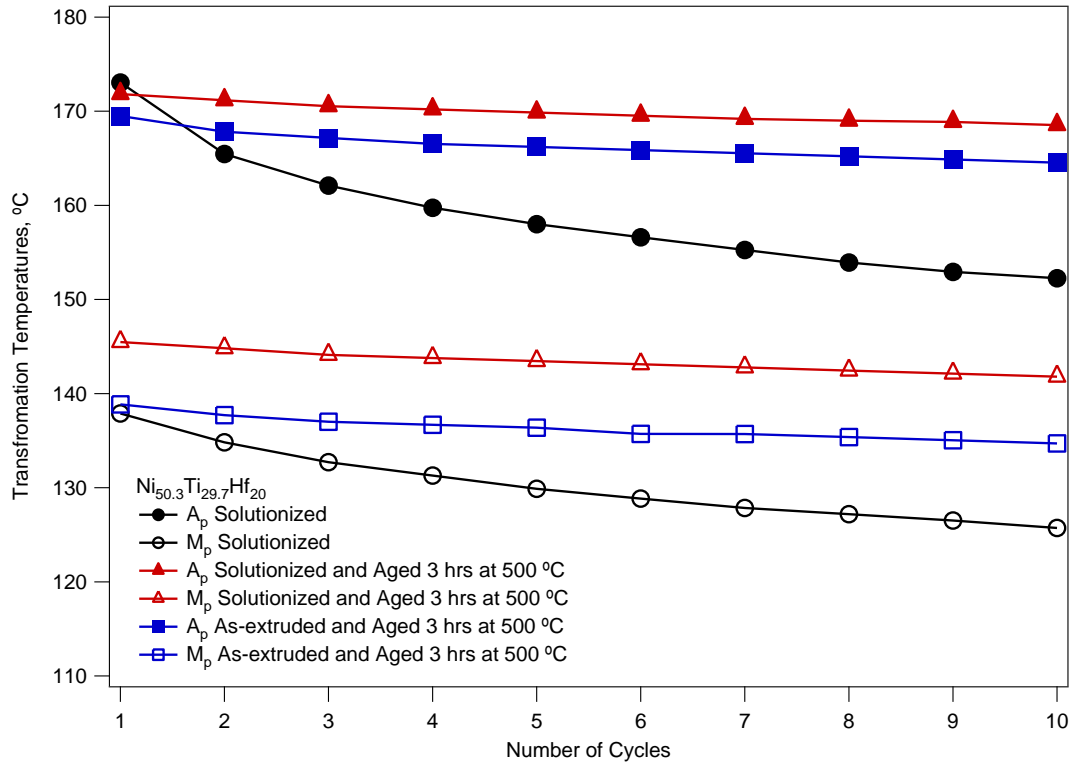
Figure 4.14: Comparison plot for transformation peaks $Ni_{50.3}Ti_{29.7}Hf_{20,}$ aged at conditions mentioned in Figure 4.13 showing the cyclic behavior for first 10 cycles.
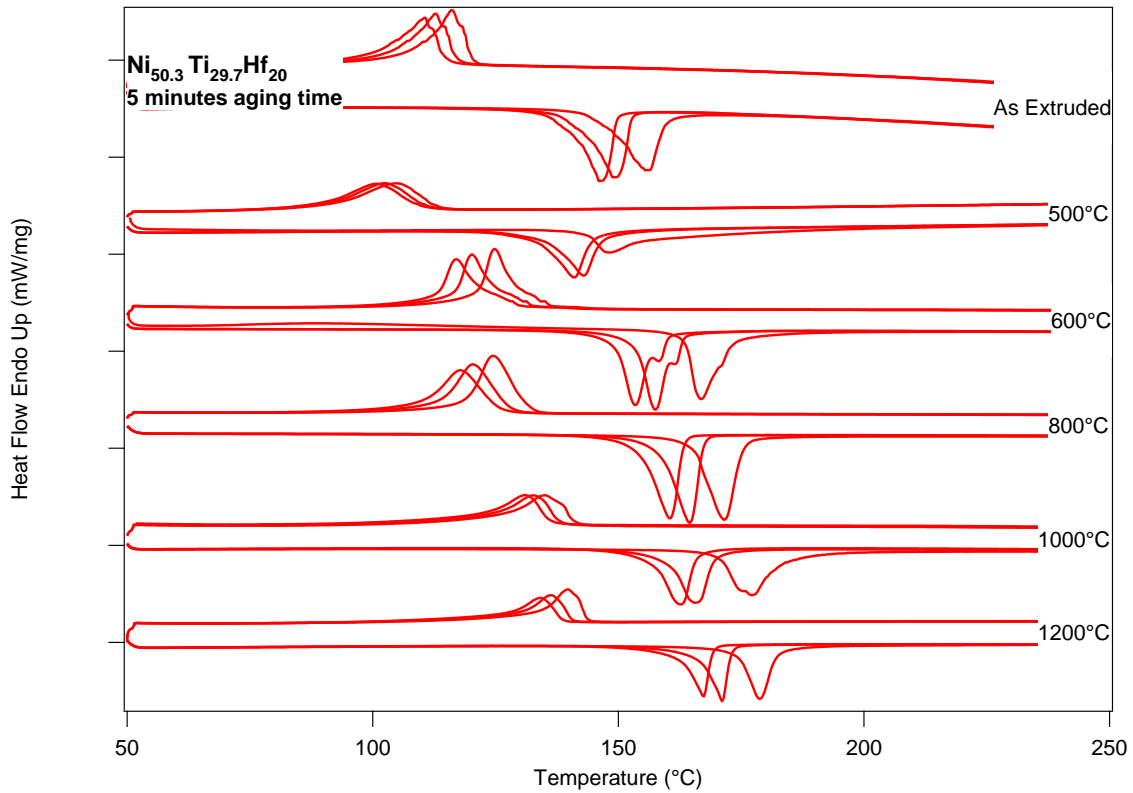
Figure 4.15: Comparison plot for transformation peaks $Ni_{50.3}Ti_{29.7}Hf_{20,}$ aged at various temperature for various 5 minutes

The Figure 4.15 represents the DSC results for $Ni_{50.3}Ti_{29.7}Hf_{20}$ aged for 5 minutes for temperatures ranging from 500°C to 1200°C. An attempt was made to investigate the effect of aging at very short times for very high temperatures ranging from 800°C to 1200°C. The results show very minute variation in TTs when the aging temperature was increased from 600°C to 1000°C. The TTs increase about 5°C for every 200°C increase in aging temperature, and reach a maximum value for A_p of 171°C for aging at 1200°C. The thermal stability did not improve with aging temperature and is visibly same for all aging temperatures. The slight increase in TTs as observed from the plot can be attributed to formation of Ni-rich precipitates heating or quenching the samples.

4.2 Hardness Results
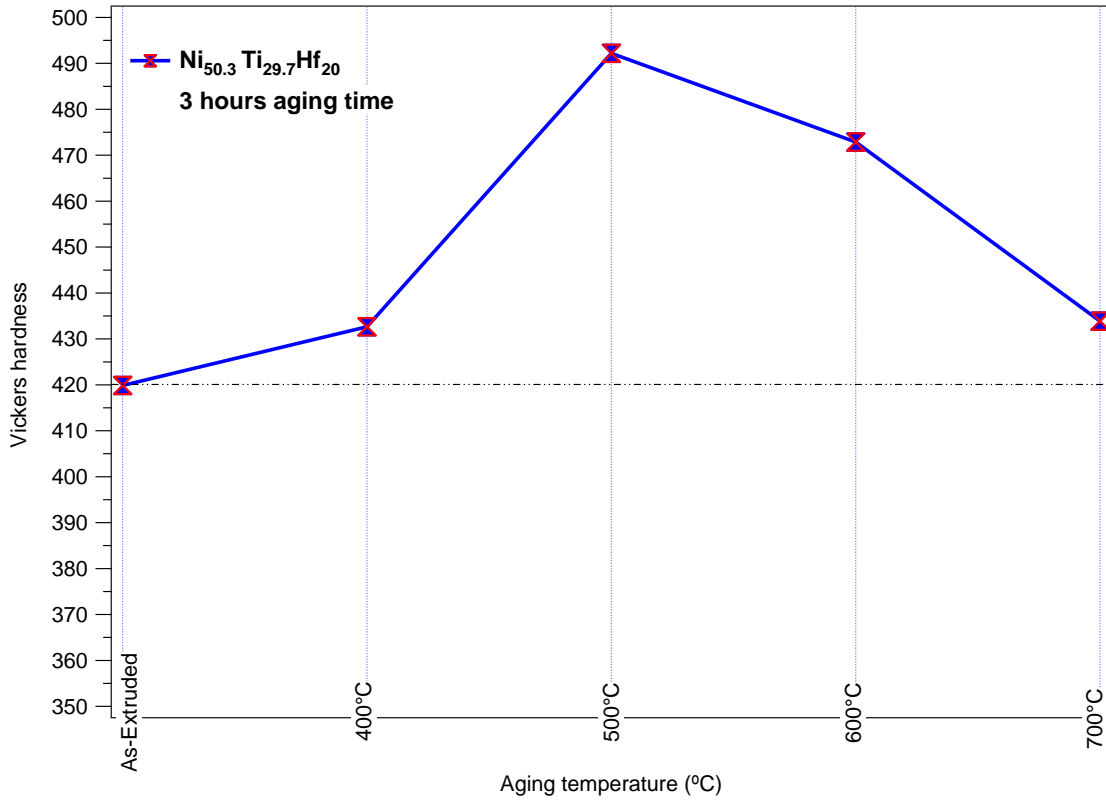
Figure 4.16: Comparison plot for hardness values of $Ni_{50.3}Ti_{29.7}Hf_{20}$, aged at selected temperatures for 3 hours

Vickers hardness values are represented in Figure 4.16 for $Ni_{50.3}Ti_{29.7}Hf_{20}$ alloy at selected temperatures for a fixed aging time of 3 hours. The hardness of the material was observed to increase with all aging temperatures studied. The hardness value increased from 421 to 435 on Vickers scale when the sample was aged for 3 hours at 400°C in comparison with as extruded sample. A substantial increment in the hardness was observed when the aging temperature was increased from 400°C to 500°C, the hardness value increased by about 60 on the Vickers scale. This hardness value was observed to be the maximum at aging for 3 hours. The hardness value was then noted to decrease with a

further increase in aging temperature. The hardness values decreased to 475 and 440 for aging at 600°C and 700°C respectively.

The trend for variation in hardness value (HV) was observed to be follow a similar trend to the variations in TTs for same aging conditions with some difference. In variance with the descent in TTs for aging at 400°C, the hardness value increased. It can be noted that in contrast with the progression of TTs which initially fell below the values of as extruded condition, the hardness value was observed to be higher than the value for as extruded sample. Higher degree of hardness was observed for aging at both 500°C and 600°C, but inverse to the trend followed by TTs which increased with increase in aging temperature from 500°C to 600°C, the hardness value decreased for the increment in aging temperature.. The trend for increment in aging temperature from 600°C to 700°C showed behavior similar to the progression of TTs, and both the attributes decreased to values comparable with as extruded condition.

The contrasting behaviors of TTs and material strength can be attributed high dependence of TTs on the compositional shift of Ni from the matrix to precipitates with the evolution of precipitates with increasing time and temperature. HV which is indicative of material strength has complex dependence on the size and interstitial distances between the precipitates. With the accruement of the precipitates into the large size, the matrix continues to deplete in Ni and hence the variation as observed in the TTs with the maximum values at aging temperature of 650°C are observed. Further increase in aging temperature results in the dissolution of the precipitates due to the proximity to recrystallization temperature. The material strength as observed from the HV results are indicative of coherent precipitates at 500°C which impart maximum strength to the alloy.

Increasing the aging temperature further increase the size of precipitates into larger in coherent precipitates which are farther apart from each other and hence the strength is observed to fall again after having reached the optimum value.

4.3 XRD Analysis
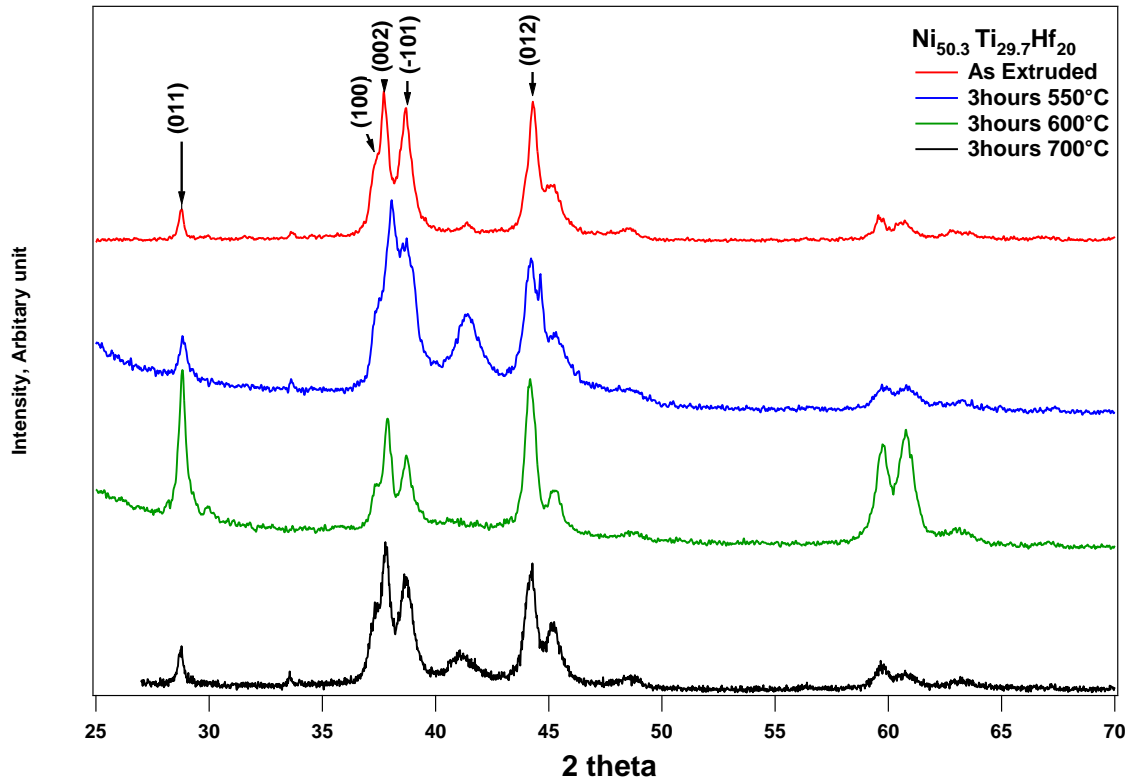
Figure 4.17: Plot for XRD at room temperature $Ni_{50.3}Ti_{29.7}Hf_{20,}$ in as extruded condition and aged at various temperature for 3 hours

Figure 4.17 represent the XRD peaks response of the $Ni_{50.3}Ti_{29.7}Hf_{20}$ samples with different aging conditions. The results for as extruded sample and three other samples aged for 3 hours at 550°C, 600°C and 700°C are presented in the plot. Very similar results were obtained for the samples tested as no visible difference in the characteristic peaks were observed. Major peaks were observed between the 2-theta range of 35° and 50° in concurrence to the results reported by Meng [62] and Tong [63] in their respective

works. The peak at about 42° of the sample aged at 550°C is from the parent phase which was found to be B2. The martensite phase for the alloy was found to be monoclinic B19' which was along the lines of the findings reported for similar alloys in the literature. The lattice parameters for the as extruded sample were analyzed using combination of two softwares by the name of PowderCell and Celref. The parameters for the as extruded sample was found to be a = 0.250nm, b = 0.401nm, c = 0.483 nm and β = 101.54° with the structure of B19'. The Figure 4.18 represents the XRD results for the as-extruded sample when measurements were done at 200°C to ensure the sample was in the austenite phase. The major peak was observed at about 42° and the structure was known to be B2 as indicated in previous works [62]. The calculations yielded the lattice parameters of a=0.31nm.
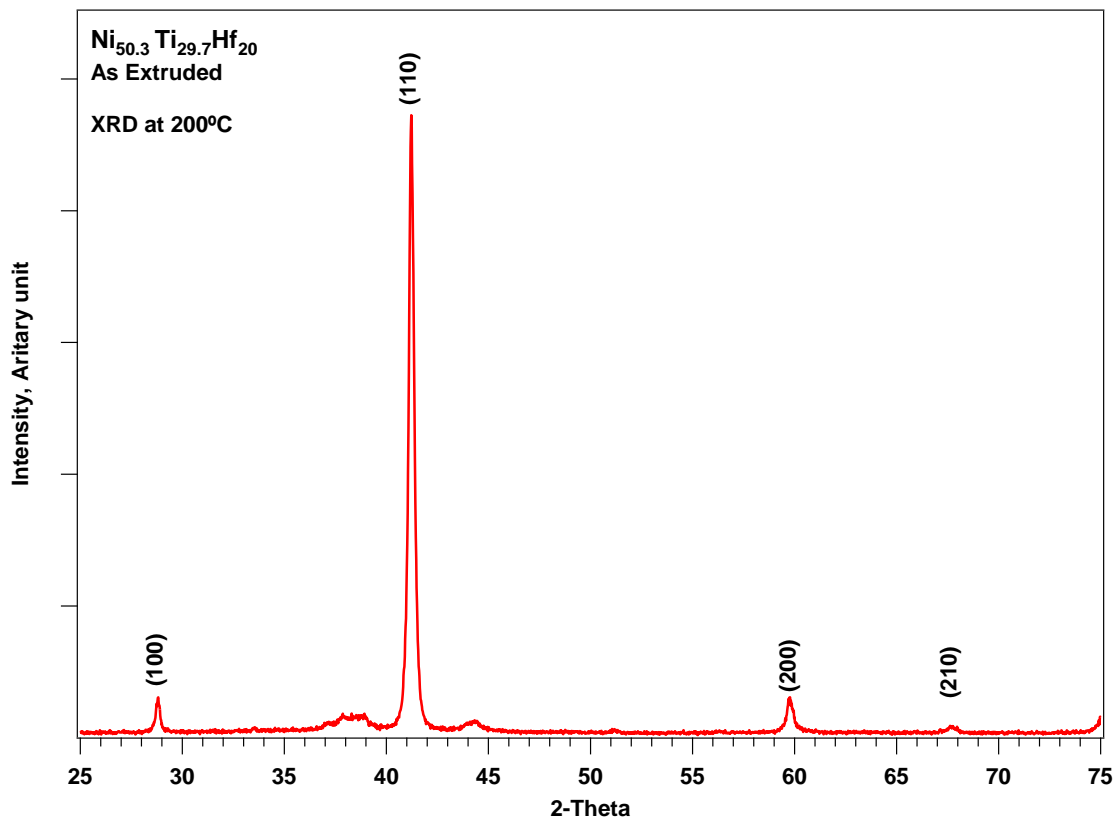
Figure 4.18: Plot for XRD at 200°C $Ni_{50.3}Ti_{29.7}Hf_{20}$ in as extruded condition.

4.4 TEM Study
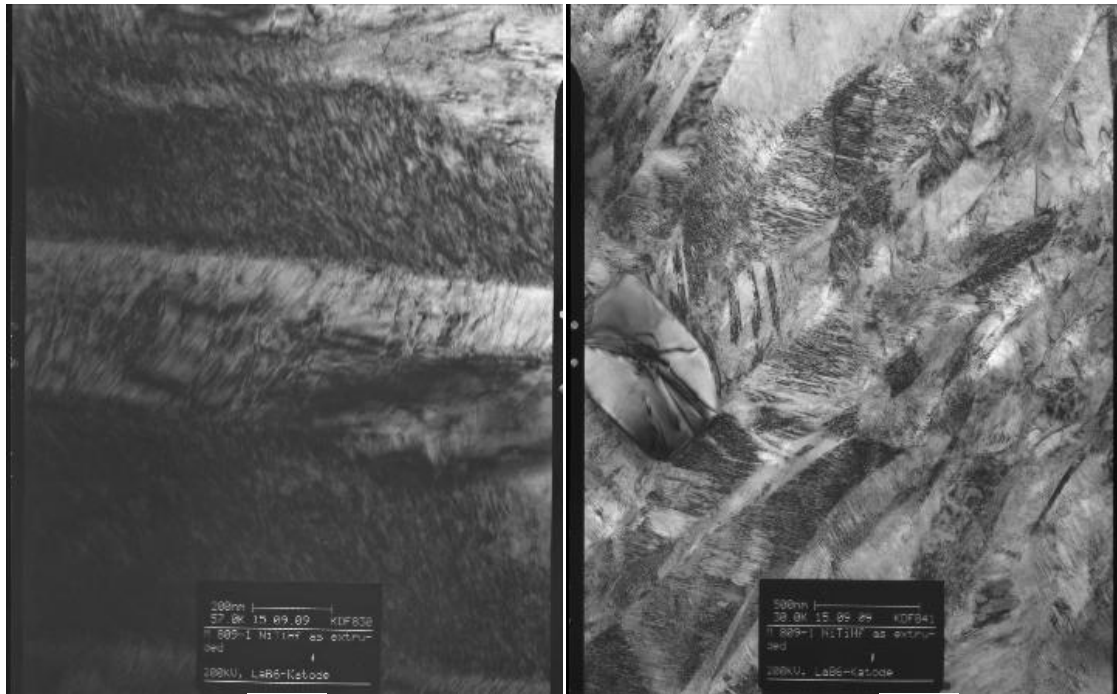
(a)

(b)

(c)

Figure 4.19: TEM micrographs of $Ni_{50.3}Ti_{29.7}Hf_{20}$ in as extruded condition

Figure 4.19 shows the TEM micrographs for $Ni_{50.3}Ti_{29.7}Hf_{20}$ in as extruded condition. Contrary to expectation, despite the extrusion at 900°C dislocations were observed in high density throughout the matrix. Figure 4.19 shows a high magnification image showing a typical area with large amount of dislocations emanating from 7:1 extrusion done at 900°C. No precipitates were visible in the alloy at the magnification used throughout the matrix. The homogenization of the alloy at 1050°C for 72 hours prior to extrusion is chiefly responsible for the absence of precipitates. The initial precipitation free structure gives an advantage in further investigations on effect of formation and evolution of precipitates with different thermo-mechanical treatments.

Figure 4.19 (c) shows the selected area diffraction (SAD) pattern for $Ni_{50.3}Ti_{29.7}Hf_{20}$ in as extruded condition. Confirming with XRD investigations presented prior to TEM micrographs the structure of martensite phase was found to be B19'. The presence of twins in the structure can be noted from the ghost like duplicate pattern in the middle.
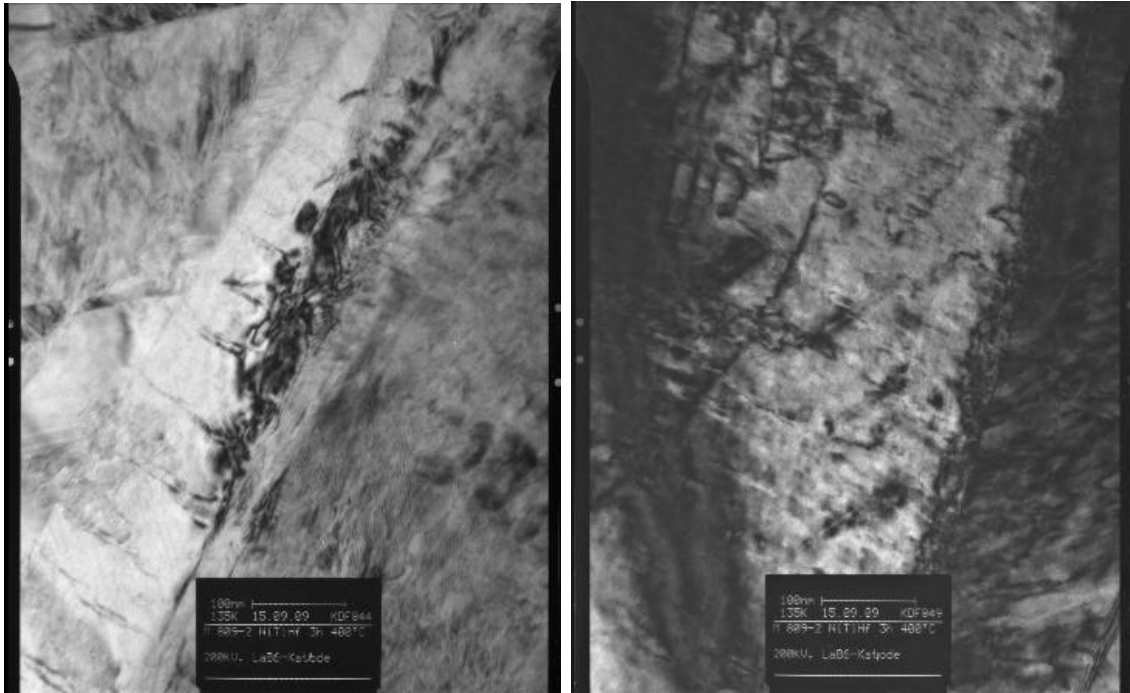
(a)

(b)

(c)

Figure 4.20: TEM micrographs of $Ni_{50.3}Ti_{29.7}Hf_{20}$ aged at 400°C for 3 hours.

Figure 4.20 (a) and (b) shows the TEM micrographs for $Ni_{50.3}Ti_{29.7}Hf_{20}$ aged at 400°C for 3 hours. Martensite lamella is observed in the center with dislocations in Figure 24.a along with some oval shaped features that should be fine precipitates. Figure 24.b shows the martensite with dislocations and very fine oval shaped precipitates. The dislocation density can be clearly observed to have decreased in comparison from the observations noted from the TEM micrographs of as extruded condition. This provides conclusive evidence for the hypothesis of initial drop in TTs when the alloy is aged at 400°C. The formation of precipitates is accompanied by the stress relief from the dislocations, and as noted from the micrographs the size of precipitates is notably small. The increment of TTs that should have occured due to formation of Ni-rich precipitates is overpowered by the stress relief due to the heat treatment which facilitates the easier motion of habit plane and hence results in overall reduction of TTs.

The SAD pattern as shown in Figure 4.20 (c) represent the alloy aged for 3 hours at 400°C. The diffraction pattern also shows twin reflections similar to the ones in as extruded specimen along with many other reflections. These reflections can be attributed to the presence of newly formed precipitates when the alloy is aged. The presence of multiple reflections clearly evidences the formation of precipitates while confirming the structure for the parent matrix same as in as extruded condition..

(a)   (b)
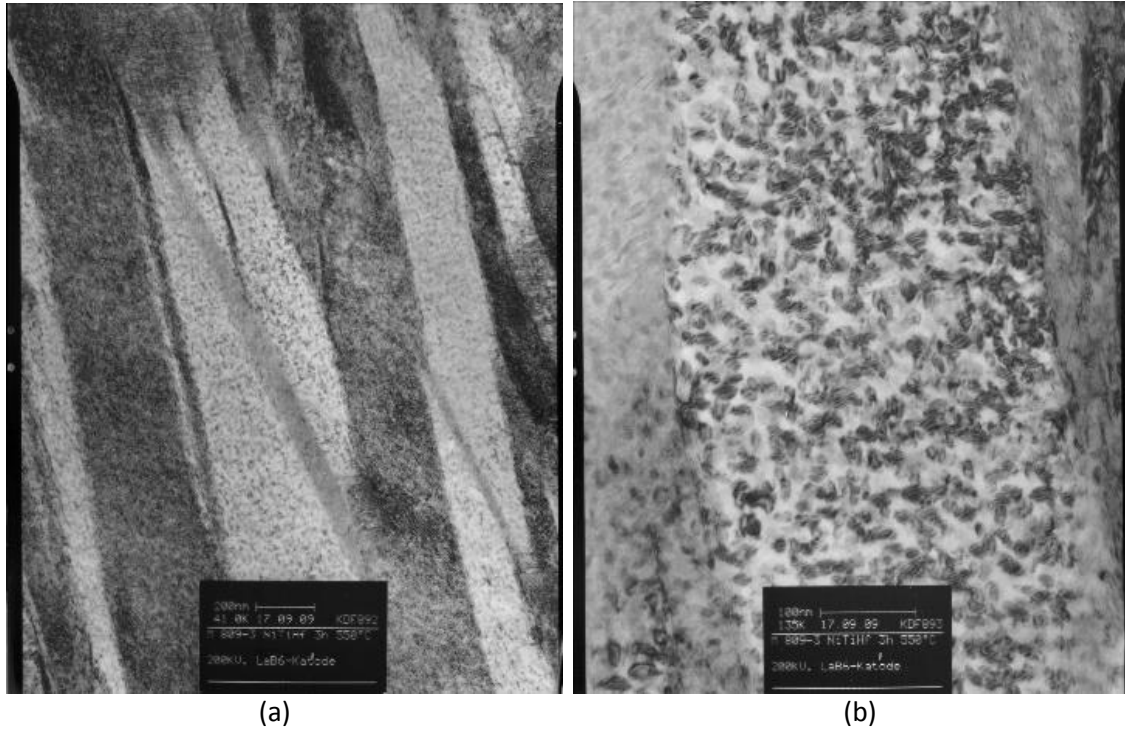
Figure 4.21: TEM micrographs of $Ni_{50.3}Ti_{29.7}Hf_{20}$ aged at 550°C for 3 hours.

Figure 4.21 represents the TEM micrograph for the $Ni_{50.3}Ti_{29.7}Hf_{20}$ aged at 550°C for 3 hours. In $Ni_{50.3}Ti_{29.7}Hf_{20}$ aged at 3 hours for 550°C we can clearly observe dislocation free martensite variants with uniformly disturbed precipitates. The average size of the precipitates is about 20nm. In the higher magnification image the precipitates are seen to be finely dispersed throughout the matrix with very less distance amongst each other. The findings are concurrent with the earlier results for TTs and HV, which are both in the vicinity of their highest respective values for the alloy system. The precipitates along with depleting the matrix of Ni, are responsible for acting as pinning sites for blocking dislocation motion. The combination effect as mentioned earlier is high thermal stability at high TTs and superior material strength. These initial finding make the $Ni_{50.3}Ti_{29.7}Hf_{20}$ alloy aged at 3 hours for 550°C a formidable candidate for detailed mechanical testing since the attributes of this particular aged specimen seems to be

optimum for exceptional high temperature shape memory properties along with good mechanical strength. The lenticular shaped particles present in the aged specimen are similar to the ones reported by Meng et. al [61]. Meng reported that the precipitation of these particles was responsible for the decrease of the ratio of Ni/Ti+Hf and hence the increment in the TTs similar to the behavior observed in this study.
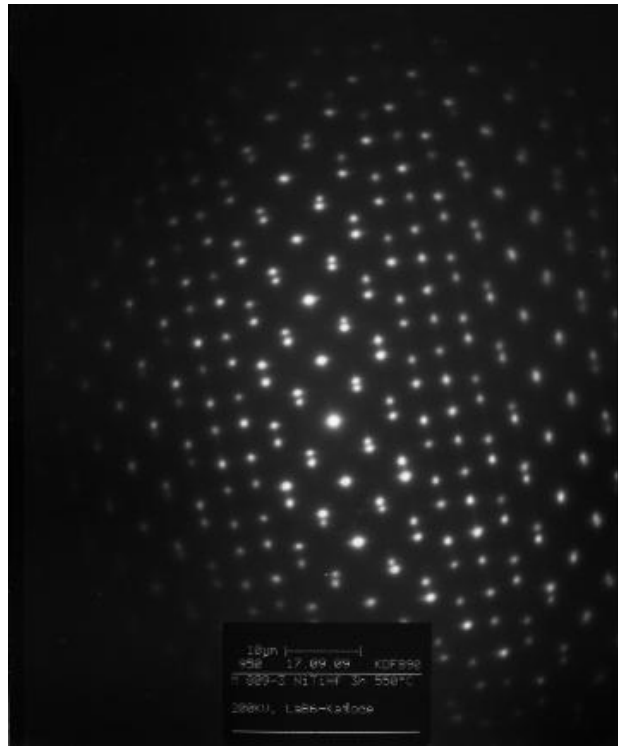
Figure 4.22: SAD pattern of $Ni_{50.3}Ti_{29.7}Hf_{20}$ aged at 550°C for 3 hours.

Figure 4.22 shows the SAD pattern for $Ni_{50.3}Ti_{29.7}Hf_{20}$ aged at 550°C for 3 hours from the area shown in Figure 4.21 (a). The SAD pattern for the alloy aged for 3hour at 550°C is noted to be similar to the one aged for same time but 400°C except for more prominent duplicate extra reflections, possible due to a notably higher ratio of bigger precipitates.

(a)   (b)
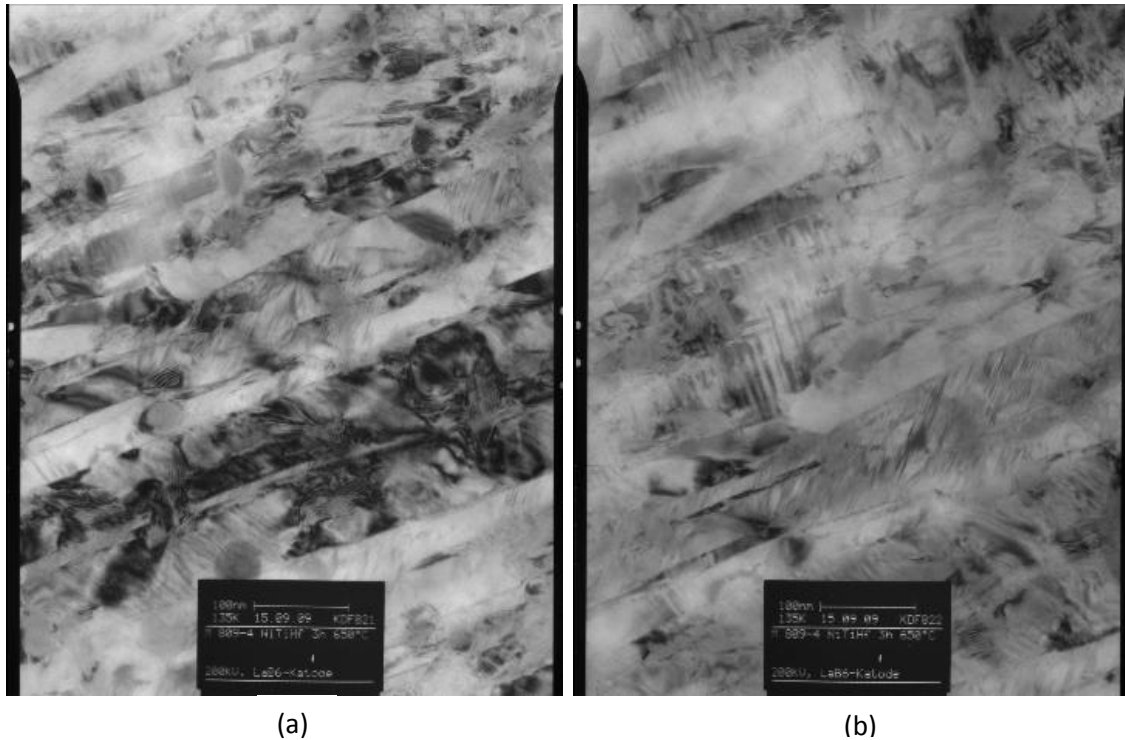
Figure 4.23: TEM micrographs of $Ni_{50.3}Ti_{29.7}Hf_{20}$ aged at 650°C for 3 hours.

The high resolution images for $Ni_{50.3}Ti_{29.7}Hf_{20}$ aged at 650°C for 3 hour is presented in Figure 4.23. Precipitates about 40-60nm, much bigger in size than the ones observed for the same aging time of 3 hours shown previously in comparison of 650°C as shown in Figure 4.21 are clearly visible. This finding is concurrent with the theory progression of size of precipitates as mentioned in earlier sections with the increase in aging time and temperature. With this growth of precipitates into apperently coarse preipitates the strength of the material decreases but the TTs continue to increase due to the further depletion of Ni from the matrix. The precipitates can be clearly observed to have grown into incoherent precipitates which are now farther apart from the previously mention aged sample. Both these factor lead to an easier motion of dislocations and hence in line with the HV results the material depreciates in material strength.

4.5 Mechanical Characterization
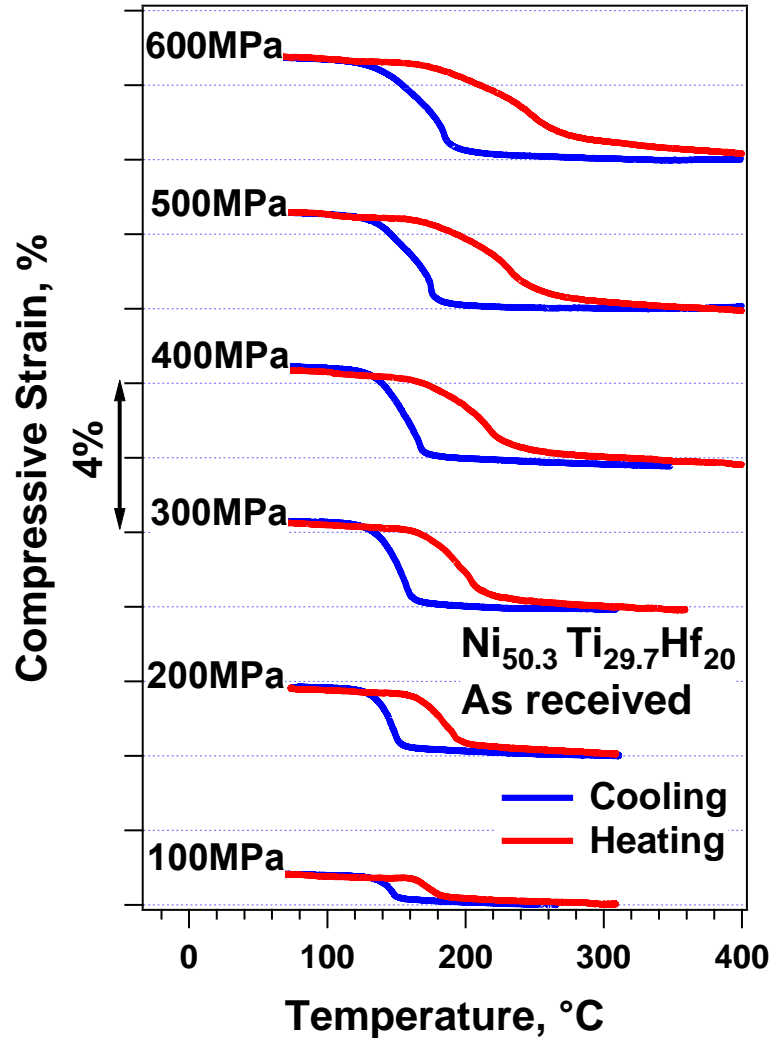
Figure 4.24: Isobaric thermal cycling of $Ni_{50.3}Ti_{29.7}Hf_{20}$ in as extruded condition.

Figure 4.24 shows the results for isobaric thermal cycling tests done on as extruded specimen with compressive loads ranging from 100MPa to 600MPa. The compression specimen was loaded at temperature well beyond A_f to ensure that the specimen was fully in austenitic state, to the desired load level. This was followed by thermal cycling at the set load level between the loading temperature and temperature lower than M_f to ensure full transformation. During the thermal cycling, when the

73

temperature reaches M_s, phase transformation starts and as visible from the graphs a rapid change in the strain is observed. The compressive strain continues to increase till it turns flat at the end of the transformation and vice versa during the heating part of the thermal cycling, along with the back transformation from martensite to austenite, due to shape memory effect the specimen change in compressive strain to its original state is observed.

In stress free transformation, no or a very small observable shape change is noted due to self accommodation of martensite variants, however when external load is applied, one or martensite variants are favored or biased and as a result a net shape change is observed. This most favored or the biased variant continues to grow with increased load levels till it is the only variant present in the structure [10, 64]. Figure 4.25 depicts the transformation strain for the as extruded sample under a compressive load of 5MPa. It is clearly visible from the plot that the load level is not enough to nucleate any biased martensite variant to result in compressive strain, instead a small strain due to selection of variant by internal stress fields. When the load is increased to 100MPa as shown in Figure 4.24, a fully recoverable strain of 0.61% is observed. The transformation strain increases notably till the load of 300MPa to 2.1% and from there on, for further loading till 600MPa the strain increases slightly to 2.6%. The increment in transformation strain along with increase in load level is because of the formation of load biased martensite variant [10]. This increment is limited to a maximum value attainable till only the most favored variant is the sole martensite variant in the whole structure. The maximum strain is also limited by the effect of dislocations that can be formed during the phase transformations. As the load levels increase, the amount of plastic deformation could also increase along with it. Some of the more notable points are the presence of no

irrecoverable strain till 300MPa as presented in Table 4.1, and small irrecoverable strain at for higher loads. The irrecoverable stain first appears at the load of 500MPa and increases slightly to 0.15% from 0.1% when load is increased from 500MPa to 600MPa. The hysteresis increases almost linearly from 27°C to 68.5°C with increase in stress from 100MPa to 600MPa. Following the Clausius–Clapeyron equation the TTs also increase with successive cycles at higher loads than preceding cycle and the maximum M_s of 190°C is observed for specimen loaded at 600MPa.
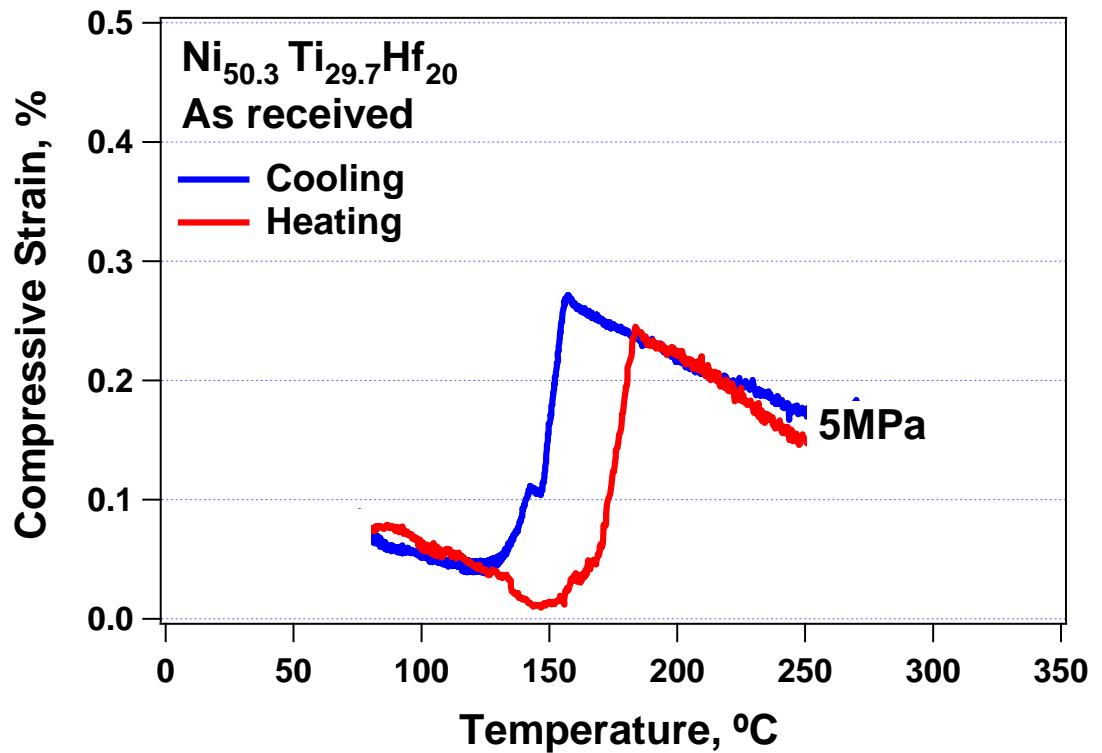
Figure 4.25: Isobaric thermal cycling under 5MPa of $Ni_{50.3}Ti_{29.7}Hf_{20}$ in as extruded condition

Table 4.1. Critical transformation parameters and strain levels for isobaric thermal cycling of $Ni_{50.3}Ti_{29.7}Hf_{20}$ in as extruded condition

Sample	Stress	Ms	Hysteresis	ε_{tr}	ε_{ir}
	100	150	27.1	0.61	0
	200	153	37	1.56	0
As Extruded	300	162.4	43	2.1	0
	400	171.4	49.4	2.2	0
	500	180	60.6	2.4	0.1
	600	190	68	2.6	0.15
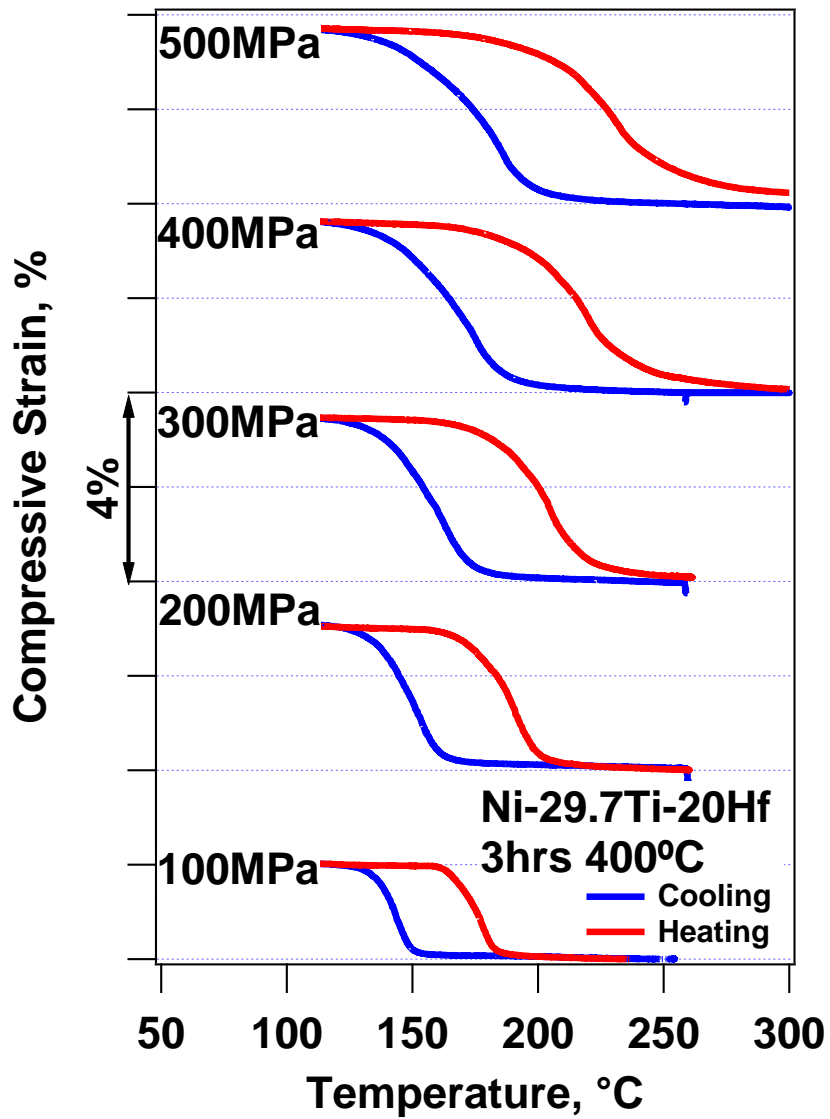
Figure 4.26: Isobaric thermal cycling of $Ni_{50.3}Ti_{29.7}Hf_{20}$ aged at 400°C for 3hours.

Figure 4.26 depicts the transformation behavior of $Ni_{50.3}Ti_{29.7}Hf_{20}$ compression sample aged at 400°C for 3hours under compressive loads varying from 100MPa to 500MPa. In accordance with DSC results reported earlier, the TTs for the specimen aged at 400°C for 3 hours were found to be lower than as extruded sample when found from mechanical tests also. The M_s for 100MPa compressive load was slightly lower as compared to the same load for as extruded specimen. The hysteresis increased in similar fashion as the as-extruded specimen where it increased linearly from 27°C to 54°C with increase in load from 100MPa to 500MPa. However it stayed lower in comparison to as extruded sample. The recoverable strain increases rapidly from 0.98% for 100MPa to 3.3% for 300MPa along with no irrecoverable strain. Slight increase in strain to 3.5% is observed for 400MPa, but the significant finding is that there was still no irrecoverable strain. The strain remained almost constant with further increase in stress levels along with introduction of irrecoveable strain in order of 0.25% as indicated in Table 4.2. This irroverable strain is much less in comparison to near equiatomic NiTi [65-66] for comparative load conditions, especially at higher load levels so much that it is only 0.25% for the alloy in current study in comparison to about 2% for NiTi

Table 4.2: Critical transformation parameters and strain levels for isobaric thermal cycling of $Ni_{50.3}Ti_{29.7}Hf_{20}$ aged at 400°C for 3hours

Sample	Stress	Ms	Hysteresis	ε_{tr}	ε_{ir}
	50	146	27.4	0.984	0
	100	149.24	31.827	1.98	0
3 hours	200	161.3	39	2.87	0
400°C	300	174	45.8	3.3	0
	400	187.8	50	3.5	0.11
	500	194.6	53.5	3.53	0.25

The trend in variation from as extruded sample was also found to be in accordance with the initial findings of the hardness results which indicated the alloy aged for 3 hours at 400°C has higher mechanical strength than the as extruded sample.

Figure 4.27 depicts the transformation behavior of $Ni_{50.3}Ti_{29.7}Hf_{20}$ compression sample aged at 500°C for 3hours under compressive loads varying from 100MPa to 500MPa. With further increment in aging temperature to 500°C while keeping the aging time constant at 3 hours, a substantial increment in TTs was observed. The M_s temperature increased notably from 150°C to 174°C. During the isobaric thermal cycling it was observed that there was no irrecoverable strain even for the highest applied stress level of 500MPa. The hysteresis was found to be very low and was observed to be only 17°C for 100MPa and it increased to 28°C for 500MPa. The strains were found to be lower in comparison of the sample aged at 400°C for the same time. The lower strain can be attributed to formation of the precipitates that decreases the volume fraction of the transforming matrix and the details of levels of strain is given in Table 4.3. The TTs increase clearly evidencing the presence of precipitates but due to the absence of dislocations, it is expected that still there is occurrence of the self accommodation of more than one variants of martensite. The most notable feature of the results from this particular aged specimen is the low hysteresis and as it will shown later in the comparison plot, it is the minimum value of all the aged specimen tested.

Table 4.3: Critical transformation parameters and strain levels for isobaric thermal cycling of $Ni_{50.3}Ti_{29.7}Hf_{20}$ aged at 500°C for 3hours

Sample	Stress	Ms	Hysteresis	ε_{tr}	ε_{ir}
3hours 500°C	100	174	17	1.2	0
	200	182	18	1.65	0
	300	191	22	2.06	0.096
	400	200	28	2.18	0.941
	500	209	28	2.23	0.67
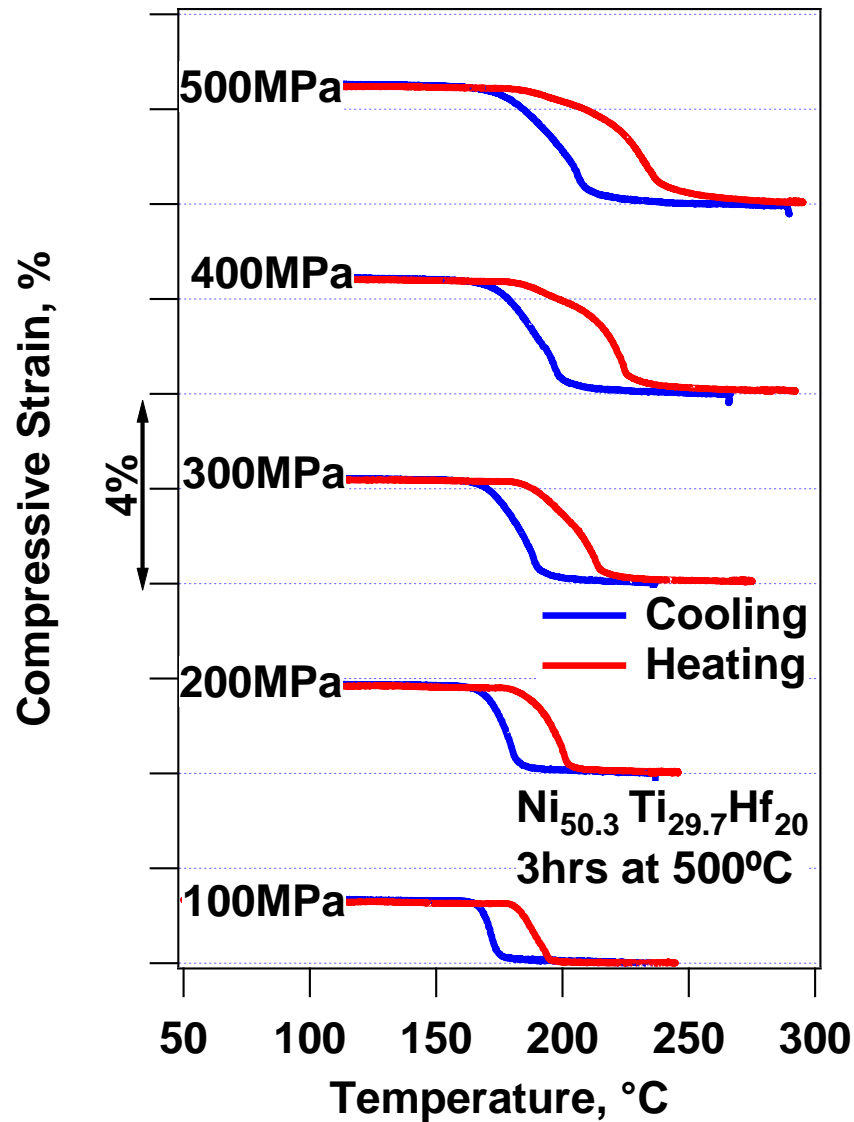
Figure 4.27: Isobaric thermal cycling of $Ni_{50.3}Ti_{29.7}Hf_{20}$ aged at 500°C for 3hours
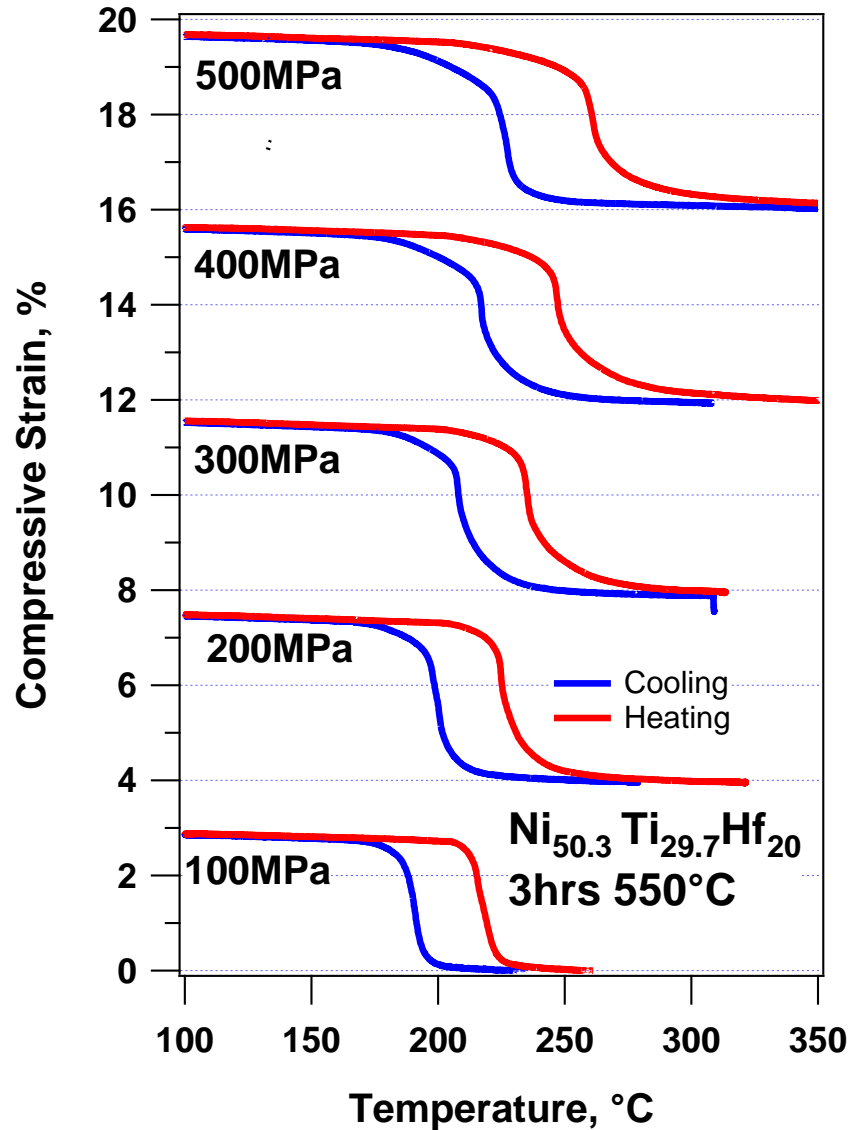
Figure 4.28: Isobaric thermal cycling of $Ni_{50.3}Ti_{29.7}Hf_{20}$ aged at 550°C for 3hours

The plot depicts the mechanical behavior of specimen aged at 550°C for 3 hours. The TEM images presented earlier showed presence of finely dispersed precipitates throughout the structure. The plot depicts very high recoverable strain upon application of even low stress levels. When the sample is loaded to 100MPa, a fully recoverable strain of 2.65% is observed, which is in fact is more than the maximum achieved strain for the same alloy aged at 500°C for 3 hours. With further increment in stress levels, the

recoverable strain increases to a maximum of 3.6% for 300MPa, and upon further loading the strain is observed to decrease very minimally to 3.3%. The details of the transformation parameters are presented in Table 4.4. Along with high recoverable strains, no irrecoveable strain is observed even for 500MPa and also the hysteresis is found to be very low and relatively constant between 25°C to 26°C for all loads tested except for 500MPa level, at which it increases slightly to 30°C. The TTs are observed to be generally very high for the specimen, the M_s for 100MPa is observed to be 195°C and it increases linearly to 230°C for 500MPa. The TTs in the vicinity of 200°C have been reported earlier for similar alloys but no or very little mechanical tests have been presented [61-62]. The findings of the present work show high TTs along with superb shape memory properties which make this aged alloy a very formidable candidate for commercial use.

Table 4.4: Critical transformation parameters and strain levels for isobaric thermal cycling of $Ni_{50.3}Ti_{29.7}Hf_{20}$ aged at 550°C for 3hours

Sample	Stress	Ms	Hysteresis	ε_{tr}	ε_{ir}
3hours 550°C	100	194.87	26.39	2.65	0
	200	202.9	26.5	3.23	0
	300	219.587	25.86	3.59	0
	400	229.05	29.27	3.375	0.184
	500	230.63	35.317	3.287	0.116
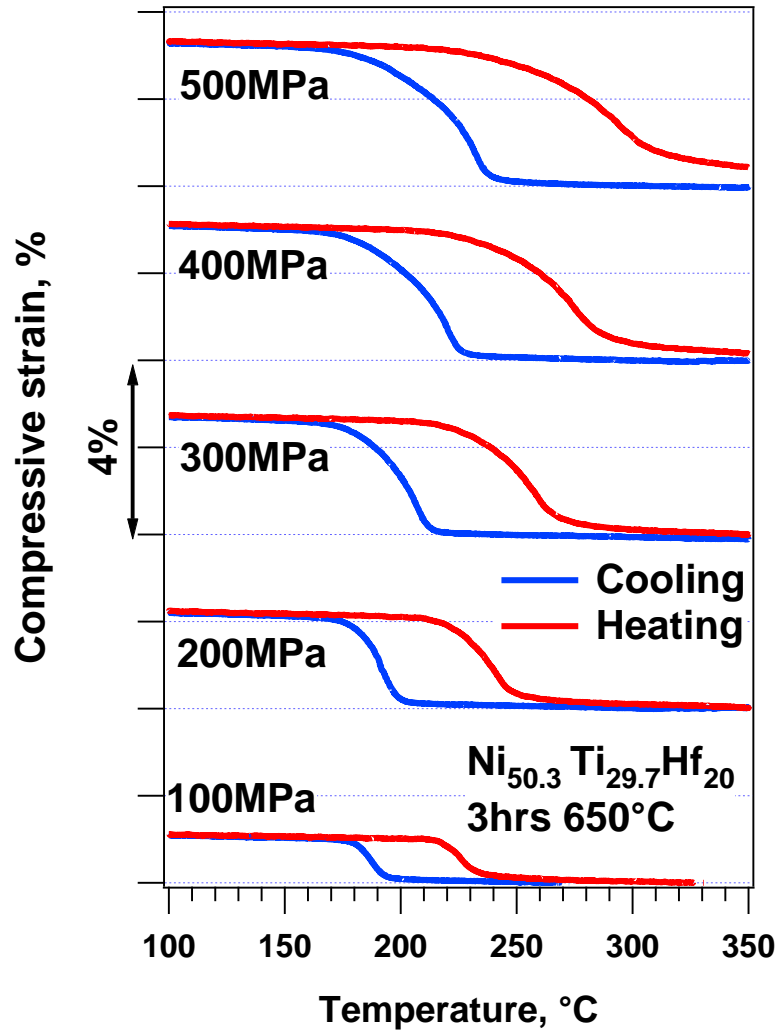
Figure 4.29: Isobaric thermal cycling of $Ni_{50.3}Ti_{29.7}Hf_{20}$ aged at 600°C for 3hours

The mechanical response for the specimen aged at 650°C for 3 hours is depicted in Figure 4.29. The TTs were found to be comparable to the previously mentioned specimen that was aged at 550°C for the same time. The recoverable strains were observed to decrease substantially in comparison to the above mentioned sample, only 1% recoverable strain was observed in comparison to 2.65% for specimen aged 3hours at 550°C. Fully recoverable strain was observed only till the loading level of 300MPa, further loading to 400MPa and 500MPa resulted in 0.15% and 0.32% irrecoverable

strain. The strain was observed to reach the maximum of 3% for 400MPa and remained

constant for further loading to 500MPa along with 0.32% irrecoverable strain as

presented in Table 4.5. This drop in strength of the material can be attributed to the large

and incoherent precipitates that were presented earlier in form TEM images.

Table 4.5: Critical transformation parameters and strain levels for isobaric thermal
cycling of $Ni_{50.3}Ti_{29.7}Hf_{20}$ aged at 650°C for 3hours

Sample	Stress	Ms	Hysteresis	ε_{tr}	ε_{ir}
3hours 650°C	100	193	38	1	0
	200	197.8	46.2	2	0
	300	212.9	52.5	2.5	0.147
	400	226.34	53	3	0.16
	500	240	67.4	3.1	0.328

The Figure 4.30 depicts the comparisons for recoverable strains under various

applied loads for the specimen aged for 3 hours at temperatures ranging from 300°C to

650°C. The strain was observed to be minimum at applied load level of 100MPa for all

specimen tested. This can be attributed to the selection of mix of martensite variants

which results in less than maximum achievable strain. The value for recoverable strain

increases with a general trend for all mentioned specimen with a steep rise till 300MPa,

after which it becomes almost constant for most cases. The strain was observed to

increase by small increment in specimen aged at 650°C but it was accompanied by

irrecoverable strain and hence the total recoverable strain remained almost constant. The

total recoverable strain for specimen aged at 550°C was observed to decrease for 400MPa

and 500MPa loads contrary to other specimen. The maximum recoverable strain of 3.6%

was observed for 3hours 550°C aged specimen at 300MPa while the minimum of 0.64%

was observed for as extruded specimen at load of 100MPa.
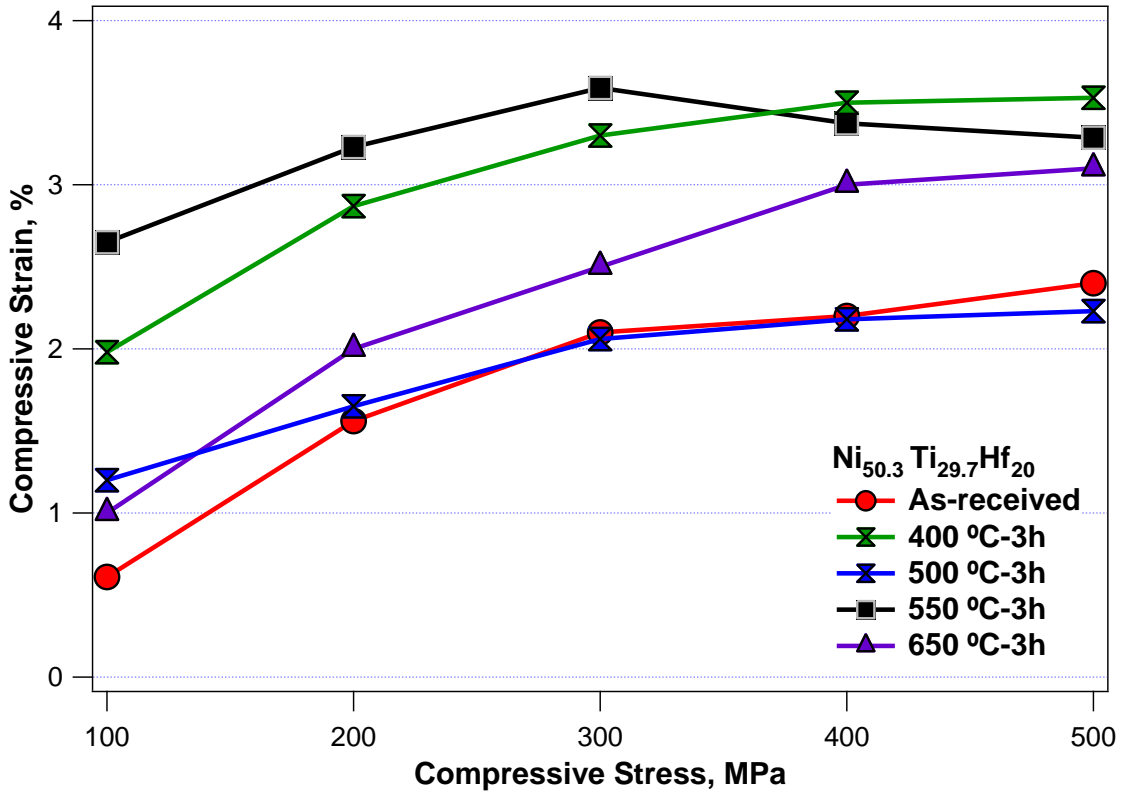
Figure 4.30: Comparison plots depicting the recoverable strain for $Ni_{50.3}Ti_{29.7}Hf_{20}$ aged at varying temperatures for 3hours

Plot depicting the comparison for thermal hysteresis is presented in Figure 4.30. Hysteresis is important for applications requiring high frequency of response and minimal values are more suited for high frequency applications. The hysteresis was generally observed to increase for all specimen with increase in applied loads except for the specimen aged at 550°C, for which it more or less remained constant and in fact was minimum for 300MPa load level which also corresponds to the maximum recoverable strain. The minimum hysteresis was observed for specimen aged at 500°C for 3hours, which increased slightly from 16°C at 100MPa to 22°C at 300MPa. The hysteresis was observed to be almost same for as extruded specimen and the one aged at 400°C for 3

hours, and except for specimen aged at 650°C for which the hysteresis was higher than the as extruded specimen, the hysteresis was decreased by aging treatment.
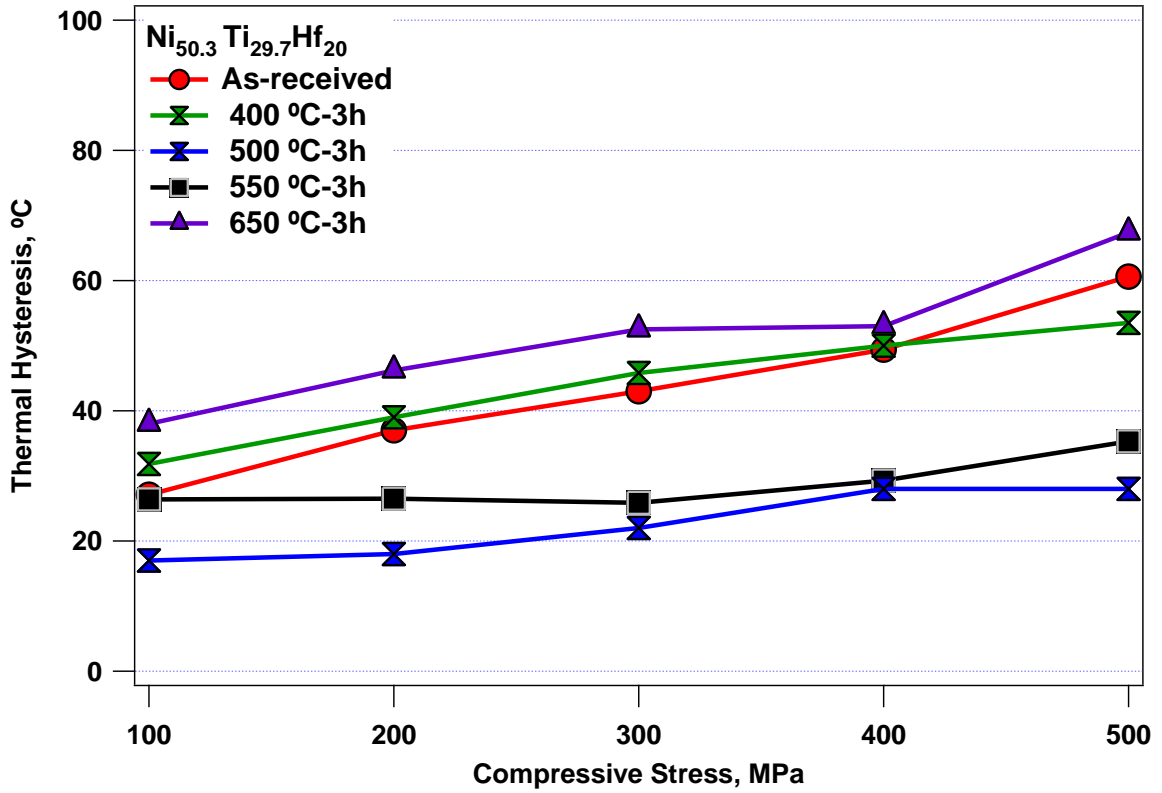
Figure 4.31: Comparison plots depicting thermal hysteresis for $Ni_{50.3}Ti_{29.7}Hf_{20}$ aged at varying temperatures for 3hours
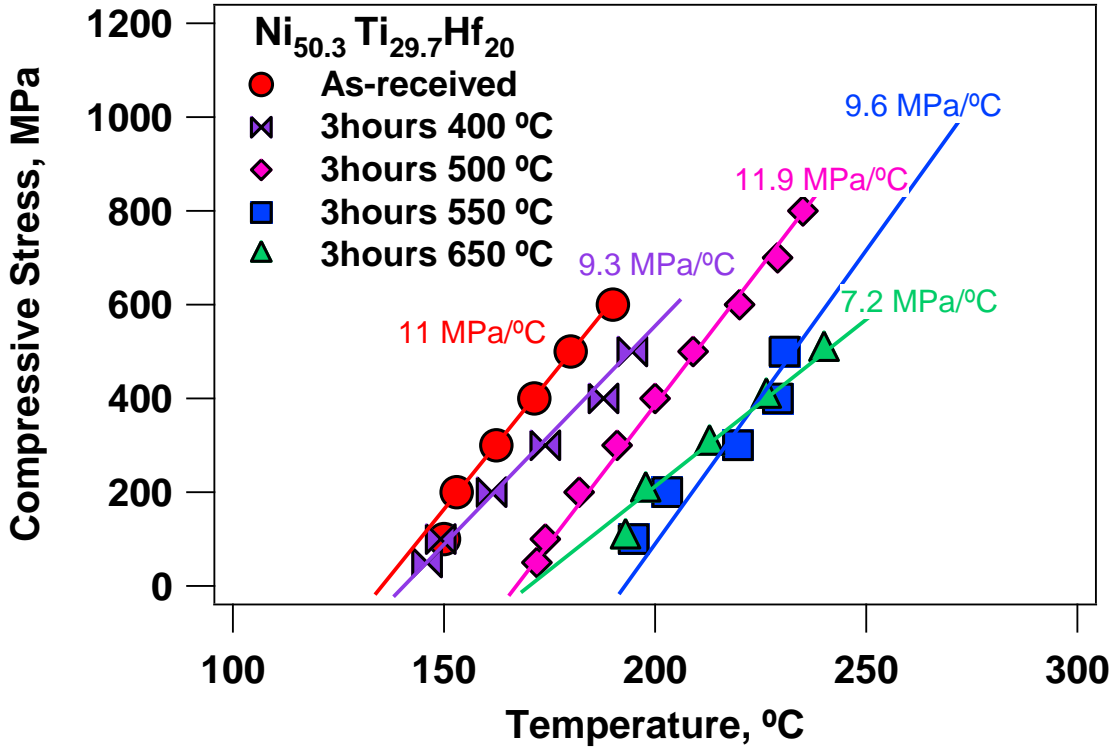
Figure 4.32: Clausius-Clayperon curves for $Ni_{50.3}Ti_{29.7}Hf_{20}$ aged at varying temperatures for 3hours with respect to M_s temperatures.

Figure 4.32 depicts the M_s temperatures under different applied compressive loads of the previously mentioned specimen. These M_s temperatures have been plotted vs the level of applied compressive stress. The curves presented in the above plot are usually referred to as Clausius-Clayperon curves. The TTs increase linearly with any corresponding increment in the load. These curves assume high significance for the prediction of the TTs under various loading conditions without having to do so experimentally and hence save effort and capital. The above plot shows the slope of the lines for each specimen tested, along the path of which the TTs for higher loads can be predicted.
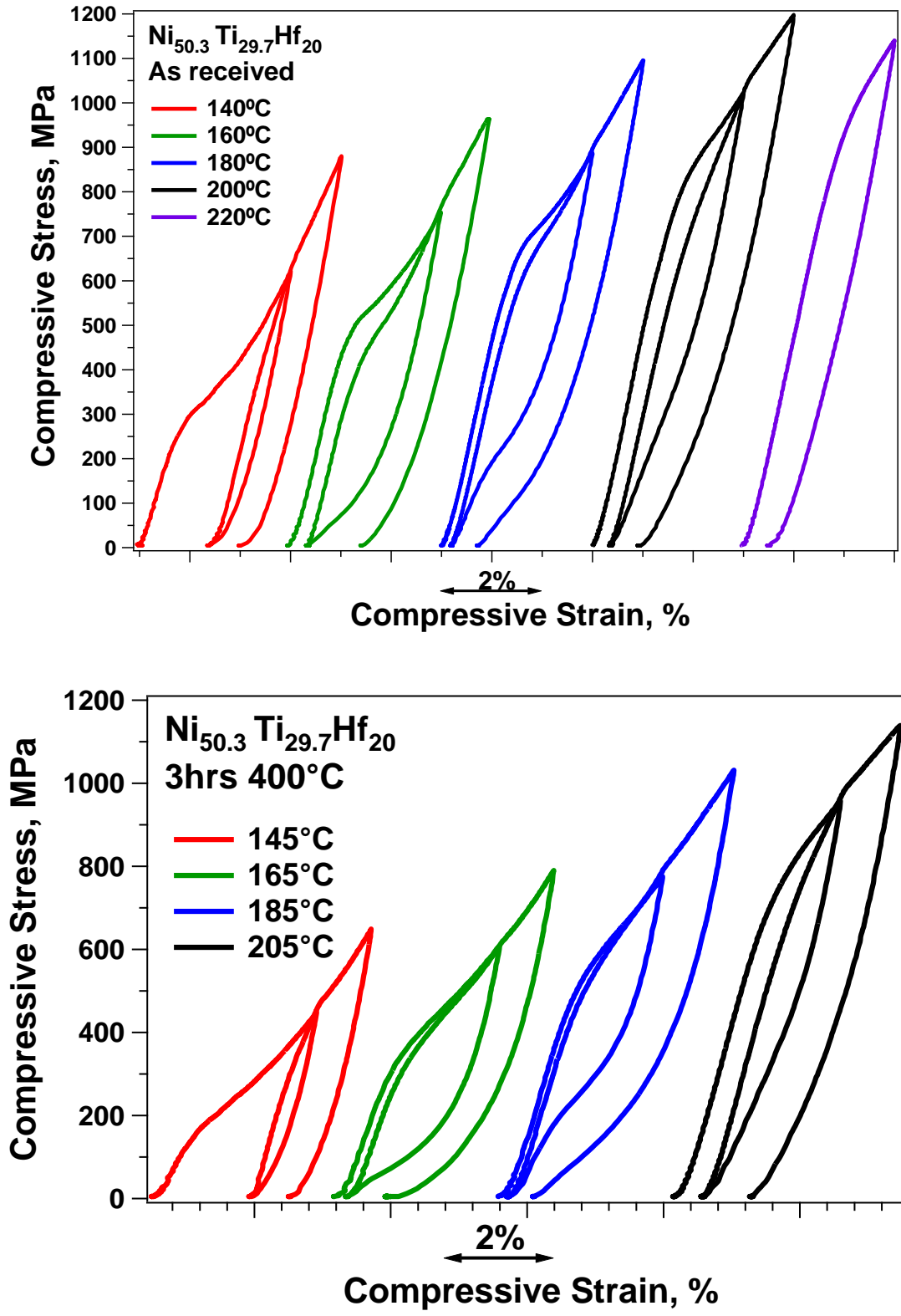
Figure 4.33: Isothermal mechanical cycling of $Ni_{50.3}Ti_{29.7}Hf_{20}$ in as extruded condition (top) and aged for 3 hours at 400°C(bottom)
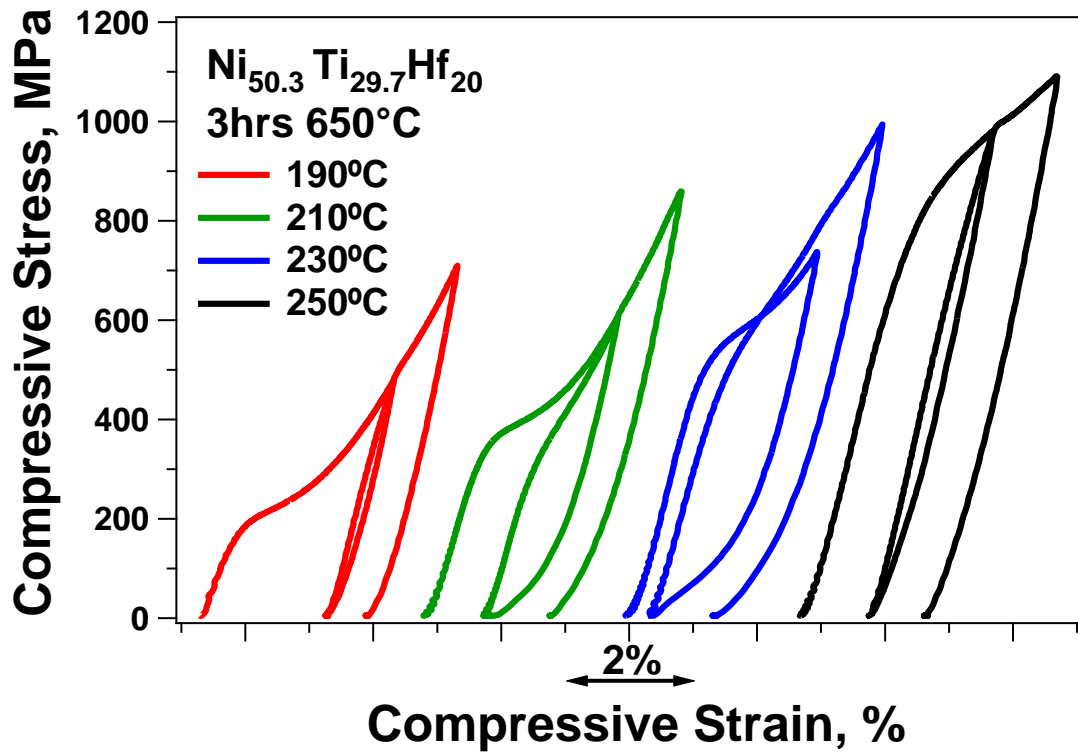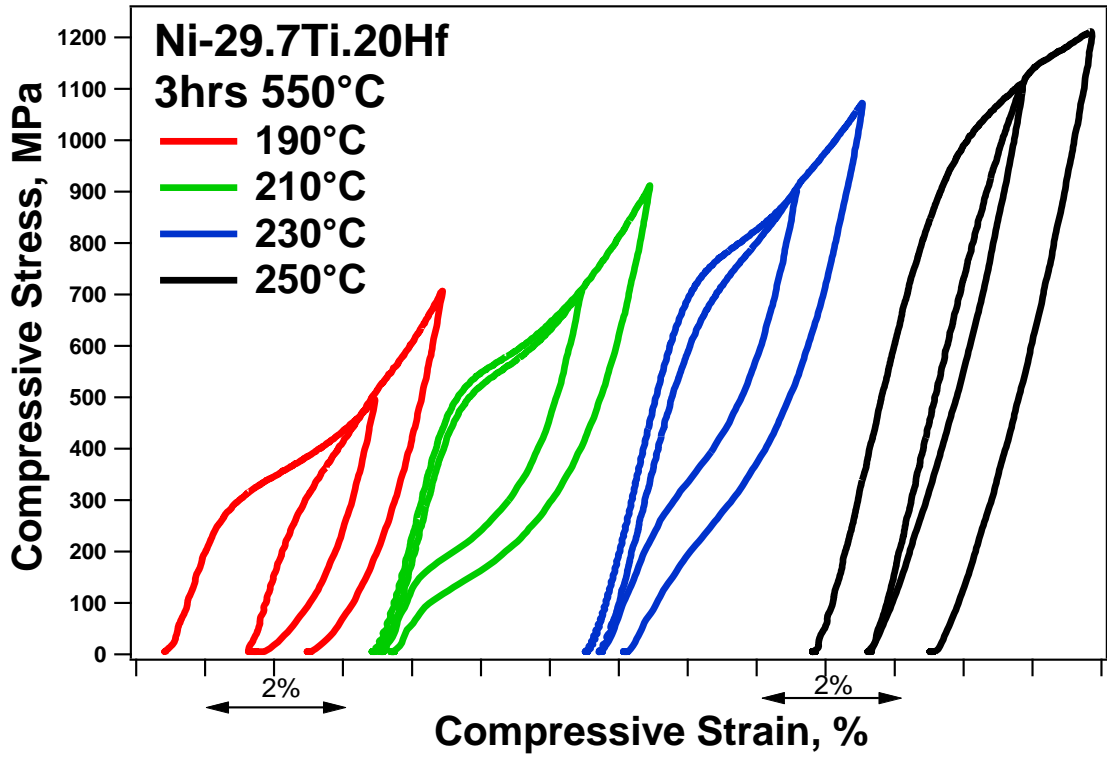
Figure 4.34: Isothermal mechanical cycling of $Ni_{50.3}Ti_{29.7}Hf_{20}$ aged for 3 hours at 550°C (top) and 650°C(bottom)

Table 4.6. Critical transformation parameters and strain levels for isothermal mechanical cycling of $Ni_{50.3}Ti_{29.7}Hf_{20}$ in as extruded condition

Sample	Testing Temperature °C	Total Strain %	Elastic Recovery%	PE Strain %	SME on heating %	Irrecover-able strain %
As extruded	140	4	1.42	0.66	1.92	0
	160	4	1.324	1.207	1.469	0
	180	4	1.6336	1.604	0.7624	0
	200	4	1.931	1.2	0.65	0.219
	220	3	1.6	1.084	0.08	0.236

The plots shown in Figure 4.33 and 4.34 depict the isothermal compressive loading and unloading curves for the specimen in as extruded condition and aged for 3 hours at 400°C, 550°C and 650°Cand the specific values for strain as depicted earlier in the schematic in Figure 1.3 are presented in Tables 4.6 to 4.10. The lowest testing temperature was selected to be 10°C higher than the M_s temperature for the specimen and the further testing was done at 20°C higher than the previous testing temperature. The temperature at which the test was run was achieved by cooling from temperature higher than A_f, to ensure that the sample was in austenitic state. The specimen was then loaded to 3% and 4% compressive strain calculated beforehand while maintaining stable temperature.

In Figure 4.33(a), the results for as extruded specimen are shown. When the specimen was loaded at 140°C, the stress induced transformation from austenite to martensite is observed but during the unloading the back transformation was not observed leaving behind 3% unrecovered strain, which however could be recovered fully upon heating. The test at 160°C yielded similar behavior but the irrecoverable strain was of the order of 1.5%. 3% loading at 180°C yielded an almost perfect PE curve with large

hysteresis, further when the sample was loaded to 4%, an irrecoverable strain of 0.8% was observed. Further tests at higher temperatures resulted in higher transformation stresses and these high stress can be held responsible for inducing dislocations in the material as plastic strain was observed in order or 1% for testing at 200°C while at 220°C the unloading curve even at 3% did not show any PE recovery and hence no further tests were done.

Table 4.7: Critical transformation parameters and strain levels for isothermal mechanical cycling of $Ni_{50.3}Ti_{29.7}Hf_{20}$ aged at 400°C for 3 hours

Sample	Testing Temperature °C	Total Strain %	Elastic Recovery%	PE Strain %	SME on heating %	Irrecover-able strain %
3hours 400°C	145	4	0.89	0.6	2.51	0
	165	4	1.1	1.73	1.17	0
	185	4	1.35	2.26	0.45	0
	205	4	1.6	1.17	0.43	0.8

As shown in Figure 4.33(b) the loading and unloading for sample aged at 400°C for 3 hours showed behavior similar to as extruded sample when tested at 145°C. The proximity of testing temperature to the M_s temperature can be held responsible for no back transformation once martensite nucleates upon application of stress. Notably the tests for 3% at both 165°C and 185°C yield almost perfect PE curves. The stress hysteresis for 185°C test is observed to be lower than 165°C test. Loading to 4% for both testing temperatures show PE recovery but a residual strain of 1% for 165°C testing temperature and 0.4% for 185°C is observed. Further increment of testing temperature to 205°C lead to transformation stress around 800MPa and possibly due to this high stress dislocations were introduced and hence plastic strain of 1.5% was observed. The

improvement of PE properties from as extruded to 3hours aging at 400°C can be attributed to presence of precipitates which strengthen the material such that the critical resolved stress is increased beyond the transformation stress and hence PE effect is observed, and this is in contrast to the attempt made by Liu and Meng in their work on similar composition [67]. In their study the HTSMA with composition $Ni_{49}Ti_{36}Hf_{15}$ was loaded at temperature above A_f between the range of 250°C to 270°C, but no PE was observed. The inexistence of the PE was attributed to the dislocation slip occurring simultaneously with stress induced martensite, which is due to the lower critical stress in contrast to the behavior observed in the aged alloy in the present study.

Table 4.8: Critical transformation parameters and strain levels for isothermal mechanical cycling of $Ni_{50.3}Ti_{29.7}Hf_{20}$ aged at 550°C for 3 hours

Sample	Testing Temperature °C	Total Strain %	Elastic Recovery%	PE Strain %	SME on heating %	Irrecover-able strain %
3hours 550°C	190	4	1.05	0.873	2.077	0
	210	4	1.2	2.544	0.256	0
	230	4	1.35	2.1	0.5	0.1
	250	4	1.512	0.78	0.3	1.4

Presence of finely dispersed precipitates were shown in TEM micrographs for the specimen aged at 550°C for 3 hours and their effect is clearly observed in PE tests as depicted in Figure 4.34 (a). At 190°C the curve is not highly representative of perfect PE curves but when loaded at 210°C and 230°C, near perfect PE curves are observed. The observed PE behavior is one of the first perfect PE behavior noted for HTSMAs at temperature range of 200°C. Full 4% recovery with very little residual strain is observed for sample loaded at 210°C while at 230°C a residual strain of 0.34% was observed. Further increment in testing temperature led to very high transformation stress and about

2% plastic strain is observed for loading the sample to 4% at 250°C. The finely dispersed particles can be attributed to strengthening the material so that even at 1000MPa, very little plastic strains are observed, and since the increment in critical stress for slip is increased beyond transformation stress levels, the near perfect PE behavior is observed. This PE behavior observed confirms the contribution of the effect of aging towards increment in critical stress for slip beyond the critical stress for transformation, which is essential for PE. Wang and Zheng [68] showed the inexistence of PE in $Ni_{49}Ti_{36}Hf_{15}$ citing occurrence of plastic deformation simultaneously with stress induced martensite, which is avoided in the present case due to higher strength of aged alloy. In comparison to the sample aged at 550°C for 3 hours, the sample aged at 650°C for the same time was observed to have larger incoherent precipitates. These incoherent precipitates have been reported in the literature to have lesser contribution to strengthening of material since the distance between them increase and it is easier for the slip to break through them. This effect is clearly observed when the PE tests for the mentioned specimen as shown in Figure 4.34 (b) are closely observed. The TTs of the 650°C, 3hour aged specimen are observed to be higher in comparison to 3 hours 550°C and this can be attributed to the larger volume fraction of the precipitates but consequently due to larger incoherent size the precipitates are unable to contribute to the strength to the extent previously as in case of 3 hours 550°C aged specimen. The loading at 190°C shows behavior similar to other specimen when aged at temperatures in vicinity of M_s. Loading at 210°C to 4% resulted in 2.1% unrecovered strain while only 0.5% irrecoverable strain was observed for 3% loading at 230°C. 4% straining of the specimen at 230°C resulted in 1.5% irrecoverable strain. The transformation stress increased to more than 900MPa for loading at 250°C

and the unloading curve was observed to be parallel to loading curve and 2% irrecoverable strain is observed for 4% loading. The diversion from PE behavior in case of the specimen aged at 650°C for 3 hours can be attributed to lower strength of material and as a result dislocations are introduced in the material even before the material transforms and hence the plastic strain instead of PE effect is observed.

Table 4.9: Critical transformation parameters and strain levels for isothermal mechanical cycling of $Ni_{50.3}Ti_{29.7}Hf_{20}$ aged at 650°C for 3 hours

Sample	Testing Temperature °C	Total Strain %	Elastic Recovery%	PE Strain %	SME on heating %	Irrecover-able strain %
3hour 650°C	190	4	0.95	0.41	2.64	0
	210	4	1.19	0.84	1.89	0
	230	4	1.478	1.14	1.06	0.322
	250	4	1.53	0.564	0.53	1.376
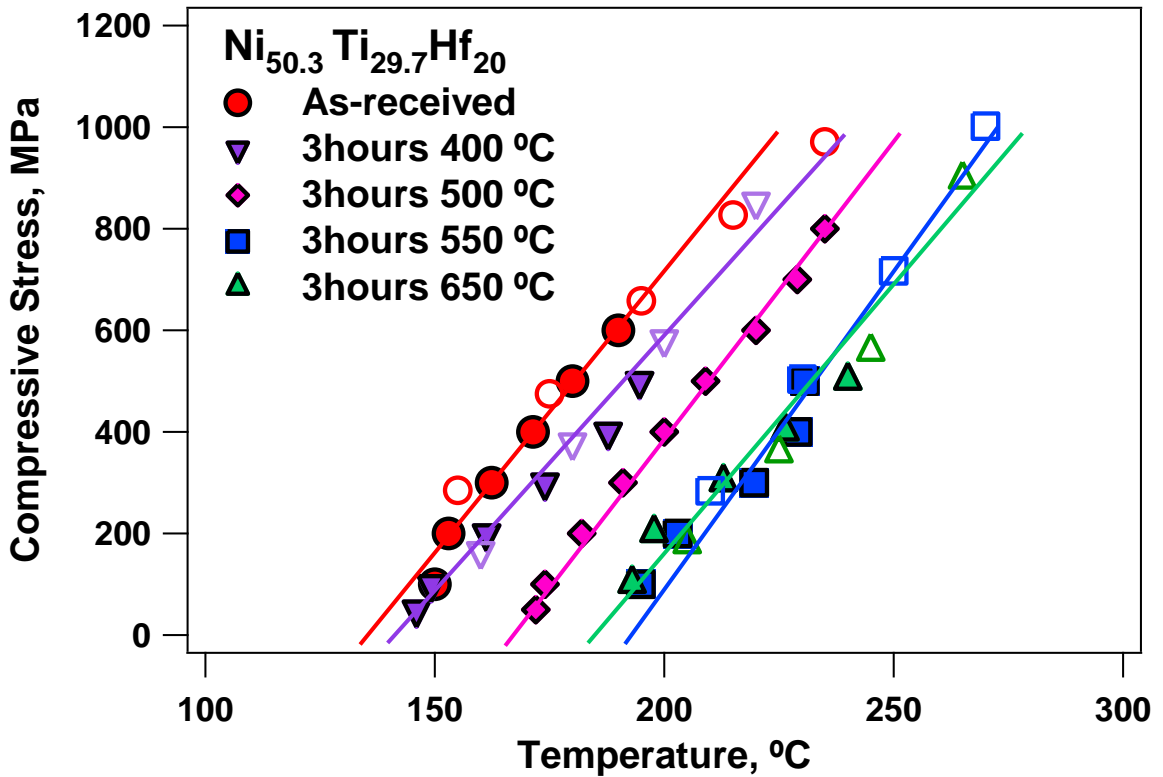
Figure 4.35: Clausius-Clayperon curves for $Ni_{50.3}Ti_{29.7}Hf_{20}$ aged at varying temperatures for 3hours with respect to M_s temperatures.

Figure 4.35 depicts the comparison of the Clausius-Clayperon curves for $Ni_{50.3}Ti_{29.7}Hf_{20}$ determined from the isobaric cycling presented in solid markers and the hollow markers presenting the results from the PE cycling of the corresponding sample. The overlapping curves further cement the validity of the results and the slope of the curve can be used in confidence for prediction of results.
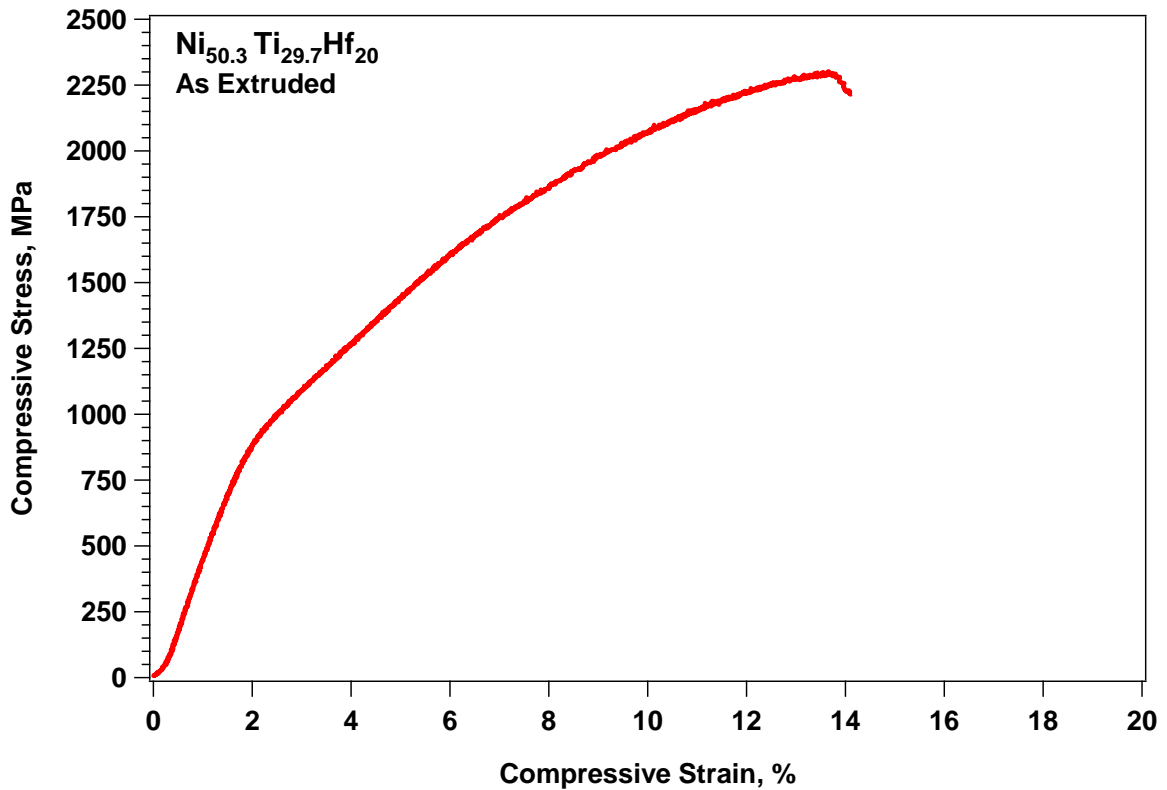
Figure 4.36: Ultimate yielding curves for $Ni_{50.3}Ti_{29.7}Hf_{20}$ compression samples in as extruded sample

The Figure 4.36 depicts the ultimate faliure stress-strain plot for $Ni_{50.3}Ti_{29.7}Hf_{20}$ sample in compression in as extruded condition. The material was found to be very strong and able to withstand till a high stress level of 2450MPa. The material failed at a strain of about 15% in compression. The sample was tested after training and hence due to presence of TWSME, the initial region of loading is missing in the plot.

Chapter Five

Experimental results $Ni_{45.3}Cu_5Ti_{29.7}Hf_{20}$

Results for $Ni_{45.3}Cu_5Ti_{29.7}Hf_{20}$ aged under different conditions have been presented in form of calotimetric analysis, TEM micrographs and XRD. The effect of the aging on the TTs is presented first followeded by observation of its effect on the microstructure of the material. The mechanical results are presented in the later sections showing the corelation of the effects of aging on the microstructure and the mechanical properties of the material.
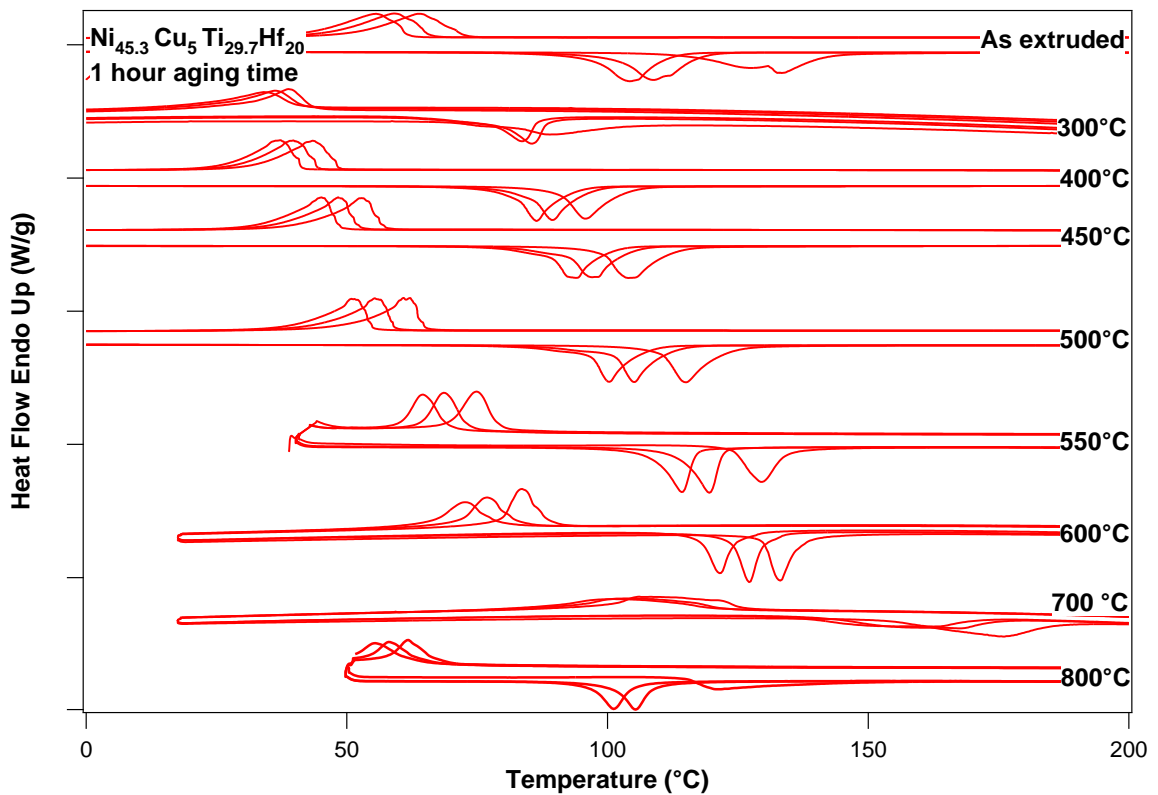
Figure 5.1: DSC plot showing the thermal cycling for $Ni_{45.3}Cu_5Ti_{29.7}Hf_{20}$ alloy aged for 1 hour ranging from 300°C to 800°C.

5.1 Calorimetry Analysis

Figure 5.1 shows the transformation behavior for $Ni_{45.3}Cu_5Ti_{29.7}Hf_{20}$ alloy aged for 1 hour at temperatures ranging from 300°C and 800°C. As explained in section 4.1, 3 cycles were run to check for cyclic stability. The TTs of $Ni_{45.3}Cu_5Ti_{29.7}Hf_{20}$ alloy were observed generally to be lower than that of $Ni_{45.3}Ti_{29.7}Hf_{20}$ alloy by about 40°C for similar aging conditions.

The TTs were observed to vary in a very linear trend after dropping initially for aging at 300°C in comparison for as extruded condition. The transformations are observed to have wide hysteresis between the start and finish of the transformation. The peaks for transformation temperatures as depicted in Figure 4.2.1 show that for all aging temperatures, the TTs decrease for every cycle by about 4-5°C. Sharpest peaks were observed for the specimen aged between 500°C and 600°C, though the cyclic stability was not observed. The maximum TTs were observed for 700°C aging temperature but the transformation was accompanied by broad peaks, second and third peaks however were noticed to be overlapping each other and showing highest degree of cyclic stability in this set of aging conditions. Further increase in aging temperature to 800°C led to fall of TTs below even the levels of as extruded condition and further aging at higher temperatures was not done.

The Figure 5.2 depicts the comparison for austenite and martensite peaks for the second cycle of the DSC curves presented in Figure 5.1. The TTs are observed to decrease significantly after aging at 300°C for 1 hour by an average of 25°C for both forward and back transformations and from there on, an increment of TTs in a linear path is observed with further increment in aging temperature to 600°C. This is followed by

sudden rise of 35°C in TTs for 700°C aging temperature followed by a steep fall for 800°C aging temperature. The TTs are observed to be lower in comparison to as extruded condition till the aging temperature of 500°C despite gradually increasing after 300°C aging temperature. The hysteresis for the transformation increased slightly for aging at 300°C and 400°C in comparison to as extruded sample, after which it stabilized in proximity of 49°C for aging temperature till 600°C. The maximum hysteresis of 60°C was recorded for aging at 700°C, after which it fell again to 47°C for aging at 800°C

$Ni_{45.3}Cu_5Ti_{29.7}Hf_{20}$ Aging for 1 hour

	As Extruded	300°C	400°C	450°C	500°C	550°C	600°C	700°C	800°C
A peak	110.27	85.238	89.34	97.88	103.68	119.2	127.14	161.86	105.8
M Peak	59.16	36.43	39.48	48.29	55.661	68.904	77.227	101.71	58.308
Hysteresis	51.11	48.808	49.86	49.59	48.019	50.296	49.913	60.15	47.492
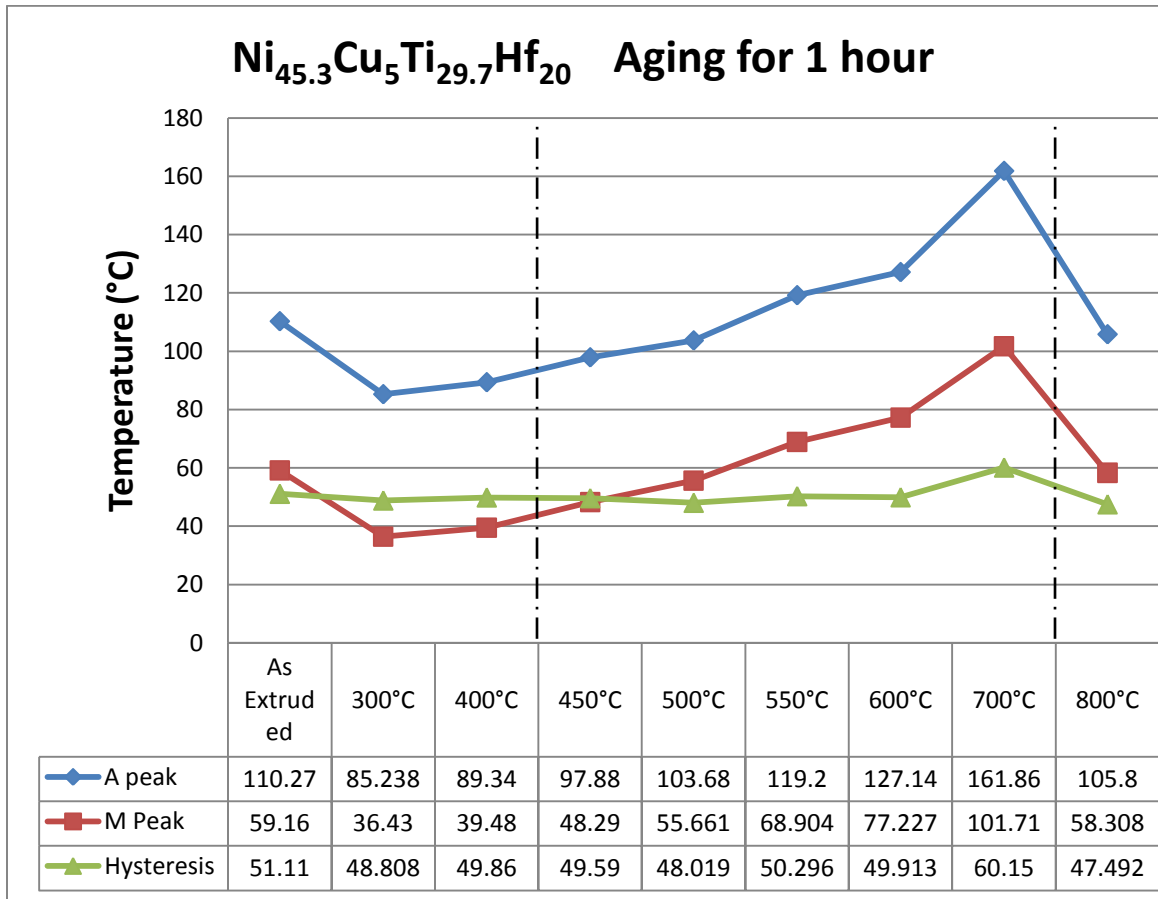
Figure 5.2: Comparison plot showing the peak temperatures for $Ni_{45.3}Cu_5Ti_{29.7}Hf_{20}$ alloy aged for 1 hour ranging from 300°C to 800°C.

Figure 5.3 depicts the transformation behavior in the DSC for 3 cycles of $Ni_{45.3}Cu_5Ti_{29.7}Hf_{20}$ alloy aged for 3 hours between the temperature range of 300°C to 800°C. Analogously to aging for 1 hour, in aging for 3 hours also, an initial descend is observed in TTs for 300°C from the as extruded condition. But contrary to the increment in TTs for aging at 400°C for 1 hour, the TTs were observed to further plummet for 400°C aging temperature for 3hours. The TTs were then observed to increase with aging temperature of 500°C and continued to increase till aging at 650°C after which it became constant for 700°C followed by drop to initial levels of as extruded condition for aging at 800°C.

Sharp peaks were first observed for the 400°C aging with the lowest TTs for the alloy, about 40°C lower than the as extruded condition. The transformation peaks stabilized significantly for corresponding temperatures when the aging time was increased from 1 hour to 3 hours. In addition to the temperatures selected for 1 hour time, 650°C for 3 hours was also done since the TTs increased substantially by increasing aging temperature from 600°C to 700°C at 1 hour, but the peaks were very broad. Aging at 650°C for 3 hours yielded TTs very similar to the 700°C but with less broader peaks. The transformation peaks for aging at 800°C were very similar to as extruded condition evidencing the recrystallization of the material and hence neutralizing the effect of any precipitates formed at lower aging temperatures.
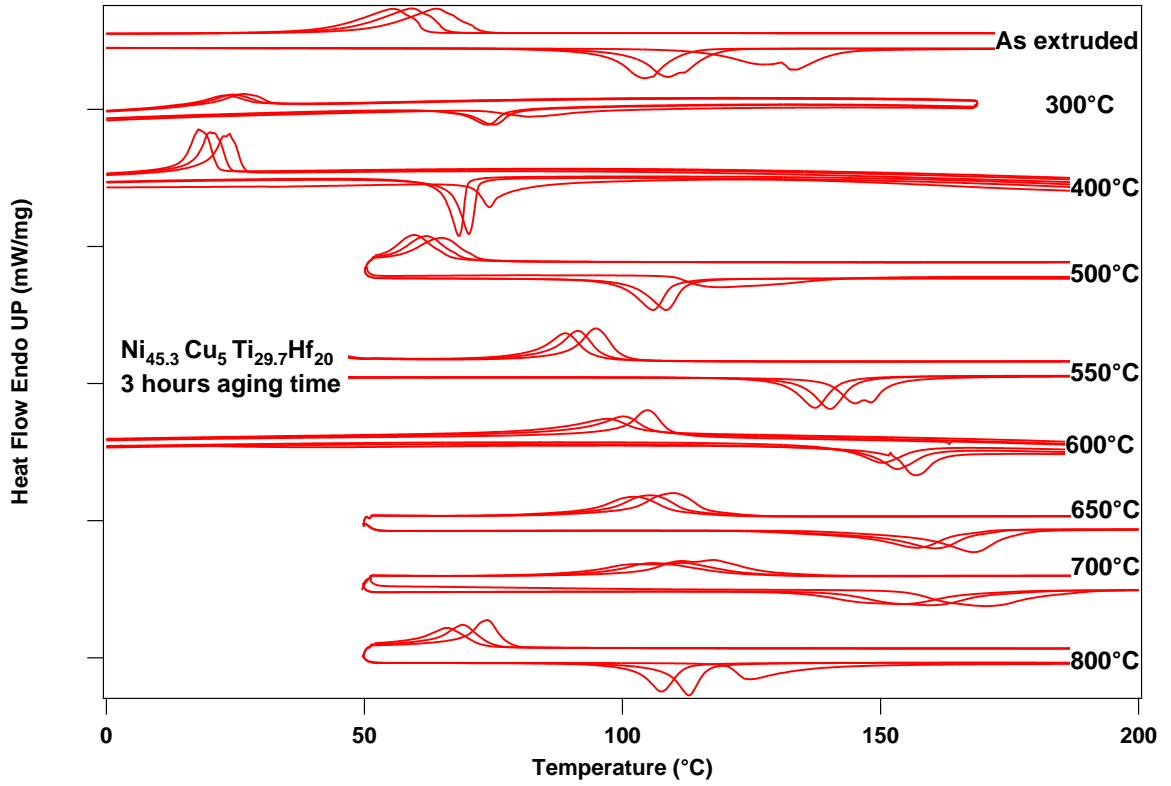
Figure 5.3: DSC plot showing the thermal cycling for $Ni_{45.3}Cu_5Ti_{29.7}Hf_{20}$ alloy aged for 3 hours ranging from 300°C to 800°C.
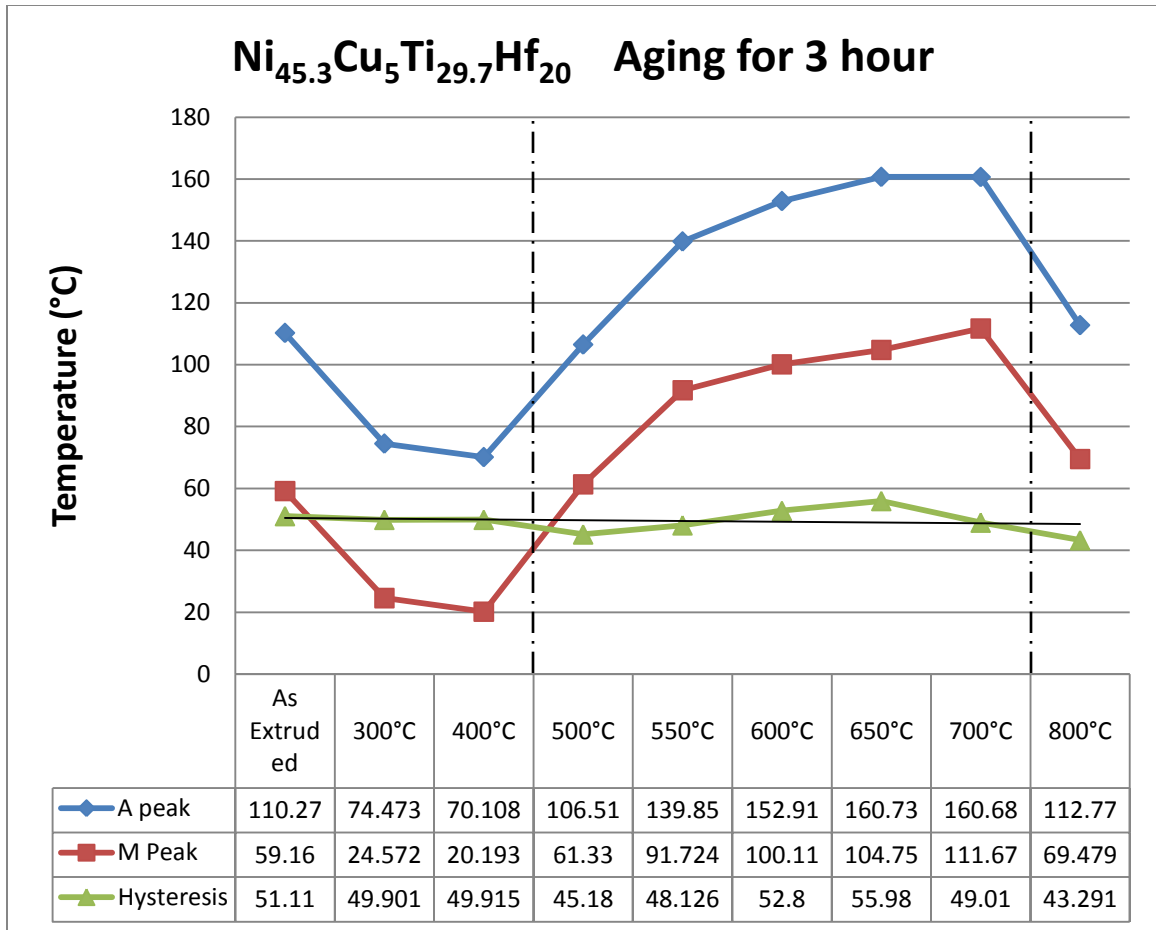
Figure 5.4: Comparison plot showing the peak temperatures for $Ni_{45.3}Cu_5Ti_{29.7}Hf_{20}$ alloy aged for 3 hours ranging from 300°C to 800°C.

Figure 5.4 depicts the transformation peaks for the DSC experiments shown in the earlier figure along with the hysteresis for the transformation. The most notable feature of the alloy is the range of the TTs that can be achieved by simply varying the aging conditions for tailoring the alloys to suit multiple working conditions. The difference between the highest and the lowest transformation is observed to be 90°C for aging at 400°C and 700°C for 3 hours each. As described earlier in the Figure 5.3, the TTs were observed to fall about 20°C initially for aging till temperature of 400°C, after which the TTs increased sharply to 50°C above as extruded condition till 550°C aging temperature. Further increment in the aging temperature yielded more subtle increase in the TTs with a

maximum of 160.7C for aging at 700°C. Similar to aging for 1 hour, aging for 3 hours at 800°C also led to decrease in the TTs to the initial level as observed for as extruded condition. The trend in variation of TTs is similar to $Ni_{45.3}Ti_{29.7}Hf_{20}$ for corresponding aging conditions, hence possible following the same trend in evolution of precipitates also. Even as the alloy was extruded under similar conditions of high temperature as for $Ni_{45.3}Ti_{29.7}Hf_{20}$, some cold working is believed to have been imparted to the material during the processing. The relief of this cold work or the dislocations introduced during extrusion by aging at 300°C and 400°C could be responsible for the decrease in TTs to such low levels, since the volume fraction of the precipitates formed in $Ni_{45.3}Ti_{29.7}Hf_{20}$ was very small under these conditions and their contribution to increment in TTs is hence observed to be overpowered by relief of dislocations.

The precipitation of Ni rich precipitates is evident from the trend in variation of TTs for aging between the temperature range of 500°C and 700°C. The depletion of Ni from the matrix continues with increment in volume fraction of Ni rich precipitates and the TTs reach their maximum value for aging at 700°C. This is followed by inversion of the trend when the temperature is too high at 800°C for the precipitates to further evolve and are then believed to have completely dissolved which can be concluded by looking upon the resemblance with transformation behavior with as extruded condition.

The hysteresis was not observed to vary largely by variation in aging conditions and mostly remained within the 10°C range about 50°C mark. Even though the hysteresis was observed to be minimum of 43°C in possibly precipitate free condition for aging at 800°C, followed by aging at 500°C, which was marginally higher at 45°C.
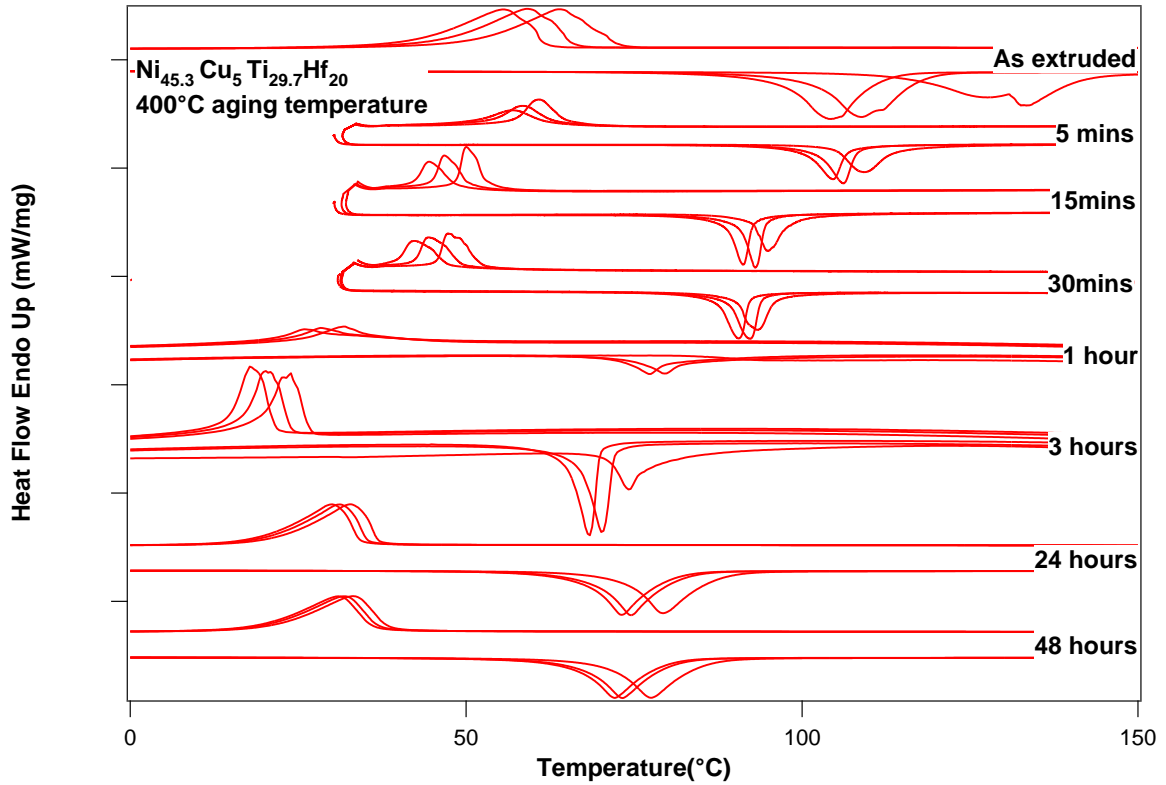
Figure 5.5: DSC plots showing the variation in TTs for $Ni_{45.3}Cu_5Ti_{29.7}Hf_{20}$ alloy aged at 400°C for time range between 5 minutes and 48 hours.

Figure 5.5 depicts the transformation behavior for $Ni_{45.3}Cu_5Ti_{29.7}Hf_{20}$ aged at 400°C for the time range between 5minutes and 48 hours. The TTs were observed to reach the minimum values for aging at 400°C for 3 hours, and hence this detailed study was conducted to check the effects of aging time for aging at 400°C. Smaller time intervals were introduced between as extruded condition and 1 hour to clearly study the effect of time, since the TTs dropped significantly in this region. Clearly visible in the plot, the TTs decrease initially very linearly till aging time of 3 hours after which the TTs were observed to stay almost constant when the time was increased to 24 hours and 48 hours. Very low cyclic stability was observed till the time of 3 hours, while when aged at

24 hours and 48 hours, second and third cycle were observed to overlap each other after the first cycle effect.
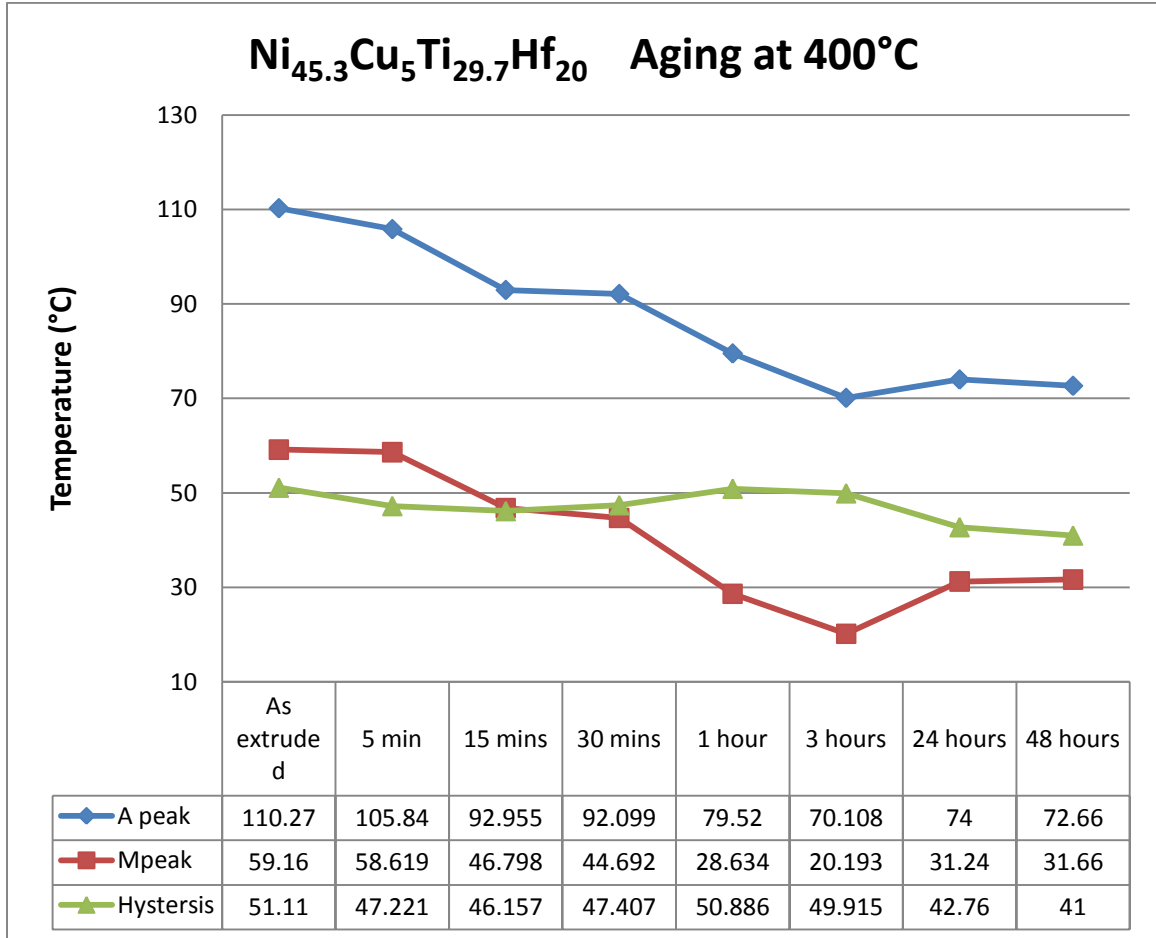
Figure 5.6: Comparison plot showing the peak temperatures for $Ni_{45.3}Cu_5Ti_{29.7}Hf_{20}$ alloy aged at 400°C for time range between 5 minutes and 48 hours.

Figure 5.6 depicts the peak temperature for the DSC cycles presented in the Figure 5.5. The detailed study showed the depression in TTs continued with increment in aging time for the temperature set at 400°C. Aging for 5 minutes did not show much variation from the TTs of as extruded specimen, possibly because the time was too short to cause any change in the microstructure. Aging for 15 minutes resulted in decrement of about 17°C for both forward and backward transformations. The hysteresis was also

observed to drop by 5°C. Further increment of aging time to 30 minutes did not yield much variation from 15 minutes but when the aging time was increase to 1 hour, the TTs dropped 12°C more and a cumulative decrement of 30°C in comparison with as extruded condition, while the hysteresis more or less remained the same. Aging for 3 hours resulted in the minimum TTs at about 40°C lower than initially observed values at as extruded condition. No further decrease in TTs was observed while increasing the aging temperature, and the TTs were observed to stabilize at +/- 1°C around 74°C for A_p and 31.5°C for M_p.
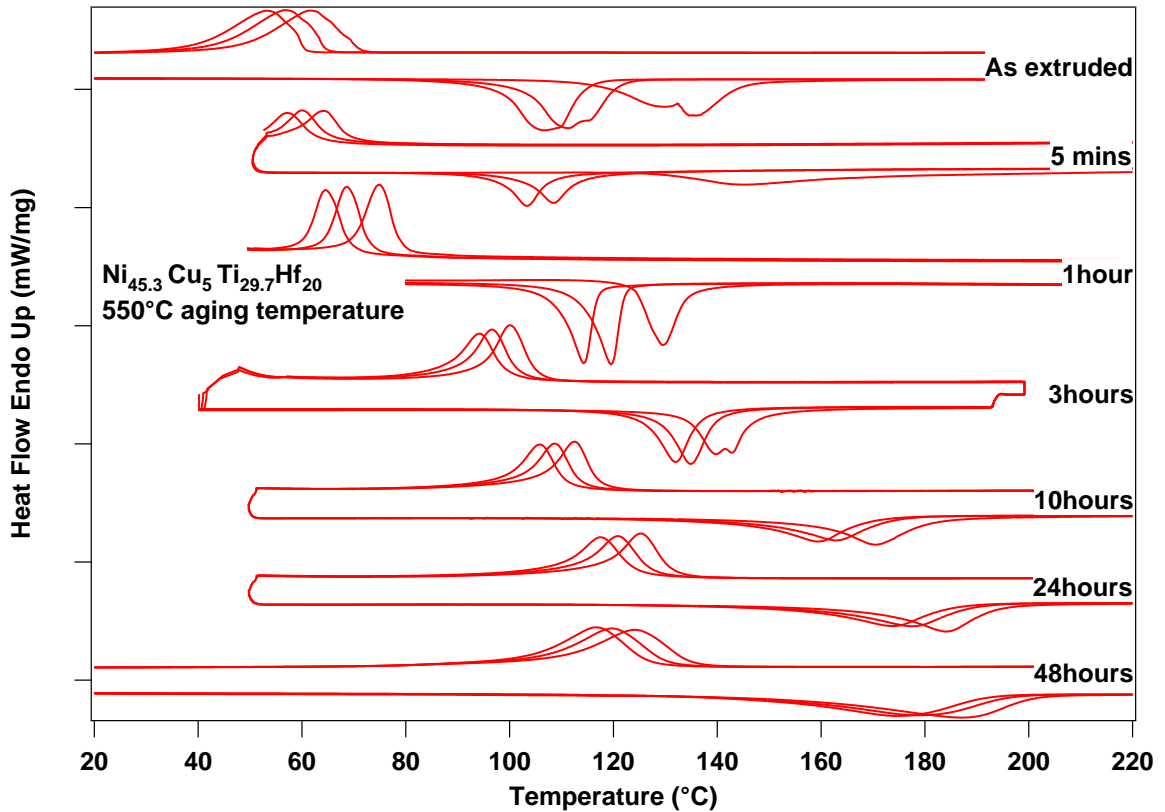
Figure 5.7: DSC plots showing the variation in TTs for $Ni_{45.3}Cu_5Ti_{29.7}Hf_{20}$ alloy aged at 550°C for time range between 5 minutes and 48 hours.
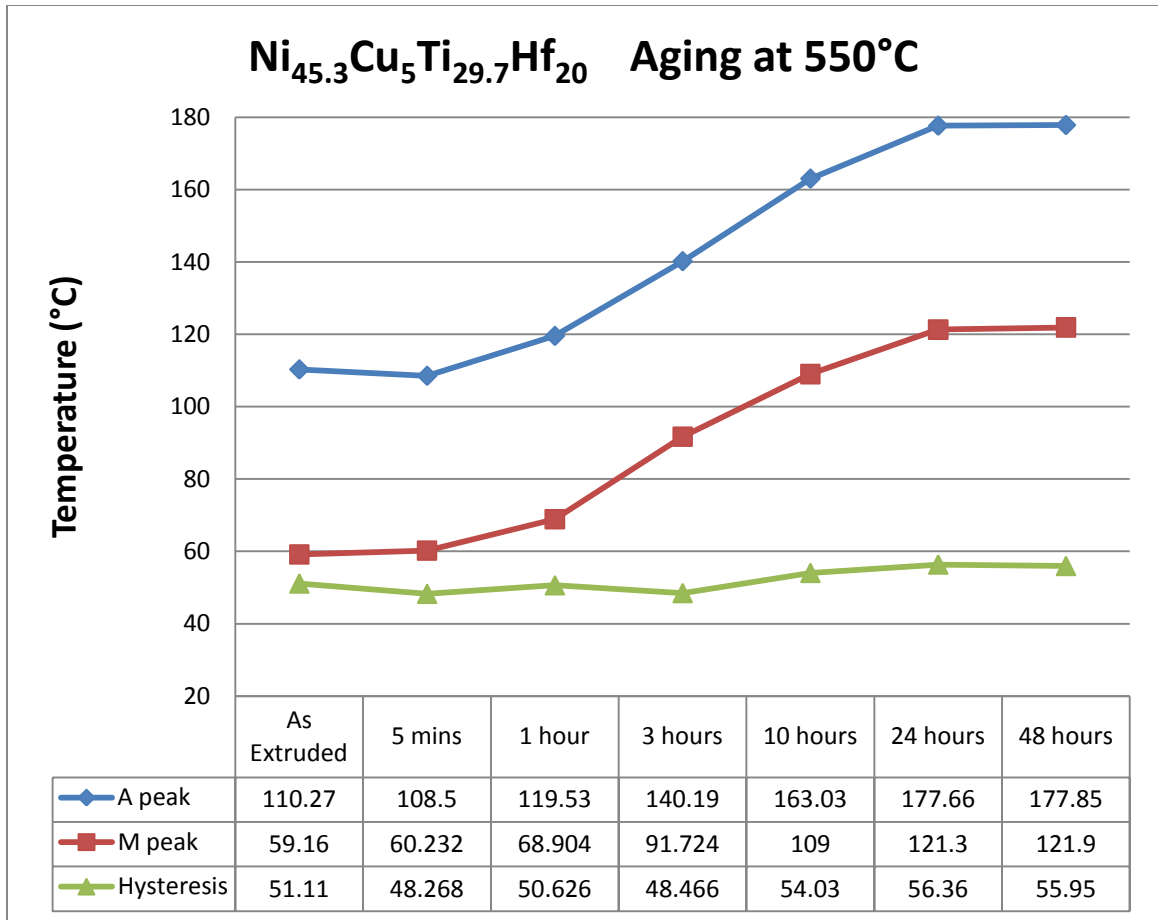
Figure 5.8: Comparison plot showing the peak temperatures for $Ni_{45.3}Cu_5Ti_{29.7}Hf_{20}$ alloy aged at 550°C for time range between 5 minutes and 48 hours.

After the drop in TTs for aging at 400°C for 3 hours, the TTs were observed to increase sharply till aging at 550°C, after which the increase in aging temperature led to a subtle increment in TTs. Figure 5.7 depicts the DSC curves for $Ni_{45.3}Cu_5Ti_{29.7}Hf_{20}$ alloy samples aged at 550°C between time of 5 minutes and 48 hours. Akin to other heat treatments done for 5 minutes, no sizable variation in TTs was observed in case of aging at 550°C for 5 minutes either. TTs were observed to increase linearly with further increment in aging time to 24 hours after which for 48 hours, the TTs were observed to stabilize at their maximum threshold noted marginally under 178°C. Sharp transformation peaks were observed for the specimen aged for 1 hour and 3 hours, while

high stability was observed for specimen aged for 3 hours only amongst the two. The TTs were observed to decrease by 5°C for each cycle for 1 hour aged specimen while the decrement for 3 hours sample was decreased to about 2°C only. The TTs were then observed to increase to higher levels with further increment in aging time. The peaks for the transformation were observed to become wider and the increment in TTs from 24 hours to 48 hours was noted to be very marginal.

Figure 5.8 depicts the transformation peak temperature for the DSC curves depicted in the Figure 5.7. The line following the locus of peak temperatures is seen to follow a steady slope of positive 20°C per increment in aging time till 24 hours after which it becomes invariable. The hysteresis is observed to be minimum at aging for 3 hours and reaches its maximum value at aging for 24 hours, though the range for hysteresis is mere 8°C.
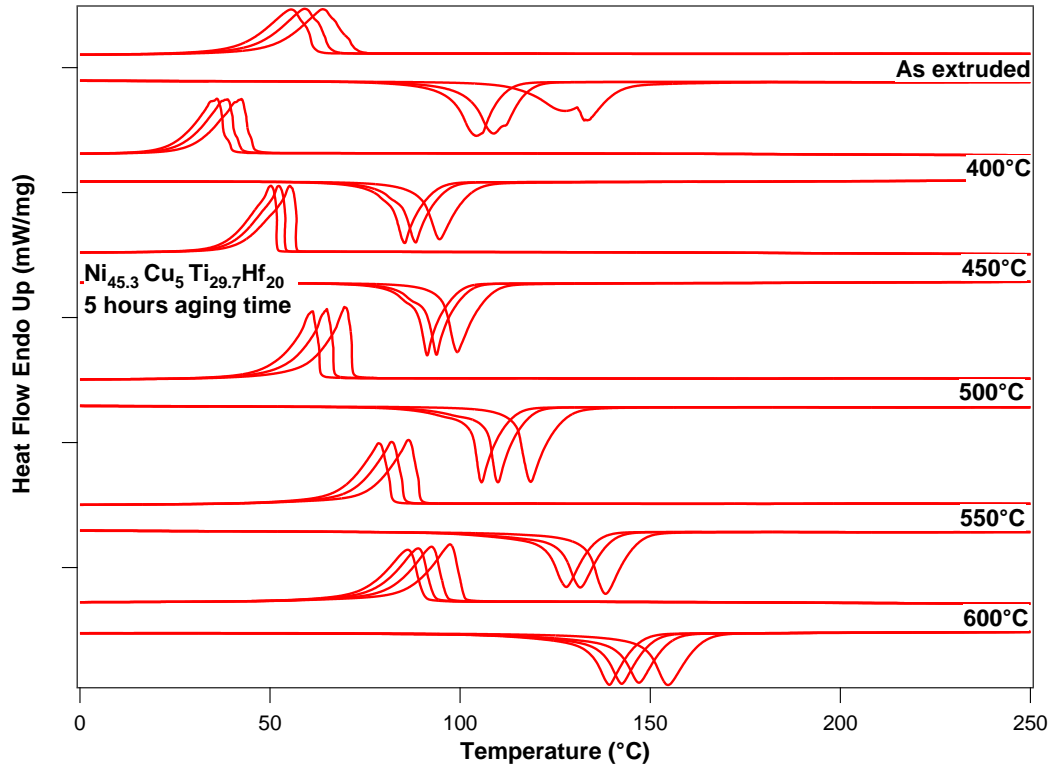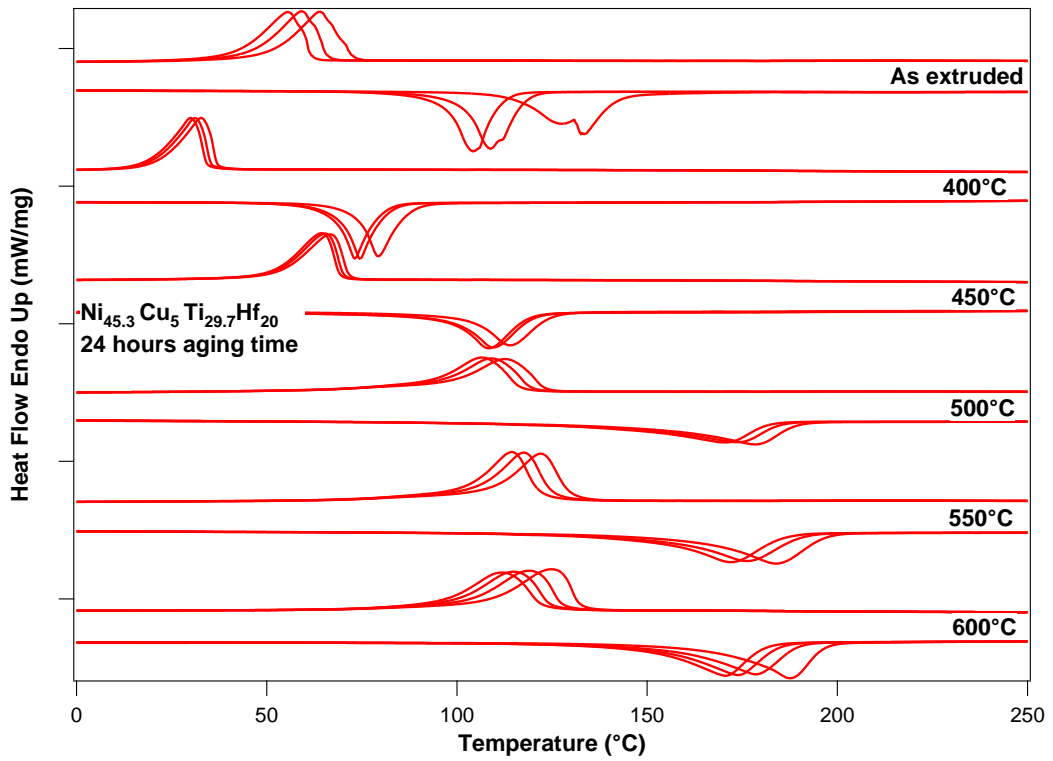
Figure 5.9 (a,b): DSC plots showing the variation in TTs for Ni$_{45.3}$Cu$_5$Ti$_{29.7}$Hf$_{20}$ alloy aged for   5 hours (a, top) and 24 hours (b, bottom) between 400°C and 600°C.
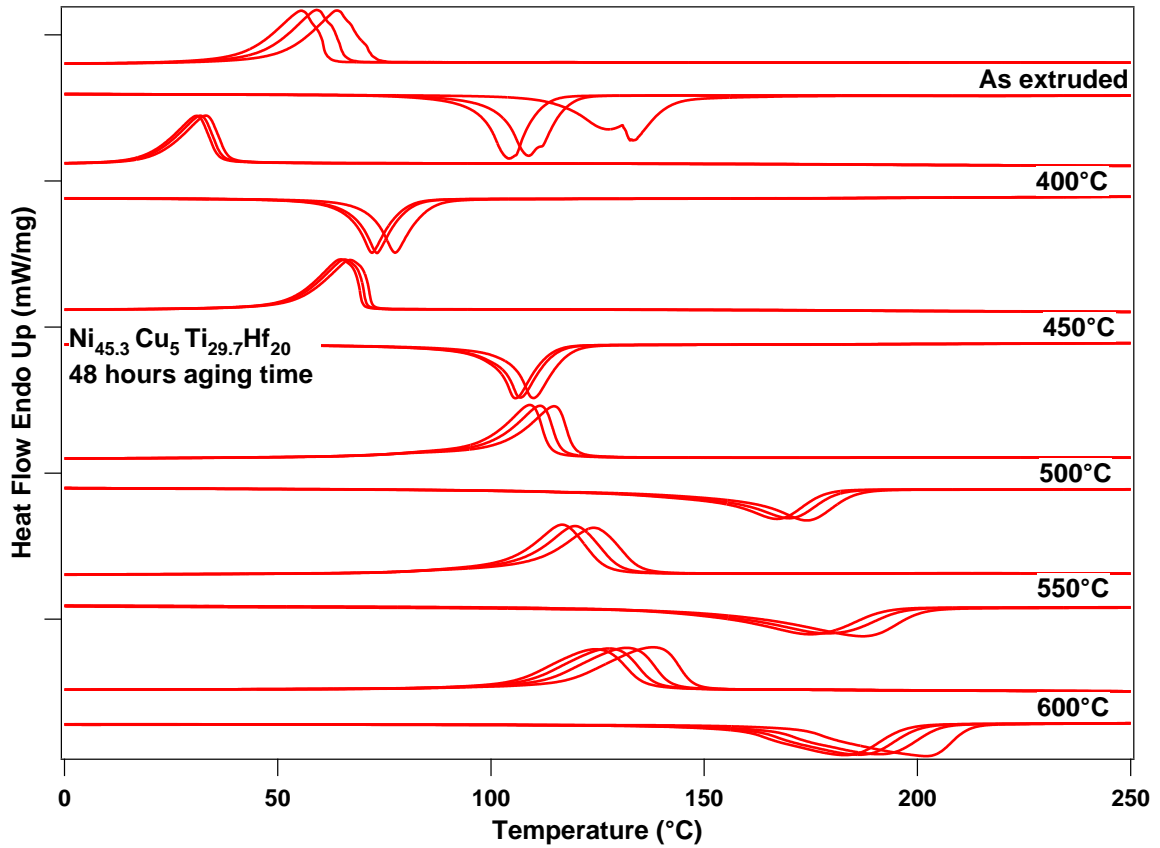
Continued Figure 5.9(c): DSC plots showing the variation in TTs for $Ni_{45.3}Cu_5Ti_{29.7}Hf_{20}$ alloy aged for   48 hours between 400°C and 600°C.

Figures 5.9 depicts the transformation behavior for $Ni_{45.3}Cu_5Ti_{29.7}Hf_{20}$ alloy aged at the selected temperatures for 5, 24 and 48 hours. Five steps between 400°C and 600°C at a difference for 50°C were chosen for this detailed study. The temperatures were chosen to include both the extreme points of minima and maxima for the varying TTs. The aging temperature of 700°C was not included for this study as the transformation peaks observed for it were very wide and the aging temperature is expected to be close to recrystallization temperature. In this case the precipitates are expected to dissolve at higher time durations and hence no information can be gathered or along with no variation in TTs as a result of it.

Figure 5.9(a) depicts the DSC curves for aging at the above mentioned temperatures for 5 hours. The variation in TTs is observed to follow similar trend to aging for 3 hours. The TTs reach their minimum values for aging at 400°C, and from here on any increase in aging temperature leads to a steady increment in the TTs. The general shape of the peaks for all the aging temperatures for 5 hours were observed to be sharp, which can be attributed to homogenous composition throughout the material matrix. Figure 5.10 depicts the transformation peak temperatures for aging for 5 hours. it can be observed that after an initial dip in the TTs, the TTs increase over a smooth slope in linear fashion to the maximum for aging at 600°C. The hysteresis was observed decrease by 10°C from ax extruded condition to aging at 450°C, after which with further increment in aging temperature led to marginal increment in hysteresis with each aging temperature, with at maximum of 54.6°C, about 3°C higher in comparison to as extruded condition.

Ni$_{45.3}$Cu$_5$Ti$_{29.7}$Hf$_{20}$ Aging for 5hrs

|	As extruded	400°C	450°C	500°C	550°C	600°C
A peak	110.27	88.33	93.84	109.98	131.63	147.05
M peak	59.16	38.86	52.27	64.95	81.97	92.43
Hystersis	51.11	49.47	41.57	45.03	49.66	54.62
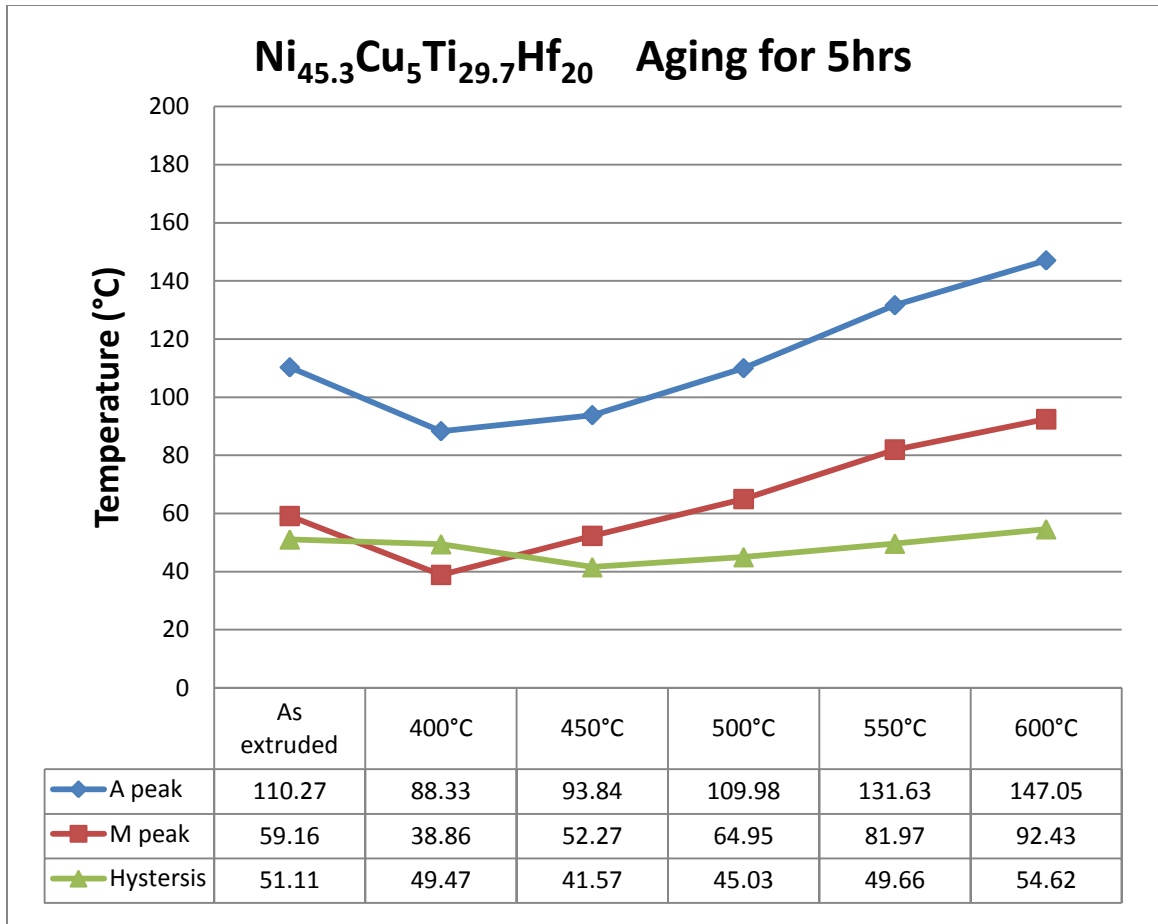
Figure 5.10: Comparison plot showing the peak temperatures for Ni$_{45.3}$Cu$_5$Ti$_{29.7}$Hf$_{20}$ alloy aged for 5 hours ranging from 400°C to 600°C.

Figure 5.9 (b) and (c) show the transformation behaviors for aging at the selected temperature for 24 hours and 48 hours respectively. Transformation behaviors were observed be very similar to each other for 24 hours and 48 hours for corresponding aging temperatures. The TTs for aging at 400°C were observed to reach their minimum values at 24 hours and remained within 1°C for further increasing aging time to 48 hours. The TTs were then observed to reach back to levels of as extruded condition when the alloy was aged for 24 and 48 hours. The most notable feature as will be mentioned for other aging temperatures for these time ranges is degree of cyclic stability achieved. After the

first cycle effect, the transformation peak were observed to almost overlap the preceding cycle. The most discriminating feature for aging for duration of 24 and 48 hours is the realization of almost the maximum TTs for aging temperature of 500°C, as opposed to earlier mentioned aging times where the TTs were observed to increase linearly till 600°C, and TTs only comparable to as extruded condition for aging at 500°C. The evolution of precipitates with the increment in time from 5 hours to 24 and 48 hours can be attributed for this behavior. As seen in case of aging time of 1,3 and 5 hours the TTs reached their maximum level for aging at 600°C, the reason for this behavior is growth of the precipitates continue with the increment in aging temperature to increase in their volume fraction. In contrast when aged at even at 500°C, the time of 24 hours is found to be sufficient for the precipitates to grow sufficiently to achieve the maximum possible TTs. The hysteresis for both 24 hours and 48 hours was also observed to replicate each other. The hysteresis decreased to its minimum by 7°C and 10°C from as extruded condition for aging at 450°C for 24hours and 48 hours respectively. The hysteresis was then observed to increase with a steep slope to about 10°C higher than initial values for aging at 500°C and followed by a slight decrement of about 3°C for 550°C and 600°C.

	As extruded	400°C	450°C	500°C	550°C	600°C
A peak	110.27	74.57	109.57	173.77	176.2	178.49
M peak	59.16	31.08	65.36	109.06	117.59	118.92
Hystersis	51.11	43.49	44.21	64.71	58.61	59.57
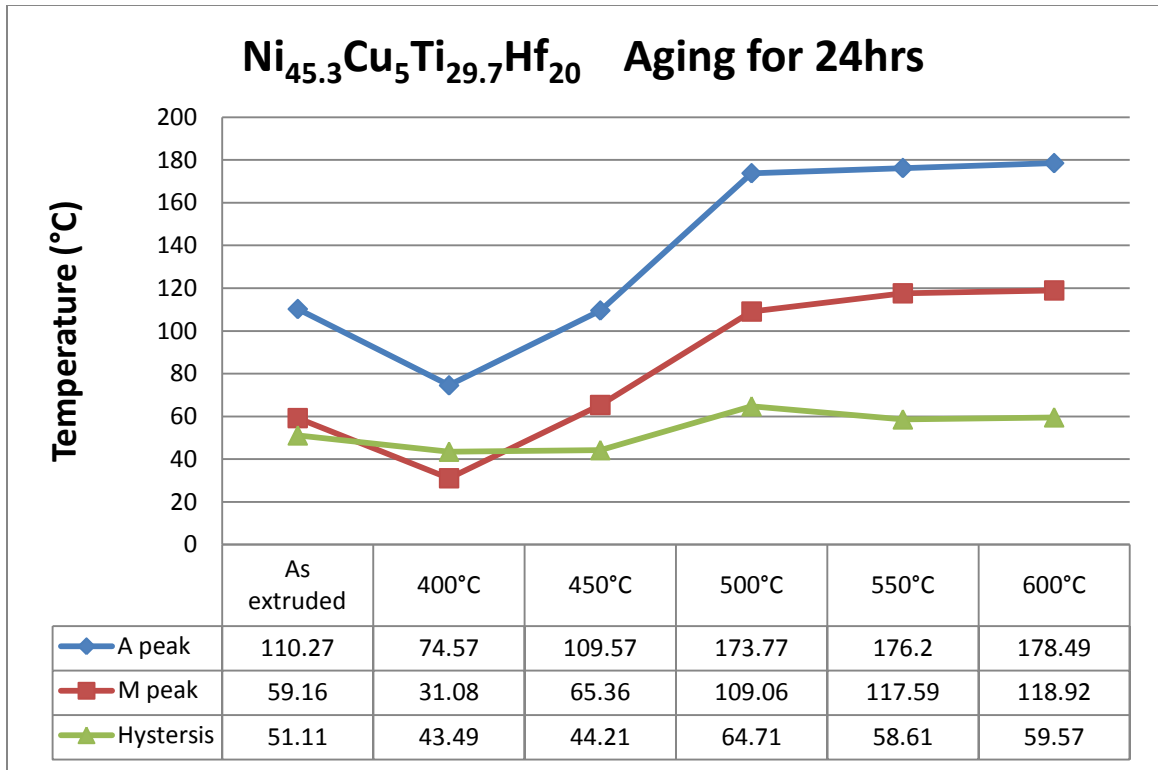
Figure 5.11: Comparison plot showing the peak temperatures for $Ni_{45.3}Cu_5Ti_{29.7}Hf_{20}$ alloy aged for 24 hours ranging from 400°C to 600°C.

	As extruded	400°C	450°C	500°C	550°C	600°C
A peak	110.27	73.24	106.9	170.04	179.08	190.98
M peak	59.16	31.86	65.75	111.59	119.72	131.8
Hystersis	51.11	41.38	41.15	58.45	59.36	59.18
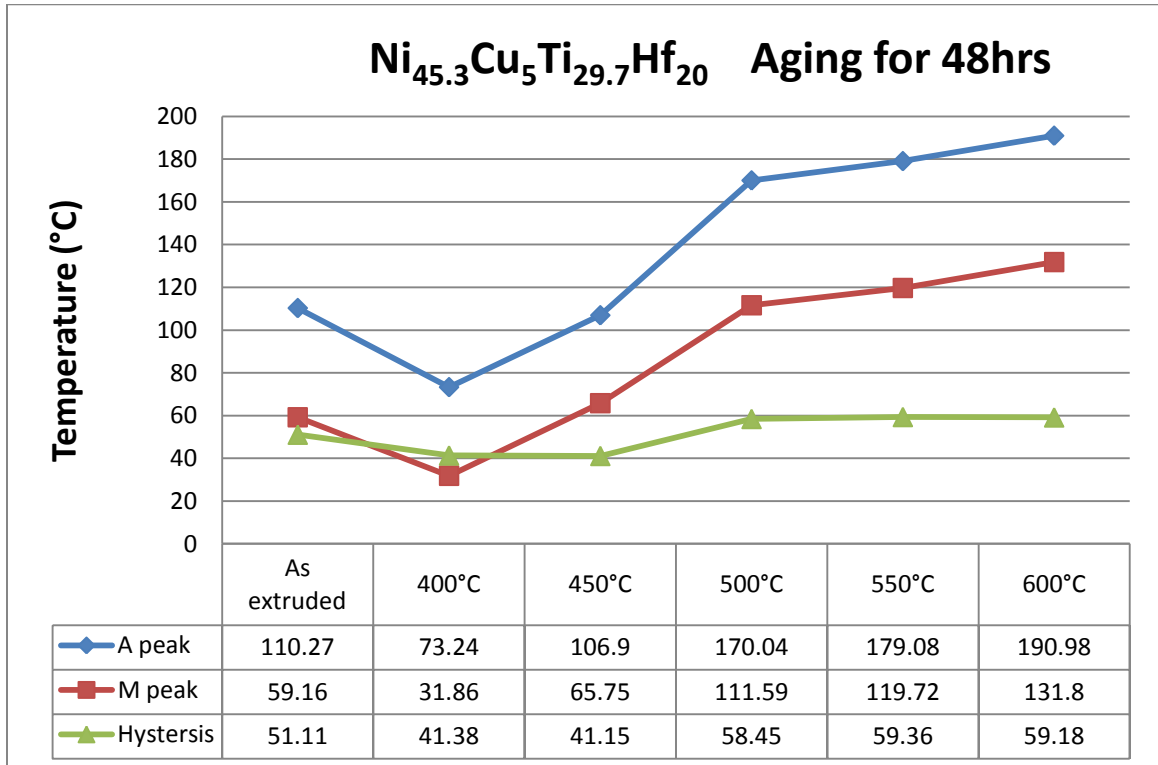
Figure 5.12: Comparison plot showing the peak temperatures for $Ni_{45.3}Cu_5Ti_{29.7}Hf_{20}$ alloy aged for 48 hours ranging from 400°C to 600°C.

5.2 TEM Study

(a)   (b)
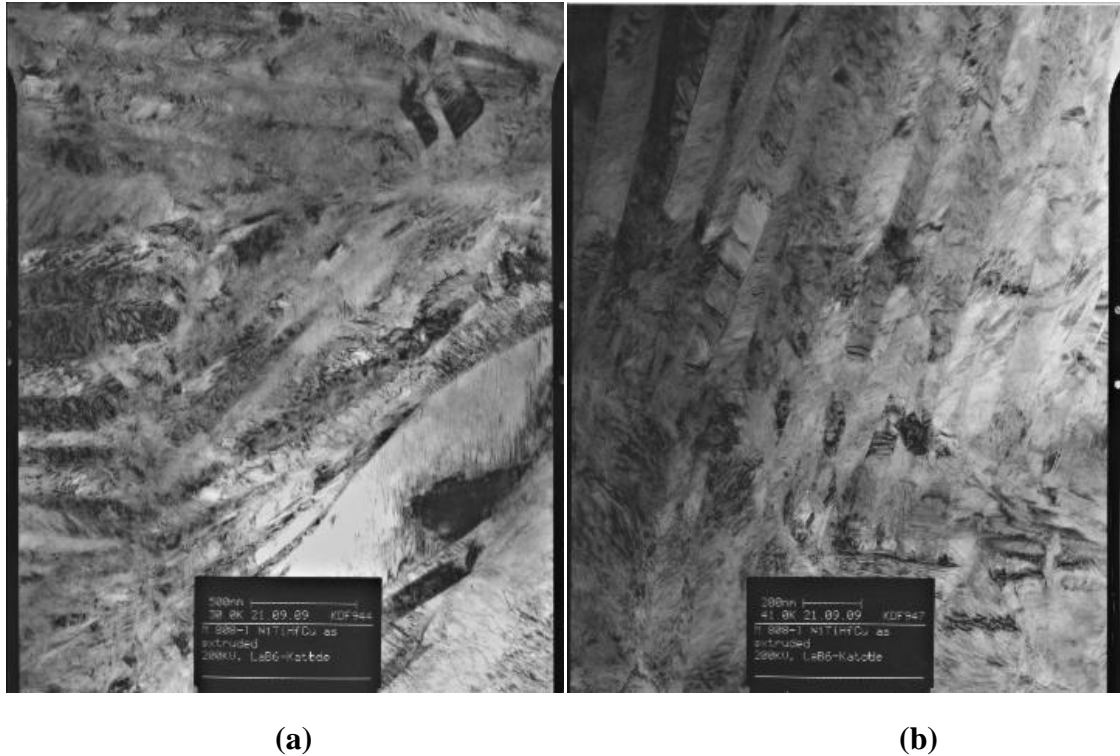
Figure 5.13: TEM micrographs of $Ni_{45.3}Cu_5Ti_{29.7}Hf_{20}$ in as extruded condition

The TEM micrographs showing the microstructure for $Ni_{45.3}Cu_5Ti_{29.7}Hf_{20}$ in as extruded condition are presented in Figure 5.13. In contrast to $Ni_{45.3}Ti_{29.7}Hf_{20}$ alloy, in as extruded condition, very large amount of dislocations were observed for $Ni_{45.3}Cu_5Ti_{29.7}Hf_{20}$ in the similar condition. The addition of Cu is responsible for the softening as well as increasing the ductility of the material. Another notable feature visible in the TEM micrographs is the presence of large volumes of internally twinned martensite. When the material is looked upon at higher resolution, internally twinned martensite along with lots of dislocations is evident. The matrix is observed to be free of any precipitates, which can be attributed to the homogenization done for 72 hours at 1050°C before extrusion at 900°C.

Figure 5.14: TEM micrographs of $Ni_{45.3}Cu_5Ti_{29.7}Hf_{20}$ aged for 3hours at 400°C

Figure 5.15: TEM micrographs of $Ni_{45.3}Cu_5Ti_{29.7}Hf_{20}$ aged for 24hours at 400°C

Figures 5.14 and 5.15 represent the $Ni_{45.3}Cu_5Ti_{29.7}Hf_{20}$ alloy aged at 400°C for 3hours and 24 hours respectively. From figure 5.14 the decrement of the TTs observed in the calorimetry experiments can be clearly inferred. Also it will be shown in the mechanical characterization, the aging at 400°C for 3 hours led to a decrement in the mechanical strength of the alloy. For increasing the aging time from 3 hours to 24 hours the dislocations are observed to further decrease but evolution of small precipitates is observed, with which a marginal improvement in the hardness values is observed but the TTs are seen to further decrease. This can be attributed to the very small volume fraction of the precipitates and hence the effect of the initiation of annihilation of dislocations overpowers the effect of precipitates and a net decline in TTs is observed.

The TEM micrographs of $Ni_{45.3}Cu_5Ti_{29.7}Hf_{20}$ alloy aged at 550°C for 3hours and 24 hours are presented in figures 5.16 and 5.17. The presence of the precipitates is clearly visible in form of worm like features in the figure 5.16. The size of precipitates is observed to be in the vicinity of 15 to 20 nm, and the reason for worm like evolution can be attributed to selection of dislocations as the nucleation site. The volume fraction is observed to have risen notably from aging the alloy at 550°C in contrast to aging at 400°C. The rise in TTs can be clearly attributed to the observations made in the TEM micrographs. With further increment in aging time to 24 hours the size and volume fraction is observed to increase, but the internally twinned martensite in observed to be still present.

Figure 5.16: TEM micrographs of $Ni_{45.3}Cu_5Ti_{29.7}Hf_{20}$ aged for3 hours at 550°C
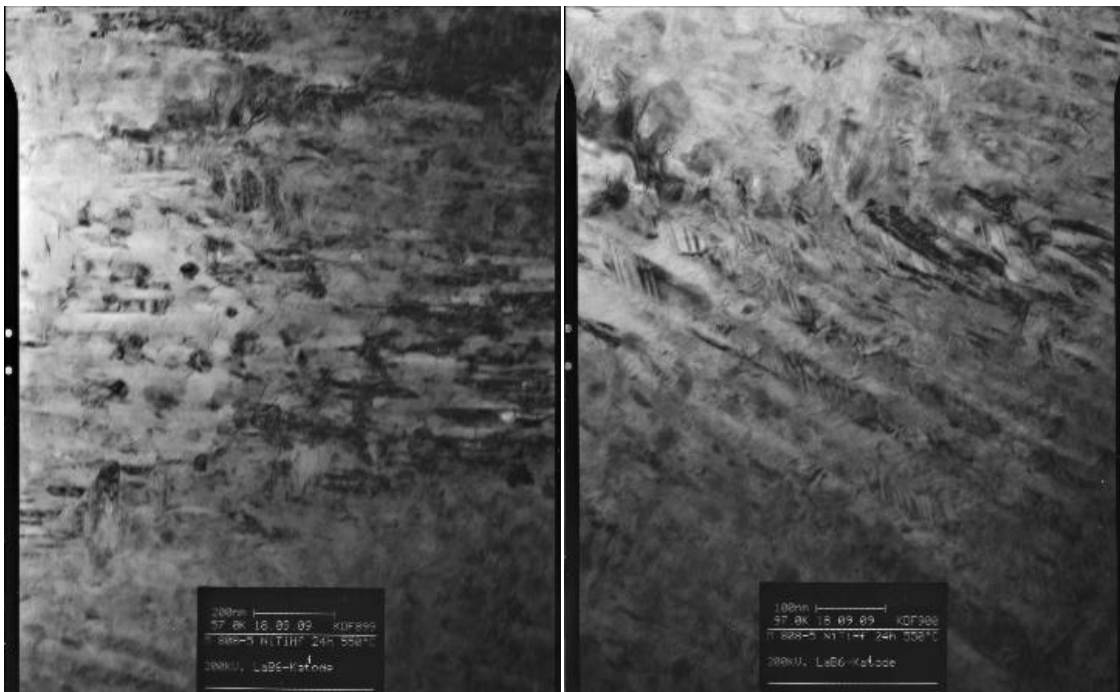
Figure 5.17: TEM micrographs of $Ni_{45.3}Cu_5Ti_{29.7}Hf_{20}$ aged for 24hours at 550°C

5.3 Hardness results
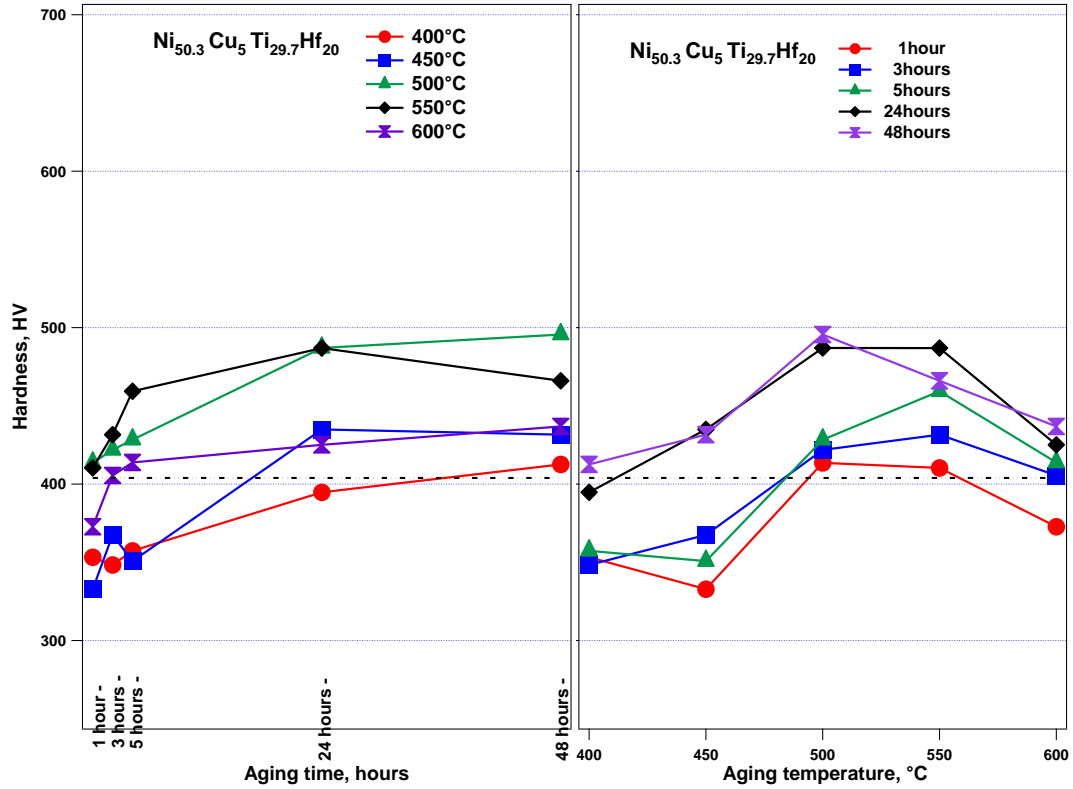
Figure 5.18: Comparison plot for hardness values of $Ni_{45.3}Cu_5Ti_{29.7}Hf_{20,}$ aged at selected temperatures for 1, 3, 5, 24 and 48 hours

The figure 5.18 depicts the variation of Vickers hardness with respect to selected aging conditions and the dotted black line running horizontally at 404 represents the hardness value for as extruded sample. The effect of the evolution and growth of precipitates shown in figures 5.13 to 5.17 can be clearly observed in figure 5.18. The TEM micrographs finding presented for aging at 400, 550°C matched nicely with the variation of TTs and are observed to match very closely to their expected effects on the material strength also. When observing the locus of Vickers hardness of sample aged at 550°C for various times, the hardness value is observed to increase sharply till aging time

of 5 hours followed by a more subtle increment till 24 hours where it reaches it maximum value. The hardness value is then observed to decrease slightly when aging time is further increased to 48 hours in contrast to no change in the TTs for the same change in aging time. The hardness values, similar to the TTs are observed to stay above the value for as extruded condition for all aging times at the aging temperature of 550°C. A clear analogy between the size of the precipitates and the hardness values can be drawn along the lines of presented in the literature. The strength of the material is observed to increase with the increment in aging time for 550°C from 1 to 5 hours which can be attributed to the increase in the size of precipitates to form finely dispersed coherent precipitates. The increment in volume fraction can be inferred from the increase in the TTs along with this process. The hardness is reported to reach its maximum value for 24 hours after which it decrease slightly, this is comparable to further growth of precipitates into incoherent size and hence cannot contribute as highly as previously to the strength of the material. On the other hand the TTs are seen to further increase due to the high dependence on the composition which continues to change as the precipitates become larger and higher in volume fraction.

Contrary to the realization of maximum strength for aging for 24 hours at 550°C, the hardness was observed to continue to increase for increment in aging time from 24 to 48 hours. This can be attributed to dependence of growth of precipitates on both time and temperature and hence at the lower temperature of 500°C the precipitates are expected continue to remain coherent even at 48 hours of aging. While observing the TEM micrographs and hardness results for aging at 400°C it is expected that the aging does not yield favorable volume fraction of precipitates along with relief from dislocations present

initially due to material processing, resulting in lower hardness of the material and suppression of TTs. Aging temperature of 450°C yields results similar to previously mentioned aging temperature of 400°C except for the observation of higher hardness values. Aging at 600°C further cements the theory behind the growth of precipitates and a steep growth is observed initially when increasing the aging time from 1 to 5 hours, after which the hardness values increase marginally, which can be explained by the quick initial growth of precipitates into coherent size followed by increase in size into incoherent precipitates which contribute marginally to the strength.
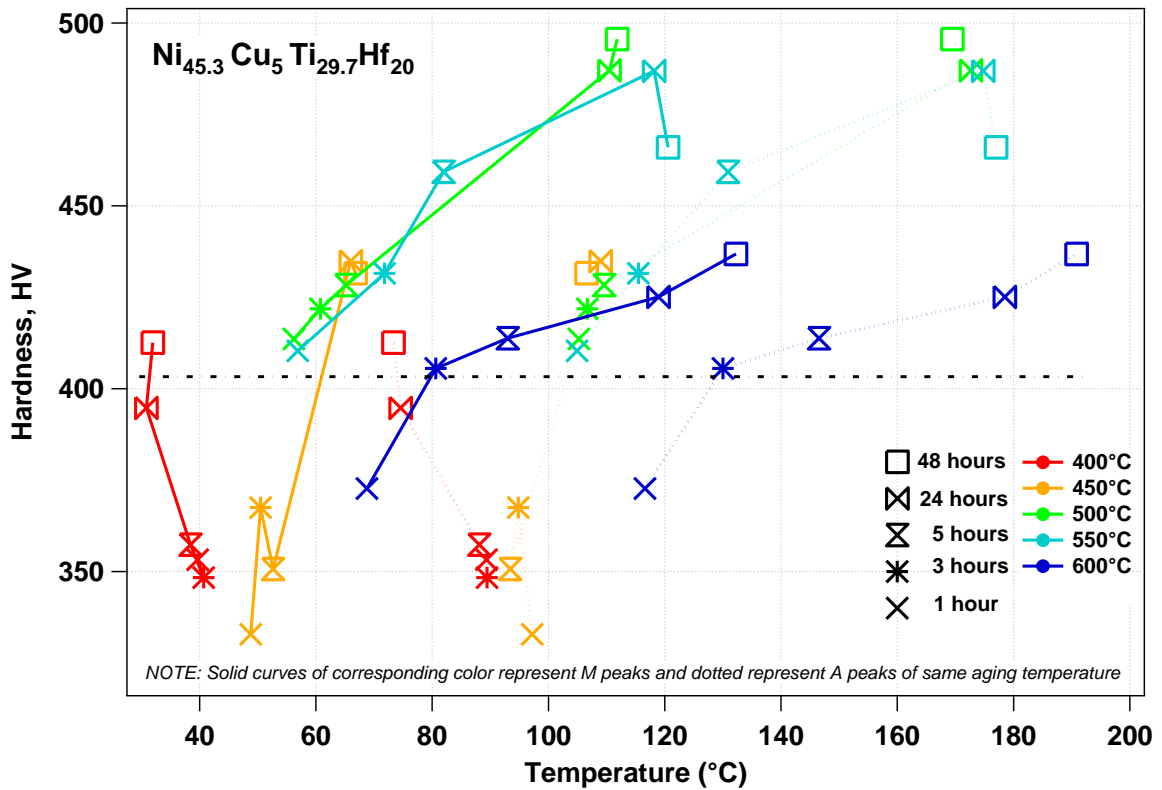
Figure 5.19: Comparison plot for hardness vs TTs for corresponding aging conditions.

Figure 5.19 represents the hardness values for the aged specimen vs TTs for the corresponding sample. The dotted line running parallel to the horizontal at 404 represents the hardness value for the as extruded sample. The curve for the sample aged at 400°C

shows the increment in the hardness value with the increment in the aging time even though the TTs decreased by a small amount. The curve for the sample aged at 450°C showed a different outlook and the hardness increased very sharply in contrast to the increment observed in the TTs. The hardness for both samples aged at 400°C and 450°C had hardness value lower than the as extruded sample for all aging times except for aging at 48 hours. The decrement in the TTs for aging in this range is responsible for making the nucleation of martensite very difficult due to presence of very small precipitates dispersed in the matrix.

Samples aged at 500°C and 550°C followed each other very closely tracing out almost similar paths for the curve. Hardness was observed to stay higher than as extruded sample for all aging times for both the samples and was observed to increase almost linearly with the increment in the TTs. The maximum hardness for the sample aged at 500°C was achieved at aging for 48 hours however the sample aged at the higher temperature of 550°C attained the maximum value of hardness at 24 hours and it was observed to fall for the increment in aging time from 24 hours to 48 hours. The different routes followed by the two samples when the aging time was increased from 24 hours to 48 hours can be attributed to the dependence of the precipitate evolution on the combination of aging temperature and time. Aging for 48 hours at the higher temperature of 550°C could be held responsible for the growth of the precipitates incoherent size in contrast to the high volume fraction of coherent precipitates at 500°C for the same aging time. The aged at 600°C followed a similar trend but the hardness was observed to be lower than the samples aged at 500°C and 550°C.

5.4 XRD Analysis
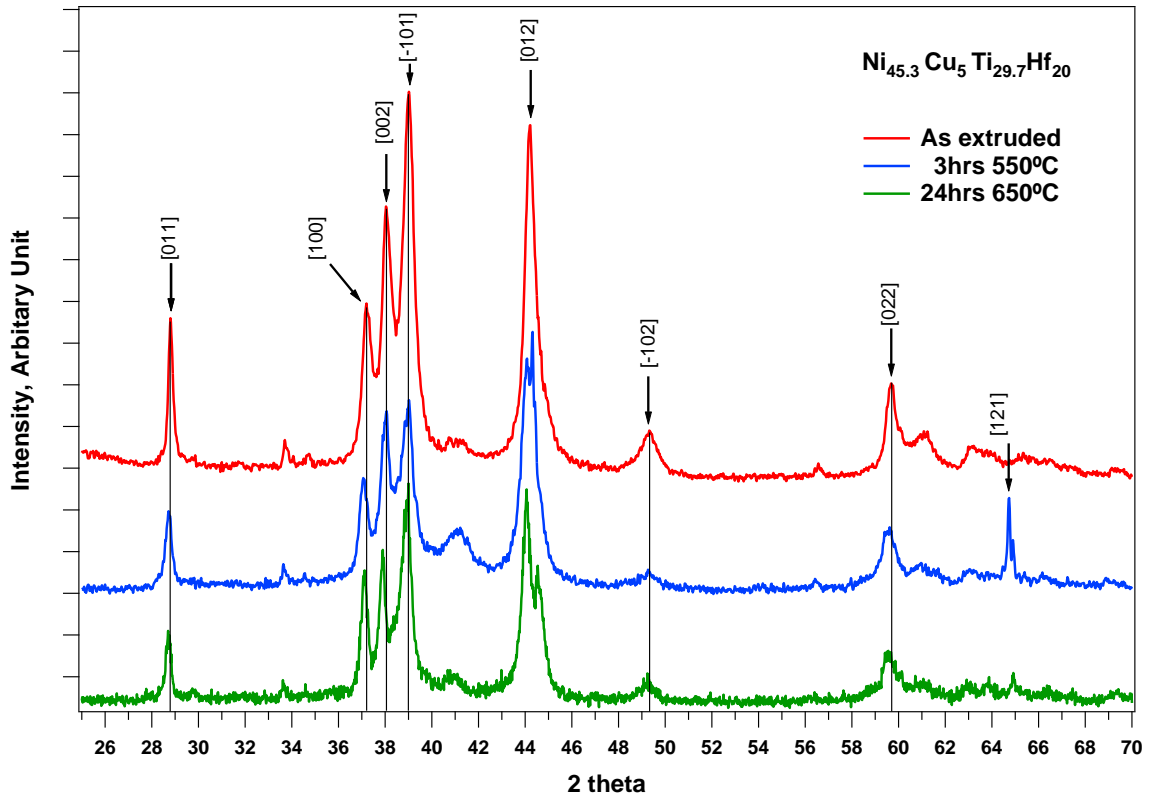
Figure 5.20(a): XRD plots for $Ni_{45.3}Cu_5Ti_{29.7}Hf_{20}$ for varying aging conditions.

Figure 5.20 depicts the results obtained from XRD of $Ni_{45.3}Cu_5Ti_{29.7}Hf_{20}$ samples aged at the conditions mentioned in the plot. Very similar results were obtained for the samples aged for 3 hours at 550°C and 24 hours at 650°C in comparison for the as extruded sample. The structure of martensite is determined to be B19'. Upon calculations the lattice parameters for the as extruded sample were indexed at a=0.24nm, b=0.41nm, c=0.48nm, β=99.29°. The sample aged at 550°C for 3 hours was found to be close with the parameters of a=0.24nm, b=0.41nm c=0.48nm, β=99.360°.
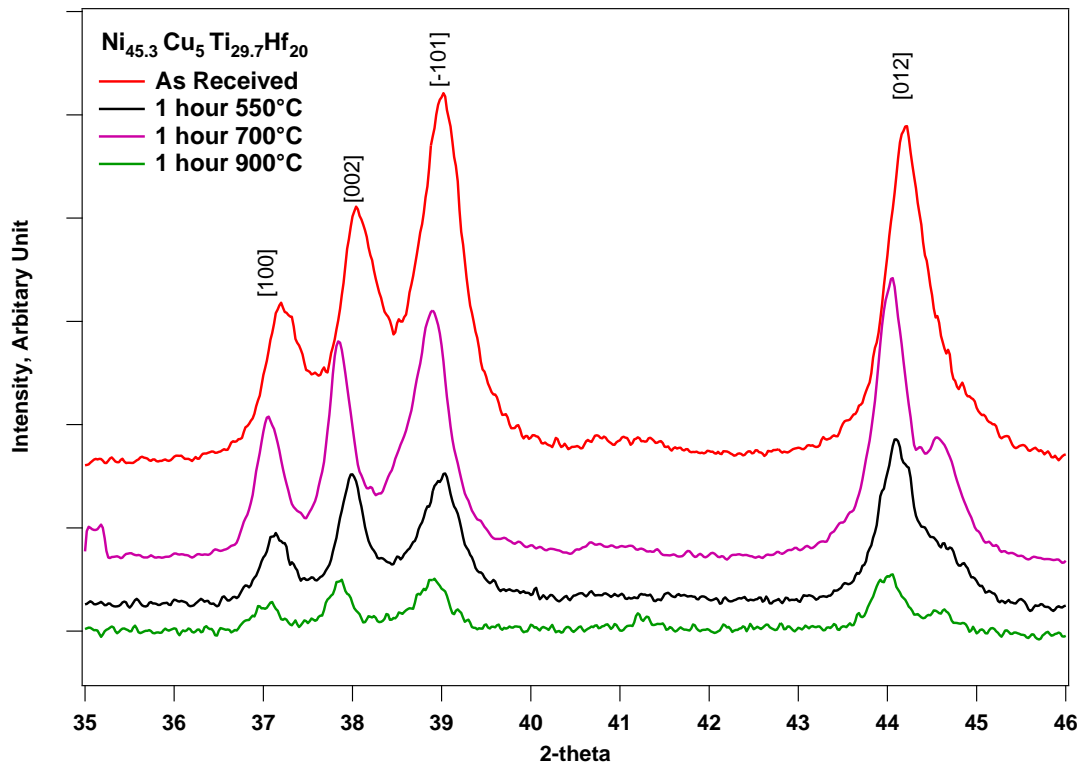
Continued Figure 5.20(b): XRD plots for $Ni_{45.3}Cu_5Ti_{29.7}Hf_{20}$ for varying aging conditions.
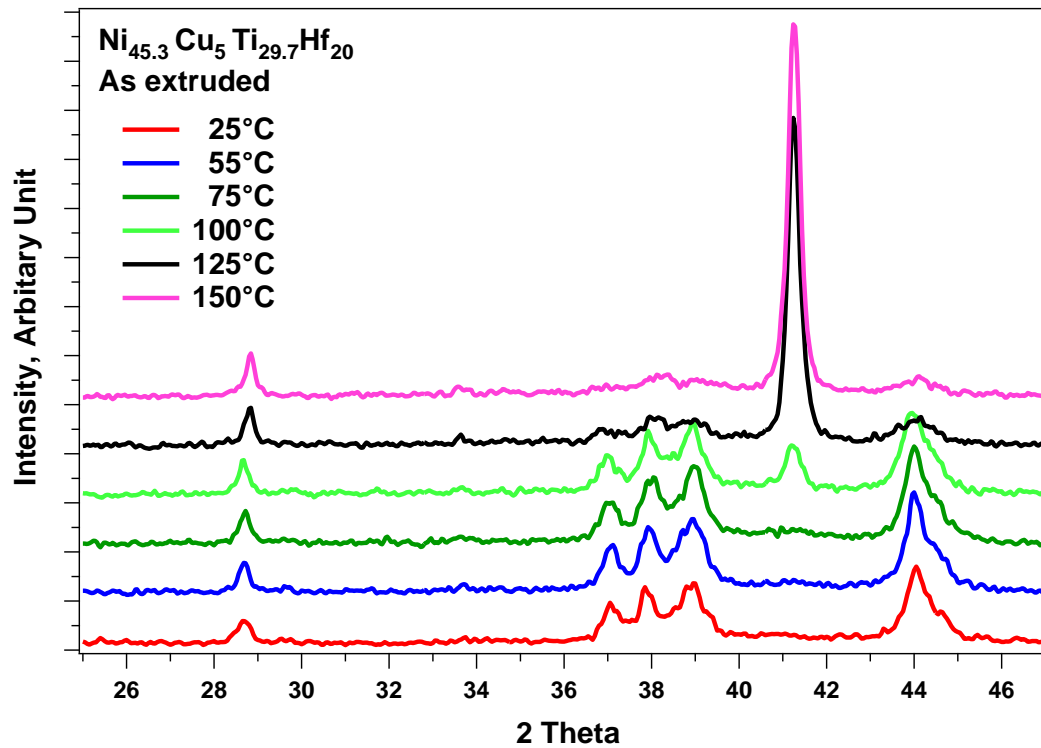
Figure 5.21: XRD plots for $Ni_{45.3}Cu_5Ti_{29.7}Hf_{20}$ in as extruded sample heated from room temperature to 150°C.

Figure 5.21 represents the sequence of XRD patterns obtained for the scan between the 2-theta range of 25° to 50° at the temperatures indicated in the color legend for the plot. While Figure 5.22 depicts similar plot the specimen aged for 3 hours at 550°C between the 2-theta range of 36° to 46°. The mentioned plots represent the transition of the crystal structure from the martensite at room temperature to the austenite phase at the higher temperature. The curves obtained till the temperature of 75°C are observed to be purely martensite, as the temperature reaches 100°C a peak is observed to evolve at about 42° which is the peak of the B2 austenite phase. The peaks observed at the lower temperatures disappeared with the increasing temperature and only peaks for austenite phase were present at 150°C. The calculations done on the XRD for the B2 phase gave the parameter of a=0.31nm.
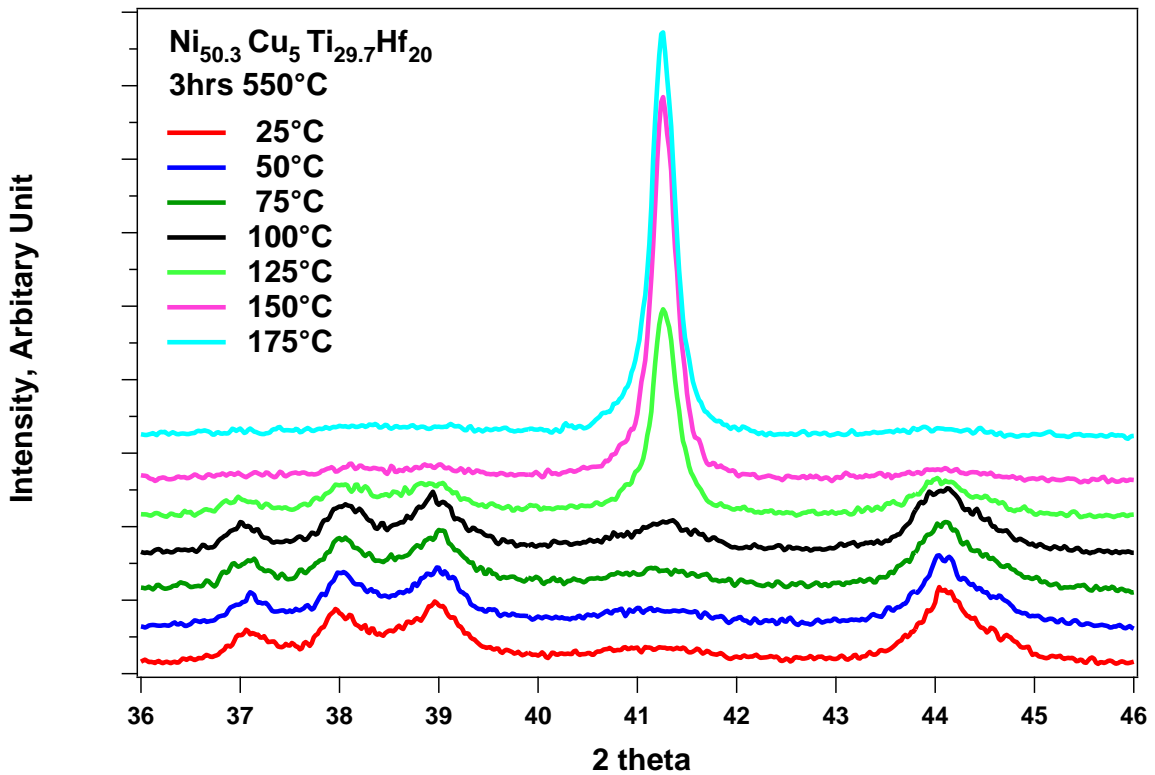
Figure 5.22: XRD plots for $Ni_{45.3}Cu_5Ti_{29.7}Hf_{20}$ aged for 3 hours at 550°C heated from room temperature to 150°C.

5.5 Mechanical Characterization
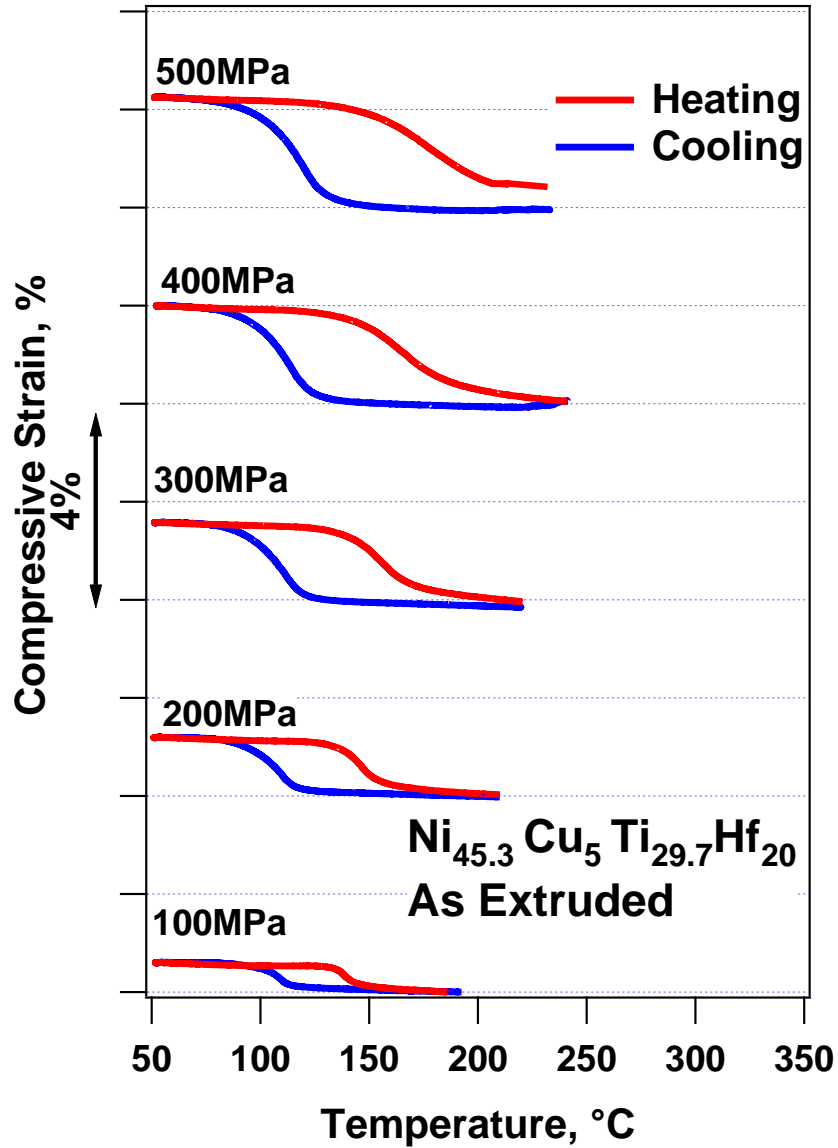
Figure 5.23: Isobaric thermal cycling of $Ni_{45.3}Cu_5Ti_{29.7}Hf_{20}$ in as extruded condition

Figure 5.23 depicts the response for isobaric mechanical response for $Ni_{45.3}Cu_5Ti_{29.7}Hf_{20}$ alloy in as extruded condition for loads varying from 100MPa to 500MPa, specific critical information for which is presented in Table 5.1. Similar procedure as used previously for $Ni_{45.3}Ti_{29.7}Hf_{20}$ was followed for the mechanical characterization of $Ni_{45.3}Cu_5Ti_{29.7}Hf_{20}$ also. The compression sample was loaded in

austenite phase followed thermal cycle of cooling below M_f and heating back to temperature above A_f. The rate of both heating and cooling for the thermal cycle was kept at 10°C/min. It is observed that thermal cycling under when loaded to 100MPa resulted in fully recoverable strain of about 0.5 %. The TTs were observed to be lower than those observed in $Ni_{45.3}Ti_{29.7}Hf_{20}$ for the same corresponding conditions, even though the M_s was still observed to be higher than 100°C for 100MPa load level. The recoverable strain increased with increase in the load levels till the highest load level of 500MPa that was applied in this test. The TTs were also observed to increase as expected along with increase in levels of applied load. The recoverable strain increased in steep fashion till 300MPa, after which the increment in the strain level was very minute. No irrecoverable strain was observed till load level of 300MPa, after which the increment of load to 400MPa and 500MPa led to very small quantity of irrecoverable strain. The hysteresis for the transformation was also noted to increase with the level of applied loads, especially with the increment of load beyond 300MPa resulted in hysteresis of 56°C and 66°C for 400MPa and 500MPa in comparison of just 31°C for 100MPa.

Figure 5.24 depicts the mechanical characteristic for $Ni_{45.3}Cu_5Ti_{29.7}Hf_{20}$ aged at 400°C for 3 hours. The results of the mechanical characterization were observed to be very analogous to the finding of TEM and hardness results. It can be observed from the figure that the with application of load, bias for martensite variant is observed to grow and hence as a consequence the total recoverable strain is also observed to grow. In contrast to as extruded sample where no irrecoverable stain was observed for load level of 300MPa, 0.2% irrecoverable strain was observed for sample aged at 400°C for 3hours. As depicted in the Table 5.2 ,further increment in load to 500MPa and 700MPa

led to an irrecoverable strain of 0.3% and 0.68% respectively. These levels of irrecoverable strains at 300MPa and 500MPa are clear indicators of the depreciation of material strength in comparison for aging at 400°C for 3 hours from as extruded condition. This increment in the observable irrecoverable strain can be attributed to the introduction of dislocations due to low material strength. This finding was earlier mentioned from the observations reported for TEM micrographs and also for hardness results. The hysteresis was observed to increase with increasing load levels and the back transformation from martensite to austenite was to be an inclined with a moderate slope in contrast to the steep transformation curve for forward transformation.

Table 5.1: Critical transformation parameters and strain levels for isobaric thermal cycling of $Ni_{45.3}Cu_5Ti_{29.7}Hf_{20}$ in as extruded condition

Sample	Stress	Ms	Hysteresis	ε_{tr}	ε_{ir}
	50	111.97	28.86	0.35	0
	100	114.61	31.32	0.48	0
As	200	116.07	39.28	1.08	0
Extruded	300	120.23	47.32	1.5	0.13
	400	123.88	56.17	1.83	0.25
	500	130.29	66.58	2.07	0.33

Table 5.2: Critical transformation parameters and strain levels for isobaric thermal cycling of $Ni_{45.3}Cu_5Ti_{29.7}Hf_{20}$ aged at 400°C for 3hours

Sample	Stress	Ms	Hysteresis	ε_{tr}	ε_{ir}
	100	115	27.8	0.6	0
3 hours	300	125	42	1.6	0.14
400°C	500	137	59.23	2.25	0.28
	700	157.2	84	2.82	0.68
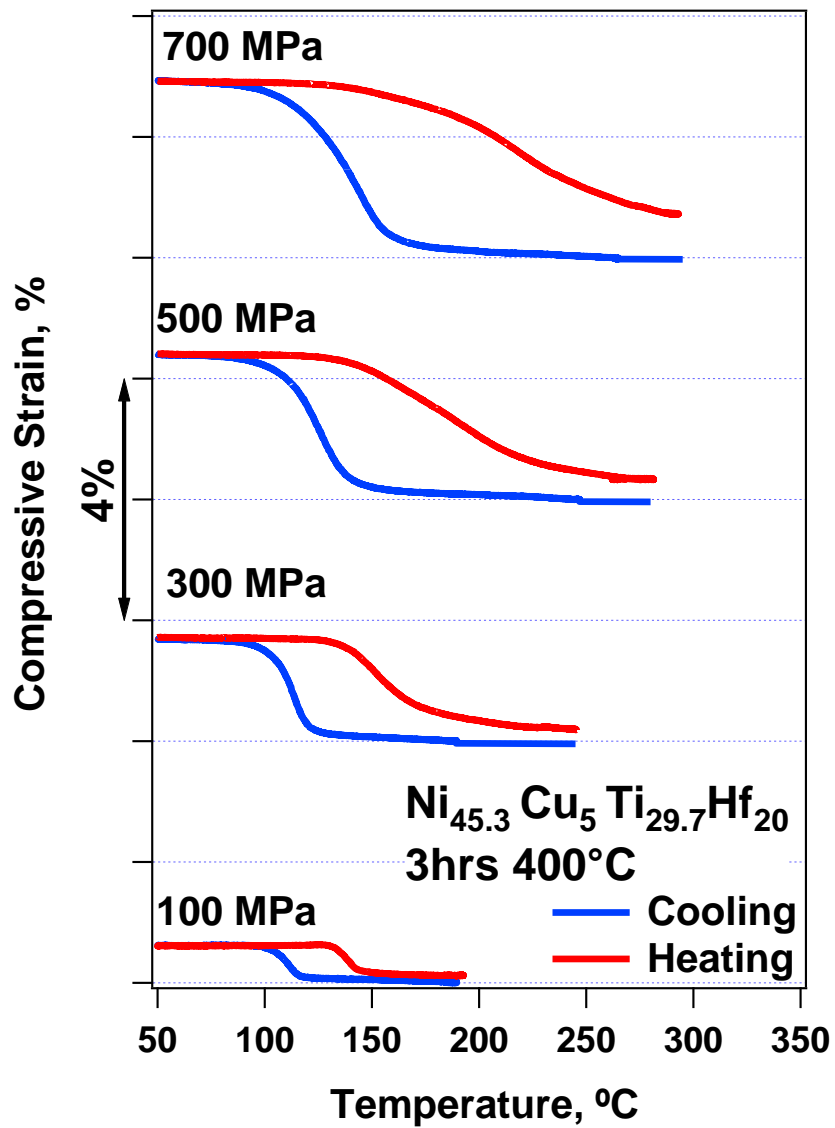
Figure 5.24: Isobaric thermal cycling of $Ni_{45.3}Cu_5Ti_{29.7}Hf_{20}$ aged for 3 hours at 400°C
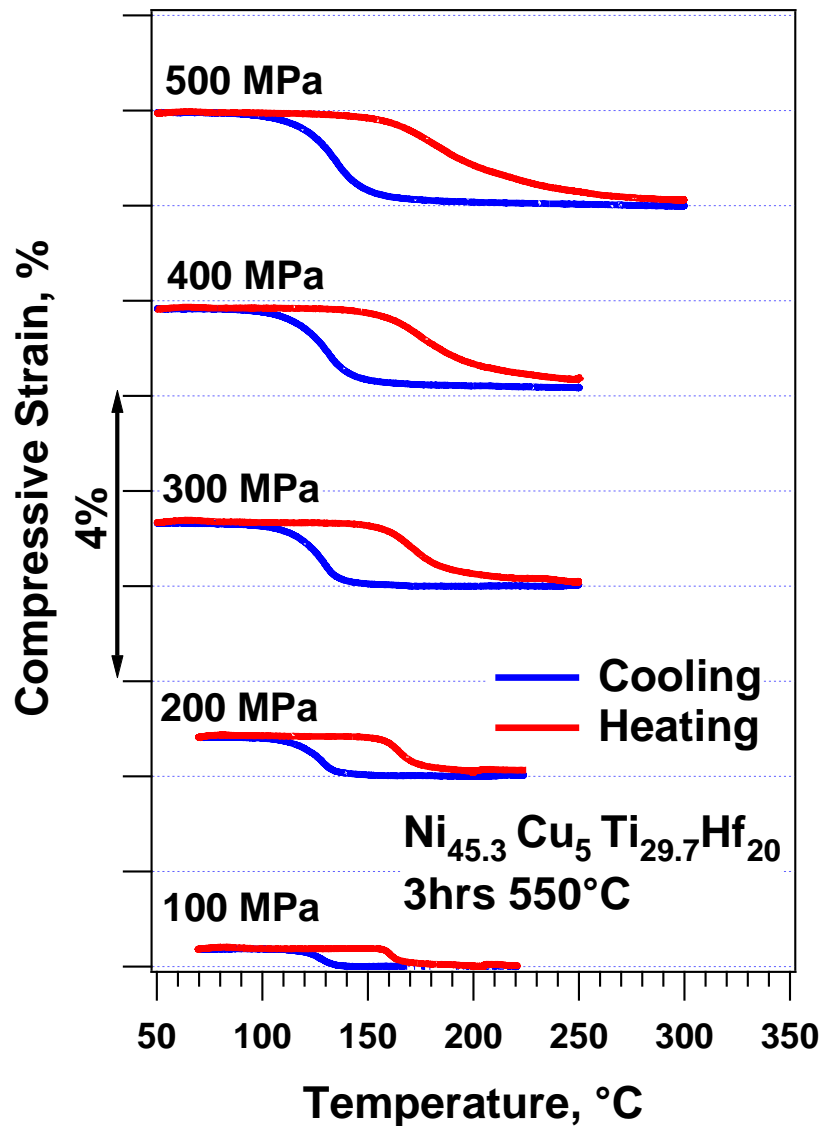
Figure 5.25: Isobaric thermal cycling of $Ni_{45.3}Cu_5Ti_{29.7}Hf_{20}$ aged for 3 hours at 550°C

Figure 5.25 depicts the transformation behavior of $Ni_{45.3}Cu_5Ti_{29.7}Hf_{20}$ aged for 3

hours at 550°C under the selected compressive loads ranging from 100MPa to 500MPa.

The transformation parameters for the same are presented in the Table 5.3. In comparison

to previously mentioned samples, the TTs were observed to increase notable by about

30°C for corresponding load levels. Akin to as extruded and sample aged at 400°C, the

load biased selection of variants is observed, and the recoverable strain is observed to

increase with applied loads. The recoverable strains were observed to increase steeply from 0.4% at 100MPa to 1.54% at 400MPa, after which the strain was observed to saturate at 1.7% at 500MPa. Negligible level of irreceverable strain was observed for loading at 400MPa and 500MPa for the sample. This can be attributed to the precipitates observed in the TEM micrographs, which strengthen the material by acting as pinning sites for dislocations and impeding the slip motion. The augmentation of the TTs is also attributed to the presence of precipitates in the material which depletes the Ni from the matrix. The hysteresis was observed to increase almost linearly from 35°C to 57°C for 100MPa and 500MPa respectively with a rather moderate slope in contrast with the sample aged at 400°C for 3 hours.

Table 5.3: Critical transformation parameters and strain levels for isobaric thermal cycling of $Ni_{45.3}Cu_5Ti_{29.7}Hf_{20}$ aged at 550°C for 3hours

Sample	Stress	Ms	Hysteresis	ε_{tr}	ε_{ir}
3hours 550°C	50	133.75	33	0.2	0
	100	134.6	35.61	0.38	0
	200	135	41.05	0.8	0
	300	139	47.54	1.27	0.11
	400	143.8	51.84	1.54	0.18
	500	150.9	57.62	1.75	0.13
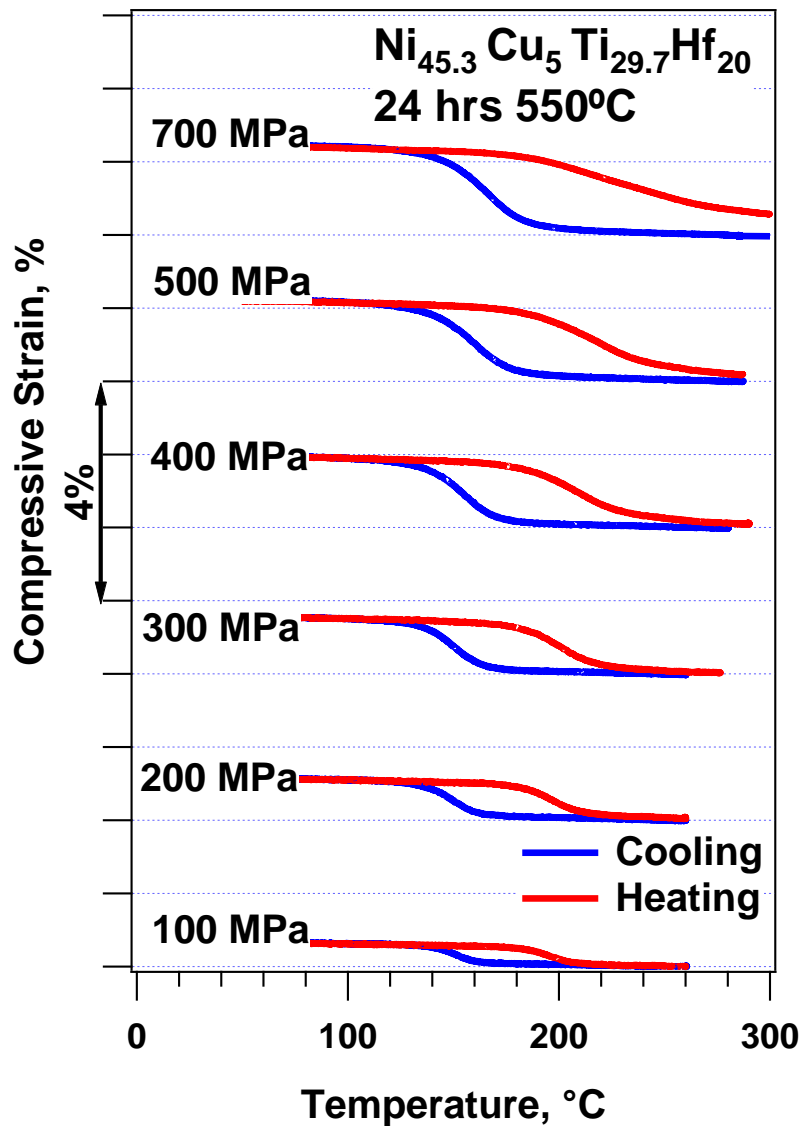
Figure 5.26: Isobaric thermal cycling of $Ni_{45.3}Cu_5Ti_{29.7}Hf_{20}$ aged for 24 hours at 550°C

The transformation behavior under stress is depicted in Figure 5.26 for the $Ni_{45.3}Cu_5Ti_{29.7}Hf_{20}$ specimen aged for 24 hours at 550°C. The TTs were observed to further increase for increment in aging time from 3 hours to 24 hours at 550°C. This observation is associated with the increment of the volume fraction of the precipitates with the increment in aging time from 3 hours to 24 hours. Apart from higher TTs, very similar behavior was observed for the samples aged for both 3 hours and 24 hours. The

recoverable strains were marginally higher for the specimen aged for 24 hours while the hysteresis was observed to be between 3 to 5°C higher in comparison with the sample aged for 3 hours. Diminutive levels of irrecoverable strain were observed at load of 500MPa which was slightly higher in contrast to specimen aged for 3 hours as presented in the table 5.4.. In contrast to the highest load level of 500MPa applied to the specimen aged for 3 hours, 700MPa was also applied to the specimen aged for 24 hours, but no increment in the transformation strain was observed and instead an irrecoverable strain of about 0.34% was observed. This suggests that the growth of precipitates observed with increment of aging time from 3 hours to 24 hours does not contribute to the mechanical strength and instead is only observed to increase the TTs.

Table 5.4: Critical transformation parameters and strain levels for isobaric thermal cycling of $Ni_{45.3}Cu_5Ti_{29.7}Hf_{20}$ aged at 550°C for 24hours

Sample	Stress	Ms	Hysteresis	ε_{tr}	ε_{ir}
24hours 550°C	50	158	39.6	0.26	0
	100	161	41.3	0.37	0
	200	161.75	46.6	0.9	0
	300	166.5	49.4	1.37	0
	400	170.1	54	1.64	0.16
	500	178.6	59.4	1.812	0.21
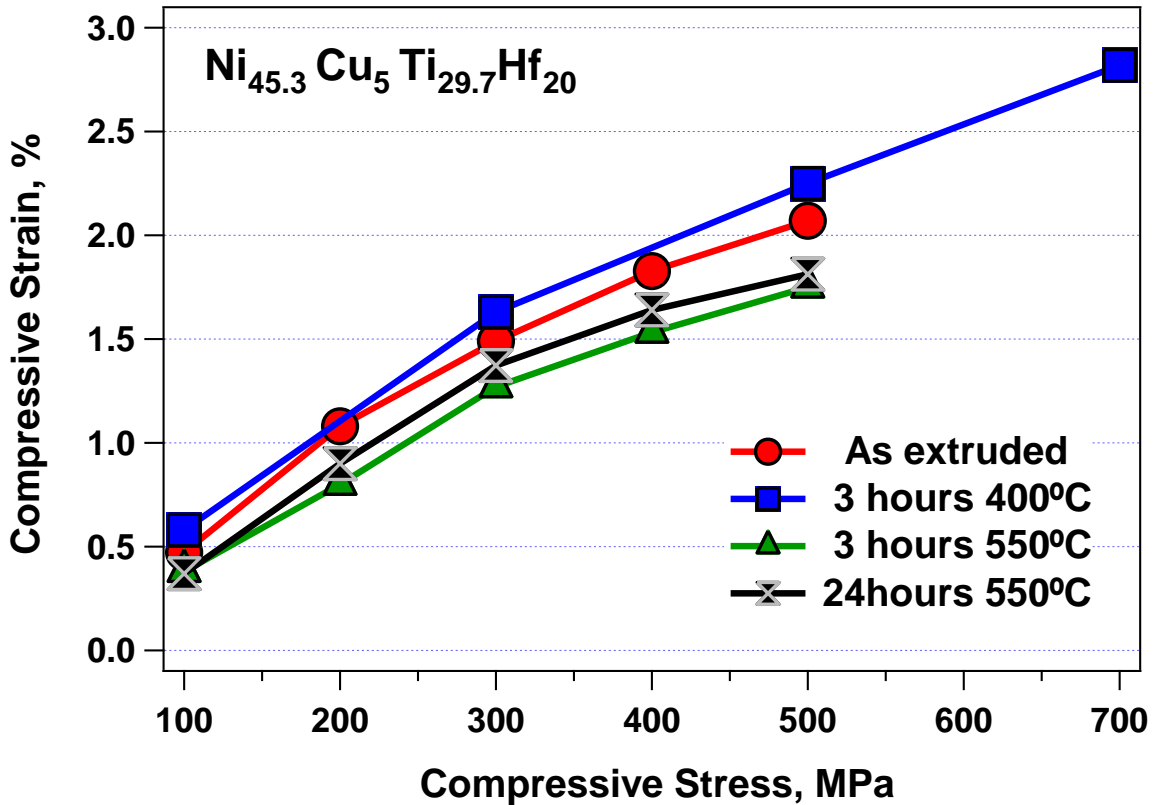
Figure 5.27: Comparison plots depicting the recoverable strain for $Ni_{45.3}Cu_5\ Ti_{29.7}Hf_{20}$ aged at varying conditions

Figure 5.27 depicts the recoverable strains for the varying loads for the specimen in as extruded condition, aged for 3 hours at 400°C and aged at 550°C for 3 hours and 24 hours.. The recoverable strain is observed to follow similar trends for all specimen under consideration. The recoverable strain was observed to be in vicinity of 0.5% for an applied load, this can be attributed to the beginning of the formation of load biased variants. These biased are observed to grow with increase in applied load levels and as a result the observed recoverable strains also increase. It should be noted from the figure that the increment in the strain level is more steep till 300MPa, which is followed by a more subtle increment. Another notable change in the mechanical behavior after loading beyond 300MPa is the introduction of irrecoverable strains. This can be attributed to the lower strength of the material, due to which loading beyond 300MPa results in formation

of dislocations in the material which the disable the alloy from recovering fully to its original position and instead a plastic deformation is introduced. The specimen aged at 400°C for 3 hours was loaded to 700MPa in contrast to other samples which were loaded to only 500MPa to check for the effect of higher loads on the recoverable strains. It was noted that the transformation strain increased with increment of load from 500MPa to 700MPa, but as reported earlier it was accompanied by about 0.67% irrecoverable strain, hence only a minute overall increment in the work output is observed. Even though the recoverable strains were observed to be marginally lower than other specimen for the samples aged at 550°C for 3 and 24 hours, due to no irrecoverable strain and high TTs makes them more suitable contender for practical applications.

Figure 5.28 depicts the comparison for the thermal hysteresis for the transformation under the varying loads for the selected alloys. The hysteresis is an important characteristic to be taken into consideration for use of SMAs in active actuation since the large amount of hysteresis would require larger time for the sample to cool down lower into martensite from austenite and this would hamper the frequency with which the actuator can be used. The hysteresis was observed to increase with the increment in the applied loads on the compression sample for the various specimen as depicted in figure 5.28. The hysteresis was determined to be minimum for the sample aged at 400°C for 3 hours, while the maximum was observed for the one aged at 550°C for 24 hours. Interestingly the hysteresis was found to be in the same order as the progression of TTs for various specimen for loading till 300MPa, such that the specimen observed with highest TTs was observed to have the highest hysteresis and the specimen with the lowest TTs was observed to have lowest hysteresis also. In general, the

hysteresis was observed to increase with the increment in applied loads. The hysteresis increased more sharply for the as extruded specimen and the one aged at 400°C for 3hours in comparison to the specimen aged at 550°C for 3hours and 24 hours.
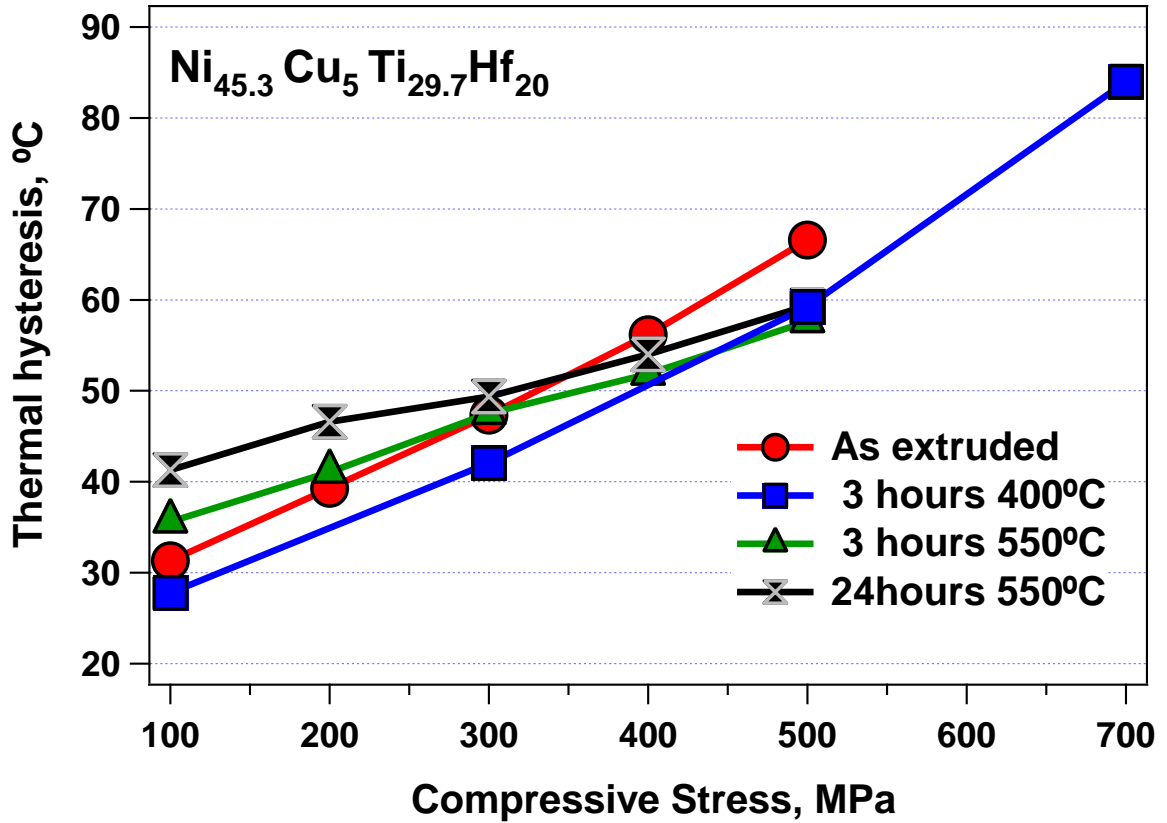
Figure 5.28: Comparison plots depicting thermal hysteresis for $Ni_{45.3}Cu_5Ti_{29.7}Hf_{20}$ aged at varying temperatures for 3hours
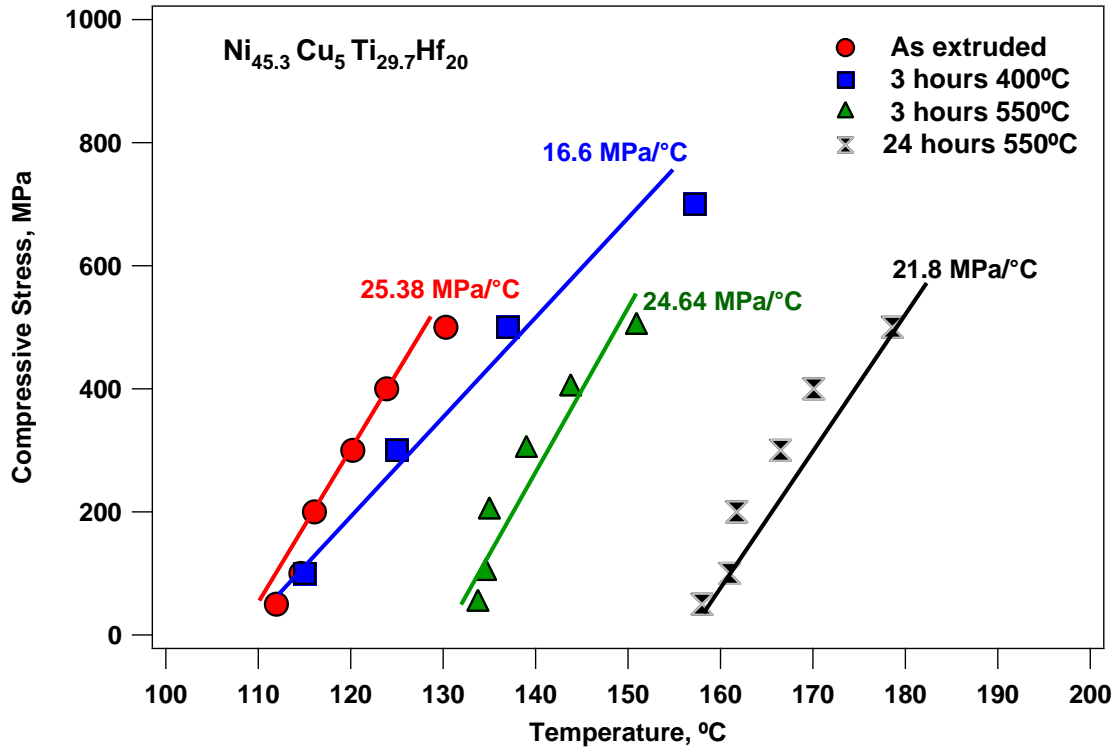
Figure 5.29: Clausius-Clayperon curves for $Ni_{45.3}Ti_{29.7}Hf_{20}$ aged at varying conditions with respect to M_s temperatures.

Figure 5.29 shows the Clausius-Clayperon extracted from the Figures 5.23 to 5.26. In the plot, the M_s temperature determined from the transformation curve obtained by isobaric thermal cycling, is plotted against the applied stress level. Linearity of the curves is expected along the lines of Clausius-Clayperon law. The difference in the slope of the curves as observed for the different specimen can be attributed to the different heat of enthalpies for the transformation for the respective samples, which was observed in the DSC curves presented in the earlier sections.
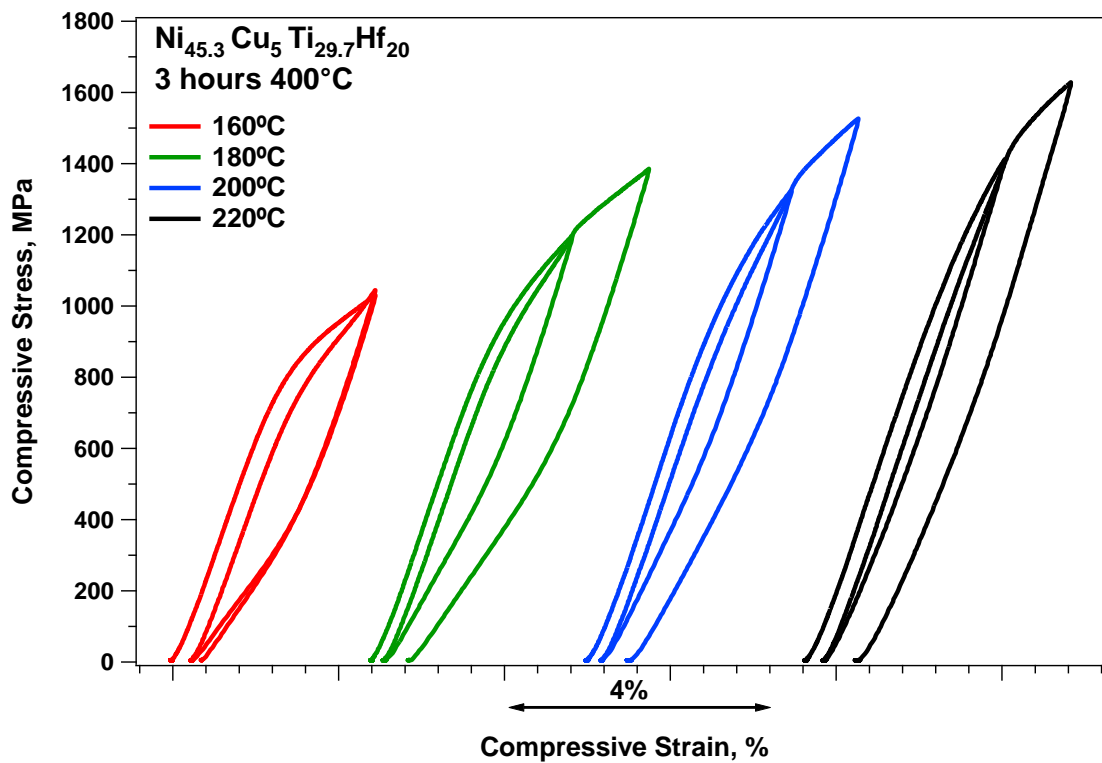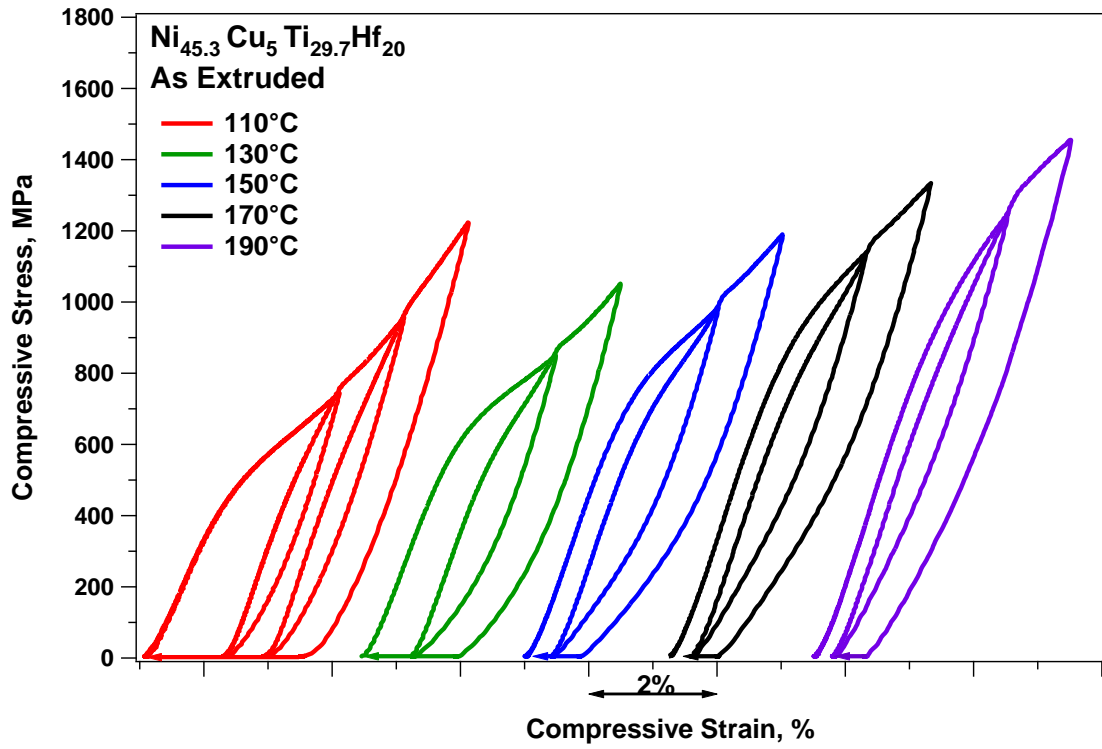
Figure 5.30: Isothermal mechanical cycling of $Ni_{45.3}Cu_5Ti_{29.7}Hf_{20}$ in as extruded condition (top) and aged for 3 hours at 400°C(bottom)
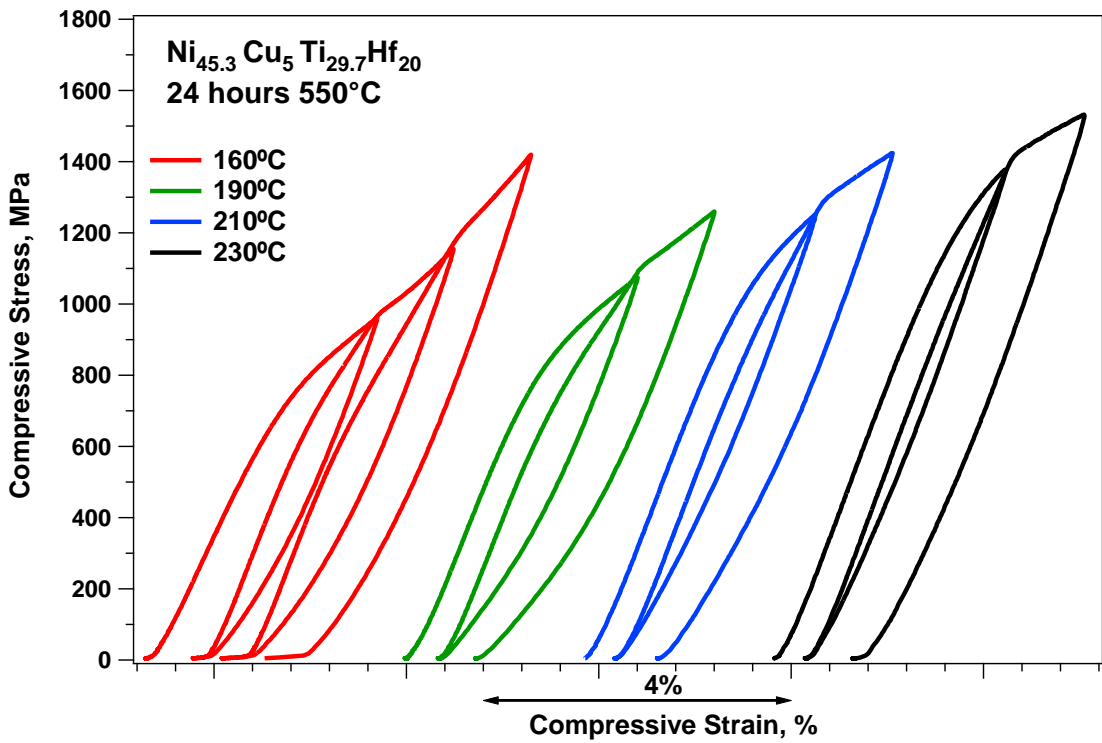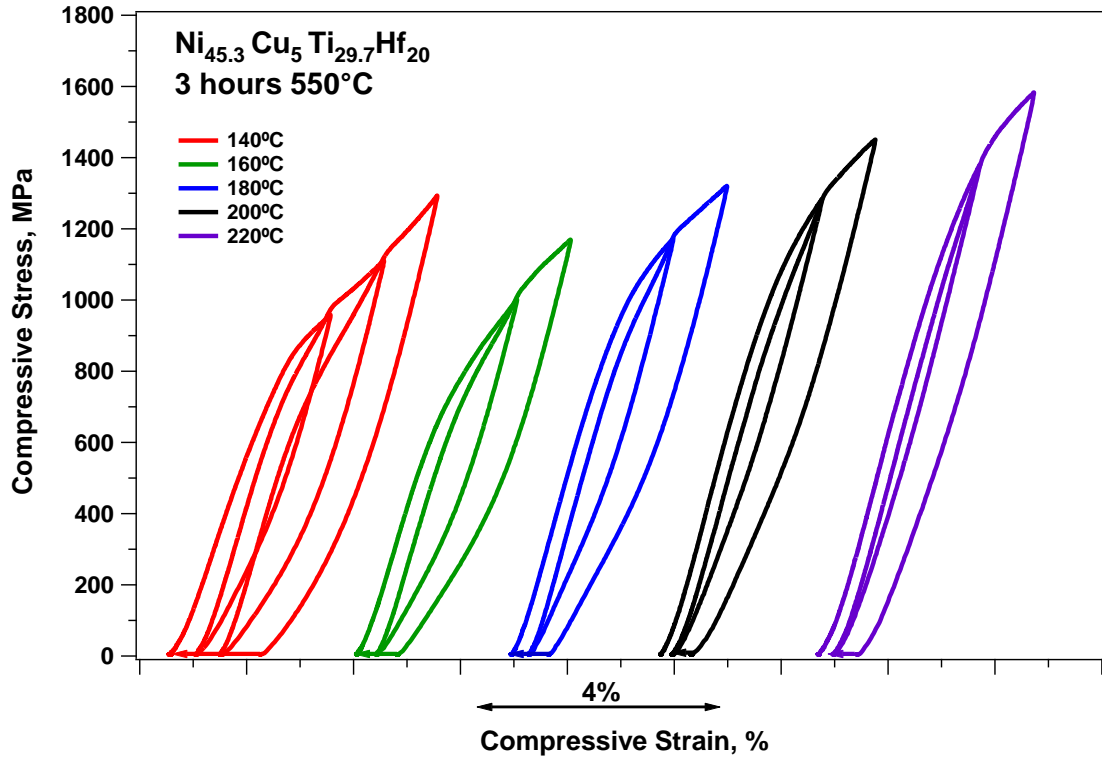
Figure 5.31: Isothermal mechanical cycling of $Ni_{45.3}Cu_5Ti_{29.7}Hf_{20}$ aged at 550°C for 3 hours (top) and 24 hours(bottom)

The plots shown in Figure 5.30 and 5.31 depict the isothermal compressive loading and unloading curves for the specimen whose results have been reported for isobaric thermal cycling in the previous section. The lowest testing temperature was selected to be 10°C higher than the M_s temperature for the specimen and the further testing was done at 20°C higher than the previous testing temperature. The testing temperature was increased more than 20°C for the samples in which no back transformation was observed at all, which meant the sample was too low to initiate the back transformation and for any PE behavior it would have to raised. The temperature at which the test was run was achieved by cooling from temperature higher than A_f, to ensure that the sample was in austenitic state. The specimen was then loaded to 3% and 4% compressive strain calculated beforehand while maintaining stable temperature.

In Figure 5.30(a) depicts the results for as extruded specimen for which the critical strain levels are presented in Table 5.5. When the specimen was loaded initially to 3,4 and 5% at 110°C, the stress induced transformation from austenite to martensite is observed but during the unloading the back transformation was not observed leaving behind 2.5% unrecovered strain upon loading to 5% strain. This pre-strained sample was heated to 350°C, whole of the irrecoverable strain was recovered and hence no plastic strain was observed. The test at 130°C yielded similar behavior but the irrecoverable strain was of the order of 1.5%, which was also recovered fully upon heating. 3% loading at 150°C yielded better PE response with large hysteresis and only about 0.5% irrecoverable strain was observed, further when the sample was loaded to 4% an additional irrecoverable strain of 0.5% was observed, which was fully recovered upon heating. Similar behavior was observed for the loading cycle at 170°C, in which a stress

of 1360 MPa was required to induce 4% strain. About 0.8% irrecoverable strain was observed upon unloading, and contrary to initial cases this irrecoverable strain was not fully recovered upon heating and a plastic strain of 0.24% was observed. Further tests at 190°C resulted in higher transformation stresses and these high stress can be held responsible for inducing dislocations in the material as plastic strain was observed in order or 1% for testing at 190°C and the unloading curve even at 3% did not show any PE recovery and hence no further loading was done.

Table 5.5: Critical transformation parameters and strain levels for isothermal mechanical cycling of $Ni_{45.3}Cu_5Ti_{29.7}Hf_{20}$ in as extruded condition

Sample	Testing Temperature °C	Total Strain %	Elastic Recovery%	PE Strain %	SME on heating %	Irrecover-able strain %
As Extruded	110	5	1.77	0.78	2.45	0
	130	4	1.47	1.12	1.4	0
	150	4	1.86	1.27	0.87	0
	170	4	1.93	1.374	0.45	0.246
	190	4	1.98	1.163	0.5	0.357

As shown in Figure 5.30(b) the loading and unloading for sample aged at 400°C for 3 hours showed behavior similar to as extruded sample when tested at 140°C. The proximity of testing temperature to the M_s temperature can be held responsible for no back transformation once martensite nucleates upon application of stress. Notably the tests for 3% at both 160°C and 180°C yield almost perfect PE curves. Loading to 4% for both testing temperatures show PE recovery but a residual strain of 0.4% at 160°C for loading to 3% strain and 0.6% at 180°C for 4% strain level is observed. These irrecoverable strains could be recovered almost completely upon heating to 350°C leaving behind no plastic strain as shown in Table 5.6. Further increment of testing

temperature to 200°C and 220°C lead to transformation stress around 1087MPa and 1250MPa respectively and possibly due to this high stress dislocations were introduced and hence plastic strain of 1% was observed which could not be recovered upon heating to 400°C.

Table 5.6: Critical transformation parameters and strain levels for isothermal mechanical cycling of $Ni_{45.3}Cu_5Ti_{29.7}Hf_{20}$ aged at 400°C for 3 hours

Sample	Testing Temperature °C	Total Strain %	Elastic Recovery%	PE Strain %	SME on heating %	Irrecover-able strain %
3 hours 400°C	160	3	1.68	0.96	0.36	0
	180	4	2.27	1.34	0.39	0
	200	4	2.48	0.9	0.3	0.32
	220	4	2.5	0.74	0.14	0.62

Table 5.7: Critical transformation parameters and strain levels for isothermal mechanical cycling of $Ni_{45.3}Cu_5Ti_{29.7}Hf_{20}$ aged at 550°C for 3 hours

Sample	Testing Temperature °C	Total Strain %	Elastic Recovery%	PE Strain %	SME on heating %	Irrecover-able strain %
3 hours 550°C	140	4	1.98	1.287	0	0
	160	4	1.834	1.375	0	0
	180	4	2.167	1.125	0	0
	200	4	2.33	1.1	0.4	0.25
	220	4	2.4	0.9	0.42	0.28

Figure 5.31 (a) and (b) depict the isothermal compressive cycling for the specimen aged at 550°C for 3 hours and 24 hours respectively. The transformation parameters for the same are presented in the Tables 5.7 and 5.8. The effect of the precipitates shown earlier for the two specimen aged at 550°C is visible from the improvement in PE response contrary to as extruded and the specimen aged at 400°C.

Perfect PE was still not observable in either of the two specimen aged at 550°C, which can be attributed to the less volume of precipitates. Due to the lesser populace of precipitates, the dislocations have relative ease to break through due to larger distance between the precipitates and as a consequence the material's critical resolved shear stress is comparable to transformation stress and hence the fully recoverable curves as expected of perfect PE curves is not observed.

Table 5.8: Critical transformation parameters and strain levels for isothermal mechanical cycling of $Ni_{45.3}Cu_5Ti_{29.7}Hf_{20}$ aged at 550°C for 24 hours

Sample	Testing Temperature °C	Total Strain %	Elastic Recovery%	PE Strain %	SME on heating %	Irrecover-able strain %
24 hours 550°C	160	5	2.054	0.9	0	0
	190	4	1.96	1.04	0	0
	210	4	2.2	0.77	0.4	0.63
	230	4	2.28	0.54	0.28	0.9
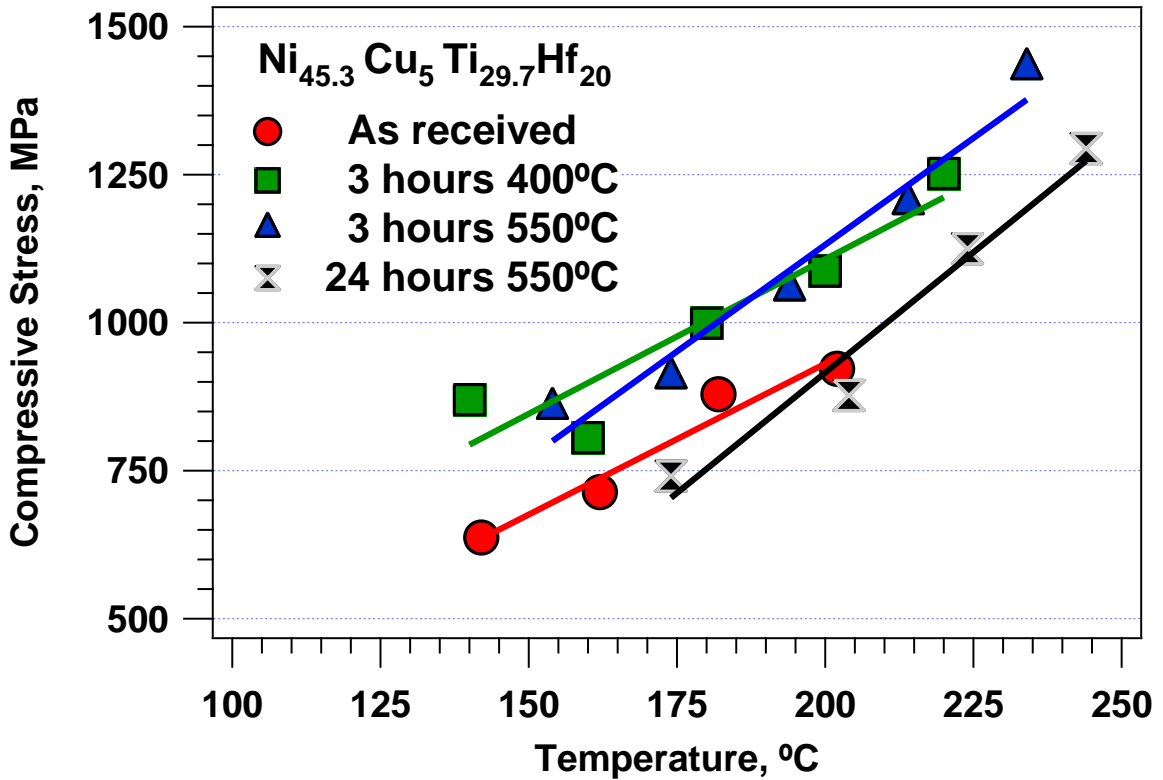
Figure 5.32: Clausius-Clayperon curves for $Ni_{45.3}Cu_5Ti_{29.7}Hf_{20}$ aged at varying time and temperatures for with respect to M_s temperatures.

Figure 5.32 depicts the comparison of the Clausius-Clayperon curves $Ni_{45.3}Cu_5Ti_{29.7}Hf_{20}$ determined from the PE cycling of the samples tested. The samples aged at 550°C for 3 hours and 24 hours had a steeper slope in comparison with the sample in as extruded condition and aged at 400°C for 3 hours. The steep slopes in range of 22-24MPa/°C for Clausius-Clayperon relation along with a lower critical stress for slip can be attributed for the imperfect PE curves obtained. The correspondence of the curves determined here from PE tests with the isobaric thermal cycling tests and linearity of the curves ensure the fact that curve can be used for predicting further results with accuracy.
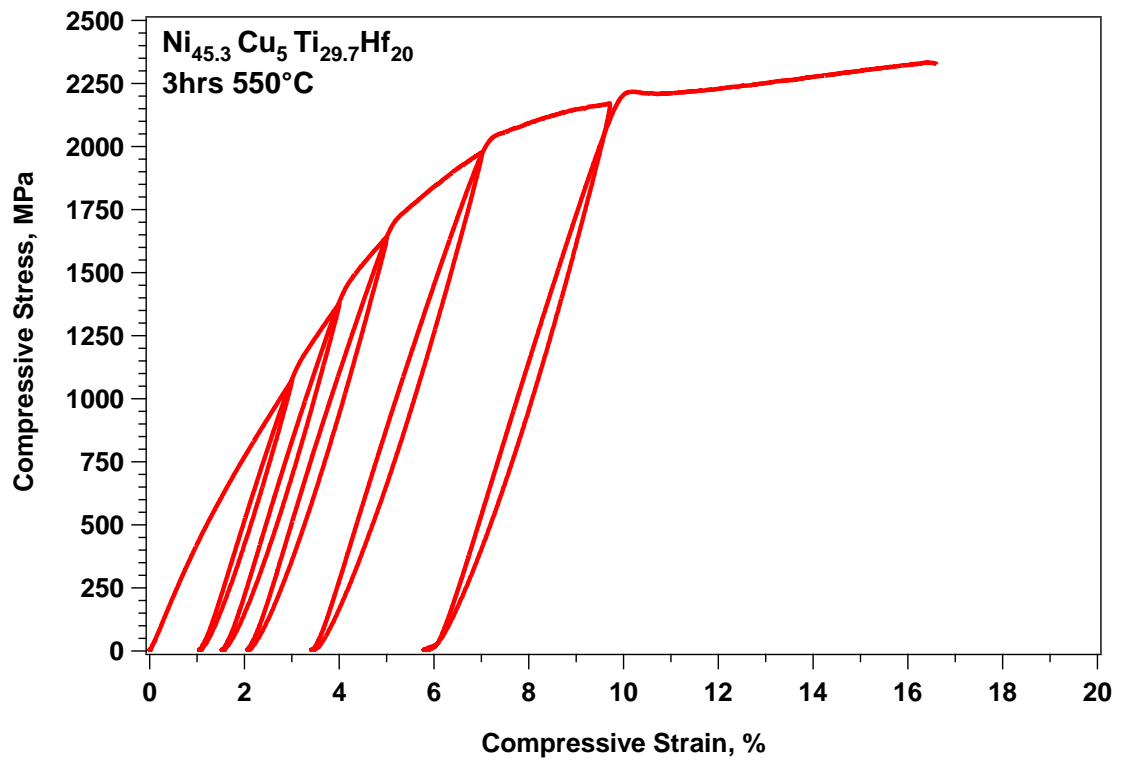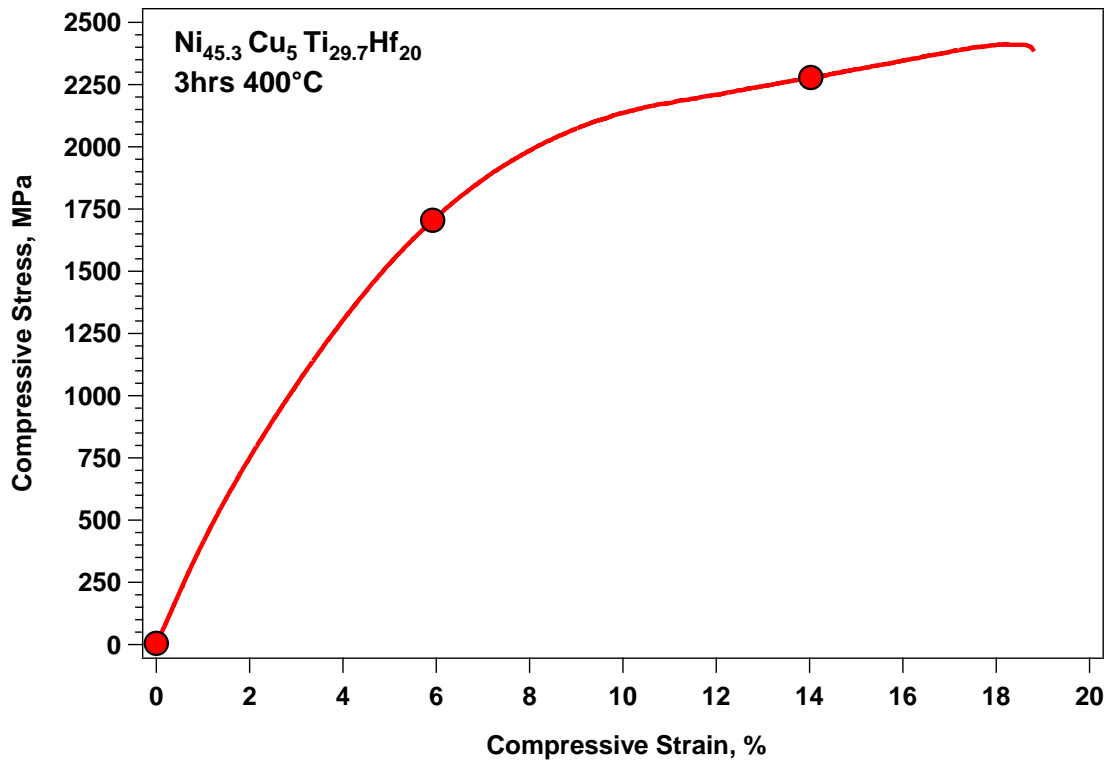
Figure 5.33: Ultimate yielding curves for $Ni_{45.3}Cu_5Ti_{29.7}Hf_{20}$ compression samples aged for 3hours at 400°C and 550°C

Figure 5.33 depicts the loading curves for $Ni_{45.3}Cu_5Ti_{29.7}Hf_{20}$ samples aged at 400°C and 550°C for 3 hours until failure. The addition of Cu to the $Ni_{50.3}Ti_{29.7}Hf_{20}$ ternary alloy with substitution for Ni can be attributed for the increased ductility of the material. This comparatively better ductility can be instrumental in solving the problem involved with the material processing into intricate shapes and further advance the possibility of usage of the material in practical applications.

Experimental Results :$Ni_{45.3}Pd_5Ti_{29.7}Hf_{20}$

6.1 Calorimetric Analysis

Effect of various heat treatments on the $Ni_{45.3}Pd_5Ti_{29.7}Hf_{20}$ alloy have been presented in this chapter in the form of DSC plots, hardness results, XRD and TEM analysis of the structure. Mechanical results are presented in the final section.
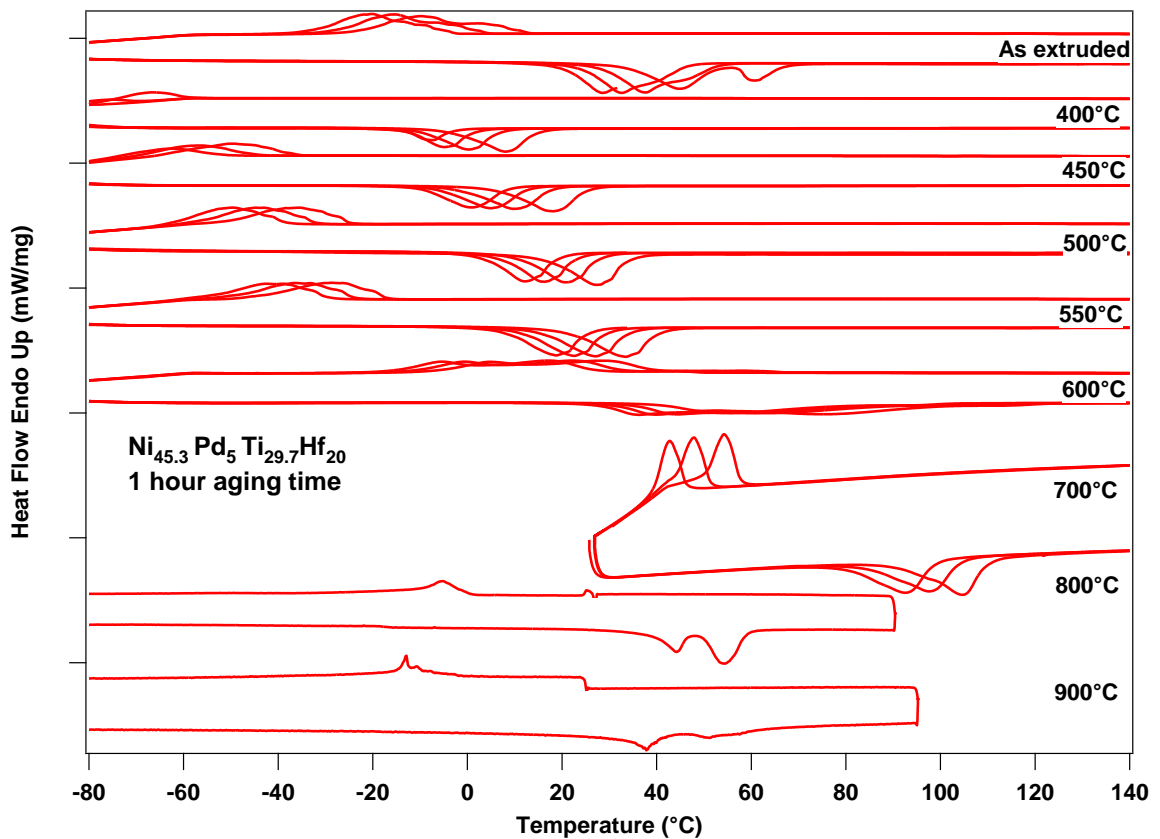
Figure 6.1: DSC plot showing the thermal cycling for $Ni_{45.3}Pd_5Ti_{29.7}Hf_{20}$ alloy aged for 1 hour ranging from 400°C to 900°C.

Figure 6.1 depicts the DSC curves for $Ni_{45.3}Pd_5Ti_{29.7}Hf_{20}$ aged for 1 hour at temperatures varying from 400°C to 900°C. The DSC curve for the as extruded sample was added on the top of the plot to give an overall outlook of the variation of the TTs.

The TTs for the alloy were observed to be the lowest of the three compositions $Ni_{50.3}Ti_{29.7}Hf_{20}$, $Ni_{45.3}Cu_5Ti_{29.7}Hf_{20}$ and $Ni_{45.3}Pd_5Ti_{29.7}Hf_{20}$ studied in the present assessment. Analogous to the $Ni_{45.3}Cu_5Ti_{29.7}Hf_{20}$, $Ni_{45.3}Pd_5Ti_{29.7}Hf_{20}$ alloy also followed the similar trend of an initial drop in the TTs when aged for 1 hour at temperatures lower than 450°C, following which the increment in the aging temperature led to increment in the TTs till the aging temperature of 700°C. Further increment in the aging temperature to 800°C and 900°C led to the decrement in the TTs. They were observed to reach their initial levels of as extruded condition before having reached their maximum values for aging at 700°C. For all aging temperatures, the cyclic stability was not quite notable and the TTs fell about 10°C for each cycle. The peaks were generally observed to be very broad, especially for the sample aged at 600°C which was observed to be the broadest. The initial decline in the TTs with aging can be attributed to the relief of dislocations introduced in the material during the extrusion process. The material was extruded at the same temperatures of 900°C similar to the previously discussed alloys, and the variation in TTs was also found to be similar.

The path traced out by the curve for variation of peak hysteresis for the sample aged for 1 hour was noted to be reverse of the TTs. The maximum peak hysteresis was 68C for samples aged at 400°C and 450°C, and minimum of 49°C for the sample aged at 700°C. The high peak hysteresis can be attributed to the hindrance in backward nucleation of martensite due to very tiny precipitates, which is also visible from extremely low TTs of the samples with higher degree of hysteresis. The hysteresis for was in order of 110°C for both aging temperatures between the M_f and A_f temperatures.
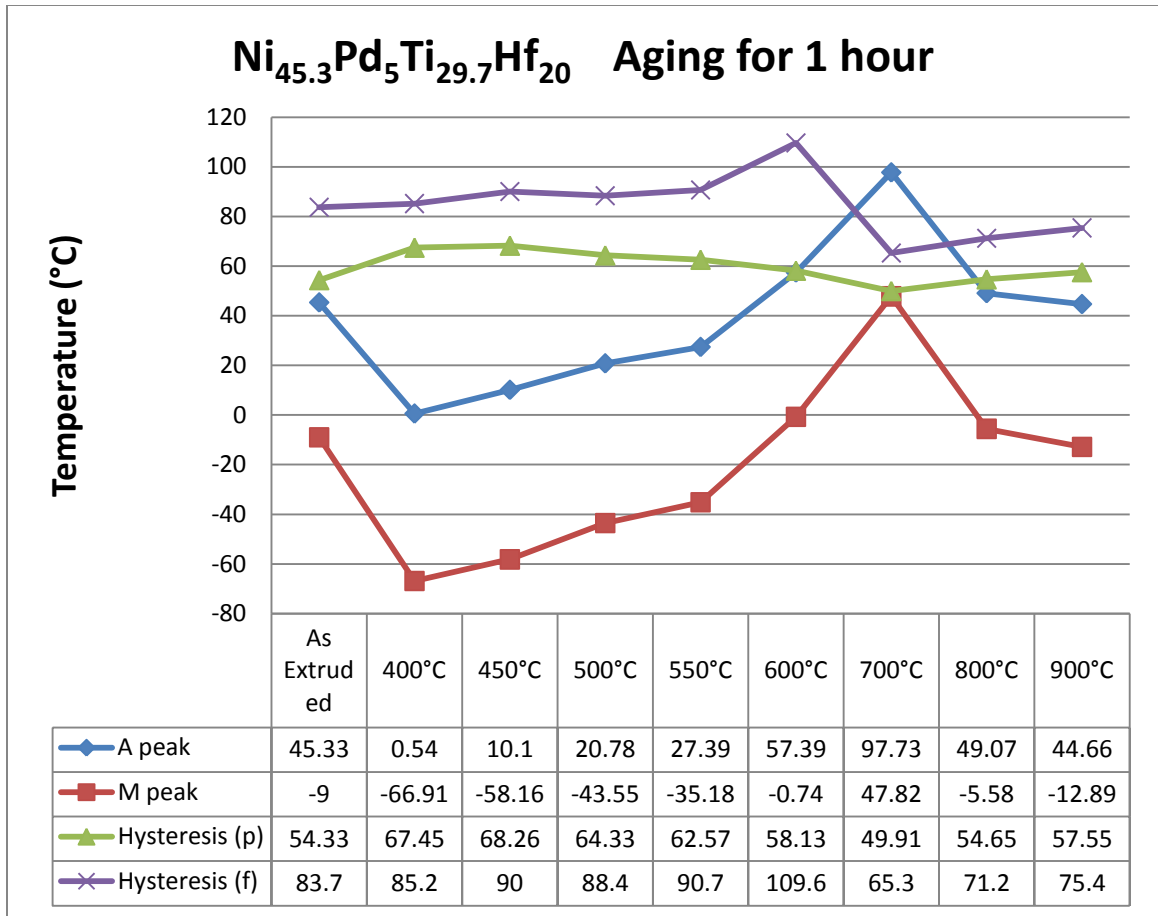
Figure 6.2: Peak transformation temperatures and hsyteresis for $Ni_{45.3}Pd_5Ti_{29.7}Hf_{20}$ alloy aged for 1 hour ranging from 400°C to 900°C.

Figure 6.2 represents the transformation peak temperature for the DSC results of the $Ni_{45.3}Pd_5Ti_{29.7}Hf_{20}$ samples aged for 1 hour ranging from 400°C to 900°C along with peak hysteresis (p) represented as the difference between the two peak temperatures and hysteresis (f) depicted as the difference of the A_f and M_f. The TTs dropped by 45°C for initially aging for 1 hour at 400°C followed by a linear rise to aging at 550°C. With further increment in aging temperature too 600°C and 700°C led to a steep rise in TTs of 30°C for increasing aging temperature from 550°C to 600°C and 40°C for finally increasing the aging temperature to 700°C. It was at aging temperature of 700°C, that the highest TTs of more than 50°C higher in contrast to as extruded condition were achieved,

along with the lowest hysteresis of little less than 50°C observed so far for the alloy system. With further increment in aging temperature to 800°C, the TTs fell down to level comparable to as extruded condition, followed by a further decrement of 5-6°C for increasing the aging temperature to 900°C.
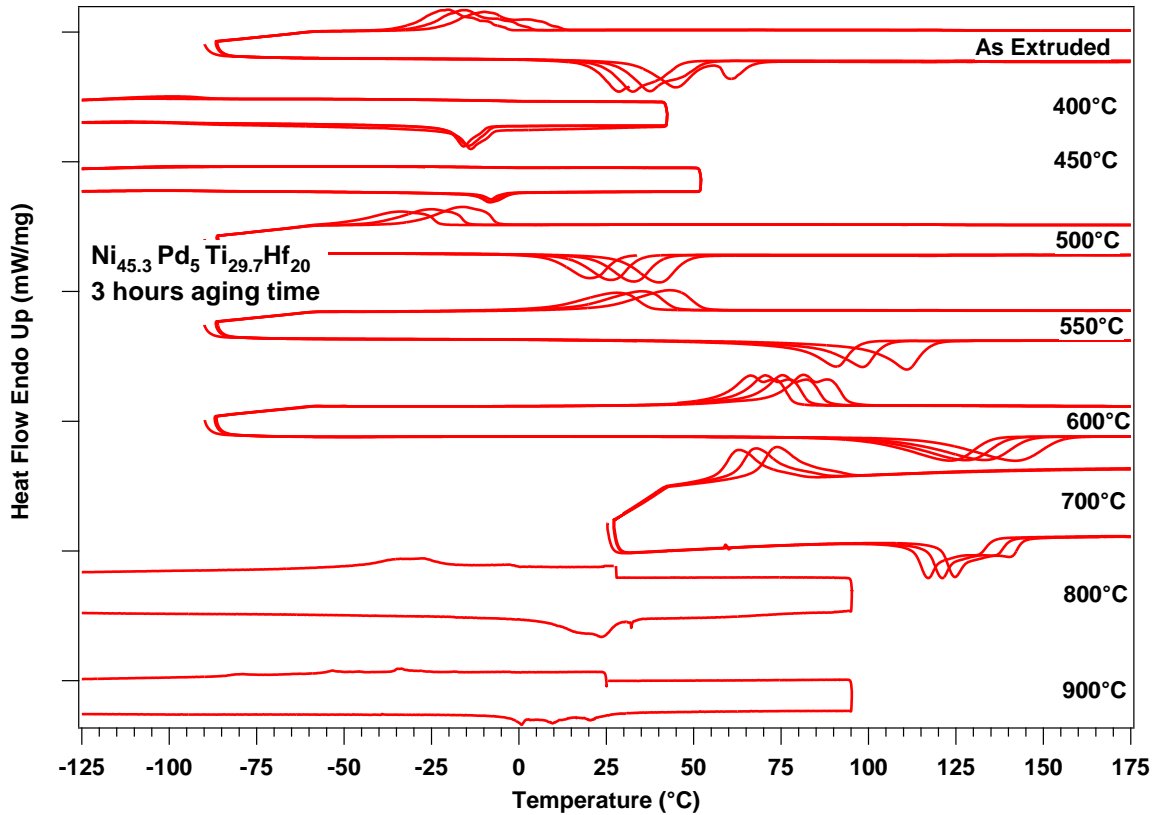
Figure6.3: DSC plot showing the thermal cycling for $Ni_{45.3}Pd_5Ti_{29.7}Hf_{20}$ alloy aged for 3 hour ranging from 400°C to 900°C.

Figure 6.3 represents the DSC curves for $Ni_{45.3}Pd_5Ti_{29.7}Hf_{20}$ samples aged at temperature varying from 400°C to 900°C for 3 hours. Huge variation in the transformation behavior is clearly visible in the plot. Parallel to the behavior for aging at corresponding temperatures for 1 hour, aging at 3 hours also resulted in sharp initial decline in the TTs when the sample was aged at 400°C. The TTs continue to be subzero for aging at 450°C also, after having increased a few degrees. Aging at 500°C led to a

reverse in the trend and the TTs started to increase sharply till increment of the aging temperature of 600°C. The realization of maximum TTs for the aging time of 3hours at 600°C in contrast to 700°C there is only a small change for 1 hour aging time can be attributed to the effect of higher aging time on the growth and dissolution of precipitates. The TTs were observed to saturate and stopped from further increment for increasing the aging temperature from 600°C to 700°C at aging time of 3 hours contrary to increment in TTs from 600°C to 700°C in case of aging for 1 hour. This can be attributed to the beginning of dissolution of precipitates at longer time at 700°C at opposed to high volume fraction of precipitates prior to their dissolution at longer time.

$Ni_{45.3}Pd_5Ti_{29.7}Hf_{20}$ Aging for 3 hours

	As Extruded	400°C	450°C	500°C	550°C	600°C	700°C	800°C	900°C
A peak	45.33	-14.8	-8.4	31.96	98.24	132.65	128.33	24.96	9.36
M peak	-9	-104.6	-99.96	-24.11	34.76	79.55	68.29	-32.65	-41.84
Hysteresis (p)	54.33	89.8	91.56	56.07	63.48	53.1	60.04	57.61	51.2
Hysteresis(f)	83.7	112.7	110.4	93.3	91.2	89.8	81.1	78.7	64.05
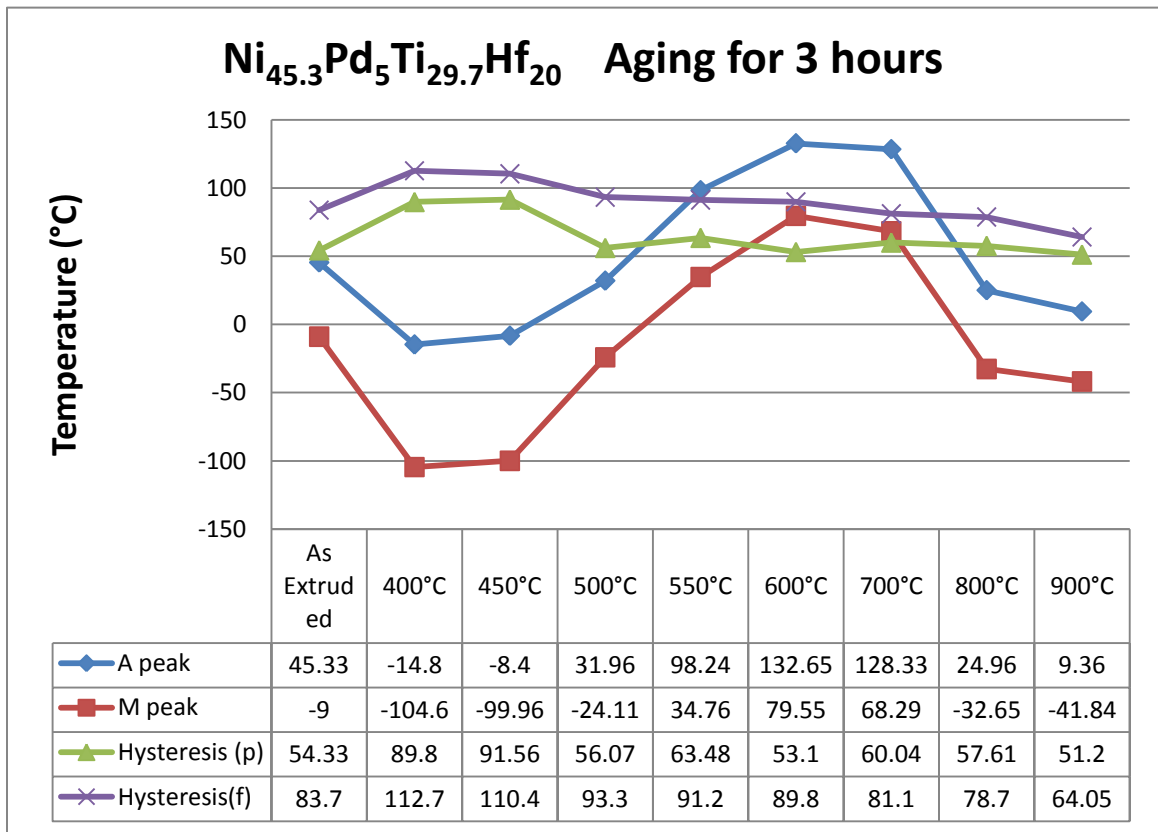
Figure 6.4: Peak transformation temperatures and hsyteresis for $Ni_{45.3}Pd_5Ti_{29.7}Hf_{20}$ alloy aged for 3 hours ranging from 400°C to 900°C.

Figure 6.4 depicts the peaks temperatures of DSC curves for $Ni_{45.3}Pd_5Ti_{29.7}Hf_{20}$ alloy aged for 3 hours shown extracted from Figure 6.3. A steep drop in the A_p of 60°C was observed in comparison to as extruded sample for the sample aged at 400°C for 3 hours, while a very broad peak was observed for transformation back to martensite and the peak temperature for the peak dropped to -104°C and the hysteresis increased to about 90°C. Hysteresis extracted from the transformation finish values of temperature remained higher than the hysteresis extracted from peak values but essentially followed the same trend. Aging at 450°C also resulted in very low TTs despite a small increment though the hysteresis still increased by another 1.5°C. Aging at 500°C resulted in a steep increment of the TTs from 450°C aging, though the TTs still remained lower in comparison for the as extruded condition and the hysteresis also dropped back to about 2°C higher than initial value. TTs continued to increase for aging at 550°C and 650°C with the highest A_p of 132.7°C for aging at 650°C. The TTs dropped marginally for aging at 700°C but for aging at 800°C and 900°C the TTs dropped about 20°C and 35°C respectively.

Table 6.1: Hysteresis depicted as a function of the difference of austenite finish and martensite finish temperatures for $Ni_{45.3}Pd_5Ti_{29.7}Hf_{20}$ aged at various temperatures for 1 hour and 3 hours

Aging Condition	1 hour			3 hours		
	M_f	A_f	Hysteresis	M_f	A_f	Hysteresis
As Extruded	-29.3	54.4	83.7	-29.3	54.4	83.7
400°C	-76	9.2	85.2	-119.4	-6.7	112.7
450°C	-71	19	90	-109.2	1.2	110.4
500°C	-57.4	31	88.4	-51	42.3	93.3
550°C	-53	37.7	90.7	16.8	108	91.2
600°C	-13.1	96.5	109.6	57.5	147.3	89.8
700°C	42.1	107.4	65.3	59.9	141	81.1
800°C	-11.4	59.8	71.2	-46.1	32.6	78.7
900°C	-14.8	60.6	75.4	-40.4	23.65	64.05

Table 6.1 depicts the hysteresis as difference between the A_f and M_f temperatures for $Ni_{45.3}Pd_5Ti_{29.7}Hf_{20}$ samples aged between 400°C and 900°C for 1 hour and 3 hours. The hysteresis is not observed to follow a clear pattern when aged for 1 hour, however the hysteresis is maximum for the aging at 400°C for 3 hours and then it is observed to gradually decrease with increment in aging time.
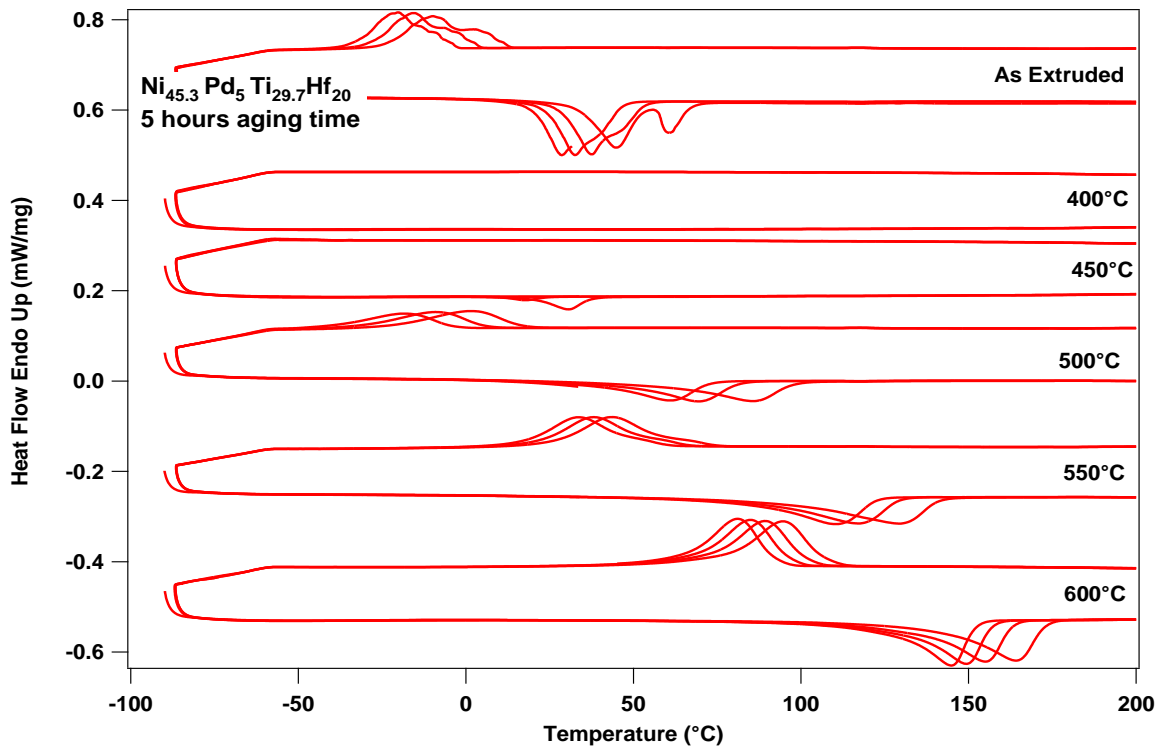
Figure 6.5: DSC plot showing the thermal cycling for $Ni_{45.3}Pd_5Ti_{29.7}Hf_{20}$ alloy aged for 5 hour ranging from 400°C to 600°C.

Figure 6.5 depicts the transformation behavior for the for $Ni_{45.3}Pd_5Ti_{29.7}Hf_{20}$ alloy samples aged for 5 hour ranging from 400°C to 600°C. Due to decrease in the TTs for aging beyond 600°C for 3 hours, the 5 hours aging was carried out for a highest temperature of 600°C only. Following the previous trend of initial decrement of TTs when aged at 400°C and 450°C, the TTs decreased to an extent that they could not be

captured by running the DSC till a temperature of -90°C for sample aged at 400°C, while only the first cycle could be captured for the sample aged at 450°C. Additional experiments at lower temperatures of a minimum of -150°C were also carried out for the two specimens but still no peaks were observed. Specimen aged at 500°C showed an increment in the TTs from as extruded condition and the TTs continued to increase with increment in the aging temperatures to 550°C and 600°C. The TTs rose higher in comparison for the corresponding aging temperatures between 500°C and 600°C in contrast of 3 hours aging. The transformation cycles were more stable for subsequent cycles thought the hysteresis increased in contrast with 3 hours aging.

$Ni_{45.3}Pd_5Ti_{29.7}Hf_{20}$ Aging for 5 hours

	As extruded	400°C	450°C	500°C	550°C	600°C
A peak	45.33		29.91	68.3	116.65	153.57
M peak	-9			-8.98	38.03	90.21
Hysteresis	54.33			77.28	78.62	63.36

Figure 6.6: Comparison plot showing the peak temperatures for $Ni_{45.3}Pd_5Ti_{29.7}Hf_{20}$ alloy aged for 5 hours ranging from 400°C to 600°C.

Figure 6.6 depicts the peak temperatures extracted from the DSC curves shown in Figure 6.5. Since no clear transformation was observed for samples aged at 400°C and 450°C, a gap in the curve depicting the varying TTs is present. The TTs for 500°C increased about 13°C in comparison to as extruded condition and the hysteresis also increased by 23°C. Aging at 550°C resulted in another increment of TTs by about 50°C for A_p and 40°C for M_p. The hysteresis increased marginally by a little over 1C. Further increment in aging temperature to 600°C to led an considerable increment in the TTs to 153°C for A_p and 90°C for M_p which is in the order of 100°C in comparison with as extruded sample. The hysteresis increase also but by comparably a small Figure of 9°C with respect to the as extruded sample.
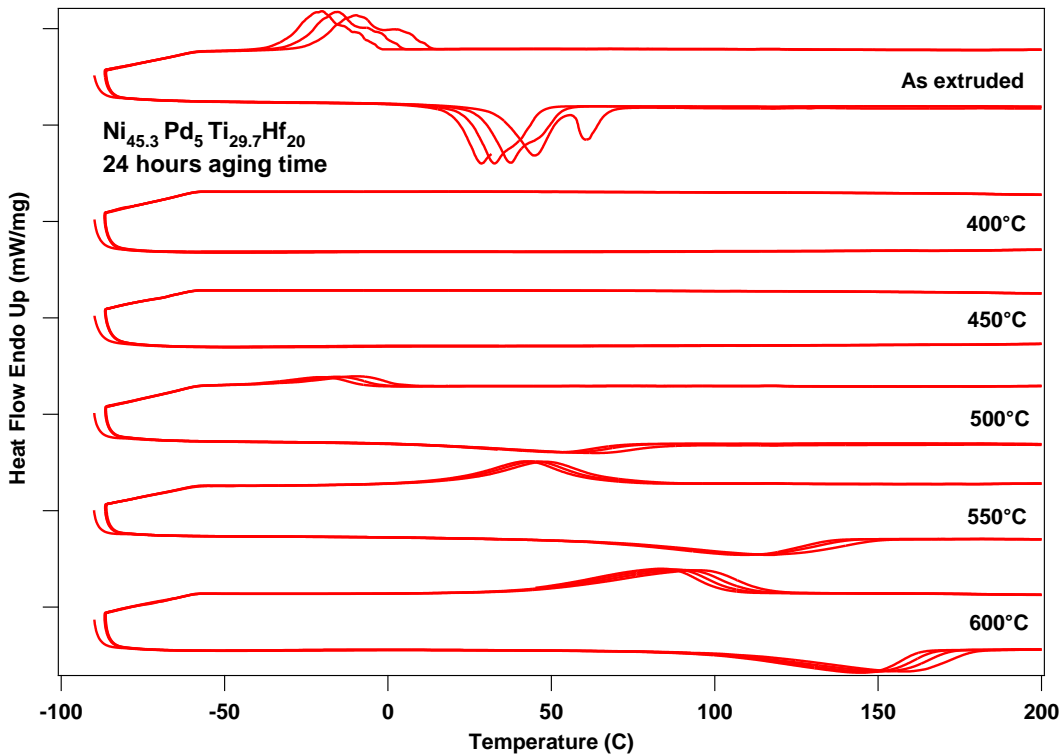
Figure 6.7: DSC plot showing the thermal cycling for $Ni_{45.3}Pd_5Ti_{29.7}Hf_{20}$ alloy aged for 24 hour ranging from 400°C to 600°C.
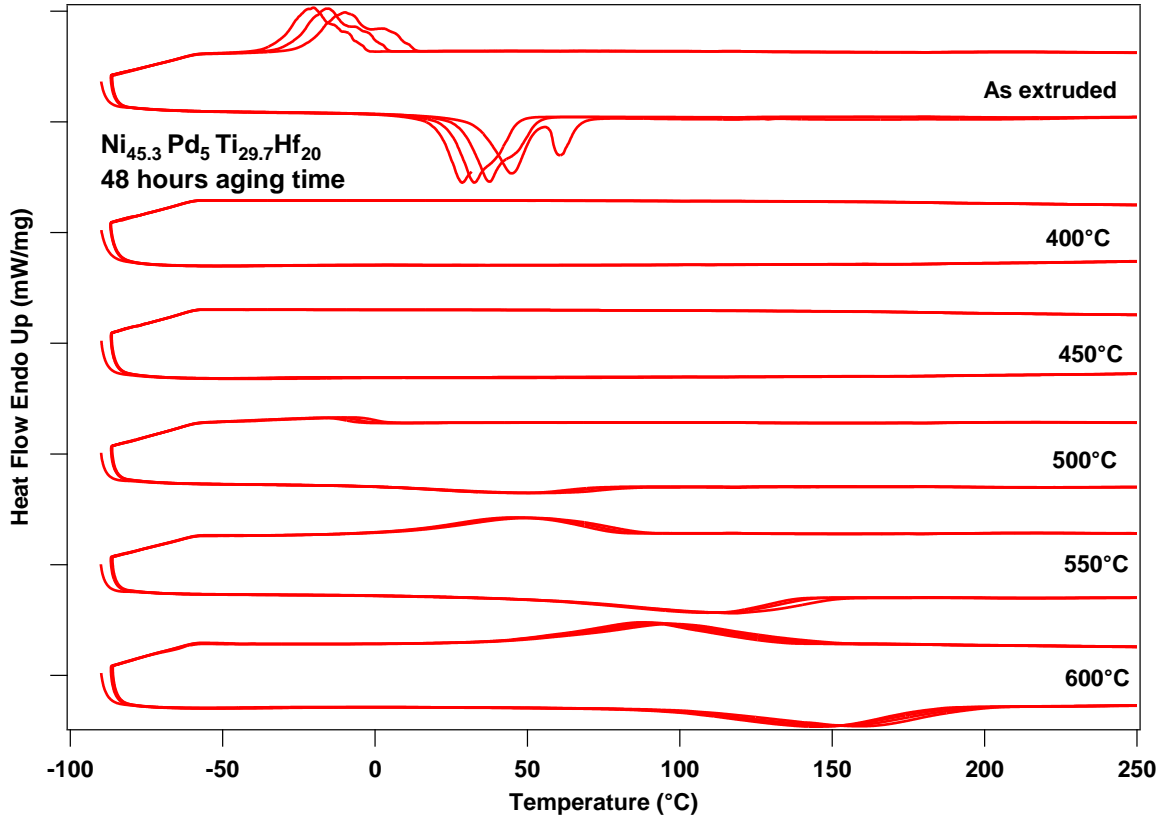
Figure 6.8: DSC plot showing the thermal cycling for Ni$_{45.3}$Pd$_5$Ti$_{29.7}$Hf$_{20}$ alloy aged for 48 hour ranging from 400°C to 600°C.

Figures 6.7 and 6.8 represent the DSC curves for the Ni$_{45.3}$Pd$_5$Ti$_{29.7}$Hf$_{20}$ alloy aged between temperatures of 400°C and 600°C for 24 hours and 48 hours respectively. No transformation peaks were observed for aging at 400°C and 450°C for either 24 hours or 48 hours. Highly repeatable curves with very broad peaks were observed for all other three aging temperatures of 500°C, 550°C and 650°C for both aging times of 24 and 48 hours. The TTs for aging at 500°C for 24 hours and 48 hours are marginally higher than the as extruded condition but peaks changed from being sharp to broad in nature. Similarly the aging at 550°C for 24 hours and 48 hours both yielded TTs sizably higher than as extruded condition. The DSC curves were highly stable and the curves overlapped the preceding curve, but the peaks were very broad and the hysteresis also increased.

154

Further increase in aging temperature to 600°C resulted in additional increment in TTs along with the same characteristics as explained for 550°C curve at both 24 and 48 hours. The sizable breadth of the DSC peaks at the long time durations of 24 hours and 48 hours can be attributed to the inhomogeneous precipitation and hence the transformation does not occur simultaneously at all sites and nucleation occur over a range of temperatures.

$Ni_{45.3}Pd_5Ti_{29.7}Hf_{20}$ Aging for 24 hours

	As extruded	500°C	550°C	600°C
A peak	45.33	59.05	111.1	149.81
M peak	-9	-13.83	45.91	91.61
Hysteresis	54.33	72.88	65.19	58.2
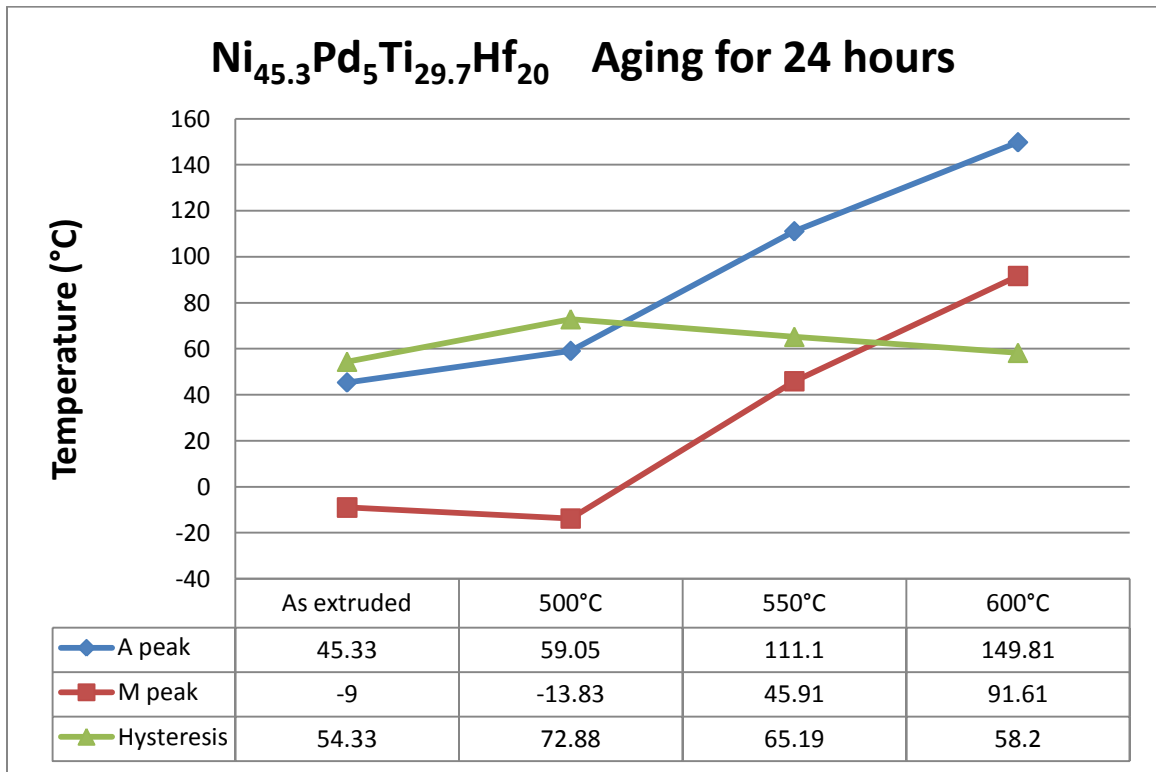
Figure 6.9: Comparison plot showing the peak temperatures for $Ni_{45.3}Pd_5Ti_{29.7}Hf_{20}$ alloy aged for 24 hours ranging from 400°C to 600°C.

Figure 6.9 represents the peak temperatures for $Ni_{45.3}Pd_5Ti_{29.7}Hf_{20}$ samples aged for 24 hours ranging from 400°C to 600°C. Since no peaks were observed for 400°C and 450°C, no results have been reported in this plot. The A_p increased by 14°C for aging at 500°C for 24 hours while the M_p fell by about 5°C in comparison with the as extruded specimen. A sizable increment of over 50°C from the preceding aging temperature of

500°C for aging at 550°C for 24 hours is observed. The hysteresis decreased in comparison to the specimen aged at 500°C, but still remained higher than the sample in as extruded sample. Both the peak temperatures increased by in excess of 45°C when the aging temperature was increased from 550°C to 600°C. Notably the hysteresis also decreased by 7°C, however it is still more than the as extruded condition.

Figure 6.10 depicts represents the peak temperatures for $Ni_{45.3}Pd_5Ti_{29.7}Hf_{20}$ alloy samples aged for 48 hours ranging from 400°C to 600°C as shown in Figure 6.8. Almost exact behavior is observed for aging at 48 hours as for 24 hours with a variation of a few degrees.

$Ni_{45.3}Pd_5Ti_{29.7}Hf_{20}$ Aging for 48 hours

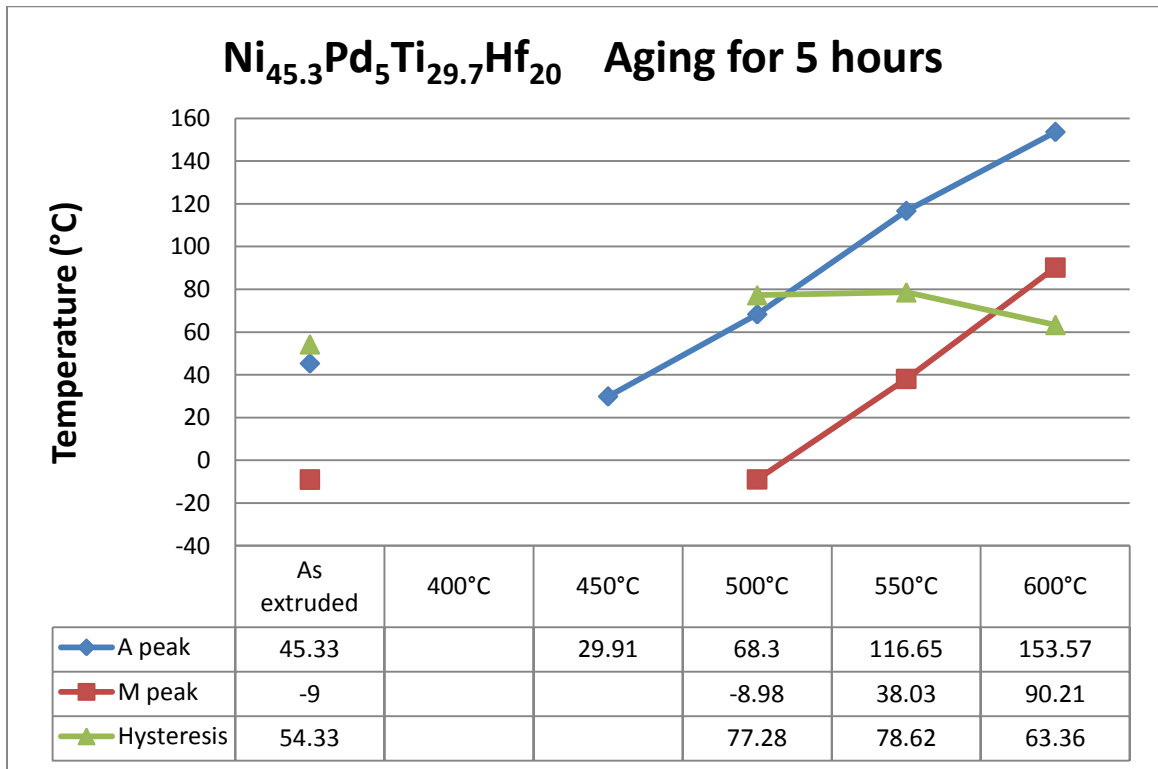|	As extruded	500°C	550°C	600°C
A peak	45.33	54.12	112.13	148.64
M peak	-9	-14.13	49.75	94.41
Hysteresis	54.33	68.25	62.38	54.23
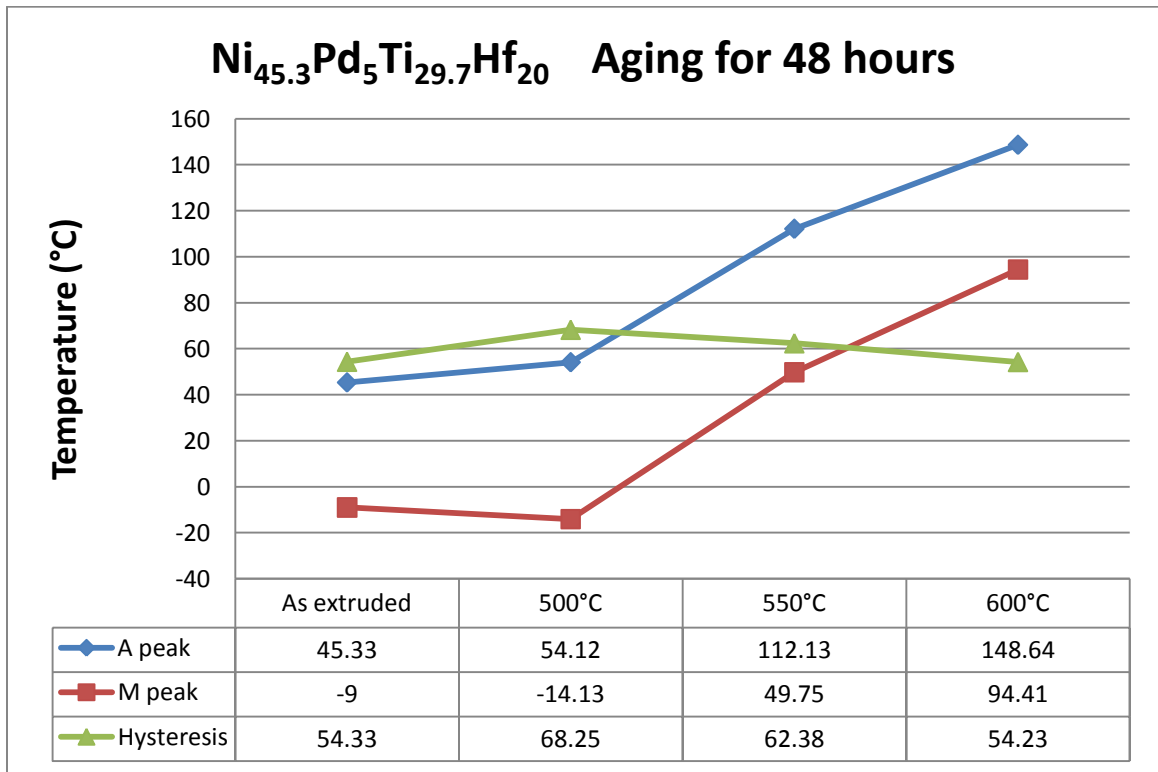
Figure 6.10: Comparison plot showing the peak temperatures for $Ni_{45.3}Pd_5Ti_{29.7}Hf_{20}$ alloy aged for 48 hours ranging from 400°C to 600°C.

Table 6.2: Hysteresis depicted as a function of the difference of austenite finish and martensite finish temperatures for $Ni_{45.3}Pd_5Ti_{29.7}Hf_{20}$ aged at various temperatures for 5 hours, 24 hour and 48 hours

Aging Condition	5 hours			24 hours			48 hours		
	M_f	A_f	Hysteresis	M_f	A_f	Hysteresis	M_f	A_f	Hysteresis
As Extruded	-29.3	54.4	83.7	-29.3	54.4	83.7	-29.3	54.4	83.7
450°C	-	-33							
500°C	-33.6	85.1	118.7	-34.25	78.6	112.9	-23.1	88.1	111.2
550°C	18.23	134.94	116.7	14.7	142	127.5	11.2	144	132.9
600°C	64.1	166.4	102.3	45.8	174	128.3	43.1	196	152.8

The hysteresis is depicted as the difference of the austenite finish and martensite finish temperatures to give an overview of the whole transformation. Results for the aging at 400°C have not be presented in the table because no transformation was observed when aged for time period higher than 3 hours, and no transformation was observed for aging at 450°C at time period higher than 5 hours. The hysteresis decreased with the increment in aging temperature at the aging time of 5 hours, which is inverse of the trend followed by the TTs. For longer time periods of 24 hours and 48 hours the hysteresis increased in comparison to as extruded condition when the aging temperature is increased. The DSC peaks became very wide and the possible reason is the inhomogenity of the matrix as a result of aging for prolonged periods.

6.2 TEM analysis
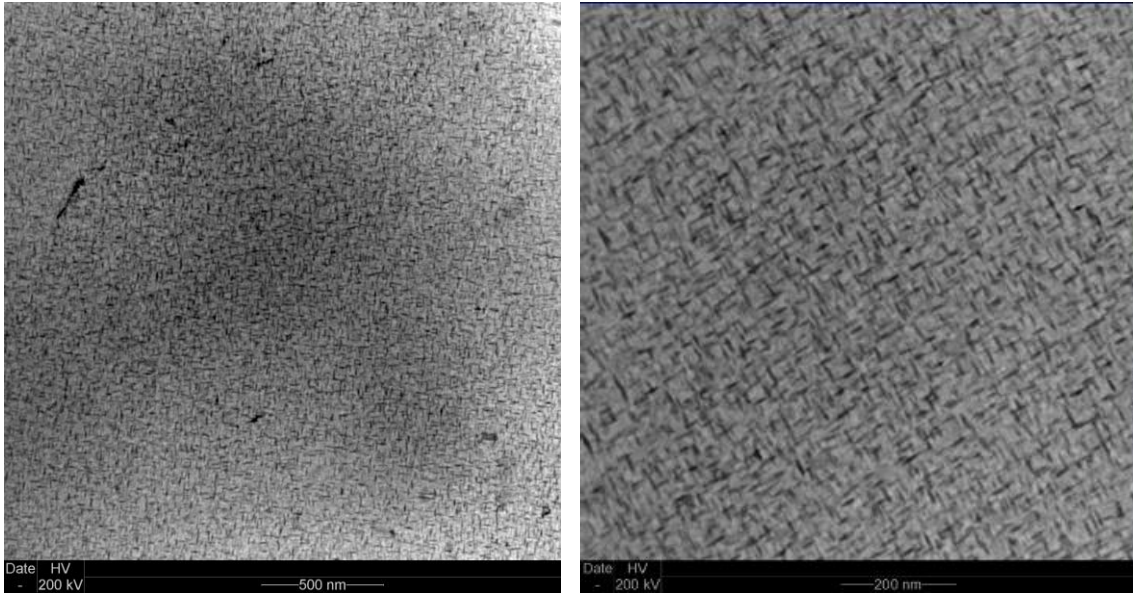
Figure 6.11: TEM micrographs of $Ni_{45.3}Pd_5Ti_{29.7}Hf_{20}$ aged for 3 hours at 550°C

Figure 6.11 represents TEM micrographs $Ni_{45.3}Pd_5Ti_{29.7}Hf_{20}$ aged for 3 hours at 550°C. In the relatively lower magnification image on the left side a finely dispersed phase can be observed throughout the material matrix, which when looked at even higher magnification revealed the presence of very fine precipitates of size less than 20nm. The precipitates were observed to be oval in shape and size of the precipitates was invariably less than 20nm. The presence of the precipitates was concurrent with the expectations and analogous with the finding for the set of the two other alloys discussed in the study. Hence, it can be inferred that the evolution of the precipitates is similar in all three alloys within a small range of variation in behavior.

Figure 6.12: Diffraction pattern of $Ni_{45.3}Pd_5Ti_{29.7}Hf_{20}$ aged for 3 hours at 550°C
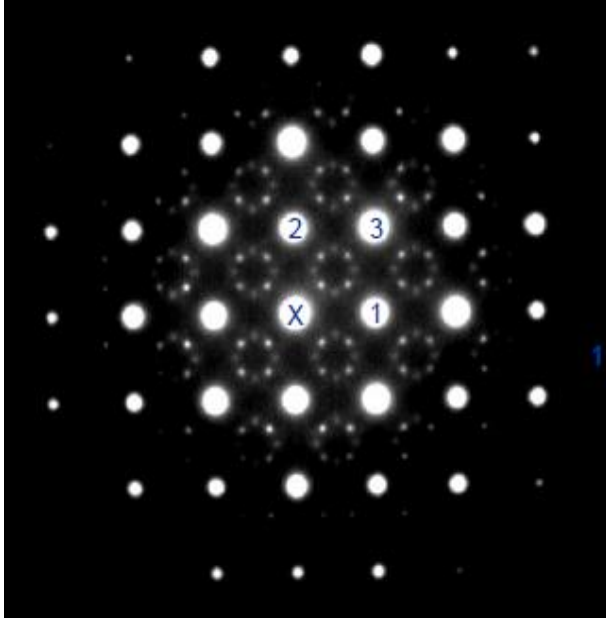
Figure 6.12 represents the diffraction pattern from the area represented in Figure 6.11. The fine phase was identified as orthorhombic precipitate (P) with parameters of a=12.6 Å, b=8.7 Å, c=26.5 Å. The orientation relationship has been mentioned in the textbox on the right side of the diffraction parameter. The austenite phase of the alloy was determined to be B2 and the its parameters were calculated to be a=0.31nm.

6.3 XRD analysis
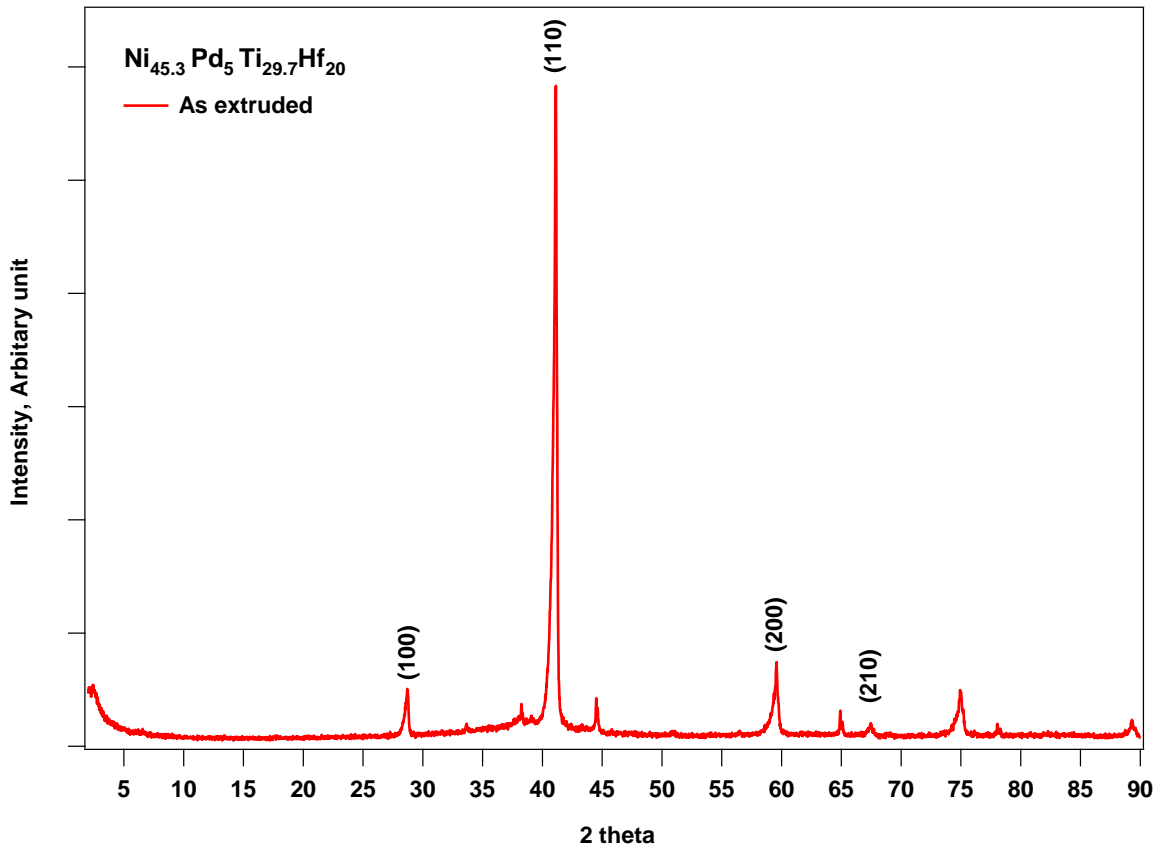
Figure 6.13: Plot for XRD at room temperature $Ni_{45.3}Pd_5$ $Ti_{29.7}Hf_{20,}$ in as extruded condition

The Figure 6.13 represents the XRD results for the as-extruded sample when measurements were done at room temperature and the sample was in the austenite phase. The major peak was observed at about 42° and the structure was determined to be B2. The calculations yielded the parameters at a =0.3103 nm. The findings of the XRD were found to be very similar to the ones yielded by TEM investigations. Figure 6.14 represents the data for the $Ni_{45.3}Pd_5$ $Ti_{29.7}Hf_{20}$ samples aged for 10 hours and 600°C and 24 hours at 650°C. This aging was done to ensure the sample had sufficiently high TTs and was in martensite phase at room temperature. The calculations for the data yielded

the parameters as a =0.245nm, b=0.41nm, c=0.48nm, β=98.90°, about the same for both

the samples.
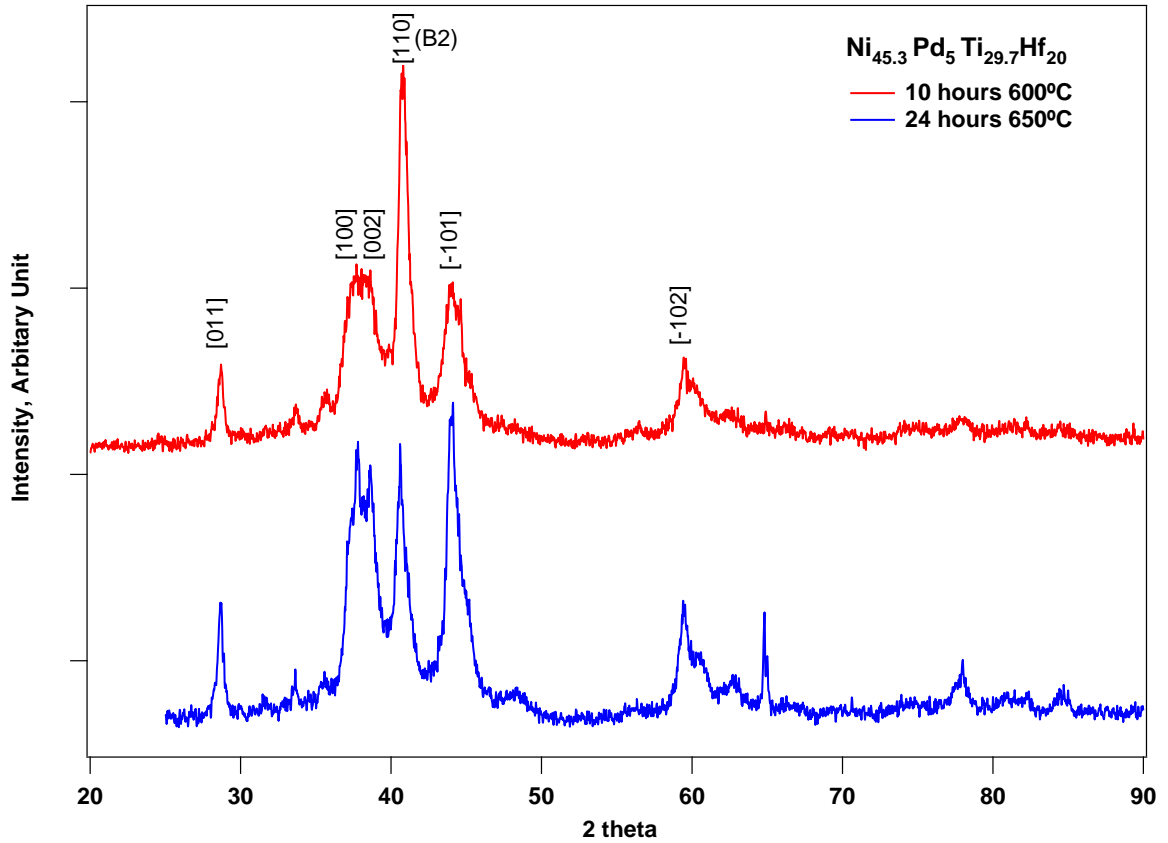
Figure 6.14: Plot for XRD at room temperature $Ni_{45.3}Pd_5 Ti_{29.7}Hf_{20,}$ aged for 10 hours at 600°C and 24 hours at 650°C

6.4 Hardness Results
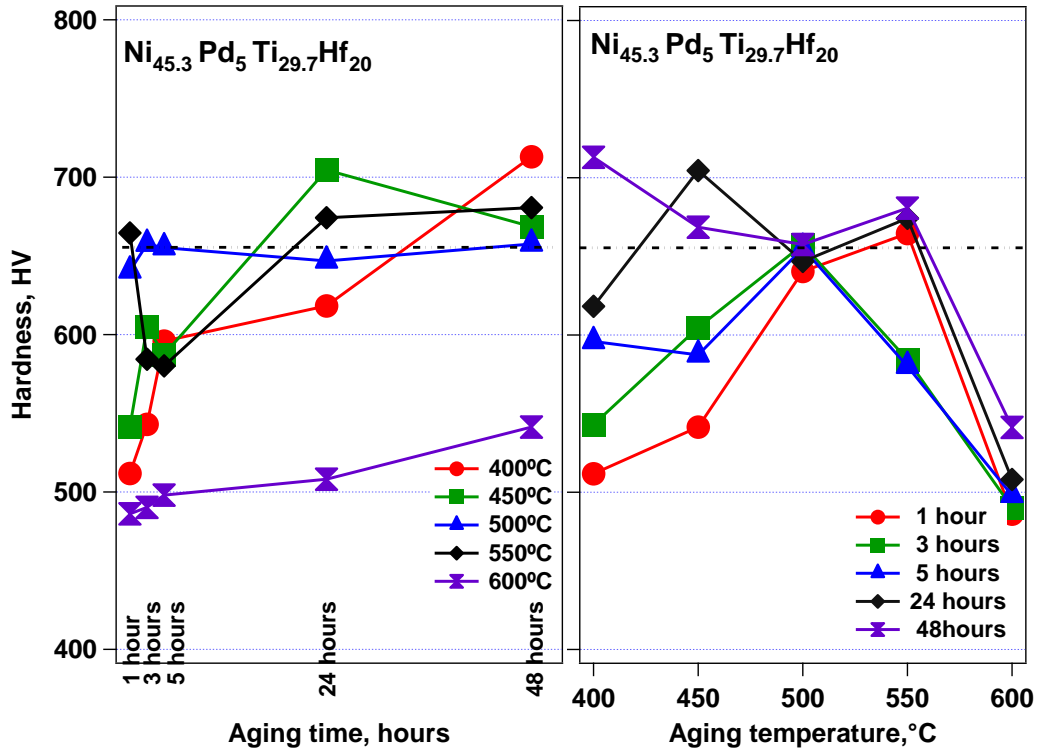
Figure 6.15: Comparison plot for hardness values of $Ni_{45.3}Pd_5Ti_{29.7}Hf_{20,}$ aged at selected temperatures for 1, 3, 5, 24 and 48 hours

Figure 6.15 represents the comparison for the hardness value of the

$Ni_{45.3}Pd_5Ti_{29.7}Hf_{20}$ samples aged at selected temperatures between 400°C and 600°C for

1, 3, 5, 24 and 48 hours. The plot on the left is plotted as a function of aging time where

the same data is represented as a function of aging temperatures on the right. The

variation of the hardness values is clearer from the plot on the left side in comparison

with the one on the right side where it is plotted as a function of aging time and each

curve follows a particular aging temperature curve. The data presented in the plot consists

of data from both the martensite phase and the austenite phase, and the phase is observed

to mostly remain same for the particular aging temperature while no such correlation can

be said for the aging time curves. An important point that should be noted is that since the

162

measurements were made at room temperature, the $Ni_{45.3}Pd_5Ti_{29.7}Hf_{20}$ aged for all mentioned time durations at 400°C, 450°C and 500°C are in austenite phase along with the sample aged for 1 hour at 550°C, while the rest of the samples were in martensite phase.

The samples in austenite phase were observed to be very hard in comparison to their counterparts in the martensite phase. The hardness value was observed to increase with the increment in aging time for all samples in the austenite phase. The sample aged at 400°C increases in hardness very significantly when the aging time was initially increased from 1 hour to 5 hours, followed by the attainment of the maximum value at 48 hours with a linear increment. Sample aged at 450°C followed a trend similar to the one aged at 400°C. The sample aged at 500°C was observed to stay almost invariable with the increment in aging time and stayed very close the hardness value of as extruded sample.

The sharp decrease in the hardness value for the sample aged at 550°C, when the aging time is increased from 1 hour to 3 and 5 hours is due to the alteration in the stable phase at room temperature, in which the material was initially in austenite but due to aging the TTs increase substantially which led to martensite being the stable phase at room temperature. Once the sample was in martensite the hardness value was observe to increase significantly with aging time. The sample aged at 600°C was observed to be martensite in all aging times, but the hardness was observed to be very low in comparison with its martensite counterpart aged at 550°C. The hardness value increased slightly with increment in aging time but it stayed much lower in comparison with the as extruded sample.

The variation in hardness values can be attributed to the presence of very finely dispersed particles as shown in the TEM micrographs for the sample aged at 550°C. The precipitates are expected to grow in size and hence become incoherent and as expected the lower values for the sample aged at 600°C are observed. The finely dispersed particles act as pinning sites for the dislocations and inhibit the slip motion. The coherent precipitates are more effective than the larger precipitates since the probability of the dislocations to break loose becomes higher as the distance between the precipitates increases. This behavior observed is analogous to the observed to $Ni_{50.3}Ti_{29.7}Hf_{20}$ reported earlier in chapter 4. The hardness for $Ni_{50.3}Ti_{29.7}Hf_{20}$ reached its maximum for the coherent precipitates at 500°C followed by a decrement in the value analogous to the large precipitates observed under the TEM for aging at 600°C for 3 hours.

Figure 6.16 depicts the relation between the variation of TTs and the hardness for the $Ni_{45.3}Pd_5Ti_{29.7}Hf_{20}$ aged under varying condition between the temperature of 400 and 600°C and time duration of 1 hour to 48 hours. The correlation for the said value cannot be clearly determined due to no observable transformation peaks for aging beyond 3 hours. The sample aged at 500°C did not show much variation in either of the TTs and hardness remained almost invariable between a small range. The sample aged at 550°C was in austenite phase at room temperature for aging for 1 hour and with sizable increment in the TTs for aging for 3 hours it became stable in martensite and remained so for further increments in aging time. The drop in hardness from 1 hour aging to 3 hours aging time was due the change in stable phase at room temperature from austenite to martensite, followed by a steep increment in the hardness and TTs with increasing the

aging time. The hardness for the sample aged at 600°C remained relatively lower but increased correspondingly with the increase in TTs.
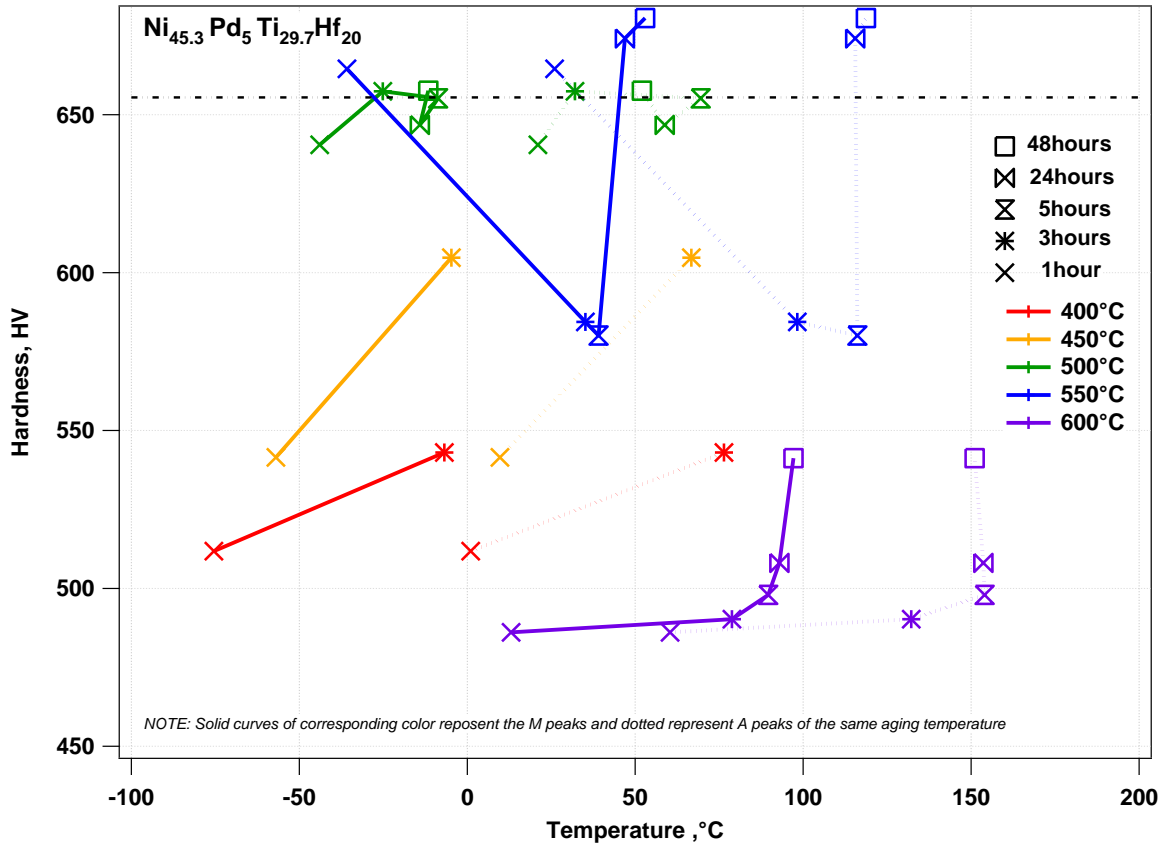
Figure 6.16: Comparison plot for hardness vs. TTs for the corresponding aging conditions.

6.5 Mechanical Characterization
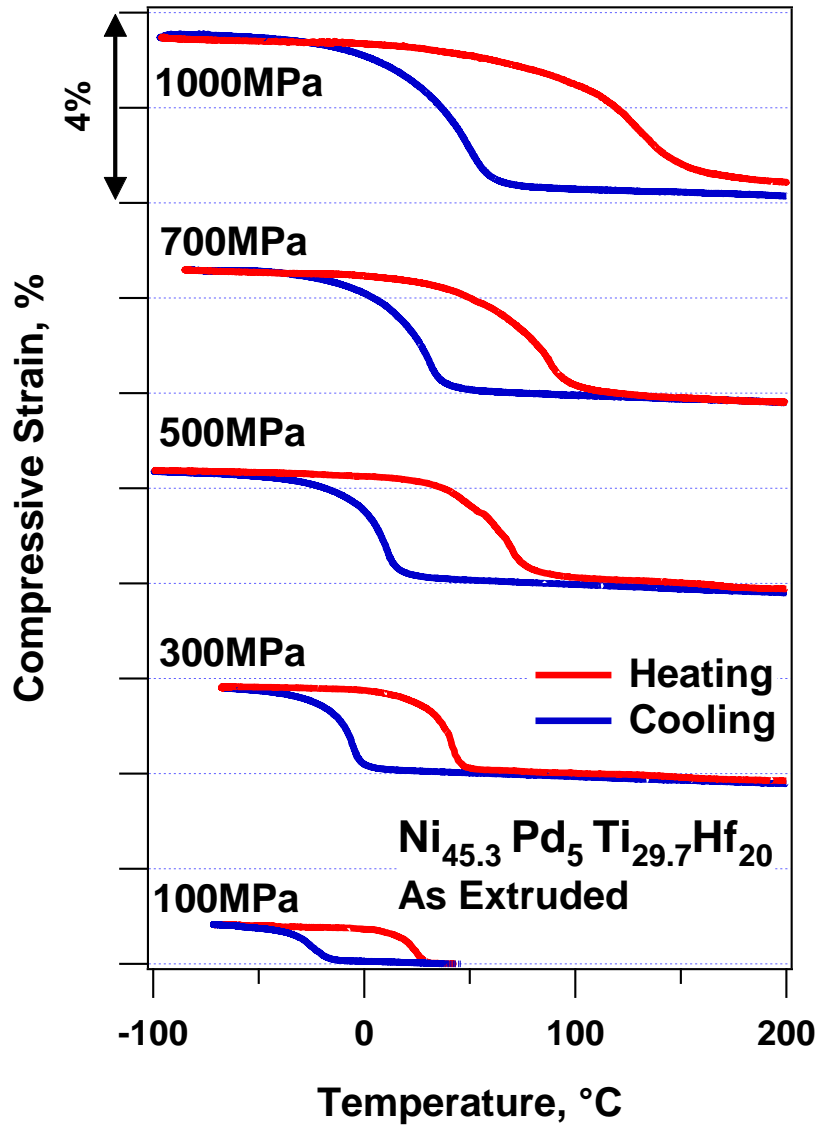
Figure 6.17: Isobaric thermal cycling of $Ni_{45.3}Pd_5Ti_{29.7}Hf_{20}$ in as extruded condition

Figure 6.17 represents the thermal cycling for $Ni_{45.3}Pd_5Ti_{29.7}Hf_{20}$ sample in as extruded condition under constant compressive stresses. The sample was loaded to in austenite to a stress level from 100MPa to 1000MPa, followed by thermal cycling with 10°C/min between a range of -100°C and 200°C. Curves for selected tests have been reported in the Figure 6.22 and the specific are presented in Table 6.1. It is observed for

the $Ni_{45.3}Pd_5Ti_{29.7}Hf_{20}$ compression sample in as extruded condition, when loaded to

100MPa resulted in fully recoverable strain of slightly less than 0.5 %. The TTs except

A_f, were lower than 0°C. The recoverable strain increased with increment in applied

loads along with a linear the increment in the TTs. The increase in the recoverable strain

can be attributed to the growth of the load biased variant of martensite which in turn leads

to the increment in transformation strain as shown in the Table 6.3. The most notable

feature for the compression sample in as extruded for $Ni_{45.3}Pd_5Ti_{29.7}Hf_{20}$ is the fully

recoverable strain is observed for the load level of 700MPa. Even under 1000 MPa, an

irrecoverable strain of less than 0.5 % is observed. This indicates that the material has

high strength that is analogous to the high hardness values discussed earlier. The

hysteresis increased very marginally when the stress level was increased till 700MPa but

with the further increment in the applied load especially under high stress of 1000MPa, it

increased very sharply from about 50°C to more than 80°C.

Table 6.3: Critical transformation parameters and strain levels for isobaric thermal
cycling of $Ni_{45.3}Pd_5Ti_{29.7}Hf_{20}$ in as extruded condition

Sample	Stress	Ms	Hysteresis	ε_{tr}	ε_{ir}
As Extruded	100	-16.62	47	0.6	0
	300	-1	46	1.7	0
	500	23	41	1.95	0
	700	37	50	2.35	0
	1000	60	82	2.93	0.3

The Figure 6.18 represents the isobaric thermal cycling for $Ni_{45.3}Pd_5Ti_{29.7}Hf_{20}$

aged for 3 hours at 400°C and the details are presented in tabular form in Table 6.4. The

TTs were even lower than for the as extruded sample by about 30°C. The trend in

variation of recoverable strain was analogous to the as extruded sample with the strains

for the aged sample being a little higher. Fully recoverable strain of 2.7% for a load of 700MPa was observed. Further loading the sample to 1000MPa resulted in 0.5% of irrecoverable strain. The hysteresis was higher than the as extruded sample and after staying almost constant till 500MPa, it increased steeply from about 75°C to 100°C for further loading to 700MPa and 1000MPa. The maximum transformation of 3.2% attained at a load of 1000MPa was comparable to the maximum strain for the $Ni_{50.3}Ti_{29.7}Hf_{20}$ aged alloy, though $Ni_{45.3}Pd_5Ti_{29.7}Hf_{20}$ had about 0.23% irrecoverable strain associated with it. The lower hardness value of the $Ni_{45.3}Pd_5Ti_{29.7}Hf_{20}$ sample aged at 400°C did not affect the SMA properties much in comparison to as extruded sample.

Table 6.4: Critical transformation parameters and strain levels for isobaric thermal cycling of $Ni_{45.3}Pd_5Ti_{29.7}Hf_{20}$ aged at 400°C for 3hours

Sample	Stress	Ms	Hysteresis	ε_{tr}	ε_{ir}
3hours 400°C	100	-46	57	0.46	0
	300	-22.43	50.6	1.65	0
	500	2.05	55.43	2.17	0
	700	24.01	74.98	2.65	0.05
	1000	60.5	95.73	3.3	0.5
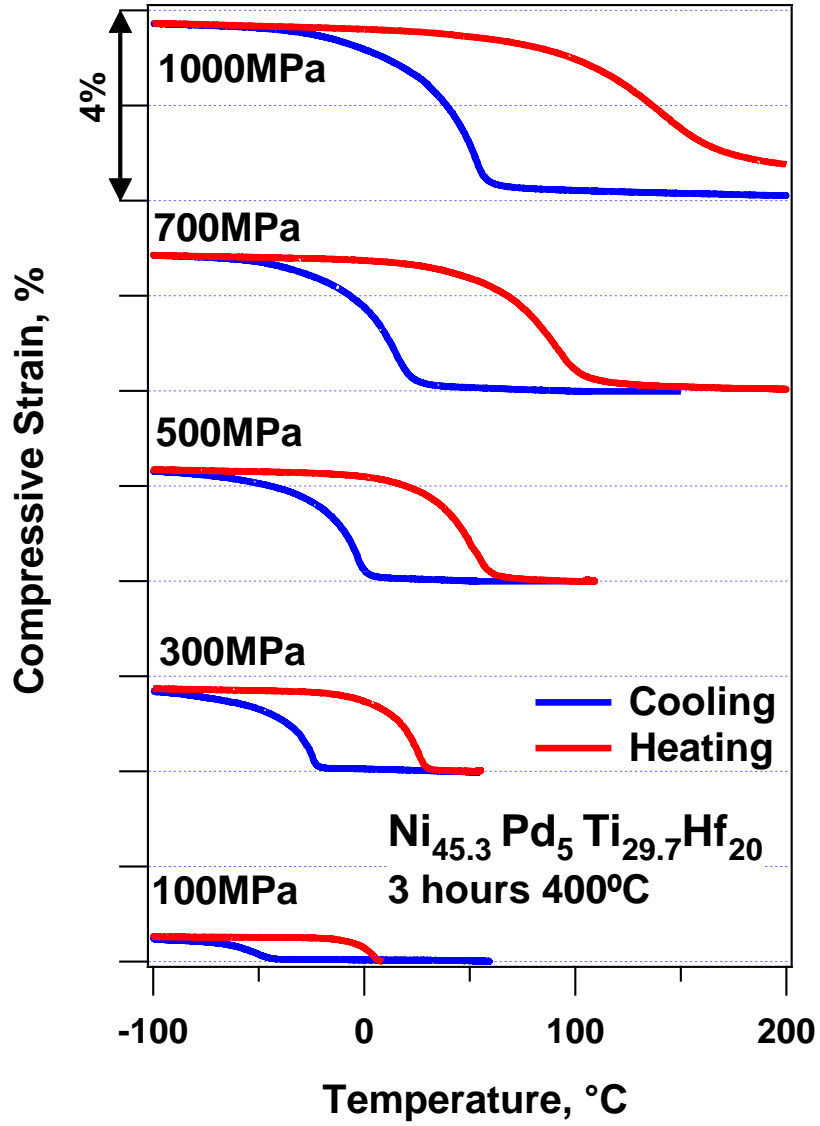
Figure 6.18: Isobaric thermal cycling of $Ni_{45.3}Pd_5Ti_{29.7}Hf_{20}$ aged for 3 hours at 400°C
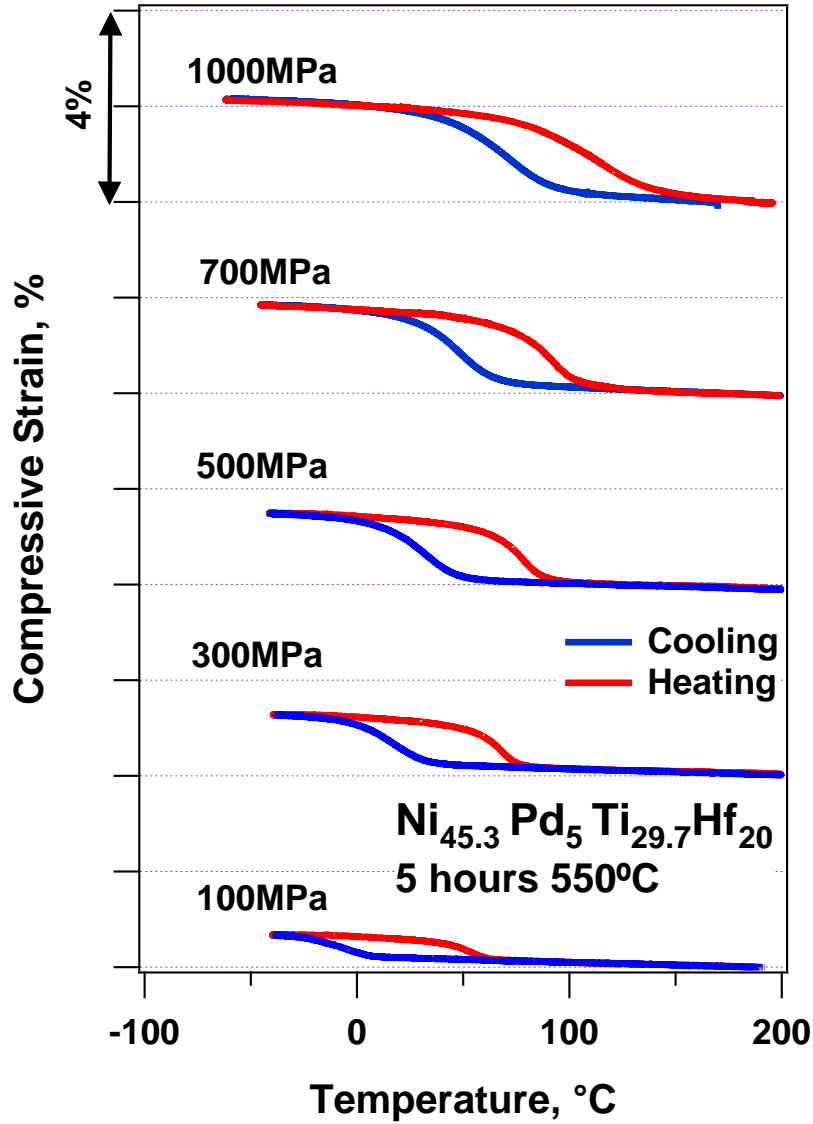
Figure 6.19: Isobaric thermal cycling of $Ni_{45.3}Pd_5Ti_{29.7}Hf_{20}$ aged for 5 hours at 550°C

Figure 6.19 represents the selected results for isobaric thermal cycling on $Ni_{45.3}Pd_5Ti_{29.7}Hf_{20}$ compression sample aged for 5 hours at 550°C between stress levels of 100MPa and 1000MPa. The increment in TTs temperatures in contrast with previous mentioned samples was analogous to the DSC findings and can be attributed to the finely dispersed precipitates observed under the TEM. The TTs were higher than 0°C except for M_f which also increased with application of stress over. The hysteresis notably varied

contrary to the earlier mention samples and it decreased with increment in applied stress. The recoverable strain was observed to be lower than previously discussed samples but it should be noted that even at load of 1000MPa a fully recoverable strain is observed which is quite remarkable in comparison with conventional SMAs. The findings are analogous to the results presented earlier in form of TEM images. The finely dispersed particles can be attributed for the high strength of the material. The closely spaced coherent precipitates are believed to act as barriers in the path of dislocation preventing slip from occurring in the material and as a result the fully closed strain loop is observed for such high levels of stress also. The low levels of transformation strains as indicated in Table 6.5 can be attributed to the high stress required for detwinning the material and decreased volume fraction of the matrix.

Table 6.5: Critical transformation parameters and strain levels for isobaric thermal cycling of $Ni_{45.3}Pd_5Ti_{29.7}Hf_{20}$ aged at 550°C for 3hours

Sample	Stress	Ms	Hysteresis	ε_{tr}	ε_{ir}
5hours 550°C	100	12.97	52.3	0.4	0
	300	32.23	46.83	0.87	0
	500	50	40	1.23	0
	700	65	38	1.38	0
	1000	93	38	1.68	0

Figure 6.20 represents the results for heating cooling under varying stress levels for $Ni_{45.3}Pd_5Ti_{29.7}Hf_{20}$ compression sample aged for 24 hours at 550°C. The result for selected tests carried out between 100MPa and 1000MPa have been presented with details in tabular format in Table 6.4. The level of transformation strain was observed to be very low, at 100MPa of applied stress there was only 0.21% of fully recoverable transformation strain. The strain value increased almost linearly with the increment in

applied stress, even though the maximum value was in proximity of 1.5%. The effect of the possibly fine precipitates was evident in the strength of the material which is visible from the fully recoverable strain even at 1000MPa. The TTs were higher than the as extruded sample and also the sample aged at 550°C for 5 hours, and increased linearly with increment in applied stresses. The hysteresis remained invariable for increment in load from 100MPa to 300MPa, after which the increment in applied stress led to a fall in hysteresis till load of 600MPa followed by a rather constant value for further increment in load levels.
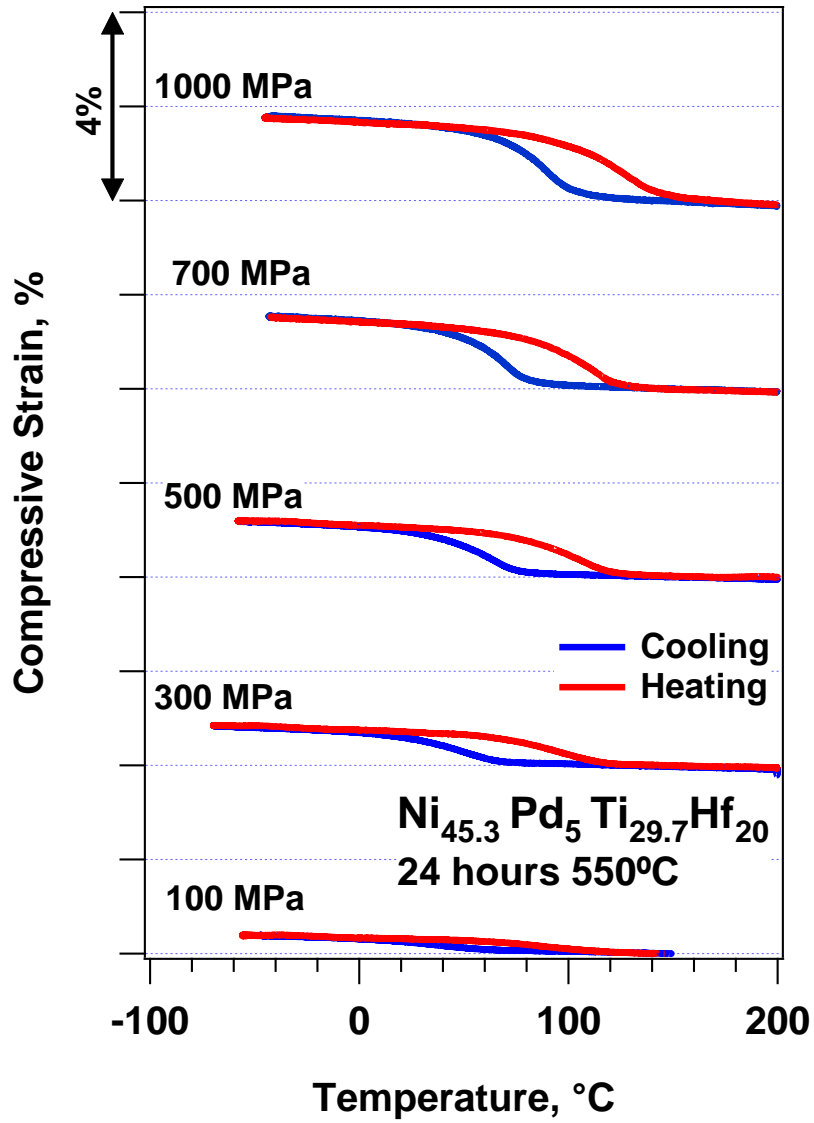
Figure 6.20: Isobaric thermal cycling of $Ni_{45.3}Pd_5Ti_{29.7}Hf_{20}$ aged for 24 hours at 550°C

Table 6.6: Critical transformation parameters and strain levels for isobaric thermal cycling of $Ni_{45.3}Pd_5Ti_{29.7}Hf_{20}$ aged at 550°C for 24hours

Sample	Stress	Ms	Hysteresis	ε_{tr}	ε_{ir}
24hours 550°C	100	61.65	43.7	0.2	0
	300	66	44.5	0.59	0
	500	75.33	39.8	0.86	0
	700	81	33	1.15	0
	1000	102	33	1.39	0

173
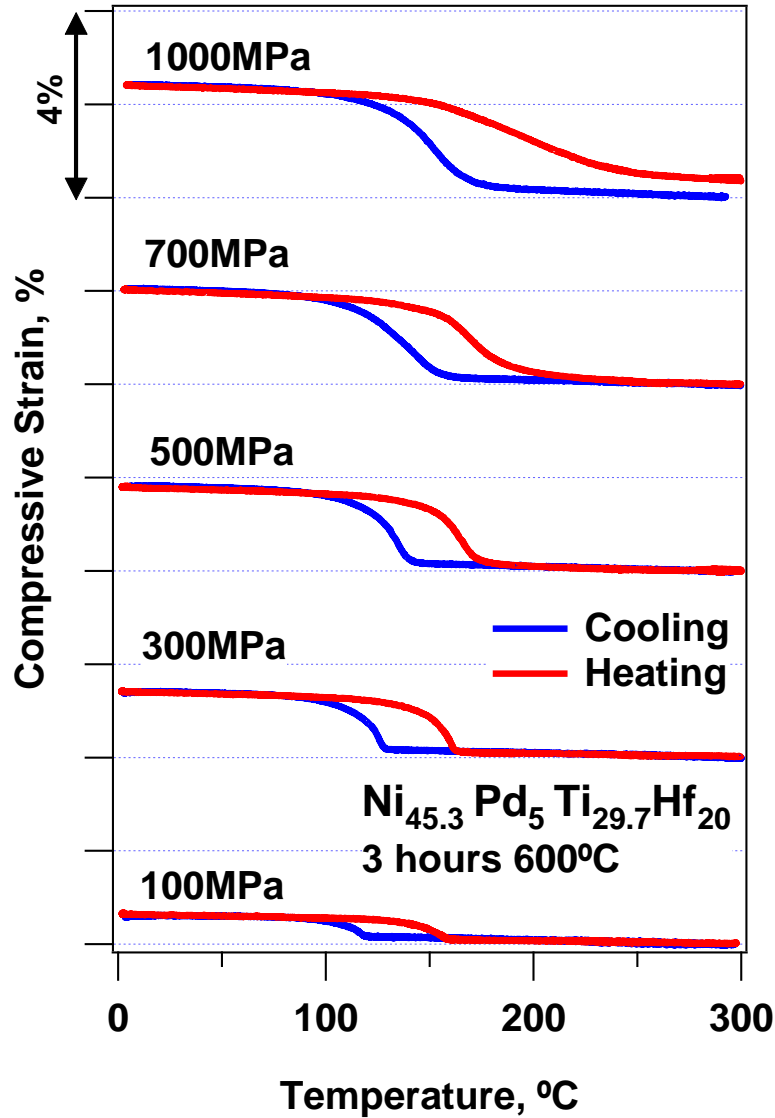
Figure 6.21: Isobaric thermal cycling of $Ni_{45.3}Pd_5Ti_{29.7}Hf_{20}$ aged for 3 hours at 650°C

Figure 6.21 depicts the transformation behavior under stress for $Ni_{45.3}Pd_5Ti_{29.7}Hf_{20}$ aged for 3 hours at 650°C. The critical points determined from the figure are presented in Table 6.7. The high TTs for the sample were in correspondence to the results observed in the DSC experiments. The evolution of precipitates into larger size thus by increase in volume fraction can be held responsible for the corresponding increment in the TTs. Low transformation strain was observed for an applied load of 100MPa though it was higher comparatively to the sample aged at 550°C for 3 hours.

The transformation strains increase linearly with applied load and with a fully recoverable strain of about 2% for 700MPa. The load of 1000MPa led to a transformation strain little higher than obtained for application of 700MPa, but an irrecoverable strain of 0.34% was associated with the transformation. The transformation temperatures were the highest observed for the various samples tested in the alloy system above 100°C. The hysteresis remained constant around 30°C till the load of 700MPa after which the further increment led to a rise of hysteresis till 50°C.

The 0.3% irrecoverable strain can be attributed to perhaps the growth of the precipitates in the range of incoherency which lead to depreciation of strengthening effect and hence the irrecoverable strain occurs. The growth of precipitates is also evident from the increment in TTs from aging at 550°C to 650°C.

Table 6.7: Critical transformation parameters and strain levels for isobaric thermal cycling of $Ni_{45.3}Pd_5Ti_{29.7}Hf_{20}$ aged at 650°C for 3hours

Sample	Stress	Ms	Hysteresis	ε_{tr}	ε_{ir}
3hours 650°C	100	119	30	0.42	0
	300	128	32	1.04	0
	500	140	30	1.4	0
	700	154	34	1.61	0
	1000	170	50	1.91	0.27
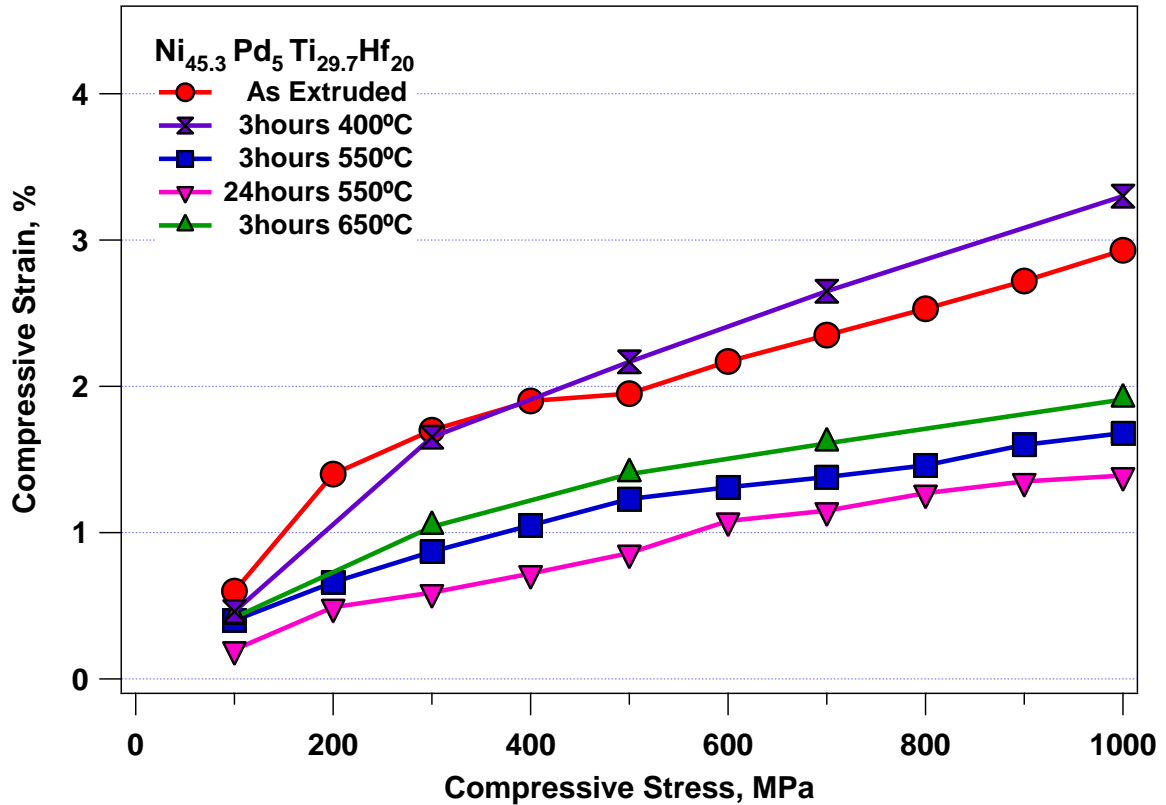
Figure 6.22: Comparison plots depicting the recoverable strain for $Ni_{45.3}Cu_5 Ti_{29.7}Hf_{20}$ aged at varying conditions

Figure 6.22 depicts the recoverable strains for the varying loads for the specimen mentioned earlier in the beginning of this section. The recoverable strain followed similar trends for all specimens under consideration while increasing linearly with increment in applied loads. The recoverable strain was observed to be in the vicinity of 0.5% for an applied load of 100MPa with the exception of the sample aged for 24 hours at 550°C which was lower at 0.23%. The increment in the recoverable strain with applied loads can be attributed to the beginning of the formation of load biased variants. These biased variants are observed to grow with increase in applied load levels and as a result the observed recoverable strains also increase. The maximum recoverable strain was at an applied load of 1000MPa, however it was accompanied by less than 0.2% of

irrecoverable strain. It should be noted than the alloys with higher TTs were observed to have lower recoverable strains, the sample aged at 650°C for 3 hours had the highest TTs , and it has the lowest recoverable strains. The samples aged at 500°C for 5 hours and 24 hours had fully recoverable strain even at 1000MPa, but the maximum recoverable strains were limited to less than 2%. The sample aged at 400°C for 3 hours had the lowest TTs and is noted to have the highest transformation strains with a maximum of about 3%. The level of recoverable strain for as extruded sample was similar in trend to the sample aged at 400°C for 3 hours but with less strain. The strain increases with the increment of applied stress however the level of stress required was much higher in comparison to the other two alloys studied. Another notable feature for the samples aged at 500°C is that the strain level were did not saturate at 1000MPa and were still increasing, hence more stress will be required to obtain the maximum possible strains from the sample.The precipitates responsible for imparting the strength to the material and increasing the TTs can also be attributed for lowering the transformation strain. With the larger volume of precipitates formed the volume of the transforming matrix decreases and as a result the overall recoverable strains are observed to decrease
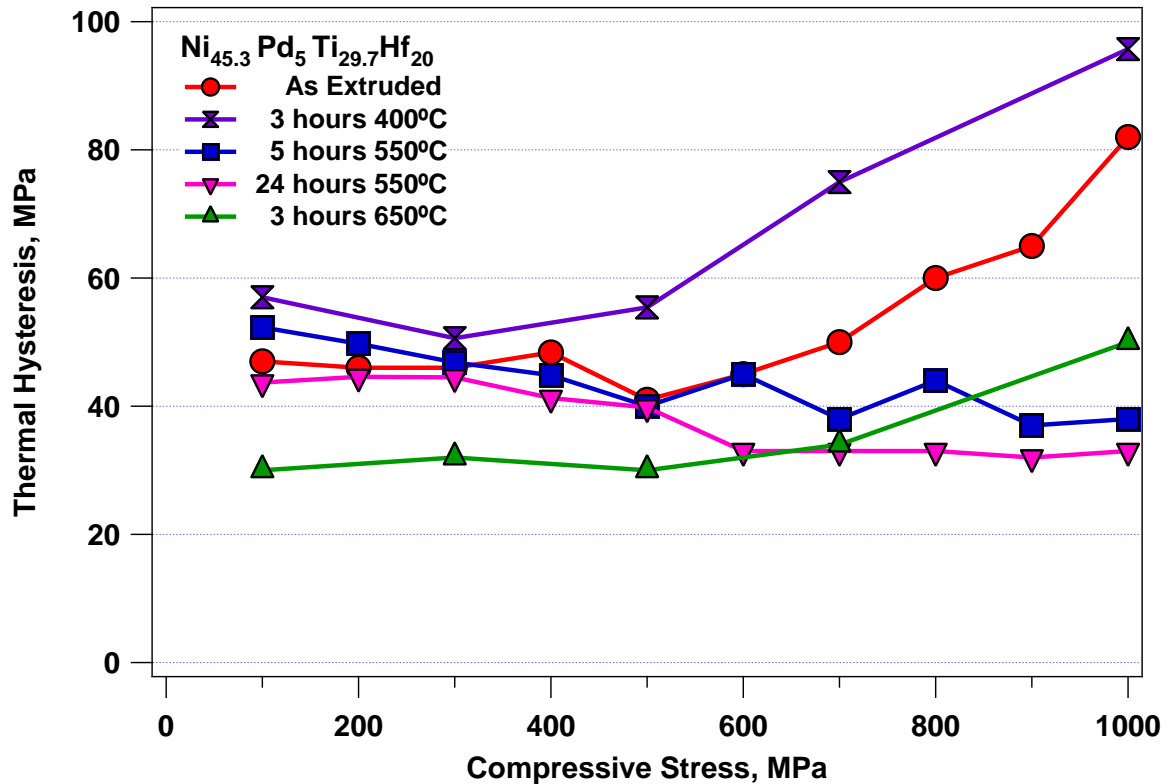
Figure 6.23: Comparison plots depicting thermal hysteresis for $Ni_{45.3}Pd_5Ti_{29.7}Hf_{20}$ aged at varying conditions

The thermal hysteresis for heating cooling under varying levels of stress for $Ni_{45.3}Pd_5Ti_{29.7}Hf_{20}$ compression previously mentioned samples are presented in Figure 6.23. The hysteresis was found to stay stable for all samples till an applied load of 500MPa after which the there were two different trends observed. The hysteresis increased linearly with further increment of loads above 500MPa with a steep slope for possibly precipitate free samples in as extruded condition and aged at 400°C for 3 hours. The hysteresis remained almost constant with increment of loads for both samples aged at 550°C for 3 hours as well as 24 hours, while hysteresis remained invariable till the load of 700MPa for the sample aged at 650°C after which it increased.
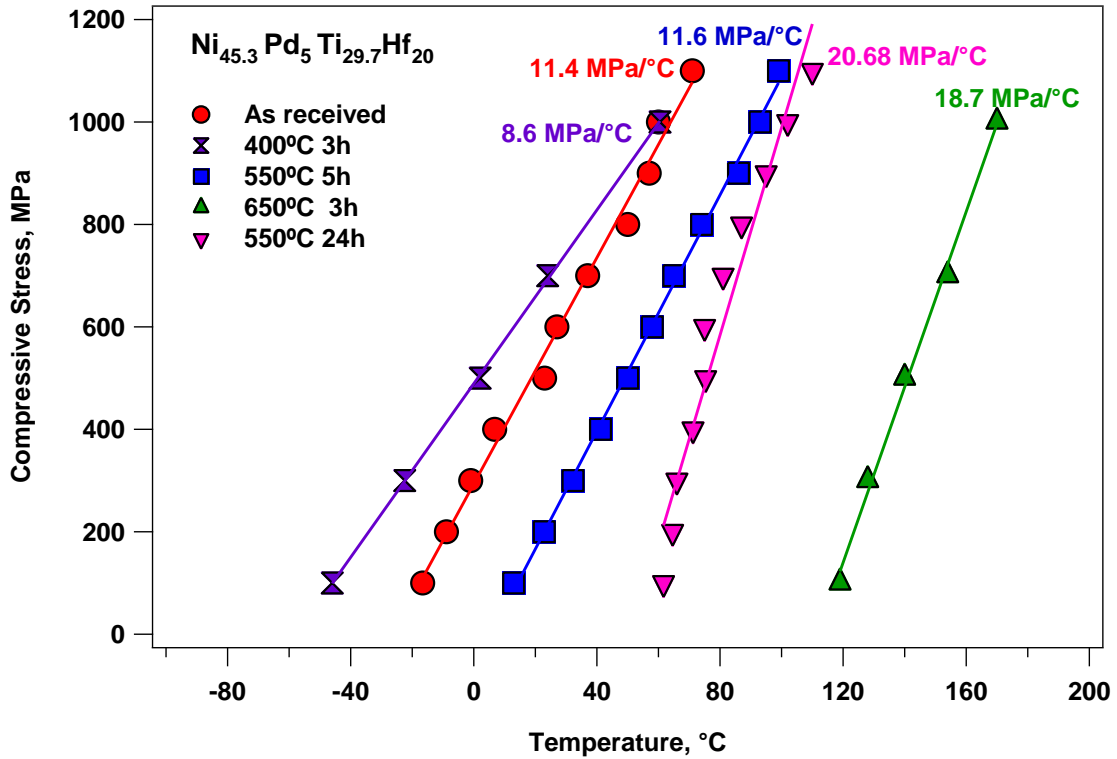
Figure 6.24: Clausius-Clayperon curves for $Ni_{45.3}Ti_{29.7}Hf_{20}$ aged at varying conditions with respect to M_s temperature.

Figure 6.24 depicts the Clausius-Clayperon curves for $Ni_{45.3}Ti_{29.7}Hf_{20}$ extracted from the M_s temperatures determined from results depicted in Figures 6.17 to 6.21. The curves for the TTs increased linearly as expected with any corresponding increment in the load. These curves assume high significance for the prediction of the TTs under various loading conditions without having to do so experimentally and hence save effort and capital. The above plot shows the slope of the lines for each specimen tested, along the path of which the TTs for higher loads can be predicted.
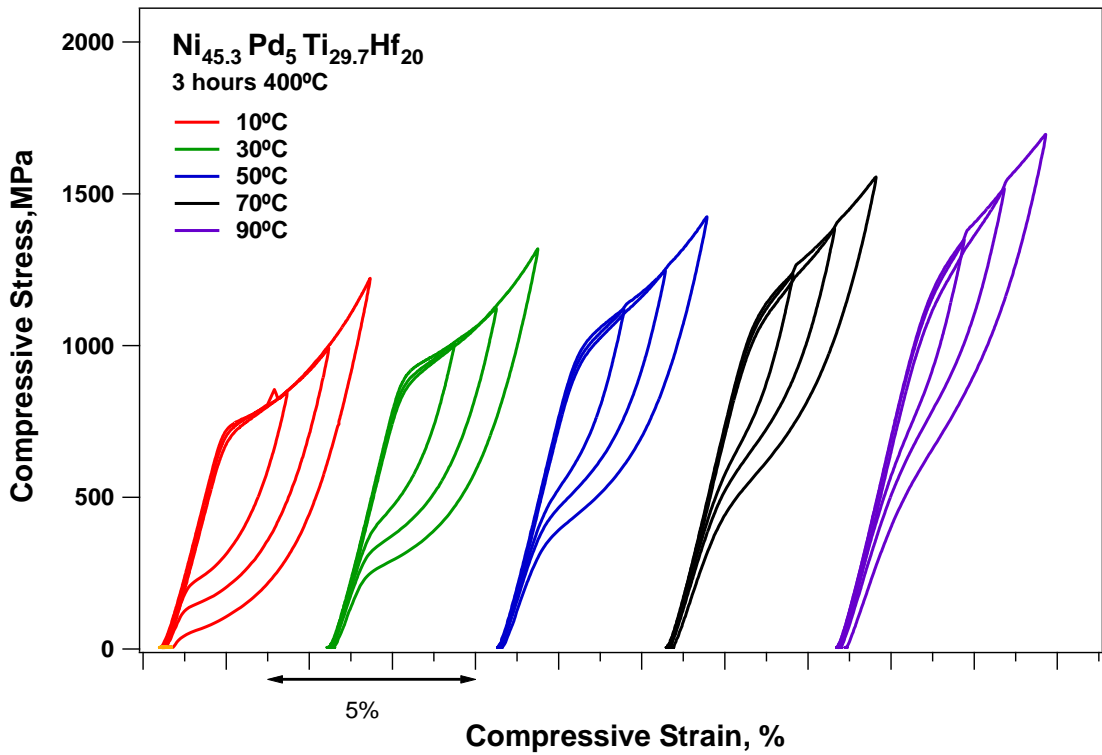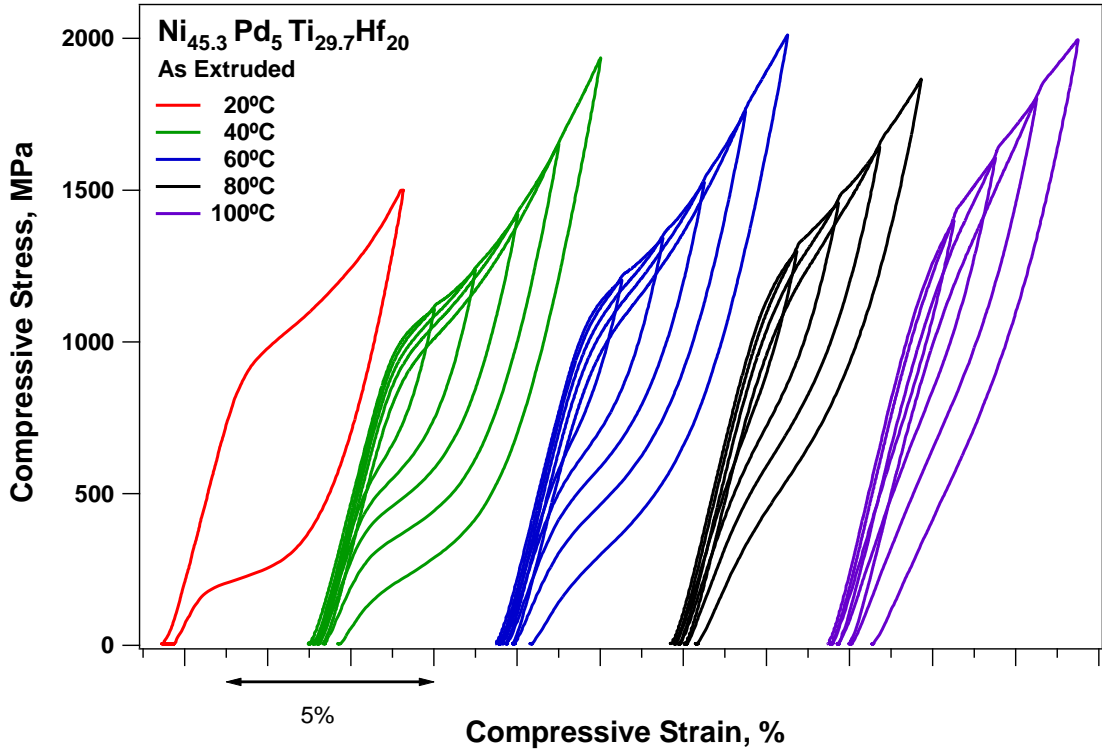
Figure 6.25: Isothermal mechanical cycling of $Ni_{45.3}Pd_5Ti_{29.7}Hf_{20}$ in as extruded condition (top) and aged for 3 hours at 400°C(bottom)
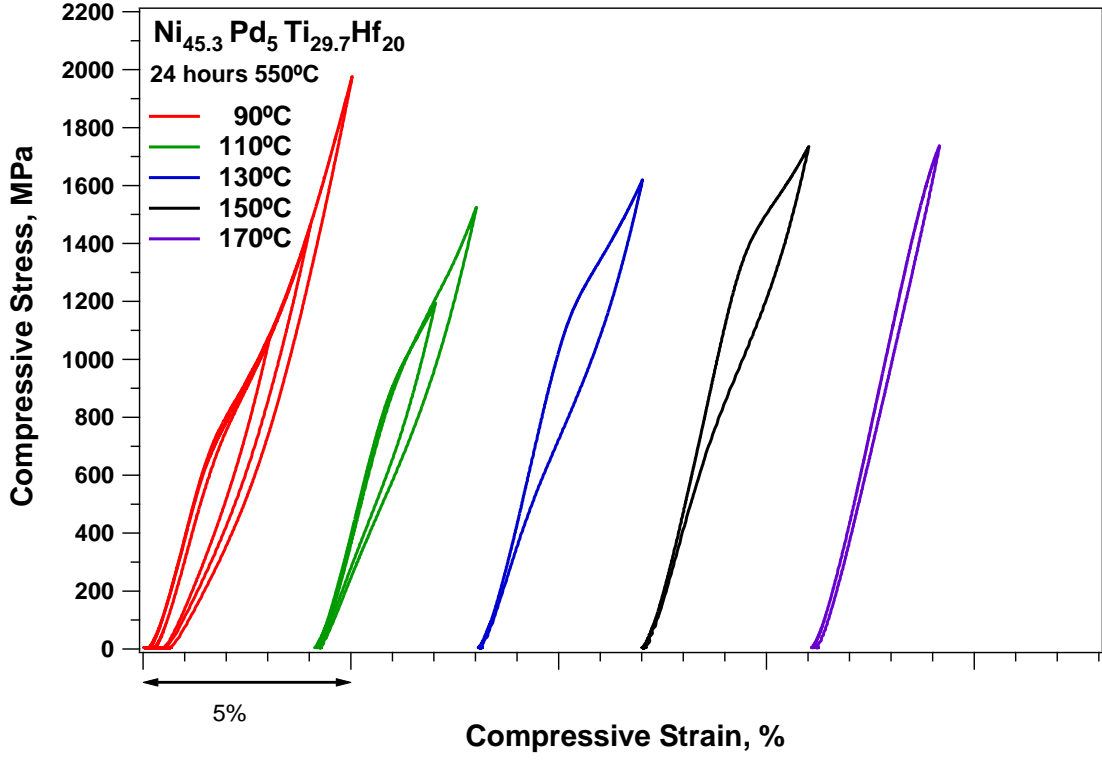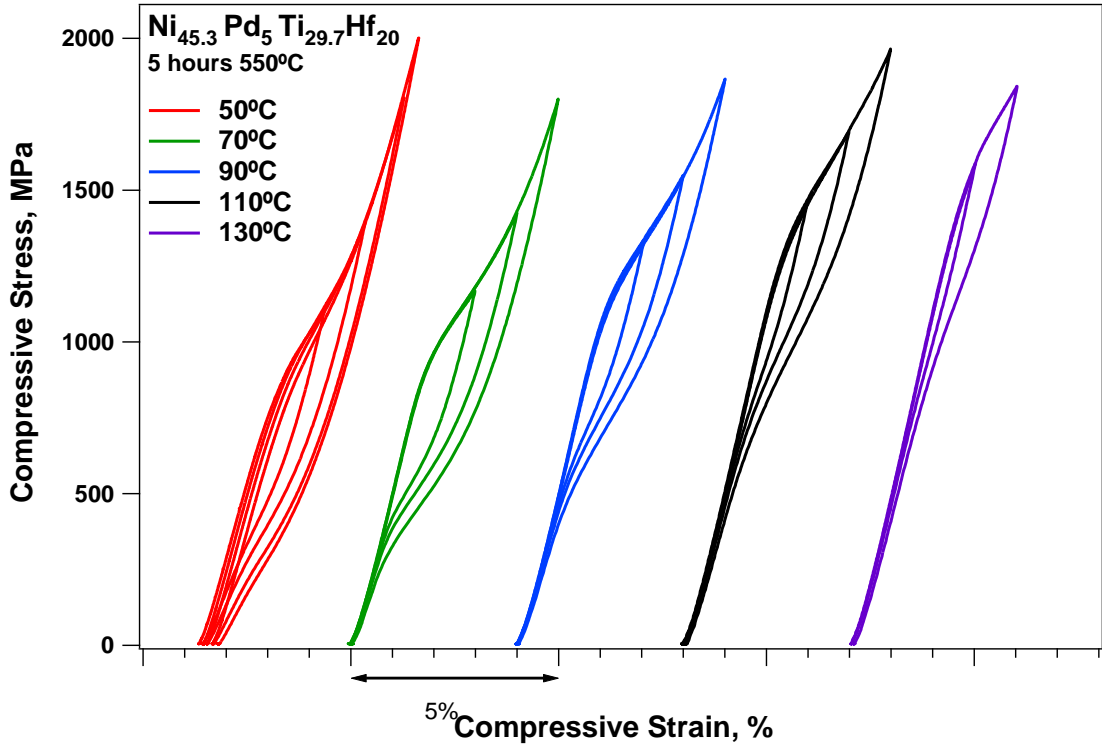
Figure 6.26: Isothermal mechanical cycling of Ni$_{45.3}$Pd$_5$Ti$_{29.7}$Hf$_{20}$ aged at 550°C for5 hours (top) and 24 hours (bottom)
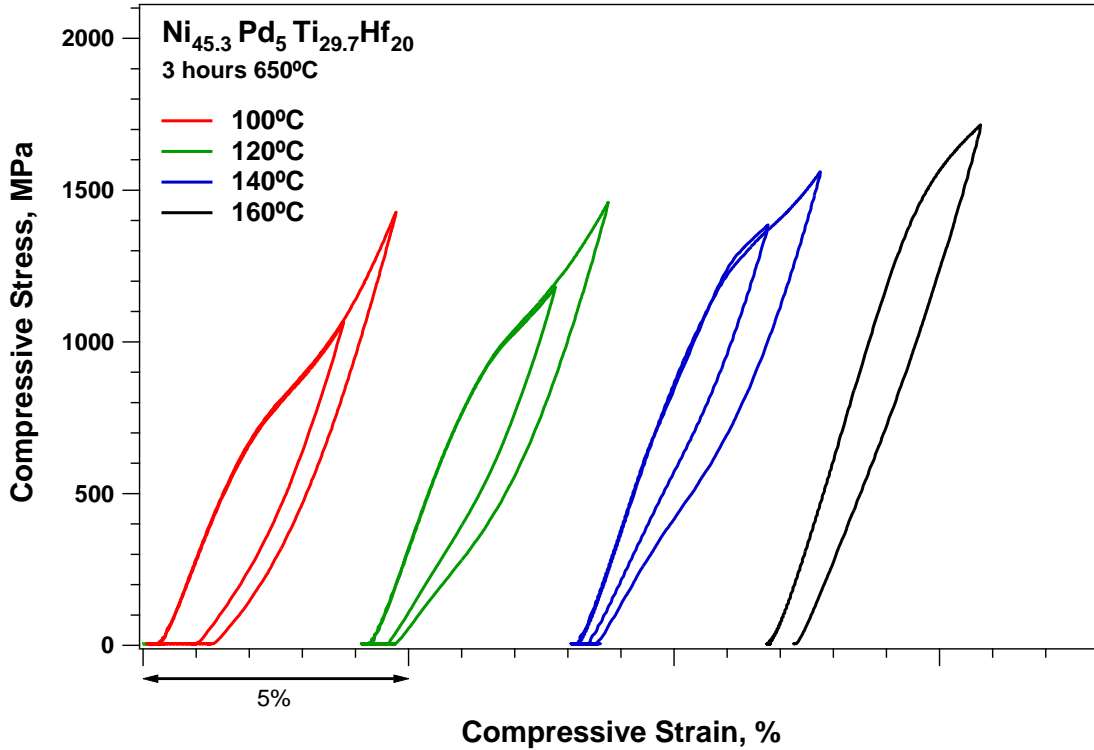
Figure 6.27: Isothermal mechanical cycling of $Ni_{45.3}Pd_5Ti_{29.7}Hf_{20}$ aged at 650°C for3
hours

The plots shown in Figures 6.25 to Figure 6.27 depict the isothermal compressive loading and unloading curves for the specimen whose results have been reported for isobaric thermal cycling in the previous section. The lowest testing temperature was selected to be 10°C higher than the A_f temperature for the specimen and the further testing was done at 20°C higher than the previous testing temperature. The testing temperature was increased more than 20°C in case the samples did not transform back to austenite at all, which meant the sample temperature was too low to initiate the back transformation. The temperature at which the test was run was achieved by cooling from temperature higher than A_f, to ensure that the sample was in austenitic state. The specimen was then loaded up to 5% in strain steps of 3%, 4% and 5% compressive strain calculated beforehand while maintaining stable testing temperature.

Table 6.8: Critical transformation parameters and strain levels for isothermal mechanical cycling of $Ni_{45.3}Pd_5Ti_{29.7}Hf_{20}$ in as extruded condition

Sample	Testing Temperature °C	Total Strain %	Elastic Recovery %	PE Strain %	SME on heating %	Irrecover-able strain %
As Extruded	20	6	2.312	3.22	0.468	0
	40	7	2.53	3.77	0.7	0
	60	7	2.74	3.335	0.78	0.2
	80	6	2.715	2.64	0.31	0.345
	100	6	2.848	2.13	0.53	0.5

Figure 6.25a represents the isobaric thermal cycling for the $Ni_{45.3}Pd_5Ti_{29.7}Hf_{20}$ in as extruded condition. The sample was initially loaded at 20°C to strain of 6% directly, and the stress induced transformation started at about 900MPa. The sample transformed back to austenite at about 250MPa and an irrecoverable strain of about 0.5% remained after unloading. The strain levels for the Figure 6.25a have been presented in Table 6.6. The sample when loaded at 40°C to a strain of 4% almost a fully recoverable strain was observed, when followed by a loading to 5% resulted in 0.7% of irrecoverable strain. This strain however was recovered completely upon heating. Loading the sample at 60°C resulted in almost similar behavior with the fully recoverable strain at a loading to 3% followed by marginal irecoverred strains of 0.2% and 0.7% for loading to 4% and 5% respectively. This left over strain was also recovered upon heating. The loading of sample at 80°C resulted in a high transformation stress of 1230MPa and as a result small amount of plastic strain was observed at loading to 4% strain itself and the sample was not loaded further. The sample transformed at 1300MPa at 100°C and the strain curve did not close for even 3% strain level. The good PE effect is analogous to the high strength of the material observed in the high values for hardness reported earlier. The high strength of

the material assured that the transformation stress was comfortably lower than the critical stress for slip.

Table 6.9: Critical transformation parameters and strain levels for isothermal mechanical cycling of $Ni_{45.3}Pd_5Ti_{29.7}Hf_{20}$ aged at 400°C for 3 hours

Sample	Testing Temperature °C	Total Strain %	Elastic Recovery %	PE Strain %	SME on heating %	Irrecover-able strain %
3hours 400°C	10	5	1.9	2.88	0.22	0
	30	5.24	2.24	3	0	0
	50	5	2.47	2.46	0	0
	70	5	2.26	2.64	0	0
	90	5	2.37	2.35	0.28	0

Figure 6.25b represents the PE curves for the experiments done on the $Ni_{45.3}Pd_5Ti_{29.7}Hf_{20}$ sample aged at 400°C for 3 hours with the specific details presented in Table 6.9. The low TTs reported earlier in the DSC ensured that the material was austenite at 10°C also, the temperature at which the sample was loaded initially. The straining of the sample to 3% resulted in fully recoverable curve and the transformation stress was much lower than the as extruded sample at 700MPa. Upon unloading from strain of 5% a very minute irrecoverable strain was left with the back transformation starting at about 200MPa. The loading of the sample to 3, 4 and 5% at the temperature of 30°C, 50°C and 70°C resulted in fully recoverable strains with fully closed cycles. The perfect PE curves can be attributed to the lowering of the transformation stress for the sample aged at 400°C for 3 hours. Fully recoverable strain was observed till loading to 4% at 90°C while a small irrecoverable strain was observed when the sample was loaded

to 5%. The transformation stress increased linearly when the sample was loaded at temperature 20°C higher than the preceding test temperature.

Table 6.10: Critical transformation parameters and strain levels for isothermal mechanical cycling of $Ni_{45.3}Pd_5Ti_{29.7}Hf_{20}$ aged at 550°C for 5 hours

Sample	Testing Temperature °C	Total Strain %	Elastic Recovery %	PE Strain %	SME on heating %	Irrecover-able strain %
5hours 550°C	50	5	2.8	2.05	0.15	0
	70	5	2.82	2.13	0	0
	90	5	2.45	2.45	0	0
	110	5	2.68	2.3	0	0
	130	4	2.9	1.1	0	0

Figure 6.26a depicts the PE behavior of the $Ni_{45.3}Pd_5Ti_{29.7}Hf_{20}$ sample aged for 5 hours at 550°C. The TTs increased notably from as extruded condition and it is reflected in the PE results also. The initial loading of the sample at 50°C resulted in incomplete recovery of the strain upon unloading representing the testing temperature to be lower than required for full recovery. The sample when loaded at 70°C resulted in perfect PE curves with transformation stress of 931 MPa. Similar behavior was observed for loading the sample at 90°C and 110°C also with the transformation stress levels increasing to about 1200MPa and 1388MPa respectively. Most notable feature of the curves is the low hysteresis.

Figure 6.26(b) represents the PE curves for the experiments done on the $Ni_{45.3}Pd_5Ti_{29.7}Hf_{20}$ sample aged at 550°C for 24 hours. The testing temperatures are indicative of the higher TTs for the sample in comparison to its counterpart aged for 5 hours at the same temperature. The sample behaved similar to the previous mentioned specimen and did not recover fully at 90°C, however the irrecoverable stains were

recovered upon heating the sample. The sample showed fully recoverable curves when loaded to 4% at 110°C, 130°C and 150°C. The division of the recoverable strains into the elastic recovery and the PE recovery as presented in Table 6.11. The sample was observed to harden substantially followed by stress induced transformation upon further loading and the stress level required to induce the 4% strain were in range of 1800MPa. The transformation stress for 150°C was notable high at 1400MPa. The transformation stress increased to 1469MPa for 170°C and upon unloading to 4% a strain of 0.2% was left, which was recovered by heating leaving behind no permanent strain.

Table 6.11: Critical transformation parameters and strain levels for isothermal mechanical cycling of $Ni_{45.3}Pd_5Ti_{29.7}Hf_{20}$ aged at 550°C for 24 hours

Sample	Testing Temperature °C	Total Strain %	Elastic Recovery %	PE Strain %	SME on heating %	Irrecover-able strain %
24hours 550°C	90	5	3.03	1.36	0.61	0
	110	4	2.6	1.39	0	0
	130	4	2.775	1.225	0	0
	150	4	2.88	1.12	0	0
	170	4	2.71	0.26	0	0

The PE testing results for the sample aged at 650°C for 3 hours is presented in the Figure 6.27. The TTs were reported to be even higher than the sample aged for 24 hours at 550°C possibly due a higher volume fraction of precipitates. The high testing temperature is indicative of high TTs since the lowest testing temperature was selected to be 10°C higher than the A_f. The sample was not observed to show fully recoverable strain for any testing temperature. This can be explained from the earlier observation of low hardness values also. The precipitates are believed to have grown into incoherent size and hence it is easier to induce slip in the sample and hence fully recoverable strains are not

observed. There was an irrecoverable strain of 0.2% left even after the sample showed

SME of 0.35% upon heating as shown in Table 6.10.

Table 6.12: Critical transformation parameters and strain levels for isothermal mechanical cycling of $Ni_{45.3}$ $Pd_5Ti_{29.7}Hf_{20}$ aged at 650°C for 3 hours

Sample	Testing Temperature °C	Total Strain %	Elastic Recovery %	PE Strain %	SME on heating %	Irrecover-able strain %
3hours 650°C	100	5	2.4	1.042	1.558	0
	120	5	2.42	1.69	0.89	0
	140	5	2.47	1.77	0.76	0
	160	4	2.75	0.69	0.35	0.21
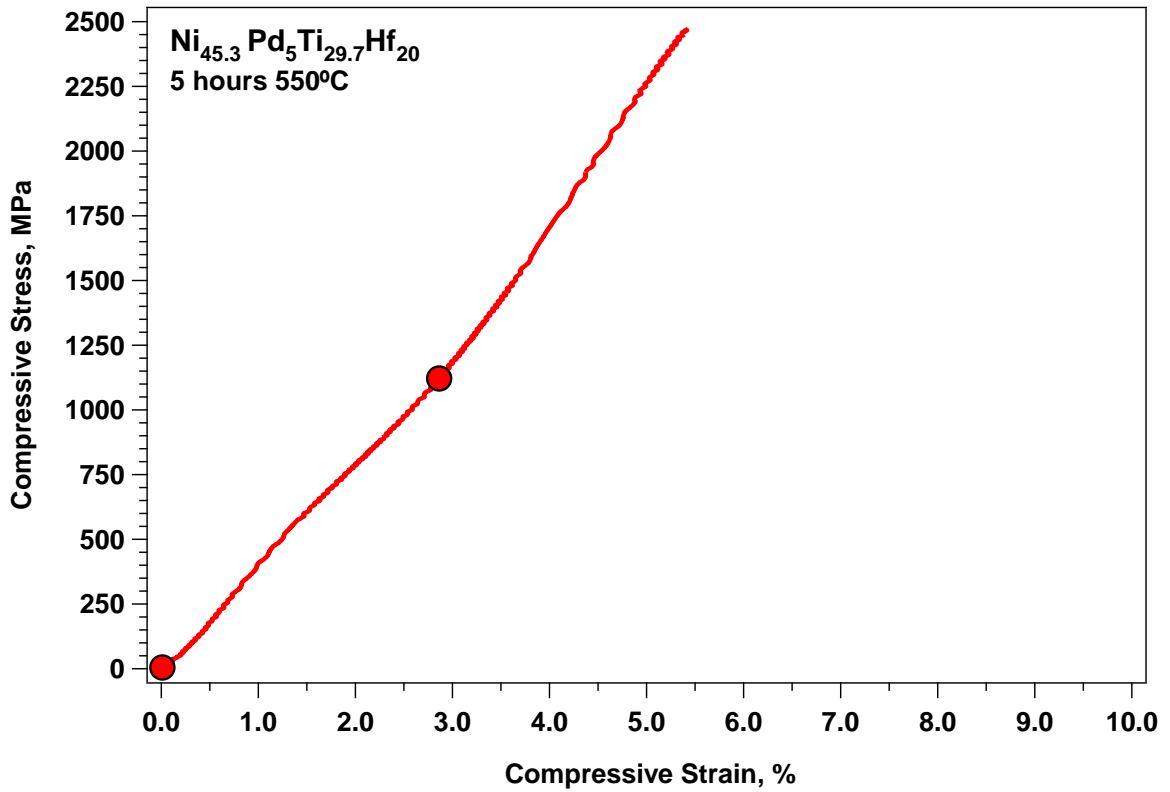
Figure 6.28: Ultimate yielding curves for $Ni_{45.3}Pd_5Ti_{29.7}Hf_{20}$ compression samples aged for 5hours at 550°C

187

Figure 6.28 depicts the ultimate failure test on the $Ni_{45.3}Pd_5Ti_{29.7}Hf_{20}$ compression samples aged for 5hours at 550°C earlier used for PE and isobaric cycling. The sample when loaded at room temperature abruptly failed at a stress of about 2500MPa with a brittle failure at a strain of about only 6%. The alloy was however still observed to be the toughest of the three alloys tested in the study but along with the highest strength it was found to be the most brittle also.

Comparisons

Comparisons between the results for the three alloys studied are presented and the compositional dependence of the material properties are shown in this chapter. The DSC, hardness and mechanical results are presented for as extruded condition and selected aging conditions. TEM micrographs are presented in the end of the chapter.

7.1 DSC results
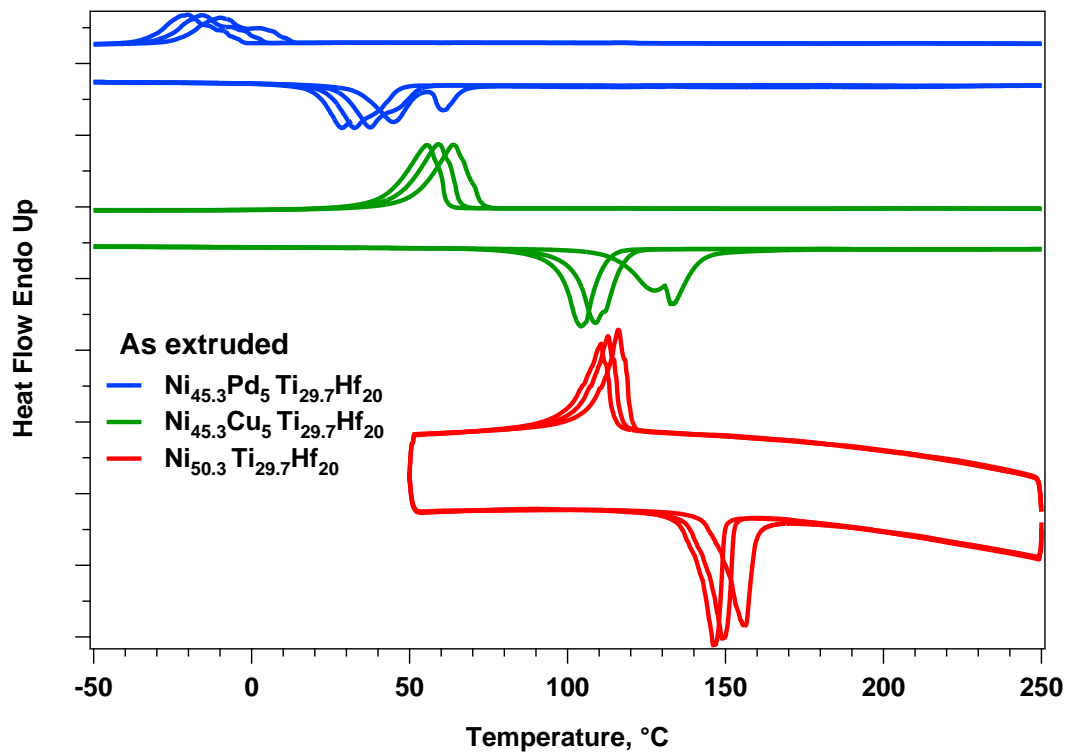
Figure 7.1: DSC curves for $Ni_{45.3}Pd_5Ti_{29.7}Hf_{20}$, $Ni_{45.3}Cu_5Ti_{29.7}Hf_{20}$, and $Ni_{50.3}Ti_{29.7}Hf_{20}$ in as extruded condition

Figure 7.1 represents the DSC curves extracted for the samples in as extruded condition for $Ni_{45.3}Pd_5Ti_{29.7}Hf_{20}$, $Ni_{45.3}Cu_5Ti_{29.7}Hf_{20}$, and $Ni_{50.3}Ti_{29.7}Hf_{20}$. The

Ni$_{45.3}$Pd$_5$Ti$_{29.7}$Hf$_{20}$ alloy has the lowest TTs, followed by the Ni$_{45.3}$Cu$_5$Ti$_{29.7}$Hf$_{20}$ and Ni$_{50.3}$Ti$_{29.7}$Hf$_{20}$ with the highest TTs. The amount of 5 at.% quaternary element added to the Ni$_{50.3}$Ti$_{29.7}$Hf$_{20}$ in substitution for Ni to obtain the Ni$_{45.3}$Pd$_5$Ti$_{29.7}$Hf$_{20}$ and Ni$_{45.3}$Cu$_5$Ti$_{29.7}$Hf$_{20}$ resulted in depression of the TTs for addition of both Cu and Pd. The TTs decreased by about 40°C for substitution of Cu for Ni and 100°C for Pd.
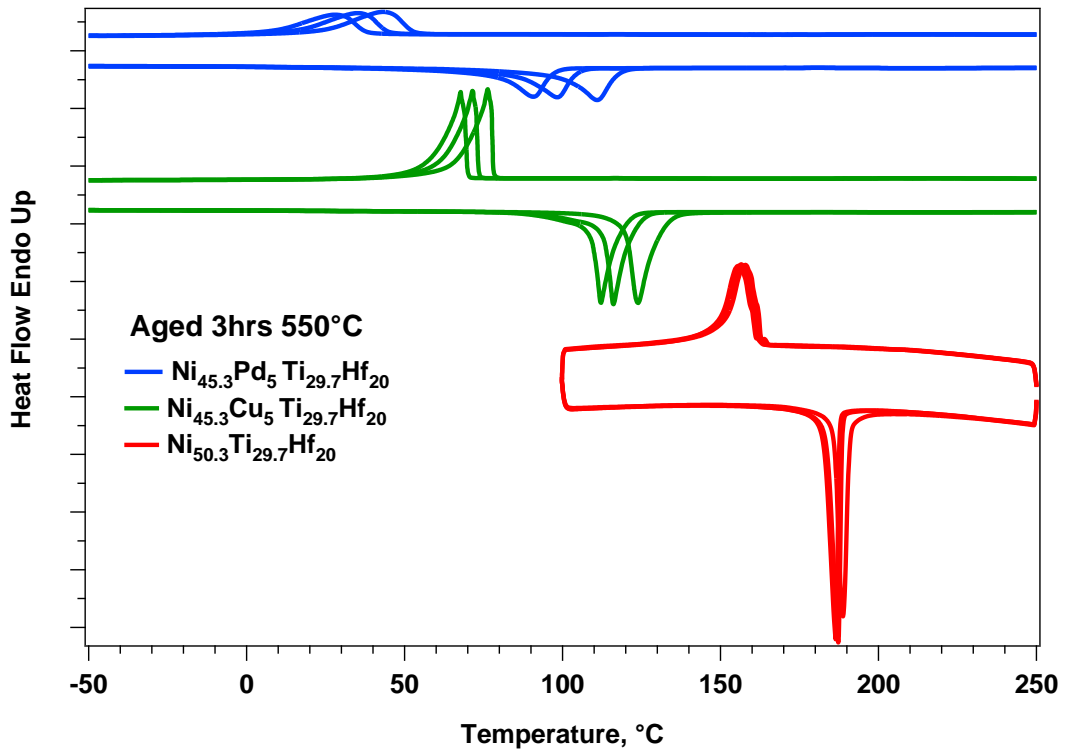
Figure 7.2: DSC curves for Ni$_{45.3}$Pd$_5$Ti$_{29.7}$Hf$_{20}$, Ni$_{45.3}$Cu$_5$Ti$_{29.7}$Hf$_{20}$, and Ni$_{50.3}$Ti$_{29.7}$Hf$_{20}$ aged for 3 hours at 550°C

Figure 7.2 depicts the DSC curves for Ni$_{45.3}$Pd$_5$Ti$_{29.7}$Hf$_{20}$, Ni$_{45.3}$Cu$_5$Ti$_{29.7}$Hf$_{20}$, and Ni$_{50.3}$Ti$_{29.7}$Hf$_{20}$ aged at 550°C for 3 hours. The temperature between range of 500°C and 600°C was observed to impart maximum augmentation in the TTs for all three alloys. The trend of TTs for the aged samples is similar to the samples in as extruded condition with the maximum TTs for Ni$_{50.3}$Ti$_{29.7}$Hf$_{20}$ and the minimum increment in the TTs was

observed for $Ni_{45.3}Cu_5Ti_{29.7}Hf_{20.}$ The aging leading to formation of precipitates is responsible for the increment in the TTs but as from the difference in increments it is visible that the type and volume fraction of precipitates formed depends strongly on the composition of the alloy. Along with the difference in the type and volume fraction of precipitates, their effects on the TTs and material strength is also different.
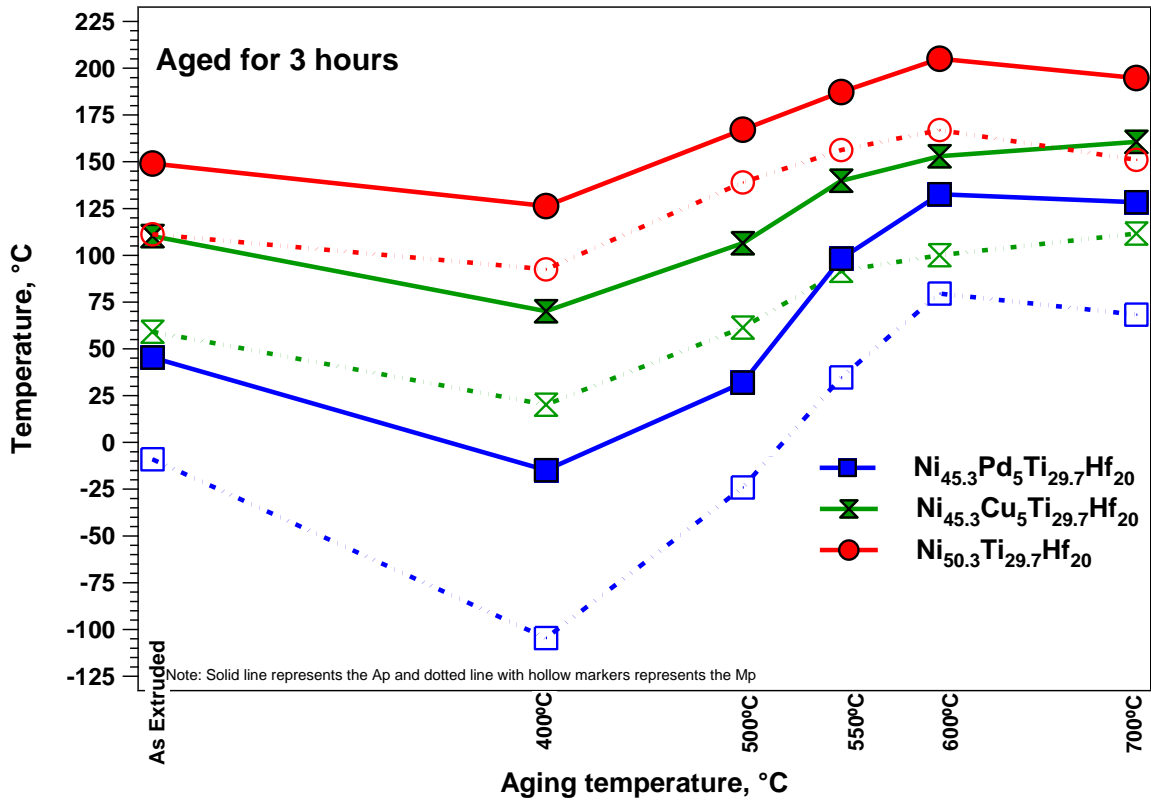
Figure 7.3: Curves depicting the A_p in solid curve and M_p in dotted curve for $Ni_{45.3}Pd_5Ti_{29.7}Hf_{20,}$ $Ni_{45.3}Cu_5Ti_{29.7}Hf_{20,}$ and $Ni_{50.3}Ti_{29.7}Hf_{20}$ aged for 3 hours at varying temperatures.

7.2 Hardness
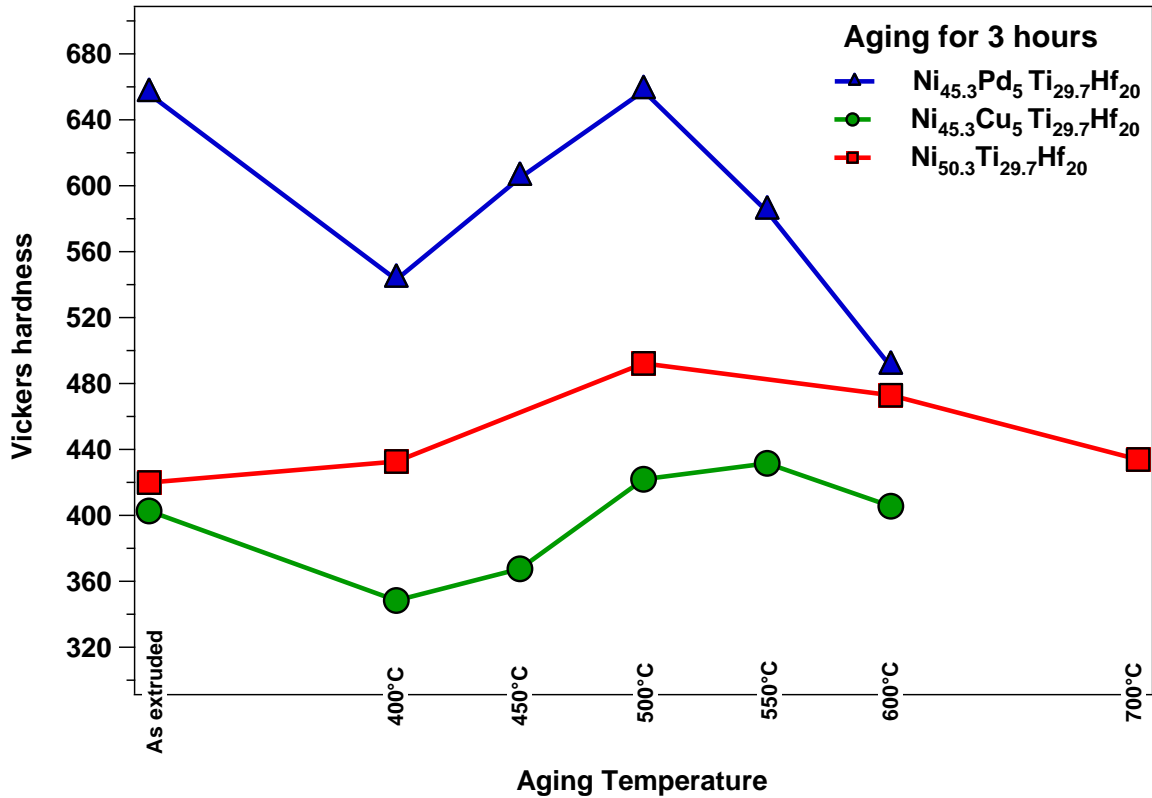
Figure 7.4: Curves depicting the hardness values for $Ni_{45.3}Pd_5Ti_{29.7}Hf_{20}$, $Ni_{45.3}Cu_5Ti_{29.7}Hf_{20}$, and $Ni_{50.3}Ti_{29.7}Hf_{20}$ aged for 3 hours at varying temperatures.

Hardness results for $Ni_{45.3}Pd_5Ti_{29.7}Hf_{20}$, $Ni_{45.3}Cu_5Ti_{29.7}Hf_{20}$, and $Ni_{50.3}Ti_{29.7}Hf_{20}$ samples aged for 3 hours at temperatures between 400°C and 700°C are presented in Figure 7.3. The $Ni_{45.3}Pd_5Ti_{29.7}Hf_{20}$ was the hardest of the three alloys, while the addition of Cu led to softening of the material. The variation in the hardness was similar for all the alloys with the maximum value observed for aging at 500°C though it should be noted that $Ni_{45.3}Pd_5Ti_{29.7}Hf_{20}$ alloy was in austenite phase at room temperature for the aging below 550°C for 3 hours.

7.3 Mechanical Results
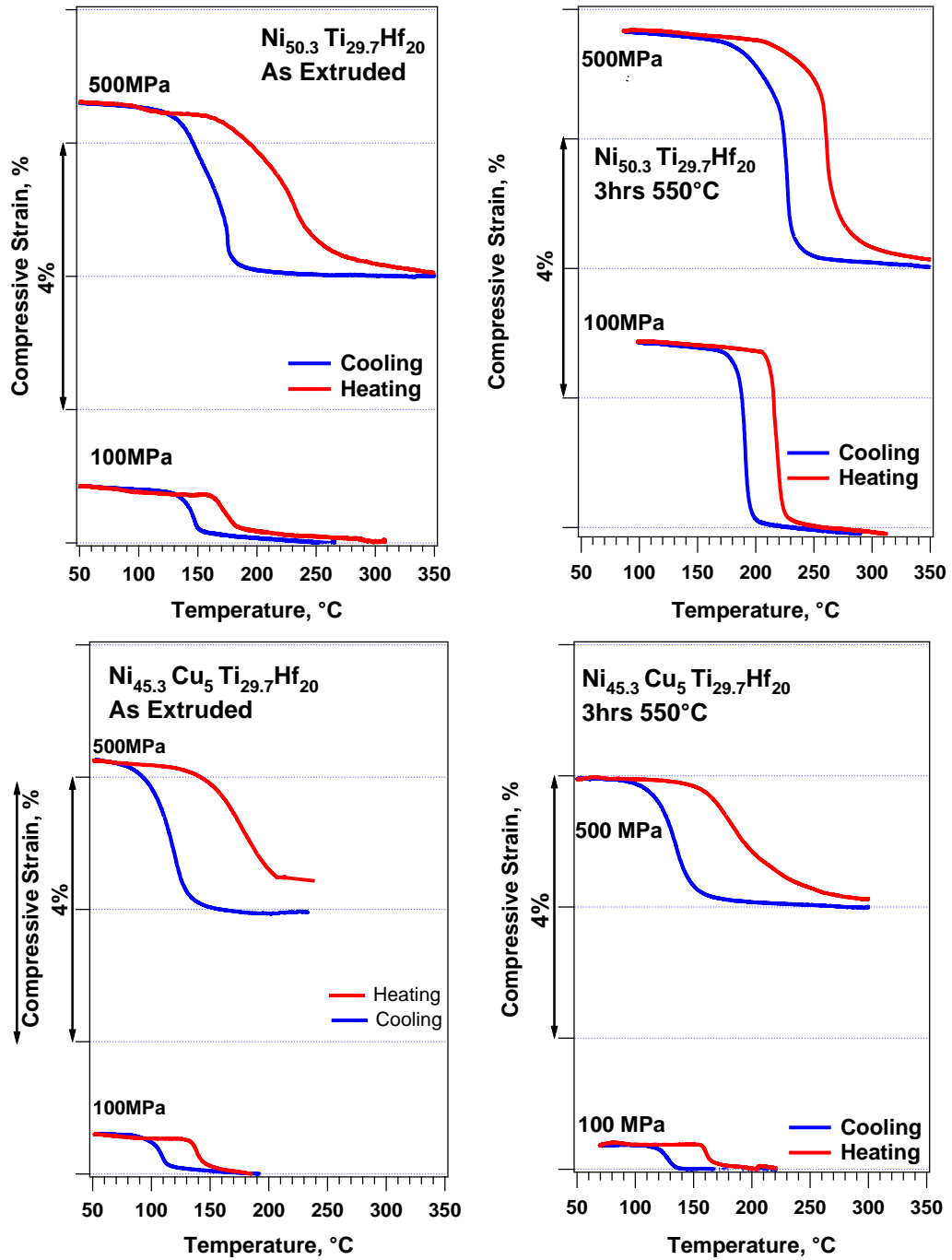
Figure 7.5 Isobaric thermal cycling plots for selected samples at 100MPa and 500MPa for $Ni_{50.3}Ti_{29.7}Hf20$ and $Ni_{45.3}Cu_5Ti_{29.7}Hf_{20.}$
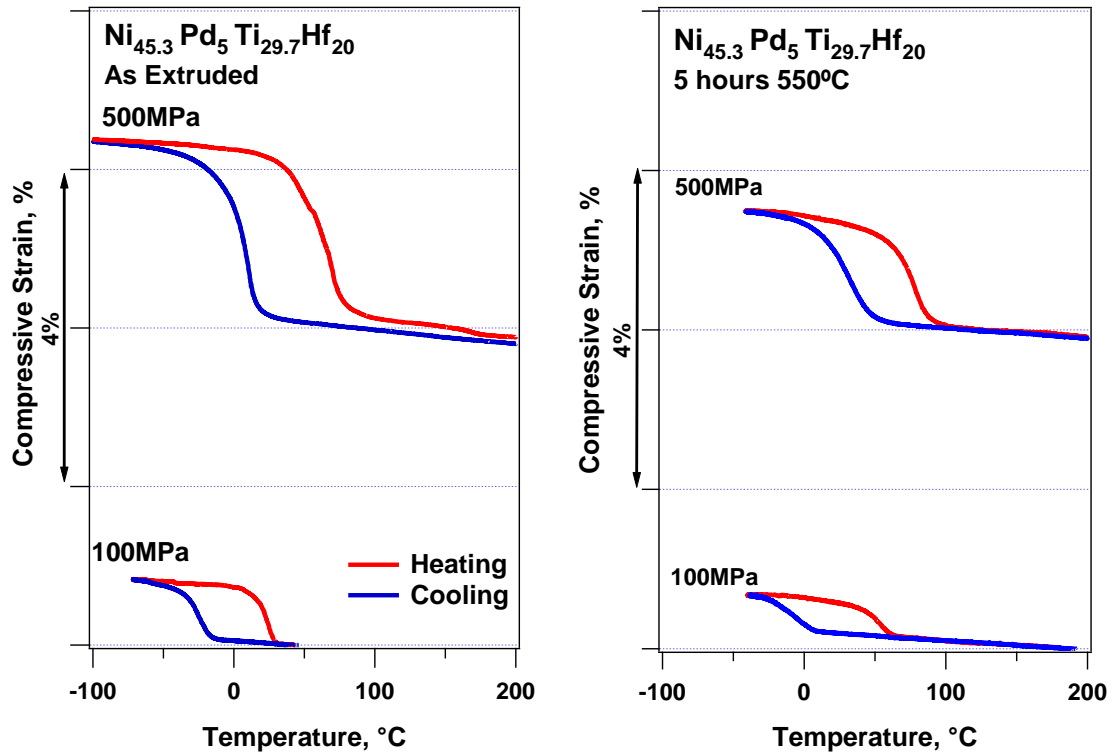
Continued Figure 7.5. Isobaric thermal cycling plots for selected samples at 100MPa and 500MPa for $Ni_{45.3}Pd_5Ti_{29.7}Hf_{20}$.

Figure 7.5 depicts a comparison between isobaric thermal cycling for sample in as extruded condition and aged at 550°C for the $Ni_{50.3}Ti_{29.7}Hf_{20}$, $Ni_{45.3}Pd_5Ti_{29.7}Hf_{20}$ and $Ni_{45.3}Cu_5Ti_{29.7}Hf_{20}$ at load levels of 100MPa and 500MPa. In correspondence to the DSC results the TTs increased for all the above samples shown in Figures 7.4 and 7.5 with aging. The precipitation of Ni-rich particles which can be attributed for the increment in TTs can also be ascribed for the higher strength of the aged specimen, in which the irrecoverable strains decreased in comparison with the as extruded samples of corresponding alloys. The hysteresis decreased significantly for $Ni_{50.3}Ti_{29.7}Hf_{20}$ and $Ni_{45.3}Pd_5Ti_{29.7}Hf_{20}$ samples, while the drop for the same was marginal in $Ni_{45.3}Cu_5Ti_{29.7}Hf_{20}$. precipitates for the aged specimen increased the level of recoverable strain in aged $Ni_{50.3}Ti_{29.7}Hf_{20}$ sample by possibly assisting in selection of biased

194

martensite variants. However the precipitates in the aged $Ni_{45.3}Pd_5Ti_{29.7}Hf_{20}$ samples can be held responsible for decreasing the volume of transforming matrix significantly, whose effect can be noted in the decreased level of recovered strains for the transformation.
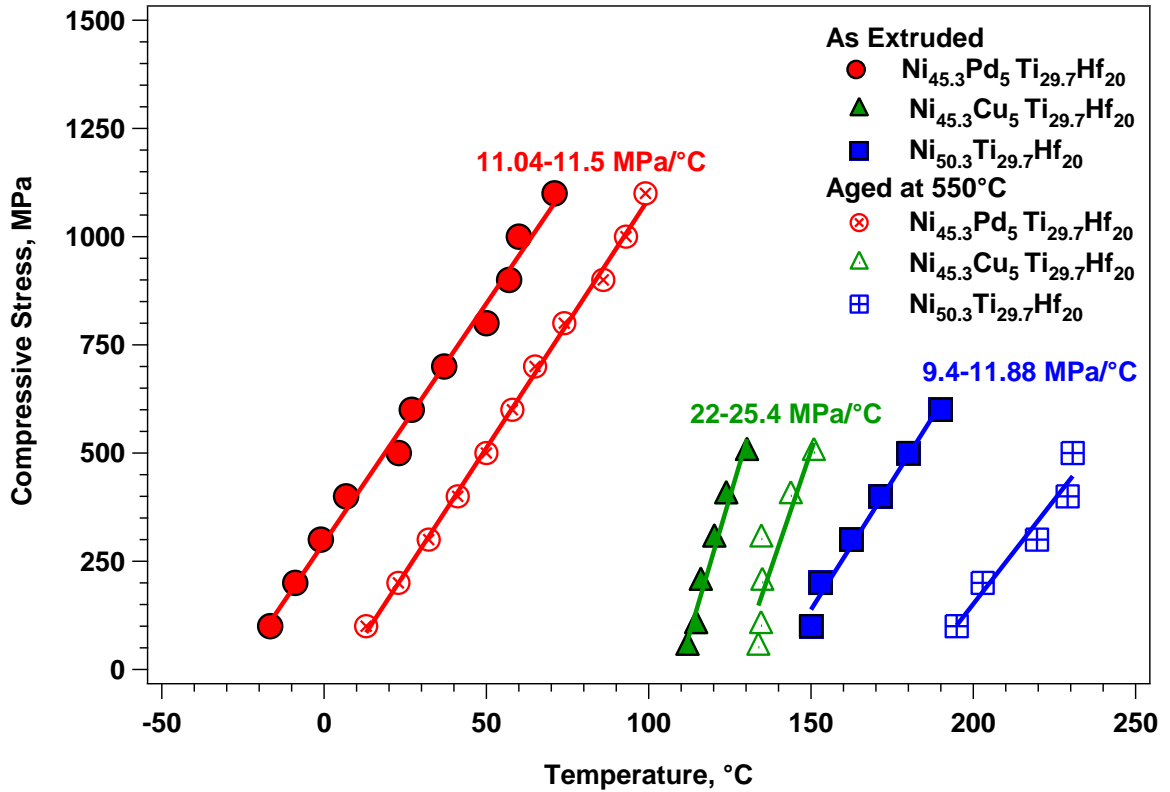
Figure 7.6: Clausius-Clapeyron curves for $Ni_{45.3}Pd_5Ti_{29.7}Hf_{20}$, $Ni_{45.3}Cu_5Ti_{29.7}Hf_{20}$, and $Ni_{50.3}Ti_{29.7}Hf_{20}$ alloys in as extruded condition and aged at 550°C.

The slopes of the Clausius-Clapeyron curves for the three alloys are presented in the figure 7.6. The combination of the steepest slope for CC curve and the least hardness can be attributed for no perfect behavior for $Ni_{45.3}Cu_5Ti_{29.7}Hf_{20}$. The CC slope for $Ni_{45.3}Pd_5Ti_{29.7}Hf_{20}$ and $Ni_{50.3}Ti_{29.7}Hf_{20}$ alloys is much lower at 9.4-11.88MPa/°C in comparison to 22-25.5 MPa/°C for $Ni_{45.3}Cu_5Ti_{29.7}Hf_{20}$. This lower slope results in a broader window of temperature range for possibility of PE behavior for

$Ni_{45.3}Pd_5Ti_{29.7}Hf_{20}$ and $Ni_{50.3}Ti_{29.7}Hf_{20}$ alloys, and as shown in discussion of results almost perfect PE is observed. Higher hardness of these two alloys can also be attributed for ensuring the possibility of PE.
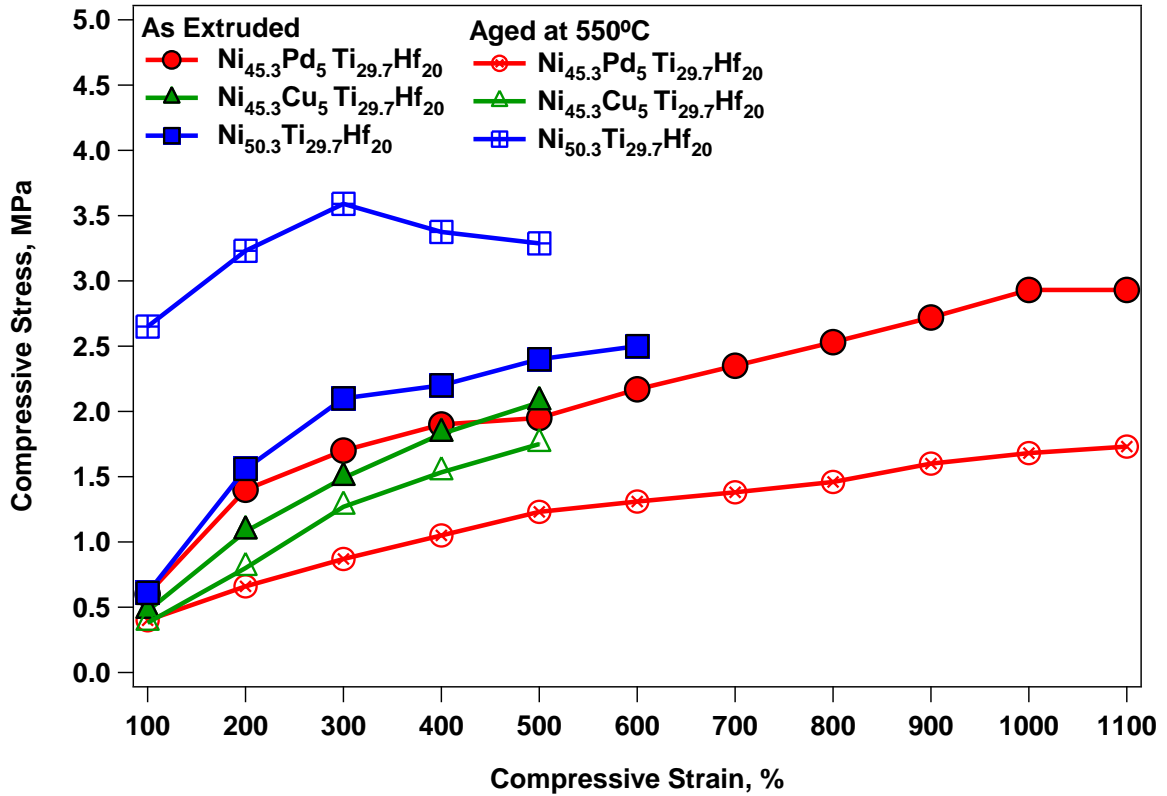
Figure 7.7. Curves representing the recoverable strains for $Ni_{45.3}Pd_5Ti_{29.7}Hf_{20,}$ $Ni_{45.3}Cu_5Ti_{29.7}Hf_{20,}$ and $Ni_{50.3}Ti_{29.7}Hf_{20}$ alloys in as extruded condition and aged at 550°C.

Figure 7.7 presents the variations in levels of recoverable strains upon application of varying loads for $Ni_{45.3}Pd_5Ti_{29.7}Hf_{20,}$ $Ni_{45.3}Cu_5Ti_{29.7}Hf_{20,}$ and $Ni_{50.3}Ti_{29.7}Hf_{20}$ alloys in as extruded condition and aged at 550°C. The recoverable strain increased as a function of applied stress and saturated at applied stress of 300MPa for $Ni_{50.3}Ti_{29.7}Hf_{20}$, while it continue to increase almost linearly for $Ni_{45.3}Pd_5Ti_{29.7}Hf_{20}$. The strains for $Ni_{45.3}Cu_5Ti_{29.7}Hf_{20}$ were accompanied by irrecoverable strain at the stress level of 300MPa and higher. The progressive increment of the recoverable strain can be attributed

196

to the evolution of stress biased martensite variants. During the cooling part of isobaric cycling, at low stress levels are assumed not to be sufficient to bias a single variant and it is accompanied by partial formation of self accommodating martensite and hence lower level of strains are observed at lower applied stress levels. The decrement in the amount of recoverable strain for $Ni_{45.3}Pd_5Ti_{29.7}Hf_{20}$ aged specimen in contrast to the as extruded specimen can be attributed to the large volume fraction of precipitates, which in turn reduces the volume of transforming matrix and hence the lower amount of observed strain. On the other hand, as is visible from TEM micrographs the comparably different type of precipitates formed in $Ni_{50.3}Ti_{29.7}Hf_{20}$ can be attributed for the selection of biased variants and hence the level of transformation strain increases. The small variation in the strain for as extruded sample and the aged sample for $Ni_{45.3}Cu_5Ti_{29.7}Hf_{20}$ can be attributed to the relatively small volume fraction of precipitates which don't contribute greatly in either way.
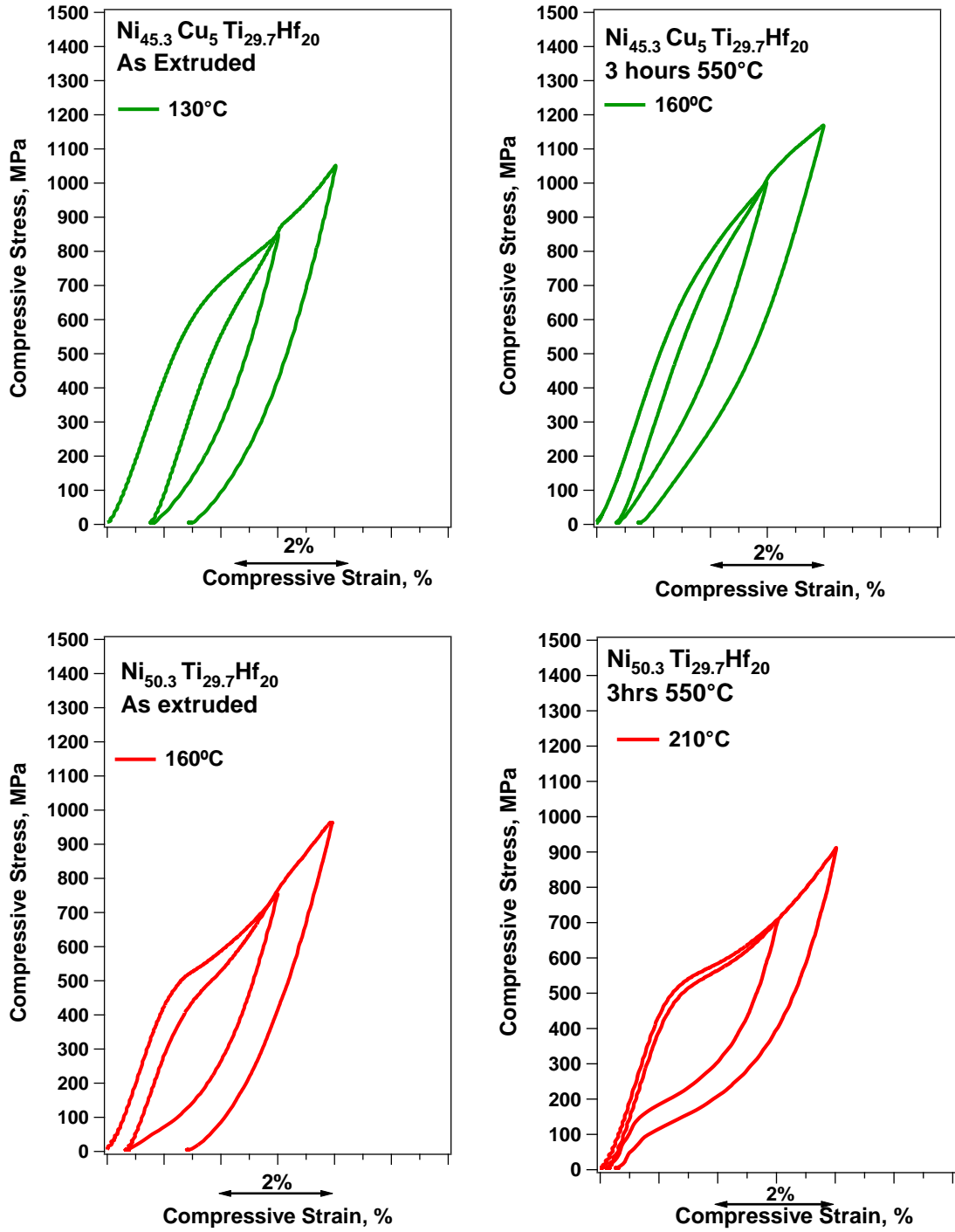
Figure 7.8. Isothermal PE cycling for selected samples at $A_f+10°C$ for $Ni_{50.3}Ti_{29.7}Hf_{20}$ and $Ni_{45.3}Cu_5Ti_{29.7}Hf_{20}$.
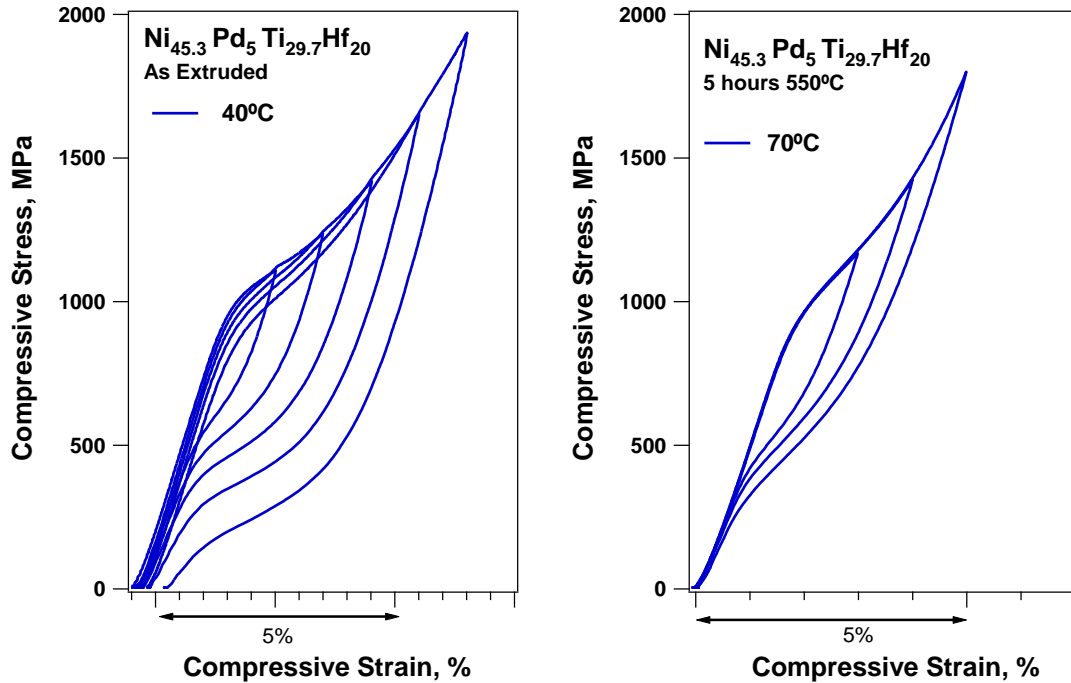
Figure 7.9. Isothermal PE cycling for selected samples at $A_f+10°C$ for $Ni_{45.3}Pd_5Ti_{29.7}Hf_{20}$.

Figures 7.7 and 7.8 present an insight of the variation of the PE cycling for the $Ni_{50.3}Ti_{29.7}Hf_{20}$, $Ni_{45.3}Pd_5Ti_{29.7}Hf_{20}$ and $Ni_{45.3}Cu_5Ti_{29.7}Hf_{20}$ from as extruded condition to aged at 550°C. The cycles for the test done at $A_f+10°C$ have been presented in the Figures 7.7 and 7.8. No significant variation between the aged and as extruded sample for the $Ni_{45.3}Cu_5Ti_{29.7}Hf_{20}$ alloy can be attributed to the lower volume fraction of the strength imparting precipitates, while the clear strengthening due to formation of precipitates is observable for $Ni_{50.3}Ti_{29.7}Hf_{20}$ and $Ni_{45.3}Pd_5Ti_{29.7}Hf_{20}$. The increased critical stress for slip due to precipitation hardening can be attributed for the fully recoverable curves for the aged specimen of the two alloys in contrast to the irrecoverable strains left over for the as-extruded specimen.

7.4 TEM results

(a)   (b)
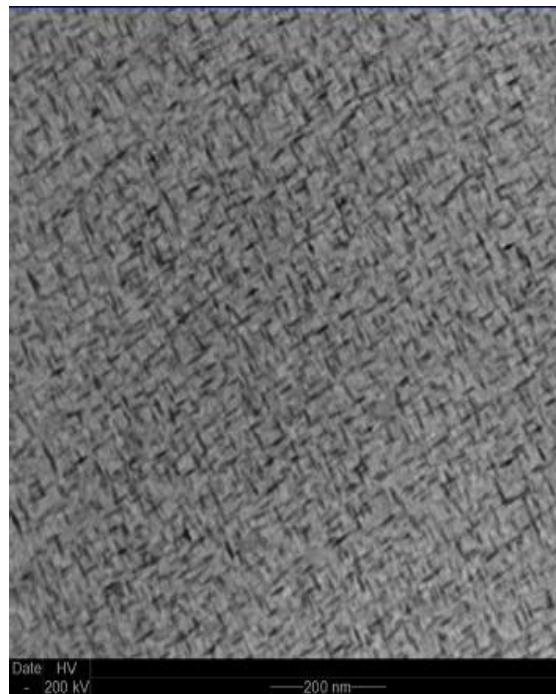
(c)

Figure 7.10. TEM micrographs of $Ni_{45.3}Cu_5Ti_{29.7}Hf_{20}$(a), and $Ni_{50.3}Ti_{29.7}Hf_{20}$(b) and $Ni_{45.3}Pd_5Ti_{29.7}Hf_{20}$ (c) aged for 3 hours at 550°C

Figure 7.10 depicts the TEM micrographs for $Ni_{45.3}Cu_5Ti_{29.7}Hf_{20}$, $Ni_{50.3}Ti_{29.7}Hf_{20}$ and $Ni_{45.3}Pd_5Ti_{29.7}Hf_{20}$ aged for 3 hours at 550°C. The variation in the formation of precipitates despite the exact same aging conditions is clearly visible. Worm like formations possible due to nucleation at site of dislocations is visible for $Ni_{45.3}Cu_5Ti_{29.7}Hf_{20}$ while oval shaped finely dispersed particle are observed for $Ni_{50.3}Ti_{29.7}Hf_{20.}$ Long rice-grain shaped precipitates are present in a very large volume fraction for $Ni_{45.3}Pd_5Ti_{29.7}Hf_{20.}$

The results presented above show the high sensitivity of compositional dependence of the various properties of the three alloys discussed in the study. The substitution of Ni from $Ni_{50.3}Ti_{29.7}Hf_{20}$ with 5 at.% Cu decreased the TTs however it also made the alloy more ductile, henceforth making the processing of the alloy significantly easier. The addition of Pd to the ternary alloy imparted high level of strength to the alloy while decreasing the TTs very significantly for certain aging conditions. The TTs were highest for the $Ni_{50.3}Ti_{29.7}Hf_{20}$ alloy, followed by $Ni_{45.3}Cu_5Ti_{29.7}Hf_{20}$ and the lowest TTs were observed for $Ni_{45.3}Pd_5Ti_{29.7}Hf_{20}$.

The properties of the alloys, including the TTs and the strength of the three alloys were found to be varying decidedly with different conditions for aging as well. The formation of precipitates with aging led to significant changes at the microstructure level of the alloys, which can be significantly used for tailoring the shape memory properties of the alloys to suit particular requirements. Very stable transformations and suitably high temperatures were observed at optimum aging conditions, including high recoverable strains and fully recoverable PE cycles.

CHAPTER 8: Summary and Conclusions

8.1 Summary

In this study a detailed investigation into the properties and transformation behavior for the Ni-rich HTSMA with the compositions of $Ni_{45.3}Cu_5Ti_{29.7}Hf_{20}$, $Ni_{50.3}Ti_{29.7}Hf_{20}$ and $Ni_{45.3}Pd_5Ti_{29.7}Hf_{20}$ was carried out. The effect of aging the three alloys as function of temperature and time was determined experimentally by using techniques such as DSC, XRD, TEM and mechanical characterization.

8.2 Conclusions

- The $Ni_{50.3}Ti_{29.7}Hf_{20}$ alloy has the highest TTs among the three alloys studied. The TTs were highly dependent on aging conditions while becoming maximum for aging at 650°C for 3 hours. Recoverable strains under isobaric cycling increased sharply till an applied load of 300MPa, followed by only a slight increment and small levels of irrecoverable strains for higher stress levels. The isobaric thermal cycling yielded recoverable strain of more than 3% at 300MPa for sample aged at 550°C for 3 hours. It showed best PE behavior for temperature range of A_f+10°C to A_f+30°C. Perfect PE curves were observed for sample aged at 550°C for 3 hours in the above mentioned temperature range.

- Substitution of Ni for 5 at.% of Cu led to slight decrement in the TTs and the material became more ductile in comparison to the $Ni_{50.3}Ti_{29.7}Hf_{20}$ alloy. The variation of the TTs for $Ni_{45.3}Cu_5Ti_{29.7}Hf_{20}$ was found to be highly sensitive to the aging analogous to the ternary $Ni_{50.3}Ti_{29.7}Hf_{20}$ alloy. Under isobaric thermal cycling the levels of recoverable strains increased with increment in levels of applied stress, however after

loading beyond 300MPa sizable amount of irrecoverable strains accompanied the transformation strain. The alloy did not show very good PE in general, though the increased ductility makes the processing of the material into intricate shapes relatively easy.

- $Ni_{45.3}Pd_5Ti_{29.7}Hf_{20}$ alloy was found to be the strongest of all the three alloys tested, though the TTs were notably lower than $Ni_{50.3}Ti_{29.7}Hf_{20}$. The TTs were extremely sensitive to the aging conditions; the TTs fell to extremely low levels for aging at 400°C and 450°C while aging at 550°C to 600°C yielded higher TTs than as extruded condition. The levels of recoverable strain were lower than both the other alloys for corresponding stress levels. The recoverable strain for isobaric cycling continued to grow with increment of applied stress to 1000MPa with almost no irrecoverable strain. PE was observed for a large range of temperature with fully recoverable strains in order of 6%, though the strain included about 2.5% elastic strain in addition to about 3.5% PE strain.

- Generally in all the three alloys the aging at 3 hours was found to be more effective than 1 hour for achieving more desirable outputs. Dependence of evolution of precipitates on time and temperature can be attributed for this effect. The TTs decreased initially for aging till 450°C, followed by a linear sizable increment for aging between 500°C and 600°C. The inhibition of martensite nucleation due to presence of very small precipitates throughout the matrix are attributed for initial decrement in TTs. The aging between a temperature range of 500°C to 600°C was found to be optimum for combination of strengthening the material along with increasing the TTs for all the three alloys. Large volume fraction of coherent

precipitates can be attributed for strengthening the material and increasing the TTs. Formation of coherent precipitates between the size of 20nm to 50nm are responsible for the increment in TTs.

- The TTs decreased for increasing the aging temperature further to 700°C, and fell back to values comparable as extruded condition for aging at 900°C. The recrystallization temperature is very close to 700°C and can be held responsible for beginning of dissolution of precipitates and hence annulling the effect of precipitates seen for aging at 500°C and 600°C. Aging at 900°C is held responsible for completely precipitate free structure and hence transformation behavior similar to as extruded condition is seen. Hysteresis was also observed to increase for substitution of Ni by both Cu and Pd.

- Aging was found to be a very effective tool for tailoring the TTs and shape memory properties of the alloys to specific requirements. Formation of Ni-rich precipitates is responsible for this effect.

- $Ni_{50.3}Ti_{29.7}Hf_{20}$ aged at 550°C for 3 hours tested decidedly positive for use in high temperature applications due to good shape memory properties and near perfect PE behavior observed. The high strength of the $Ni_{45.3}Pd_5Ti_{29.7}Hf_{20}$ along with the large range of temperature in which the alloy showed perfect PE behavior makes it a formidable candidate for both high temperature and biomedical applications.

8.3 Future Work

- More indepth TEM analysis need to be done to establish the fundamental understanding on the effects of aging on the microstructure. The high resloution TEM

is required to reveal the properties and microstructure of the nano-sized precipitates formed in the alloys

- TEM study to investigate the evolution of dislocations and detwinning behavior should be carried out.

- High stress level tests need to be done in future to fully understand the behavior of $Ni_{45.3}Pd_5Ti_{29.7}Hf_{20}$ along with TEM analysis of samples with very low TTs.

- Cyclic mechanical tests need to be done to positively conclude the feasibility of $Ni_{50.3}Ti_{29.7}Hf_{20}$ and $Ni_{45.3}Pd_5Ti_{29.7}Hf_{20}$ in aerospace applications.

- Further work is required to establish the composition-microstructure property relationship.

References:

1. Chang, L.C. and T.A. Read, *PLASTIC DEFORMATION AND DIFFUSIONLESS PHASE CHANGES IN METALS - THE GOLD-CADMIUM BETA-PHASE.* Journal of Metals, 1951. **3**(1): p. 47-52.
2. Lagoudas, D.C., *Shape Memory Alloys: Modeling and Engineering Applications*. 2008, New York: Springer.
3. Buehler, W.J., R.C. Wiley, and J.V. Gilfrich, *EFFECT OF LOW-TEMPERATURE PHASE CHANGES ON MECHANICAL PROPERTIES OF ALLOYS NEAR COMPOSITION TINI.* Journal of Applied Physics, 1963. **34**(5): p. 1475-&.
4. Miyazaki, S. and K. Otsuka, *DEVELOPMENT OF SHAPE MEMORY ALLOYS.* ISIJ International, 1989. **29**(5): p. 353-377.
5. Schetky, L.M., *SHAPE-MEMORY ALLOYS.* Scientific American, 1979. **241**(5): p. 74-82.
6. Wayman, C.M. and J.D. Harrison, *THE ORIGINS OF THE SHAPE MEMORY EFFECT.* Jom-Journal of the Minerals Metals & Materials Society, 1989. **41**(9): p. 26-28.
7. Schetky, L.M., *The industrial applications of shape memory alloys in North America*, in *Shape Memory Materials*, T. Saburi, Editor. 2000, Trans Tech Publications Ltd: Zurich-Uetikon. p. 9-16.
8. Miyazaki, S., et al., *Fatigue life of Ti-50 at.% Ni and Ti-40Ni-10Cu (at.%) shape memory alloy wires.* Materials Science and Engineering A, 1999. **273-275**: p. 658-663.
9. Duerig, T., *Engineering aspects of Shape memory alloys*. 1990, London: Butterworth-Heinemann.
10. Otsuka, K.a.W., C.M, *Shape memory materials*. 1998, Cambridge; New York: Cambridge University Press.
11. Mavroidis, C., *Development of advanced actuators using shape memory alloys and electrorheological fluids.* Research in Nondestructive Evaluation, 2002. **14**(1): p. 1-32.
12. Funakubo, H., *Shape Memory Alloys*. Precision Machinery and Robotics, ed. H. Funakubo. 1987, Amsterdam: Gordon and Breach Science Publishers S.A.
13. Melton, K.N. and O. Mercier, *THE MECHANICAL-PROPERTIES OF NITI-BASED SHAPE MEMORY ALLOYS.* Acta Metallurgica, 1981. **29**(2): p. 393-398.
14. Noebe R, B.T., Padula SA *NiTi-Based High-Temperature Shape-Memory Alloys: Properties, Prospects, and Potential Applications*, in *Advanced Structural Materials: Properties, Design Optimization, and Applications*, S.T. Soboyejo WO Editor. 2007, Taylor & Francis Group: NW.
15. Firstov, G., J. Van Humbeeck, and Y. Koval, *High Temperature Shape Memory Alloys: Problems and Prospects.* Journal of Intelligent Material Systems and Structures, 2006. **17**: p. 1041-1047.
16. Otsuka, K. and X. Ren, *Recent developments in the research of shape memory alloys.* Intermetallics, 1999. **7**: p. 511-528.
17. Meng, X.L., et al., *Phase transformation and precipitation in aged Ti-Ni-Hf high-temperature shape memory alloys.* Materials Science and Engineering a-Structural Materials Properties Microstructure and Processing, 2006. **438**: p. 666-670.
18. Van Humbeeck, J., *High temperature shape memory alloys.* Journal of Engineering Materials and Technology-Transactions of the Asme, 1999. **121**(1): p. 98-101.

19.	Fonda, R., H. Jones, and R. Vandermeer, *The Shape Memory Effect in Equiatomic TaRu and NbRu Alloys.* Scripta Materialia, 1998. **39**(8): p. 1031-1037.

20.	Ma, Y.Q., et al., *Thermal stability of the Ni54Mn25Ga21 Heusler alloy with high temperature transformation.* Scripta Materialia, 2003. **48**(4): p. 365-369.

21.	Hamilton, R.F., et al., *Transformation of Co-Ni-Al single crystals in tension.* Scripta Materialia, 2005. **53**(1): p. 131-136.

22.	Van Humbeeck, J., in *ICOMAT 1986*. 1986, Japan Institute of Metals. p. 862-867.

23.	Viahhi, I.E., Pridaki, A.I, Pulnev, S.A., Yudin, V.I. in *SMST Proceedings: Second International conference on Shape memory and Superelastic Technologies*. 1997. Santa Clara, USA.

24.	Elst, R., et al., *GRAIN-REFINEMENT DURING SOLIDIFICATION OF BETA-CU BASED ALLOYS.* Zeitschrift Fur Metallkunde, 1986. **77**(7): p. 421-424.

25.	Yang, W.S., Mikhola, D.E. in *MRS-Proc.* 1992.

26.	Potapov, P.L., *THE ELASTIC ENERGY INDUCED BY MARTENSITIC-TRANSFORMATION IN NIMN(TI).* Scripta Metallurgica Et Materialia, 1994. **31**(9): p. 1243-1248.

27.	Potapov, P.L., *MARTENSITIC TRANSFORMATIONS AND HIGH-TEMPERATURE SHAPE-MEMORY EFFECT IN THE INTERMETALLIC NIMN ALLOYED WITH TI.* Metal Science and Heat Treatment, 1993. **35**(9-10): p. 520-525.

28.	Potapov, P.L., O.P. Maksimova, and E.Z. Vintaikin, *PHASE-COMPOSITION AND PLASTICITY OF ALLOYS WITH SHAPE-MEMORY OF THE SYSTEM NI-MN-TI.* Metal Science and Heat Treatment, 1994. **36**(1-2): p. 48-53.

29.	Potapov, P.L., et al., *The martensitic structure and shape memory effect in NiMn alloyed by Ti and Al.* Zeitschrift Fur Metallkunde, 1996. **87**(1): p. 33-39.

30.	Udovenko, V.A., et al., *ON CHARACTER OF ALLOTROPIC TRANSFORMATION IN MNNI INTERMETALLIDE ALLOYED BY TI AND AL.* Fizika Metallov I Metallovedenie, 1993. **75**(3): p. 65-68.

31.	Kainuma, R., et al., *Microstructural evolution in ductile beta(B2)+gamma'(L1(2)) Ni-Al-Fe alloys.* Intermetallics, 1996. **4**(1): p. 37-45.

32.	Kainuma, R., K. Ishida, and T. Nishizawa, *THERMOELASTIC MARTENSITE AND SHAPE MEMORY EFFECT IN B2 BASE NI-AL-FE ALLOY WITH ENHANCED DUCTILITY.* Metallurgical Transactions a-Physical Metallurgy and Materials Science, 1992. **23**(4): p. 1147-1153.

33.	Sozinov, A., et al., *Giant magnetic-field-induced strain in NiMnGa seven-layered martensitic phase.* Applied Physics Letters, 2002. **80**(10): p. 1746-1748.

34.	Sozinov, A., A.A. Likhachev, and K. Ullakko, *Crystal structures and magnetic anisotropy properties of Ni-Mn-Ga martensitic phases with giant magnetic-field-induced strain.* Ieee Transactions on Magnetics, 2002. **38**(5): p. 2814-2816.

35.	Boriskina, N.G., Kenina, E. M., *Phase equilbria in the Ti-TiPd-TiNi system alloys*, in *Titanium 80, Science and Technology, 4th International Conference on Titanium*, H. Kimura, Izumi, O., Editor. 1980, The Metallurgical Society of AIME, Warrendale, PA. p. 2917-2987.

36.	Shimizu, S., et al., *Improvement of shape memory characteristics by precipitation-hardening of Ti-Pd-Ni alloys.* Materials Letters, 1998. **34**(1-2): p. 23-29.

37.	Yang, W.S. and D.E. Mikkola, *DUCTILIZATION OF TI-NI-PD SHAPE MEMORY ALLOYS WITH BORON ADDITIONS.* Scripta Metallurgica Et Materialia, 1993. **28**(2): p. 161-165.

38.	Wasilews.Rj, et al., *HOMOGENEITY RANGE AND MARTENSITIC TRANSFORMATION IN TINI.* Metallurgical Transactions, 1971. **2**(1): p. 229-&.

39.	Yang, J.H. and J.W. Simpson, *Stress-induced transformation and superelasticity in Ni-Ti-Nb alloys.* Journal de Physique IV, 1995. **5**(C8): p. 771-776.

40. Eckelmeyer, K.H., *EFFECT OF ALLOYING ON SHAPE MEMORY PHENOMENON IN NITINOL.* Scripta Metallurgica, 1976. **10**(8): p. 667-672.

41. Donkersl.Hc and J.H. Vanvucht, *MARTENSITIC TRANSFORMATIONS IN GOLD-TITANIUM, PALLADIUM-TITANIUM A PLATINUM-TITANIUM ALLOYS NEAR EQUIATOMIC COMPOSITION.* Journal of the Less-Common Metals, 1970. **20**(2): p. 83-&.

42. Hosoda, H., et al., *Phase stability and mechanical properties of Ti-Ni shape memory alloys containing platinum group metals*, in *Thermec'2003, Pts 1-5*, T. Chandra, J.M. Torralba, and T. Sakai, Editors. 2003. p. 2333-2338.

43. Mulder, J.H., Beyer, J., Donner, P., and Peterseim, J. *On the high temperature shape memory capabilities of Ni-(TiZr) and Ni-(TiHf) alloys*. in *SMST 94-First international conference on Shape-memory and Superelastic Technologies* 1994. Pacific Grove, USA.

44. AbuJodom, D.N., Thoma, P.E., and Kao, M., Angst, D. R., *High treansformation temperature shape memory alloy*. 1992: U.S.A.

45. Angst, D., P. Thoma, and M. Kao, *The Effect of Hafnium Content on the Transformation Temperatures of $Ni_{49}Ti_{51-x}Hf_x$ Shape Memory Alloy.* Journal de Physique IV, Colloque, 1995. **C8**: p. 747-752.

46. Besseghini, S., E. Villa, and A. Tuissi, *Ni-Ti-Hf Shape Memory Alloy: effect of aging and thermal cycling.* Materials Science & Engineering A, 1999. **273-275**: p. 390-394.

47. Nishida, M., C.M. Wayman, and T. Honma, *PRECIPITATION PROCESSES IN NEAR-EQUIATOMIC TINI SHAPE MEMORY ALLOYS.* Metallurgical Transactions a-Physical Metallurgy and Materials Science, 1986. **17**(9): p. 1505-1515.

48. Zhu, Y.R., Pu, Z. J., Li, C., and Wu, K.H., *The stability of NiTi-Pd and NiTi-Hf high temperature shape memory alloys*, in *Proceedings of the International Symposium on Shape Memory Materials*, C. Yougi, and Hailing, T.U., Editor. 1994, International Acedemic Publishers: Beijing, China. p. 253-257.

49. Meng, X., et al., *Effect of Aging on the phase transformation and mechanical behavior of $Ti_{36}Ni_{49}Hf_{15}$ high temperature shape memory alloy.* Scripta Materialia, 2000. **42**: p. 341-348.

50. Olier, P., et al., *Investigation of Transformation Temperatures, Microstructure and shape memory properties of NiTi, NiTiZr and NiTiHf alloys.* Journal de Physique IV, 1995. **C8**: p. 741-746.

51. Han, X.D., et al., *The martensite structure and aging precipitates of a TiNiHf high temperature shape memory alloy.* Journal de Physique IV, 1995. **5**(C8): p. 753-758.

52. Firstov, G., J. Van Humbeeck, and Y. Koval, *Comparison of High Temperature shape memory behaviour for ZrCu-based, Ti-Ni-Zr and Ti-Ni-Hf alloys.* Scripta Materialia, 2004. **50**: p. 243-248.

53. Meng, X.L., et al., *Microstructure of stress-induced martensite in a Ti-Ni-Hf high temperature shape memory alloy.* Scripta Materialia, 2001. **45**(10): p. 1177-1182.

54. Eucken, S. and T.W. Duerig, *THE EFFECTS OF PSEUDOELASTIC PRESTRAINING ON THE TENSILE BEHAVIOR AND 2-WAY SHAPE MEMORY EFFECT IN AGED NITI.* Acta Metallurgica, 1989. **37**(8): p. 2245-2252.

55. Meng, X.L., et al., *Stress-induced martensitic transfonnation behavior of a Ti-Ni-Hf high temperature shape memory alloy.* Materials Letters, 2002. **55**(1-2): p. 111-115.

56. Meng, X.L., et al., *Effect of Cu addition on phase transformation of Ti-Ni-Hf high-temperature shape memory alloys.* Materials Letters, 2002. **57**(2): p. 452-456.

57. Meng, X.L., et al., *Effect of aging on martensitic transformation and microstructure in Ni-rich TiNiHf shape memory alloy.* Scripta Materialia, 2006. **54**(9): p. 1599-1604.

58. William D. Callister, J., *Material Science and Engineering An Introduction*. Seventh ed. 2007: Wiley.

59. Zheng, Y.F., et al., *Effect of ageing treatment on the transformation behaviour of Ti-50.9 at.% Ni alloy.* Acta Materialia, 2008. **56**(4): p. 736-745.

60. Han, X.D., et al., *A new precipitate phase in a TiNiHf high temperature shape memory alloy.* Acta Materialia, 1997. **46**(1): p. 273-281.

61. Meng, X.L., et al., *Phase transformation and thermal stability of aged Ti-Ni-Hf high temperature shape memory alloys.* Journal of Materials Science & Technology, 2006. **22**(5): p. 691-695.

62. Meng, X., et al., *Effect of aging on martensitic transformation and microstructure in Ni-rich TiNiHf shape memory alloy.* Scripta Materialia, 2006. **54**: p. 1599-1604.

63. Tong, Y.X., et al., *Microstructure and martensitic transformation of Ti49Ni51-xHfx high temperature shape memory alloys.* Materials Letters, 2009. **63**(21): p. 1869-1871.

64. Cai, W. and K. Otsuka, *Martensite Aging Effect and Thermal Cyclic Characteristics in Ti-Pd and Ti-Pd-Ni High Temperature Shape Memory Alloys.* Journal of Materials Science and Technology, 2001. **17**(3): p. 359-362.

65. Ishida, A., et al., *Effect of heat treatment on shape memory behavior of Ti-rich Ti-Ni thin films.* Materials Transactions Jim, 1995. **36**(11): p. 1349-1355.

66. Ishida, A., et al., *Effect of heat treatment on shape memory behavior of Ti-Ni thin films.* Journal de Physique IV, 1995. **5**(C8): p. 701-705.

67. Liu, L.H., et al., *Stress-induced martensitic transformation and microstructure of a Ti36Ni49Hf15 high-temperature shape-memory alloy*, in *Shape Memory Materials and Its Applications*, Y.Y. Chu and L.C. Zhao, Editors. 2001. p. 447-450.

68. Wang, Y.Q., et al., *The tensile behavior of Ti36Ni49Hf15 high temperature shape memory alloy.* Scripta Materialia, 1999. **40**(12): p. 1327-1331.

VITA

Date and Place of Birth

21st November 1984, Amritsar India

Educational Institutions Attended and Degrees Awarded

1. Bachelor of Technology, Mechanical Engineering, 2003 – 2003
   Punjab Technical University, Jalandhar, India
   D.A.V. Institute of Engineering and Technology, Jalandhar, India

2. Master of Science, Mechanical Engineering, January 08 – Present
   University of Kentucky, Lexington, Kentucky, USA

Scholastic and Professional Honors

1. Research Assistant (Mechanical Engg. Dept., University of Kentucky)

2. Teaching Assistant (Mechanical Engg. Dept., University of Kentucky)

Professional Presentations and Publications

ESOMAT' 09 European Symposium on Martensitic Transformations: Shape Memory Behaviour of Ni-rich NiTi(Cu,Pd)Hf HighTemperature Shape Memory Alloys (HTSMAs)   H. E. Karaca, G. Ded, R. Noebe, A. Hatemi, M. Souri, Y. I. Chumlyakov

Ms&T'09 Structural Materials for Aerospace and Defense: Development of NiTi(Cu,Pd)Hf High Temperature Shape Memory Alloys (HTSMAs) for Aerospace Applications
G. Ded, H. E. Karaca, M. Souri, S. Sagayian, R. Noebe , A. Garg, Y. I. Chumlyakov

ASME 2009 Conference on Smart Materials, Adaptive Structures and Intelligent Systems: Characterization of Ni-rich NiTi(Cu,Pd)Hf High Temperature Shape Memory Alloys (HTSMAs)
G. Ded, H. E. Karaca, A. Hatemi, R. Noebe , Y. I. Chumlyakov

SPIE Smart Structures and Materials+Nondestructive Evaluation and Health Monitoring:Mechanical characterization of Ni-Ti-Hf high temperature shape memory alloys, Gurdish Ded, Haluk E. Karaca, (Univ. of Kentucky); Ronald D. Noebe, NASA Glenn Research Ctr. ; Burak Basaran, Univ. of Kentucky

Gurdish Singh Ded